Julius-Maximilians-Universität Würzburg
Graduate School of Science and Technology

Doctoral thesis

for the doctoral degree

Doctor rerum naturalium (Dr. rer. nat.)

Novel Poly(2-oxazoline) Based Bioinks

Neuartige Poly(2-oxazolin) Basierte Biotinten

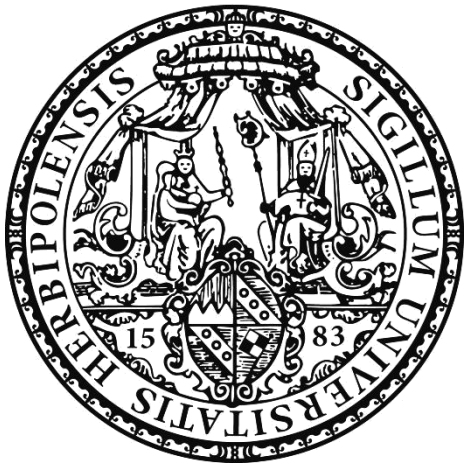

Submitted by

M.Sc. Thomas Lorson

from

Würzburg

Würzburg, 2018

Submitted on: October 22th, 2018

Members of thesis committee

Chairperson: Prof. Dr. Christoph Lambert

1. Reviewer and Examiner: Prof. Dr. Robert Luxenhofer

2. Reviewer and Examiner: Prof. Dr. Paul D. Dalton

3. Examiner: Prof. Dr. Katrin Heinze

Additional Examiners: Prof. Dr. Sebastian Seiffert

Day of thesis defense: May 09th, 2019

“The isolated man does not develop any intellectual power. It is necessary for him to be immersed in an environment of other men, whose techniques he absorbs during the first twenty years of his life. He may then perhaps do a little research of his own and make a very few discoveries which are passed on to other men. From this point of view the search for new techniques must be regarded as carried out by the human community as a whole, rather than by individuals.”

Alan Mathison Turing

Die vorliegende Arbeit wurde in der Zeit von Oktober 2014 bis August 2018 am Lehrstuhl für Chemische Technologie der Materialsynthese der Julius-Maximilians-Universität Würzburg unter der Betreuung von Herrn Prof. Dr. Robert Luxenhofer angefertigt.

Danksagung

An dieser Stelle möchte ich mich bei all denjenigen bedanken, die zum Gelingen dieser Arbeit beigetragen haben.

Mein besonderer Dank gilt meinem Doktorvater Prof. Dr. Robert Luxenhofer für die herzliche Aufnahme in seine Arbeitsgruppe (als ersten Nicht-Dresdner), die interessante und freie Themengestaltung, den unkomplizierten Umgang, seine unermüdliche Diskussionsbereitschaft sowie seine motivierende Art. Darüber hinaus bin ich sehr dankbar dafür, dass ich an verschiedenen Konferenzen in Dresden, Riva del Garda, Utrecht, Freiburg, Philadelphia, Peking, Würzburg, San Sebastian und Barcelona teilnehmen konnte sowie für die Möglichkeit bei Kooperationspartnern in Mainz und München zu forschen.

Herrn Prof. Dr. Paul Dalton sowie Frau Prof. Dr. Katrin Heinze danke ich für ihre Bereitschaft, meine Promotion an der Graduate School of Science & Technology zu betreuen sowie für die stets motivierenden und bereichernden Diskussionen. In diesem Zusammenhang möchte ich ebenfalls Herrn Dr. Schröder-Köhne für seine Hilfsbereitschaft bei organisatorischen Fragen danken.

Allen Mitarbeitern des Lehrstuhls für Chemische Technologie der Materialsynthese sowie den Mitarbeitern von FLUX Polymers danke ich für die stets gute und motivierende Atmosphäre, unzählige fachliche und private Diskussionen, vier feuchtfröhliche und (teilweise) erfolgreiche ChemCup Teilnahmen, zahlreiche Meetings und Grillabende sowie das alljährliche Boßeln. Ganz besonders bedanken möchte ich mich bei Markus, Niklas, Juliane, Corinna, Joachim, Anita, Michael, Miya, Claudia, Daniel, Christine, und Jochen, die meine Zeit am Lehrstuhl unvergesslich gemacht haben.

Meinen Bachelor- und Masteranden Miriam Komma, Simon Ziegler, Marc Lauter, Jonas Herrmann, Ralph Winkler, Jennifer Stubenrauch, Adrian Deiwiks und Nick Hüttner

danke ich für die gute Zusammenarbeit. Es war mir eine Freude euch auf einem Teilstück eurer Ausbildung begleiten zu dürfen und ich hoffe, dass ihr von mir ebenso viel gelernt habt wie ich von euch. In diesem Zusammenhang möchte ich mich auch bei allen Praktikanten, Projektstudenten und HiWis für die gute Zusammenarbeit bedanken.

Ein besonderer Dank gilt Christian May, der mit seiner ruhigen, gewissenhaften und freundlichen Art als Hilfe im Laboralltag unverzichtbar war und mir jederzeit mit Rat und Tat zur Seite stand.

Bei Guntram Schwarz möchte ich mich für seine Hilfsbereitschaft und Diskussionsbereitschaft bei Computerproblemen und rheologischen Fragestellungen bedanken.

Für die Einführung in die komplexe Welt der Lichtstreuung und die Möglichkeit Messungen selbst durchzuführen, bedanke ich mich bei Prof. Dr. Sebastian Seiffert und insbesondere bei Dr. Karl Fischer.

Dr. Sebastian Jaksch danke ich für seine Hilfe bei den durchgeführten SANS Experimenten und der Auswertung der gewonnenen Daten. Ohne die Förderung durch das JCNS wären diese Messungen nicht möglich gewesen werden, dafür vielen Dank.

PD Dr. Tessa Lühmann, Marcus Gutmann und Marco Saedtler vom Lehrstuhl für Pharmazeutische Technologie und Biopharmazie sowie Prof. Juraj Kronek und Dr. Zuzana Kroneková vom Polymer Institue der Slovak Academy of Sciences danke ich für die Durchführung von Zellviabilitätsexperimenten.

Prof. Dr. Ann-Christin Pöppler und Dr. Matthias Grüne vom Institut für Organische Chemie danke ich für ihre Hilfe bei der Durchführung von NMR-Messungen sowie für ihre Bereitschaft zur Diskussion wissenschaftlicher Fragestellungen.

Prof. Dr. Jürgen Groll und Tomasz Jüngst vom Lehrstuhl für Funktionswerkstoffe der Medizin und Zahnheilkunde danke ich für die Möglichkeit, die vorhandenen 3D Drucker zu nutzen sowie für die Unterstützung beim 3D Druck von zellbeladenen Biotinten.

Für das Korrekturlesen dieser Arbeit danke ich Martina Raschig und Prof. Dr. Robert Luxenhofer.

Deanna Nicdao danke ich für ihr künstlerische Unterstützung bei der Erstellung mancher Abbildungen.

Der Gesellschaft Deutscher Chemiker, der GlaxoSmithKline Stiftung, der International Society for Biofabrication, dem Deutschen Akademischen Austauschdienst, der Deutschen Forschungsgemeinschaft, dem Jülich Centre for Neutron Science sowie dem Freistaat Bayern danke ich für die Finanzierung meiner Forschung und Konferenzreisen.

Nicht zuletzt gilt mein Dank meiner Familie und meinen Freunden für ihre Unterstützung abseits der wissenschaftlichen Arbeit.

Publikationsliste

“Peptoids and Polypeptoids at the Frontier of Supra- and Macromolecular Engineering”
N. Gangloff, J. Ulbricht, T. Lorson, H. Schlaad and R. Luxenhofer
Chemical Reviews, 2016, 116(4), 1753 – 1802

“A Thermogelling Supramolecular Hydrogel with Sponge-Like Morphology as a Cytocompatible Bioink”
T. Lorson, S. Jaksch, M. M. Lübtow, T. Jüngst, J. Groll and R. Luxenhofer
Biomacromolecules, 2017, 18(7), 2161 – 2171

“Investigating the influence of aromatic moieties on the formulation of hydrophobic natural products and drugs in poly(2-oxazoline) based amphiphiles”
L. Hahn, M. M. Lübtow, T. Lorson, F. Schmitt, A. Appelt-Menzel, R. Schobert and R. Luxenhofer
Biomacromolecules, 2018, 19(7), 3119 - 3128

“Poly(2-oxazoline)s based Biomaterials: A comprehensive and critical update”
T. Lorson, M. M. Lübtow, E. Wegener, M. S. Haider, S. Borova, D. Nahm, R. Jordan, M. Sokolski-Papkov, A. V. Kabanov and R. Luxenhofer
Biomaterials, 2018, 178, 204 – 280

“More is sometimes less: Curcumin and paclitaxel formulations using poly(2-oxazoline) and poly(2-oxazine) based amphiphiles bearing linear and branched C9 side chains”
M. M. Lübtow, L. Keßler, A. Appelt-Menzel, T. Lorson, N. Gangloff, M. Kirsch, S. Dahms, R. Luxenhofer
Macromolecular Bioscience, 2018, DOI: 10.1002/mabi.201800155

“Melt Electrowriting of Electroactive Poly(vinylidene difluoride) Fibers”
S. Florczak, T. Lorson, T. Zheng, M. Higgins, M. Mrlik, D. W. Hutmacher, M. Higgins, R. Luxenhofer, P. Dalton
Science and Technology of Advanced Materials, submitted

Contents

Abbreviations and Symbols

ABBREVIATIONS

ACF	autocorrelation function
ACN	acetonitrile
AFA-LIFT	absorbing film-assisted laser-induced forward transfer
AM	Additive Manufacturing
CAD	computer-aided design
CLIP	continuous liquid interface production
CMC	critical micelle concentration
DMEM	Dulbecco's Modified Eagle Medium
DMF	dimethylformamide
DLS	dynamic light scattering
DOD	drop-on-demand
DP	degree of polymerization
DSC	dynamic scanning calorimetry
(d)ECM	(decellularized) extra cellular matrix
EPC	ethyl-4-piperidinecarboxylate
EPS	bacterial extracellular polysaccharides
FACS	fluorescence-activated cell sorting

FBS	fetal bovine serum
FDA	U.S. Food and Drug Administration
FDA	fluorescein diacetate
FDM	fused deposition modelling
GelMA	gelatin methacrylate
GPC	gel permeation chromatography
HA	hyaluronic acid
HaCat cells	human immortalized keratinocytes
HEMA	2-hydroxyethyl methacrylate
HFIP	hexafluoroisopropanol
IR	infrared
LCROP	living cationic ring opening polymerization
LCST	lower critical solution temperature
LDPE	low-density polyethylene
LIFT	laser-induced forward transfer
LVE	linear-viscoelastic
MALDI	matrix-assisted laser desorption/ionization
MAPLE-DW	matrix-assisted pulsed laser evaporation direct writing
MEW	melt electro writing
MMCP	methyl 3-mercaptopropionate
MS	mass spectrometry
NMR	nuclear magnetic resonance
ONs	*p*-nitrobenzenesulfonate
OTf	trifluoromethanesulfonate
OTs	*p*-toluenesulfonate
PAA	poly(acrylic acid)
PAAm	poly(acrylamide)

P*n*BuOx	poly(2-*n*-butyl-2-oxazoline)
P*n*BuOzi	poly(2-*n*-butyl-2-oxazine)
PBS	phosphate-buffered saline
PCL	poly(ε-caprolactone)
PEG	poly(ethylene glycol)
PEI	poly(ethylene imine)
PEtHepOzi	poly(2-(3-ethylheptyl)-2-oxazine)
PEtOx	poly(2-ethyl-2-oxazoline)
PEtOzi	poly(2-ethyl-2-oxazine)
PhCN	benzonitrile
PI	propidium iodide
PIPOx	poly(2-isopropenyl-2-oxazoline)
PLA	poly(lactic acid)
PLGA	poly(lactic-*co*-glycolic acid)
PMAA	poly(methacrylic acid)
PMeOx	poly(2-methyl-2-oxazoline)
PNiPAAm	poly(N-isopropylacrylamide)
P*n*NonOx	poly(2-*n*-nonyl-2-oxazoline)
P*n*NonOzi	poly(2-*n*-nonyl-2-oxazine)
POx	poly(2-oxazoline)
POzi	poly(2-oxazine)
PP	polypropylene
PPG	poly(propylene glycol)
P*n*PenOzi	poly(2-*n*-pentyl-2-oxazine)
PPhOzi	poly(2-phenyl-2-oxazine)
P*c*PrOx	poly(2-*cyclo*-propyl-2-oxazoline)
P*i*PrOx	poly(2-*i*so-propyl-2-oxazoline)

P*n*PrOx	poly(2-*n*-propyl-2-oxazoline)
P*n*PrOzi	poly(2-*n*-propyl-2-oxazine)
PS	polystyrene
PSR	polysarcosine
PVA	poly(vinyl alcohol)
RGD	arginine-glycine-aspartic acid
RM	regenerative medicine
SANS	small angle neutron scattering
SD	standard deviation
SDD	sample-detector distance
SEM	scanning electron microscopy
SLA	stereolithography
SLS	static light scattering
TE	tissue engineering
TOF	time of flight
UCST	upper critical solution temperature
UV	ultraviolet
WST	water soluble tetrazolium

SYMBOLS

2D	two-dimensional
3D	three-dimensional
°C	degree Celsius
Å	Ångström, 10^{-10} m
c	centi, 10^{-2}
Đ	dispersity ($Đ = M_w/M_n$)
d	characteristic domain size (periodicity)
D	diffusion coefficient
(k)Da	(kilo)Dalton
dn/dc	refractive index increment
eq	equivalent
(k)g	(kilo)gram
G’	storage modulus
G’’	loss modulus
(k)Gy	(kilo)Gray
γ	strain
$\dot{\gamma}$	shear rate
η	dynamic viscosity
h	hour
(k)Hz	(kilo)hertz
K	Kelvin
K	flow consistency index
k_B	Boltzmann constant
k_e	equilibrium rate constant
k_i	initiation rate constant

k_p	propagation rate constant
k_t	termination rate constant
L	liter
λ	wavelength
m	meter
m	milli, 10^{-3}
M	molar
µ	micro, 10^{-6}
min	minute
M_n	number-average molar mass
M_w	weight-average molar mass
n	nano, 10^{-9}
n	flow behavior index
N_A	Avogadro constant
(k)Pa	(kilo)pascal
ppm	parts per million
q	scattering angle
q^2	scattering vector
rad	radian
R_g	radius of gyration
R_h	hydrodynamic radius
s	second
t	time
T	temperature
tan δ	loss factor
T_{CP}	cloud point temperature
T_g	glass transition temperature

T_{Gel}	gelation temperature
T_m	melting temperature
τ	shear stress
(k)V	(kilo)volt
vol%	volume percent
W	watt
wt%	weight percent
w/v	weight per volume
ξ	correlation length

1 Introduction

Polymers: With them it all began. About 3.4 billion years ago, bacteria were the first living things on earth. Their origin and development was based on biopolymers. The same applies for us human beings who started to subdue the earth and dominate it about 150 000 years ago. Although the complex interaction of polymers inside the human body is quite robust for some time, it is still vulnerable to infections, diseases, and irradiation. Consequently, life expectancy was rather low in the former times (30 – 35 years around 1800)[1] as health care was not existent just like knowledge of hygiene or diseases spreading. However, life expectancy has increased linearly at almost three months per year over the past 160 years based on improvements in nutrition, public health and sanitation.[2] According to the world factbook, the highest life expectancy at birth is approximately 88 years (in Japan and Singapore) at the moment.[3]

It appears that even though the human body is quite resistant, it sooner or later stops to function properly or at least certain parts of it. Today, organ transplantation is a well-established procedure to extend life or to maintain quality of life the longest possible. Consequently, there is a growing demand for organs which dramatically exceeds the number of organ donors which is declining since 2010, at least in Germany. Even worse, today the lack of transplant tissue is estimated to be one of the leading causes of death in the U.S. Assuming a further increase of life expectancy in combination with a decrease of available organ donors the situation will become even worse in the next years. A very promising approach to overcome this dramatic organ shortage is presented by the young but rapidly growing field of biofabrication. Here polymers, either natural or synthetic, are intended to be used to build up biologically functional products through bioprinting. However, before being able to print a highly complex organ many challenges have to be mastered. To name just one example among many: Being able to ensure proper vascularization of a thick and metabolically-active organ tissue. A solution of this challenge would have such a huge impact that NASA is offering a $500 000 prize for it.[4]

For printing technologies, suitable substances are urgently needed which is why many research groups currently work on the development of printable polymeric materials. On the one hand it is important to develop new materials or to realize new material properties to broaden the field of application, on the other hand a continuous advancement of well-established polymers either by post modification or different processing techniques is crucial for future developments. This is the basis for all following investigations regarding, e.g. cytocompatibility, cell damage during printing, or tolerability *in vitro*.

A frequently discussed alternative to poly(ethylene glycol) (PEG), at the moment the "gold standard" of synthetic polymers used for biomedical applications, are poly(2-oxazoline)s (POx). From a chemical point of view POx exhibit a significantly higher synthetic variability as the side chain of every monomer unit could be functionalized while PEG only allows for the attachment of two functional groups at the chain end. The synthesis of POx takes place via living cationic ring opening polymerization (LCROP) and the physicochemical properties can be adjusted over a wide range by changing the substituent of the amid function. Furthermore, POx exhibit excellent cytocompatibility.

Although POx are well investigated in the context of drug delivery system and exhibit lower critical solution temperature (LCST) behavior, prior to this work no reports can be found describing physically cross-linked hydrogels solely based on POx, analogous to PEG based systems.

2 State of Knowledge

The chemical or physical interconnection of polymer chains results in networks which are termed gels if swollen in a liquid. A strict definition and delimitation against other classes of material remains difficult as gels unite characteristics of solids as well as liquids. They possess the capability to store energy or work, respectively, and can recover to their initial shape after deformation. Generally, a distinction is made between organo-gels and hydrogels, whereby the former are swollen in organic solvents and the latter are swollen in water. Accordingly, hydrogels consist of hydrophilic polymers that are cross-linked into an insoluble, but highly hydrophilic structure. These functional materials find application *inter alia* as biomaterials, which will be discussed in more detail in the following chapter.

2.1 Polymer Based Hydrogels for Biomedical Applications

For almost 70 years, hydrogels have been used and investigated as biomaterials and make an irreplaceable contribution to everyday life nowadays. For the first time mentioned in the late 19th century[5], the term hydrogel generally denotes a solid, jelly-like, absorbent and water containing material with mechanical properties ranging from soft and weak to hard and tough. Important to note, the system consisting of a three-dimensional network must not flow when in the idle state. In 1974, Flory classified gels in 4 main types (**Tab. 2.1**).[6]

Table 2.1| Hydrogel classification according to Flory.

Flory-Type	Definition
I	Well-ordered lamellar structures, including gel mesophases.
II	Covalent polymeric networks; completely disordered.
III	Polymer networks formed through physical aggregation; predominantly disordered, but with local regions of order.
IV	Particulate disordered structures.

Accordingly, the polymer chains can be cross-linked either covalently (Type II) or non-covalently (Type I, III & IV), resulting in chemical or physical gels, respectively. While the former are connected irreversibly but in the context of biomaterials mostly degradable, physical gels are only linked reversibly. For either type, gelation can be induced by certain stimuli like pH value, salt concentration, temperature and/or many more. Micellar crystallites, helices, glassy entanglements, micro-phase separation, ionic or

hydrophobic interactions as well as H-bonds can be the reason for physical gelation. Therefore, these gels are heterogeneous, due to the formation of clusters or domains. The different types of gelation transitions according to Rubinstein are summarized in **Fig. 2.1**.[7]

An alternative classification based on morphological considerations was presented by Russo.[8] On the one hand, he defined *Fishnet gels* where cross-links, whether reversible or covalent, provide the strong points of the structure and are separated by flexible strands which provide elasticity. On the other hand, *Lattice gels* where the division of the structure into cross-links and strands is inappropriate, i.e., the mechanical distinction between cross-links and strands is obscure, but nonetheless, a space filling structure exists.

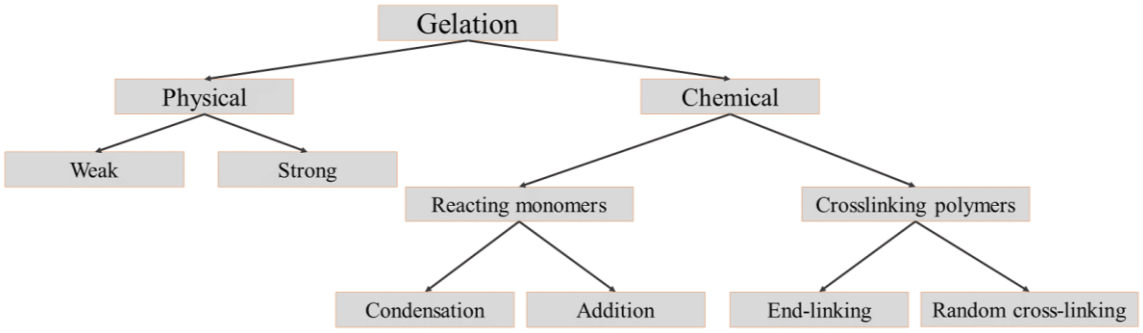

Fig. 2.1| Classification of gelation transition.

Notwithstanding the cross-linking mechanism, some crucial cross-linking requirements having a major impact on material performance need to be fulfilled to obtain a hydrogel applicable for medical applications. The correlation length or distance between two adjacent cross-links (ξ), the degree of cross-linking as well as the character of the bound water determine the overall transport of nutrients or drugs in and cellular products out of the hydrogel. For example, a short correlation length consequently results in tight meshes that are not desirable as cells with a diameter between 1 and 30 µm have to migrate through the hydrogel.

In general, hydrogels must meet a large number of design criteria to be considered for biomedical application in the human body and to function appropriately in this demanding environment. These criteria include both biological as well as physicochemical parameters. One critical parameter relates to the material's ability to exist within the body without damaging adjacent cells or leading to significant scarring or otherwise trigger a response that is detrimental to its desired function. This may be particularly problematic as the inflammatory response to a hydrogel can influence the immune response towards transplanted cells and *vice versa*.[9] Although it is controversially discussed, materials that

fulfill the mentioned criteria are still commonly termed biocompatible. Even worse, however, is the sometimes rapid generalization of the attribute biocompatibility for a certain material, based on *in vitro* cytotoxicity tests with a few selected cell lines/types. It is more reasonable to distinguish between biotolerant, bioinert and bioinstructive materials and term them cytocompatible if only cytotoxicity was investigated. In the last decades, several natural as well as synthetic polymers have been investigated and already used for biomedical applications. Hereinafter, the most promising candidates, either naturally derived or synthetic, will be discussed with respect to their gelation mechanism, occurrence and characteristic properties.

2.1.1 Hydrogels Based on Naturally Occurring Polymers

Although, all of the biopolymers mentioned below can be blended or mixed with each other and of course with synthetic polymers, this will not be taken into consideration in the following subchapters.

2.1.1.1 Polypeptides/Proteins

Collagen is the main organic constituent of natural extra cellular matrix (ECM) and the most abundant protein in mammalian tissue including bone, skin, cartilage, tendon and ligament.[10,11] Most of the 29 different types of collagen in the human body are fibrillary with type I collagen being the most common type. All fibrous collagen types exhibit a triple-helical structure with three left-handed polypeptide helices, coiling around each other and forming a right-handed triple-helical chain.[11,12] Typically, collagen is sourced from rat tail tendon or bovine skin and tendon.[13,14] Increasing the pH value of a collagen I solution initiates collagen fibril self-assembly, which does not harm cells dispersed in the solution/gel.[15] Collagen is naturally degraded by metalloproteases, particularly collagenase and serine proteases, allowing degradation to be locally controlled by cells.[16] However, problems with regard to sterilization[17], limited long-term stability as well as poor mechanical properties with elastic moduli of around 1 kPa are reported.[14,18,19] Although, the material properties can be improved by cross-linking[20], this drastically alters biodegradability.

Gelatin is a partially denatured collagen, formed by breaking its natural triple-helix structure into single-strand molecules.[21] A distinction is made between gelatin A that is prepared by acidic treatment and subsequent thermal denaturation, and gelatin B that is processed by alkaline treatment resulting in a high carboxylic content. Beneficially, gelatin

retains natural cell-adhesive motifs arginine-glycine-aspartic acid (RGD) and is less immunogenic compared to its precursor material collagen. Aqueous solutions of gelatin are thermoresponsive and solidify as collagen triple helices partially reform below their upper critical solution temperature (UCST) of 27 °C – 32 °C, depending on the polymer concentration (Flory type III).[22] Therefore, gelatin based hydrogels are not stable under physiological temperature and require chemical cross-linking. In addition to the methods used for collagen, commonly gelatin is photo-cross-linked after modification with methacrylate or free thiol groups. Gelatin methacrylate (GelMA) has been used in 2D and 3D cell culture[23], tissue engineering[24] (TE) and was extensively investigated in the new and up-coming field of biofabrication as potential bioink[25-27].

Another collagen-based hydrogel that has been widely used for TE applications, mostly cell culture studies, is Matrigel®. Developed in the Laboratory of Developmental Biology and Anomalies 30 years ago, Matrigel® is the solubilized mixture of basement membrane proteins extracted from Engelbreth-Holm-Swarm mouse sarcoma tumors that are rich in laminin, and collagen type IV.[28] Furthermore, it contains entactin/nidogen, heparin sulfate proteoglycans, and various growth factors. Depending on the composition, the gelation occurs rapidly and irreversibly between 24 °C and 37 °C. Although Matrigel® enables stem cells to maintain self-renewal and pluripotency, it promotes tumorigenicity and the growth of tumor cells *in vivo* due to the present growth factors.[29]

Fibrin is a naturally occurring polymer formed during wound coagulation[30] and has been used for various biomedical applications[31-33] in the recent years. Selective cleavage of the dimeric glycoprotein fibrinogen – the circulating dormant precursor of fibrin monomers – by the serine protease thrombin results in the formation of fibrin molecules that interact through a series of disulfide bonds.[34,35] Consequently, the mechanical and morphological properties are determined by the initial thrombin and/or fibrinogen concentration.[35,36] Fibrin is inherently cytocompatible, cell adhesive due to present RGD and alanine-glycine-aspartic acid-valine (AGDV) sites[33,37], and enzymatically degradable through activated plasmin within two weeks in the absence of fibrinolytic inhibitors like aprotinin.[38] Although fibrin hydrogels display non-linear elasticity, represented by an increasing storage modulus (G') with increasing deformation[39] the overall mechanical properties are poor with an elastic modulus ≤0.1 kPa. However, for applications like matrix models for neurons that usually reside in very soft tissue such as the brain, soft gels are imperatively necessary. The long-term

stability is still a remaining challenge as the best fibrin hydrogels with mechanical integrity were stable and optical clear for 3 weeks.[32]

Silks are natural protein fibers produced by *Arthropoda* such as spiders of the class *Arachnida* as well as insects of the order *Lepidoptera*.[18] Some spiders, such as female orb-weavers, are able to produce up to seven distinct types of silk, all with different mechanical properties and for specialized application. Native silk proteins are extremely repetitive and feature crystalline domains periodically interrupted by helical or amorphous regions.[40] Furthermore, silk is particularly of interest as a biomaterial due to slow degradation, outstanding mechanical properties, and absence of cytotoxicity and immunogenicity.[41,42]

Recently, decellularized extracellular matrix (dECM) comes in the focus of research.[43] Compared to hydrogels composed of individual ECM components like collagen, dECM-based hydrogels preserve the full well-matched biochemical complexity of the native tissue, and unlike Matrigel®, are not composed of a protein source that is the product of a tumorigenic cell line. The hydrogel formation is a collagen-based self-assembly process which is controlled in part by the presence of proteoglycans, glycosaminoglycans and other ECM proteins.[44] Very recently, the *in vivo* applications of state-of-the-art dECM-based hydrogels were comprehensively reviewed by Spang and Christman.[45]

In summary, naturally derived polypeptides are generally regarded as non-cytotoxic which is beneficial for any biomedical application. However, due to their varying composition (batch-to-batch or source-to-source) and purity they have the potential to induce inconsistent or unwanted biological response. Furthermore, apprehensions regarding immunogenic response and disease transmission are justified, as the proteins mentioned-above are mainly isolated from mammalian tissue.[46]

2.1.1.2 Polysaccharides

Simple sugars or monosaccharides are the building blocks of polysaccharides and are linked together via O-glycosidic linkages. Polysaccharides constitute an important group of biomaterials with varying chemical functionalities and physical properties. Additionally, most of them are able to form hydrogels in aqueous solution, for example on the basis of intermolecular hydrogen bonds (e.g. agarose) or intermolecular electrostatic (ionic) interactions (e.g. alginate). Due to synthetic modifications, the scope of hydrogel

formation pathways was significantly broadened and opened up possibilities to synthesize polysaccharides with tailor-made mechanical, biological, and physicochemical properties.

Hyaluronic acid (HA), discovered by Meyer and Palmer in 1934[47], is an immunoneutral linear polysaccharide consisting of alternating disaccharide units of [β(1,4)-D-glucuronic acid-β(1,3)-N-acetyl-D-glucosamine] linkages. Furthermore, it is the only non-sulfated glycosaminoglycan and plays a crucial role in wound healing, angiogenesis as well as matrix organization.[48] Moreover, HA is an essential component of the ECM and can be degraded in the body by hyaluronidase[49], which is ubiquitous in serum and cells. Many cross-linking mechanisms have been developed over the last decades, whereby usually, the hydroxyl, carboxylic acid, or N-acetyl groups are addressed for modification. These were reviewed in detail by Burdick and Prestwich.[50]

Alginate or alginic acid, one of the most frequently used polymers for biomedical applications, is a hydrophilic and linear unbranched anionic polysaccharide containing homopolymeric blocks of 1,4-linked β-D-mannuronic acid and its C-5 epimer α-L-guluronic acid in different proportions and varying in sequence. Primarily derived from brown seaweed, it is generally regarded as safe by the U.S. Food and Drug Administration (FDA) and has the capability to support cell survival and differentiation in culture.[51] At pH-values below 3, alginate self-assembles into acidic gels by the formation of inter-molecular hydrogen bonds.[52] Moreover, a physical gel is formed by cooperative binding with divalent cations such as Ca^{2+}, Mg^{2+}, Ba^{2+}, or Sr^{2+}. The selective storage of divalent cations into the zigzag structure of the α-L-guluronic acid blocks is commonly described in a model referred to as the egg-box model.[53] However, ionically cross-linked alginate hydrogels have the disadvantage of uncontrolled degradation via an ion exchange process under physiological conditions. A further limitation is the lack of bioactive binding sites requiring the modification, for instance, with lectin or RGD to enhance interactions with cells. In combination with a cationic polymer, polyelectrolyte complexes are formed which can be used as carrier systems.

Such a cationic polymer is chitosan, produced by partial deacetylation of chitin. It is composed of randomly distributed *β*-(1,4)-linked D-glucosamine and N-acetyl-D-glucosamine units and is structurally similar to naturally occurring glycosaminoglycans. An important characteristic of the macromolecule is the degree of deacetylation or the fraction of glucosamine units in the chemical structure. Chitosan is

considered a biodegradable polysaccharide, which can be metabolized by certain human enzymes such as lysozyme.[54] For pH values below its pK_a (pH < 6.2), chitosan is water-soluble and positively charged following the protonation of the free amine groups, causing electrostatic repulsion between the molecules.[55] On the one hand physical gels can be obtained by carefully adjusting the pH, on the other hand it was shown that β-glycerol phosphate disodium salt induces a sol-gel transition at physiological pH and temperature.[56] Moreover, chemically cross-linked chitosan hydrogels can be prepared by different strategies for example enzyme-catalyzed cross-linking[57] or Michael addition reactions[58].

Another prominent linear polysaccharide that needs to be mentioned in this context is agarose. It is extracted from marine red algae and one of the main components of agar, consisting of 1,3-linked *β*-D-galactopyranose and 1,4-linked 3,6-anhydro-*α*-L-galactopyranose as basic unit and ionized sulfate groups in varying proportions.[59] The gelation is based on the formation of intermolecular hydrogen-bonds upon cooling, resulting in the aggregation of double helices by the entanglement of anhydro bridges.[60] These physical agarose gels exhibit elastic moduli between <1 kPa and a few thousand kPa depending on the molecular weight and the polymer concentration.[61] These values cover the whole stiffness range of natural tissue except bones, enabling a broad scope of applications. Just like other polysaccharides native agarose is bioinert consequently comprising no bioactive signals. However, these can be introduced by physical blending-in or chemical modifications as shown by different groups throughout the last years.[62]

Recently, a vast number of bacterial extracellular polysaccharides (EPSs) have been reported to have improved physical properties compared to those extracted from plants or algae making them particularly interesting for medical applications.[63] The best-known examples of EPSs are gellan gum, xanthan gum, dextran, bacterial cellulose and bacterial alginate.[64] Their properties are mainly determined by their average molecular weight, chemical composition, molecular structure and distribution. Gellan gum is of particular interest as it forms a physically cross-linked macroscopic gels. It is a high molecular weight heteropolysaccharide secreted by the bacterium *Pseudmonas elodea* containing repeating units of D-glucose, L-rhamnose, and D-glucuronic acid in the molar ratios 2:1:1.[65] At elevated temperatures (~ 30 °C), the linear molecules are in a disordered coiled state which turns into double helical form upon cooling.[66] If the concentration of the gellan gum is sufficiently high (> 2%, w/v), the double helices transform into thicker rod-like aggregates what caused the formation of a gel.[67] The final mechanical properties of the gel strongly

depend on the degree of acylation. Thermoreversible, flexible, and elastic gels were obtained if the acylated form was used. In contrast, the de-acylated type formed hard, non-elastic, and brittle gels.[68] However, compared to polysaccharides recovered from plant or algae sources, EPSs are more expensive due to their higher production costs, mostly related to substrate costs and downstream processing.

2.1.2 Hydrogels Based on Synthetic Polymers

Compared to natural polymers, synthetic polymers are typically more controllable and reproducible. They can be synthesized with predetermined molecular weight, composition and degree of cross-linking. Furthermore, their physical, chemical and biological properties can be modified application-specific by introducing functional groups and degradable linkers. However, the intrinsic biological activity is generally much lower. Since the pioneering work of Wichterle and Lim in 1960 on cross-linked 2-hydroxyethyl methacrylate (HEMA) hydrogels for biological use as contact lenses[69], synthetic polymers like poly(acrylic acid) (PAA)[70], poly(methacrylic acid) (PMAA)[71], poly(acrylamide) (PAAm)[72], poly(N-isopropylacrylamide) (PNiPAAm)[73], poly(vinyl alcohol) (PVA)[74], synthetic polypeptides[75], poly(phosphazene)s[76], PEG[77] and POx[78–80] have been investigated intensively as hydrogels for biomedical applications. Furthermore, a huge variety of copolymers was synthesized to increase mechanical, physical or biological properties. As an example, poly(lactic acid) (PLA), poly(lactic-*co*-glycolic acid) (PLGA) and poly(ε-caprolactone) (PCL) can be utilized to design hydrolytically biodegradable copolymers.[81] In principle, every hydrophilic polymer can be used as a hydrogel as long as it is cross-linked sufficiently. As the main focus of this work will be on physically cross-linked thermoresponsive POx gels, only a very limited selection of thermoresponsive hydrogels will be discussed in detail in the following.

Hydrogels based on PNiPAAm belong to the most extensively investigated thermoreversible system. For the first time, the non-biodegradable polymer was described in the 1950s.[82] An aqueous solution of PNiPAAm exhibits a phase transition at the lower critical solution temperature (LCST) which is around 32 °C. Below this temperature, the polymer exists as flexible, extended coils. Increasing the temperature leads to an entropy-driven collapse at the LCST prior to aggregation into globular particles.[83] The underlying mechanism of the phase separation is the thermally induced release of water molecules bound to the isopropyl side chains, which results in increasing intra- and inter-molecular

interactions between the hydrophobic side groups above the LCST.[84] Increasing the polymer concentration of an aqueous solution a reversible sol-gel transition was reported at 28 – 30 °C.[85] Furthermore, the authors reported no marked concentration effect on the elasticity. However, these gels are turbid making them unsuitable for imaging techniques e.g. in cell culture. Copolymerization of NiPAAm with more hydrophilic monomers increases the LCST due to an overall higher hydrophilicity. The opposite effect is achieved by using a more hydrophobic monomer.[86] Due to the fact that PNiPAAm is not biodegradable, many efforts have been made on imparting this feature by addition of various monomers into the polymer structure.[87] Over the past decade, PNiPAAm was copolymerized for example with HEMA[88], PEG[89], gelatin[90] hyaluronic acid[91], or chitosan[92] to obtain thermosensitive hydrogels with tunable properties. Nonetheless, a strong hysteresis of the thermal solubility transition[93] as well as vitrification of the collapsed polymer globules due to the high glass transition temperature[94] are reported and spearheaded as disadvantages.[95]

The fact that PEG is already approved by the FDA for certain applications accelerated the research on hydrogels based on pure PEG as well as on PEG containing copolymers and currently made them the gold-standard. However, the extensive use of PEG is not undisputed among scientist as concerns regarding the biocompatibility and immunogenicity are voiced.[96,97] Nonionic ABA-type triblock copolymers comprising two flanking PEG blocks and a poly(propylene glycol) (PPG) core, commonly referred to as poloxamers are of great interest due to their thermoresponsive behavior. A variety of more than 30 different formulations is commercially available under the tradename Pluronic with a broad range in molecular weights and PEG/PPG block ratios. Pluronic F127 (F127, M_n: 12.6 kg/mol, 70 wt% PEO) is of particular interest as it gels at a concentration of 20 wt% at 25 °C and has been approved by FDA for use as food additives and pharmaceutical ingredients.[98,99] As hydrogels based on F127 will be used as a benchmark in the present work, this polymer will be discussed in more detail. Although the gelation mechanism of aqueous solutions has been investigated extensively in the recent years, it is still not fully understood and therefore debated. At low temperatures and concentrations below the critical micelle concentration (~ 0.1 wt%) F127 exists as individual coils (unimers).[100] Thermodynamically stable spherical micelles are formed with increasing copolymer concentration at the critical micelle temperature as a result of PPO block dehydration.[101] Due to the fact that the unimer-to-micelle transition is not sharp, both

coexist over a relatively wide temperature and concentration range.[102,103] Mortensen *et al.* conducted small angle neutron scattering (SANS) experiments at different F127 concentrations and temperatures.[104] At polymer concentrations above 5 wt% they found an increasing peak revealing a spatial correlation between neighboring micelles. This correlation peak becomes more pronounced with increasing concentrations until a gelation occurs at 20 wt%. The authors observed slight narrowing of the correlation peak and interpret this as micellar ordering on a crystalline lattice. At temperatures above 65 °C a micellar transformation from spherical to rod-like structures could by observed. In a more comprehensive work, Mortensen *et al.* compared four different Pluronics (P85, F87, F88 and F127) with respect to their self-associated assemblies in water at different polymer concentrations and temperatures.[102] When the micelle volume fraction (ϕ) is increased above 0.53 a first-order phase transition from a micellar liquid to cubic crystal takes place. By performing single-crystal crystallography the authors were able to demonstrate that the micelles arrange on a body-centered cubic lattice which is in contrast to most classical hard-sphere systems which tend to crystallize on a face-centered cubic lattice. Another hypothesis was published by Cabana *et al.* who suggest a mechanism of gelation based on packing of micelles and micelle entanglements.[105] Over the last three decades, F127 has been investigated and used for various biomedical applications like drug[106] and protein delivery[107], TE[108] and also biofabrication[109–112]. In this context, poloxamers were mostly termed biocompatible, non-toxic or something similar without scrutinizing this fact. However, several studies have found evidence for severe problems caused by poloxamers if used *in vivo*. Already in 1992, Wout *et al.* illustrated that an intraperitoneal injection of F127 into rats resulted in sustained hypercholesterolemia and hypertriglyceridemia more than 96 h after injection.[113] These findings were corroborated a few years later by Li *et al.* as well as by Palmer *et al.* who obtain similar results using mice.[114] Zhang and co-workers reported a certain cytotoxicity for P123 micelles due to accumulation of non-degradable micelles *in vivo*.[115] The possibility to use F127 as a vitreous substitute and intraocular drug delivery system was evaluated by Davidorf *et al.* For this purpose, a total vitrectomy was performed on New Zealand rabbits. Two weeks after surgery eyes containing F127 showed marked destruction of the retina. Recently, Hwang *et al.* published a comparable study investigating the intraocular biocompatibility of Matrigel®, F127 and PEtOx-*b*-PCL-*b*-PEtOx in albino rabbits.[116] Two month after injection severe cataract with iris anthropic change was found in eyes containing Matrigel® and F127. Furthermore, Thonhoff *et al.* found that a 30 wt% solution of F127 was toxic to human neural stem cells.[117] Taken

together, these studies clearly illustrate major issues for the *in vivo* application of F127 and emphasize the need for promising alternatives.

Yoshioka *et al.* reported a series of papers on commercially available Mebiol® Gel (Cosmo Bio), which is composed of thermoresponsive poly(NiPAAm-*co*-*n*-butyl methacrylate) blocks and hydrophilic PEG blocks.[118] It has been used as drug delivery system[119], wound dressing[120] and quite extensively as three-dimensional culture matrices for various cell types[121]. However, the broad sol-gel transition, which stretches over a relatively wide temperature range (~ 20 °C), has to be regarded as potential draw back. Furthermore, a storage modules below 1 kPa seems rather low for more demanding applications than cell culture. A chemical modification with e.g. biological moieties is only possible to a limited extent due to the restricted possibilities for polymer analogue modifications of PEG and PNiPAAm. Two other commercial PEG-based block copolymers worth mentioning are ReGel™ and InGell gamma™. The former is a ABA block copolymer, composed of PLGA-PEG-PLGA [122] whereas the latter is an aliphatically modified triblock copolymer with two flanking poly(L-lactide-*co*-caprolactone) blocks and a central PEG block[123]. Either hydrogel was synthesized to deliver drugs whereby the PCL present in InGell gamma™ is reported to stabilize the network allowing a better control over drug releasing characteristics in contrast to ReGel™.[124]

Another class of polymers suitable for formation of hydrogels for biomedical applications are POx. Recently, they were discussed comprehensively as promising alternative especially to PEG in some excellent reviews[97,125-127] and will be described in detail in the corresponding chapter 2.2.4.

2.1.3 Naturally derived *versus* Synthetic Polymers – A Comparison

Naturally derived as well as synthetic polymers have been extensively investigated as hydrogels for biomedical applications whereby both reveal characteristic advantages and disadvantages. Owing to their inherent good cytocompatibility and structural similarity to the ECM, natural polymers had the dominant role for biomedical applications in the last decades. Despite these advantages, many issues, including batch-to-batch variations due to the dependence on the biological source, complexities associated with purification, pathogen transmission and immunogenicity have incited the development of synthetic biomaterials as cellular substrates. Furthermore, economical, ecological, and ethical

aspects need to be considered carefully. Due to their high adaptability with regard to biodegradation, mechanical strength and chemical as well as biological response to stimuli, hydrogels based on synthetic polymers are nowadays used in a broad variety of biological applications, *inter alia* in cell culture and encapsulation, TE, drug delivery, and biofabrication. Furthermore, by incorporating biological sequences, hydrogels based on synthetic polymers are able to mimic certain aspects of function or structure of natural extracellular microenvironment. Although, the preliminary results regarding the cytocompatibility are promising, the long-term effects remain unknown and need to be investigated imperatively before widespread use *in vivo*.

2.2 Poly(2-oxazoline)s and Poly(2-oxazine)s as Thermoresponsive Biomaterials

The versatile class of poly(2-alkyl/aryl-2-oxazoline)s, referred to as POx, was initially reported by four independent research groups in 1966.[128–131] POx are often classified as pseudo-polypeptides due to their structural resemblance of naturally occurring polypeptides.[132] While POx received much attention resulting in a detailed investigation and continuous development of POx based materials, poly(4H-5,6-dihydro-1,3-oxazine)s – the higher homologue of POx – referred to as poly(2-oxazine)s (POzi), were almost forgotten although they were almost simultaneously reported.[131,133] Both are tertiary polyamides and typically lack chiral centers in the polymer backbone. In contrast to polypeptides, the formation of secondary structures via hydrogen bonding is hindered. Compared to PEG, POx as well as POzi provide an almost infinitely diversity of material properties as functionalities can be readily introduced in the side chains. This also allows for the straightforward tuning of basic characteristics like thermal properties, solubility or crystallinity.

The 50th anniversary of the discovery of POx and POzi in 2017 caused a plethora of review articles dealing with different aspects from synthesis over general properties to applications to which the reader should refer for more detailed information.[126,134-138] For the sake of completeness, however, a brief overview will be given in the following subchapters.

2.2.1 The Monomers – Five and Six Membered Cyclic Imino Ethers

The heterocyclic building blocks of POx – 2-substituted 2-oxazolines, referred to as 2-oxazoline in the following – were first successfully synthesized in 1889 by Gabriel.[139] However, the reported 2-amino-2-oxazoline which was synthesized by isomerization of the free base of 2-cyanoethyl-1-ammonium chloride, is not suitable for the LCROP due to the presence of the nucleophilic secondary amine. For the same reason unprotected thiols and alcohols have to be avoided in the monomer structure. Aside from their usage as monomers for the synthesis of POx, 2-oxazolines were applied as protecting groups for carboxyl acids groups[140], structural component of natural products[141], and as ligands in complex chemistry e.g. as asymmetric catalysis[142]. With increasing demand for new monomers a wide variety of synthetic approaches towards 2-oxazoline were developed throughout the years.[143,144] The most commonly applied procedures are the direct synthesis via

non-activated carboxyl acids[145,146], the Wenker method[147], the Witte-Seeliger synthesis[148] and the α-deprotonation route[149,150] (**Fig. 2.2**). The latter is primarily used for preparation of more complex 2-oxazolines. These synthesis routes are in general also applicable for 2-oxazines which consistently form the corresponding monomers of POzi.[133,151–154] Furthermore, Litt *et al.* reported the vapor-phase cyclodehydration for the preparation of 2-methyl- and 2-ethyl-2-oxazine. Of course 2-oxazolines can also be substituted at the 4- and/or 5-position. Although these polymers have been synthesized[153,155], the LCROP is significantly slowed down due to the steric hindrance.

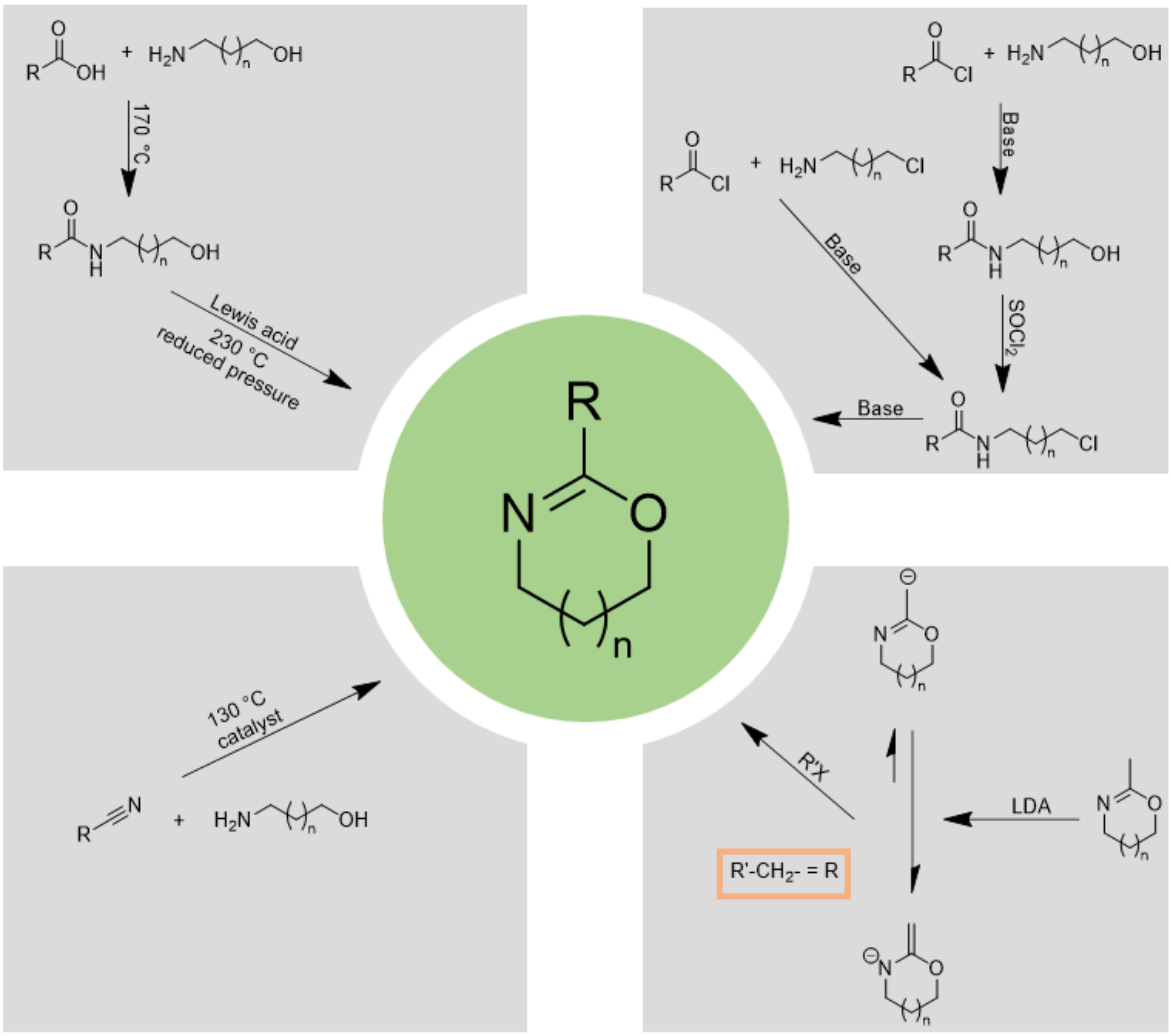

Fig. 2.2| Most common synthetic pathways towards 2-oxazolines (n = 0) and 2-oxazines (n = 1). Top left: Synthesis via non-activated carboxyl acids; Top right: Wenker method; Bottom left: Witte-Seeliger synthesis, and Bottom right: α-deprotonation route.

2.2.2 Living Cationic Ring-Opening Polymerization of 2-Oxazolines and 2-Oxazines

The LCROP of 2-oxazolines and 2-oxazines is commonly divided into initiation, propagation, and termination and can proceed in a living manner if some crucial parameters are met. In particular, all chemicals used, have to be completely dry and extremely pure as every nucleophile has the potential to terminate the polymerization at an early stage resulting in undesired broad molar mass distributions accompanied by higher dispersities (Đ) and low molar mass impurities. However, if these requirements are fulfilled, little or no unwanted termination or chain transfer should occur during polymerization in an ideal environment. Of course this is not the case in reality and these reaction cannot be suppressed completely.

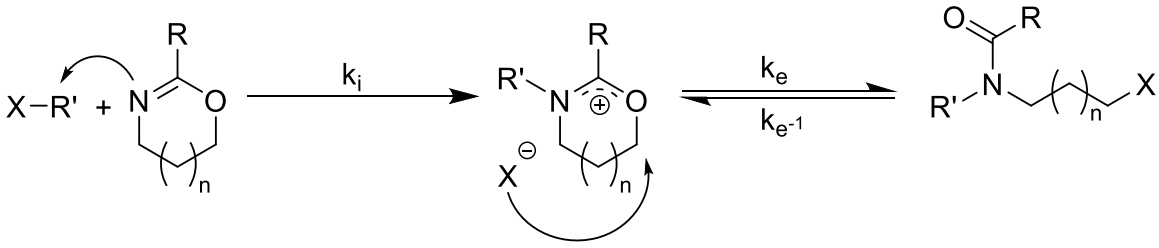

Fig. 2.3| Mechanism of the initiation of the LCROP of 2-oxazolines (n = 0) and 2-oxazines (n = 1) and the equilibrium between covalent and cationic species including the corresponding rate constants.

The initiation of the LCROP, with the initiation rate constant k_i, takes place by nucleophilic attack of the imino nitrogen of the 2-oxazoline or 2-oxazine onto an electrophilic initiator such as Brønsted or Lewis acids[128,129], silyl or acid halides[156], or alkylating agents[143,157,158] (**Fig. 2.3**). Additionally, this step allows the introduction of a functional end group.[159] When aiming for well-defined polymers with narrow molar mass distributions (Đ < 1.2) the initiation step has to be quantitative and fast compared to the propagation (propagation rate constant $k_p \ll k_i$). The resulting oxazolinium cation is resonance stabilized and can be isolated as initiator salt which constitutes a smart approach to overcome difficulties like a slow initiation. However, nowadays mainly *p*-toluenesulfonates (tosylate, OTs), *p*-nitrobenzenesulfonates (nosylate, ONs), and trifluoromethanesulfonates (triflate, OTf) are used due to their fast initiation even at ambient temperature.[157] The choice of the initiator prejudices the propagation as the nucleofugicity of the resulting counter ion strongly influences the equilibrium between the oxazolinium cation and its covalent species (k_e). For OTf, providing the highest

nucleofugicity, the propagating species was reported to be ionic for any type of 2-oxazoline including those with a perfluorated side chain.[143,160]

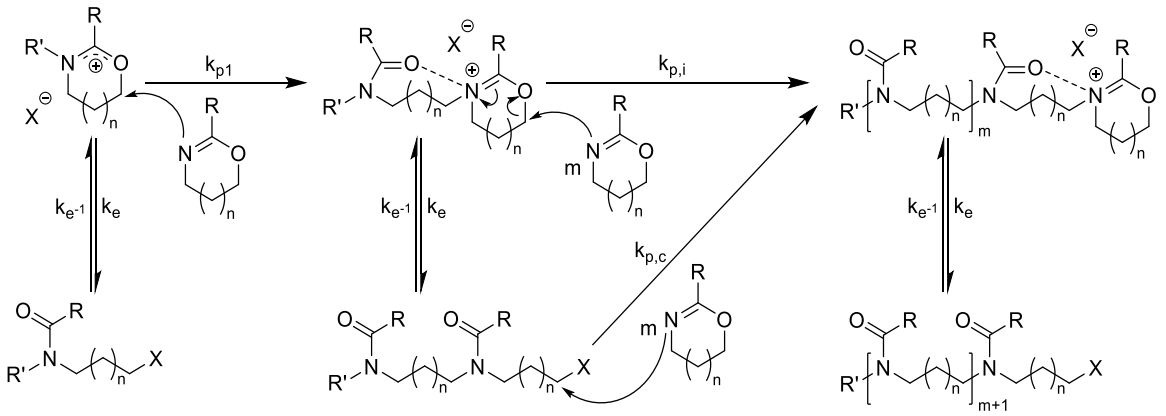

Fig. 2.4| Mechanism of the propagation of the LCROP of 2-oxazolines (n = 0) and 2-oxazines (n = 1) including the corresponding rate constants ($k_{p,i} > k_{p,c}$). For better visibility the addition of the first monomer was only drawn for the cationic species although this step can also happen at the covalent species.

Both species that can arise during initiation are electrophilic and can be attacked by further monomers resulting in continuous chain propagation (**Fig. 2.4**). It is important to note that the propagating species is at any time in equilibrium between the oxazolinium ion and the covalent species. However, the ionic species shows an increased propagation rate with respect to the covalent species ($k_{p,i} > k_{p,c}$). The average magnitude of k_p is directly proportional to the percentage of cationic species.[161] Furthermore, it is necessary to distinguish between the addition of the first monomer to the product formed during initiation (k_{p1}) and every further addition ($k_{p,i}$, $k_{p,c}$). By investigating the polymerization of 2-methyl-2-oxazoline (MeOx) Saegusa and Ikeda found that the addition of the first monomer is rather slow making it the rate-determining step.[162] An intramolecular, dipole-ion polarization effect that stabilizes the transition state might be the reason for the increase of the propagation rate after addition of the first monomer as the equilibrium is shifted towards the cationic species.[135] This equilibrium can be further influenced by the solvent, temperature, and concentration. In general, the polymerization of 2-oxazolines and 2-oxazines is thermodynamically driven as the formed tertiary amide in the backbone is more stable than the cyclic imino ether moiety of the monomer. Thus, the free energy change of isomerization compensates for the entropically unfavorable ring-opening.[163] Furthermore, it has been argued that by forming a linear polymer chain the ring strain is released leading to a minor contribution.[133,164] After complete monomer consumption the propagating species can either be terminated or a second monomer can be added, which enables the straightforward synthesis of diblock copolymers. Accordingly, multiblock

copolymers can be synthesized. Furthermore, the simultaneous addition of different monomers results in random or gradient-copolymers if the $k_{p,i}$ is different.[153] This step additionally allows the combination of POx and POzi which was only once demonstrated by Kobayashi *et al.* in a single report dealing with surfactants.[165]

Compared to initiation and propagation the termination, with the termination rate constants $k_{t,i}$, $k_{t,c}$, and $k_{t,2}$ is the least investigated part of the chain-growth polymerization. In general, any nucleophile (e.g. amines, azides, carboxylates, and thiolates) can be utilized as terminating agent (**Fig. 2.5**). As mentioned for the initiators, this step offers great potential for the introduction of functional groups by using functionalized, maybe partially protected, terminating agents.[166] It is often presumed, without further verification that the termination reliably takes place at the 5-position for 2-oxazolines. However, Nuyken *et al.* reported that water and potassium hydroxide have the tendency to terminate in 2-position. As a result a secondary amine and an cleavable ester containing end group are formed.[167] Based on the lesser interest in 2-oxazines no study regarding the termination reaction is available, although it might by highly insightful.

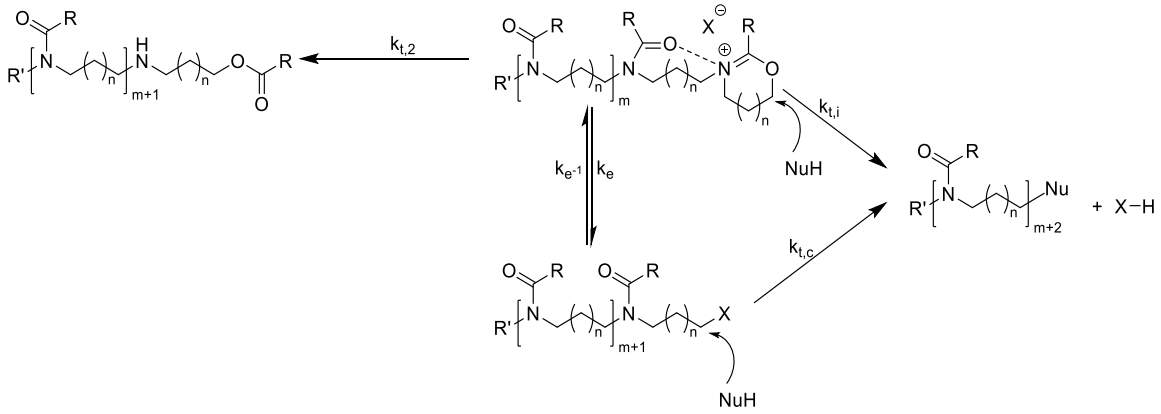

Fig. 2.5| Mechanism of the termination of the LCROP of 2-oxazolines (n = 0) and 2-oxazines (n = 1) including the corresponding rate constants. On the left side termination at 2-position is visualized.

As previously mentioned, chain transfer reactions, also denoted as β-elimination, occur to some extent in bulk as well as in solution (**Fig. 2.6**).[168,169] A proton is abstracted form the substituent of the propagating species in 2-position resulting in a new proton-initiated POx chain and a non-propagating chain bearing a cyclic enamine terminus.[168,170] The latter can lead to branching as it can take part in coupling reactions. Very recently, Schubert and co-workers combined gel permeations chromatography (GPC) and MALDI MS to investigate chain transfer reactions in more detail. They were able to unambiguously identify a low molar mass peak in the GPC elugrams as proton-initiated POx chain.[171] Furthermore, it is reported that the chain transfer reaction is strengthened by high

temperatures, extended reaction times, high monomer concentrations and high degrees of polymerization (DPs).[170] Especially the latter mentioned as well as polymerization times of hours or even days, were major drawbacks for a long period. Schubert and co-workers published a series of papers utilizing microwave technology for LCROP leading to a considerable acceleration (~350 times) of the polymerization.[172–174] This technique was also used to prepare poly(2-phenyl-2-oxazine), however, only an acceleration by factor 1.8 could be achieved.[151]

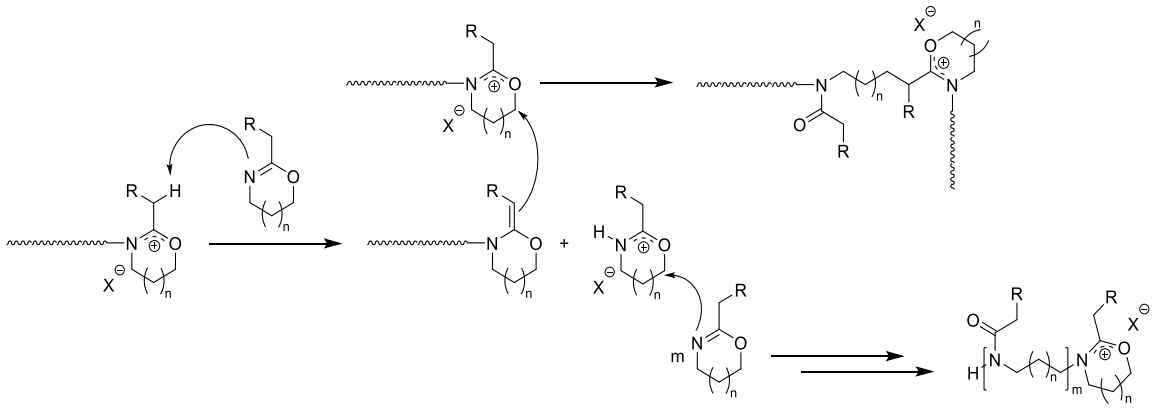

Fig. 2.6| Schematic representation of the chain transfer and coupling reactions during the LCROP of 2-oxazolines (n = 0) and 2-oxazines (n = 1).

Wiesbrock *et al.* found that the electromagnetic waves do not directly influence the process but merely ensure a rapid and particularly homogenous heating.[172] Additionally, the authors found a minimum of side reactions at an ideal temperature around 140 °C. However, the DP for well-defined POx (Đ < 1.2) was limited to 100 monomers with some exceptions for which 300 repeating units were reported.[173] Very recently, Hoogenboom and Monnery patented their approach to achieve high molar mass POx with DPs ≫ 250 and low dispersities. Although they described the synthesized polymers as uniform in the patent title, the typical dispersities are below 1.25 according to paragraph 0074. This perfectly illustrates the erroneous use of the word uniform which should only be used for polymers having one specific molar mass and not a molar mass distribution. The patented approach combines low polymerization temperatures with the sacrificial initiator method (purification of solvent and monomer over living POx chains) resulting in poly(2-ethyl-2-oxazoline) (PEtOx) with an average molar mass of 110 kDa and a dispersity of 1.02.[175] However, it remains questionable if such a cumbersome process is suitable for the production of larger quantities which will be needed if current and future studies proof the exceptional potential of POx and POzi based materials.

2.2.3 Properties

The main reason for the increasing popularity of POx are presumably their tunable properties which can be diversified over a broad range by simple variation of the 2-substituent of the monomer. The same applies for POzi, however, only limited data are available. A common approach to further tune polymer properties is to synthesize copolymers which was of course done for POx. In the following, the most commonly investigated characteristics, namely solubility and thermal properties are briefly discussed. Mechanical properties will not be addressed, as POx mainly forms brittle materials due to the inaccessibility of high molar masses which is connected to poor chain entanglement.[176,177]

2.2.3.1 Solubility of Poly(2-oxazoline)s and Poly(2-oxazine)s

The aqueous solubility of POx and POzi strongly depends on the side chain. For the shortest, namely methyl, the solubility is determined by the hydrophilicity of the polyamide backbone. Thus, poly(2-methyl-2-oxazoline) (PMeOx) is highly soluble in water but exhibits poor solubility in many common organic solvents especially at higher molar mass. Increasing the side chain leads to a LCST behavior[178] which was previously mentioned for PNiPAAm. However, it is important to take the DP and end groups into account as they strongly influence the cloud point temperature (T_{CP}).[179] For PEtOx values between 60 °C up to 100 °C have been reported.[180] Very recently, Konefał *et al.* investigated the structural changes of PEtOx during temperature-induced phase transition in D_2O utilizing ^1H NMR and dynamic light scattering (DLS).[181] They were able to show that structures on molecular level which are formed during heating are preserved during subsequent cooling. Increasing the side chain leads to a further decrease of the LCST until poly(2-*n*-butyl-2-oxazoline) (P*n*BuOx) is essentially insoluble in water. By changing the constitution of the propyl side chain T_{CP} can by varied between ~25 °C (poly(2-*n*-propyl-2-oxazoline) (P*n*PrOx))[182], ~30 °C (poly(2-*cyclo*-propyl-2-oxazoline) (P*c*PrOx))[183] and ~40 °C (poly(2-*iso*-propyl-2-oxazoline) (P*i*PrOx))[183,184] (**Fig. 2.7**). Very recently, Jung *et al.* reported that T_{CP} of P*i*PrOx can be significantly shifted to higher temperatures by synthesizing cyclic P*i*PrOx showing the end group effect.[185] Furthermore, external influences like the presence of salts need to be taken into account as these can drastically effect T_{CP} in both directions.[186–188]

In general, the T_{CP} of POzi follows the trend described for POx, however, it is considerably lower than for the corresponding POx. The only publication dealing with the LCST behavior of POzi was published by Bloksma *et al.* where they reported a T_{CP} of 56 °C for poly(2-ethyl-2-oxazine) (PEtOzi) with a DP of 100 (PEtOzi with DP = 50 did not show a LCST behavior) and 12 ± 1 °C for poly(2-*n*-propyl-2-oxazine) (P*n*PrOzi) with a DP of 50, 100 and 150 (**Fig. 2.7**).[152] Here too, poly(2-*n*-butyl-2-oxazine) (P*n*BuOzi) and POzi with longer side-chains appeared completely water insoluble.

In order to modulate the T_{CP}, different monomers can be copolymerized either statistically or as block copolymers.[178,184,189,190] Additionally, most of these block copolymers are amphiphiles which self-assemble into aggregates like micelles above a critical concentration and/or temperature in aqueous solution. This forms the basis for many applications which will be discussed in chapter 2.2.4.

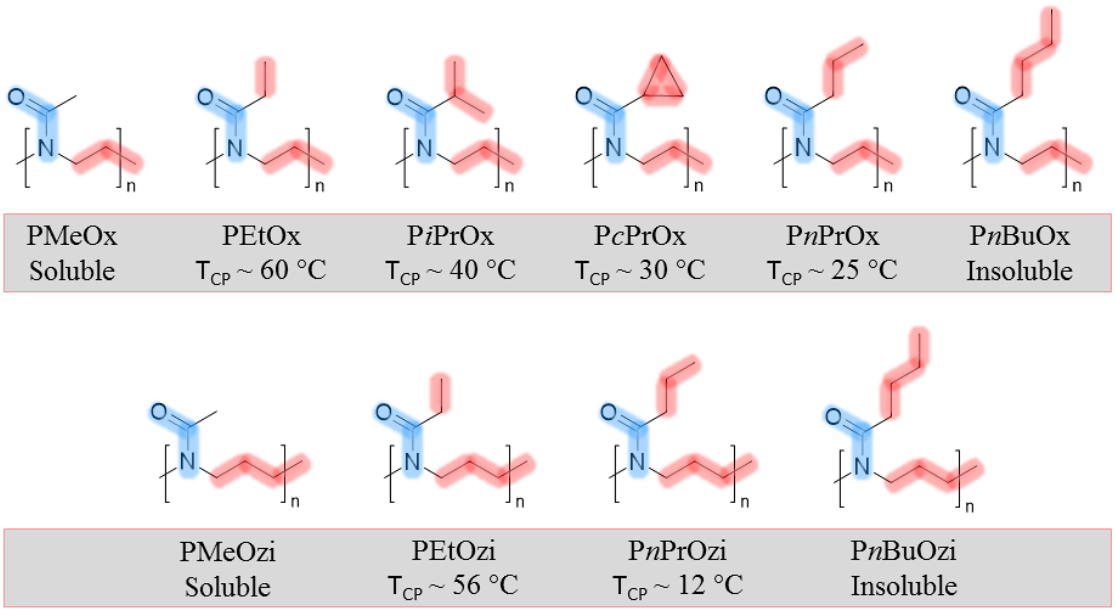

Fig. 2.7| Selected overview of the cloud point temperatures (T_{CP}) of different POx und POzi homopolymers with increasing hydrophobicity (from left to right).

Not only the solubility itself, but also the conformation of the polymer chain in solution is important for potential applications. Very recently, Filippov and co-workers thoroughly investigated the conformational parameters (equilibrium rigidity, the Kuhn segment length, and the diameter of the polymer chain) of PEtOx with molecular weights ranging from 11.2 kg/mol up to 260 kg/mol in phosphate-buffered saline (PBS) at physiological temperature.[191] The authors were able to resolve the equilibrium rigidity values, which are similar to PEG, and additionally proved that the rigidity of PEtOx is

directly influenced by its thermosensitivity. Once more, these findings stress the potential of PEtOx as promising alternative to PEG in the future.

2.2.3.2 Thermal Properties of Poly(2-oxazoline)s and Poly(2-oxazine)s

It is well established that POx are thermally stable up to temperatures of ~300 °C[192,193,194] what is comparable to other water soluble, organic polymers such as PEG[195]. Depending on the number of carbon atoms in the side chain, POx can either occur as amorphous or semicrystalline. While the latter exhibit melting temperatures (T_m) around 150 °C regardless of the length of the side chain[145,174,177,194,196], the glass transition temperature (T_g) of POx decreases almost linearly with increasing side chain length[174,177] due to the increasing flexibility. However, this trend is only valid for non-branched alkyl side chains. It is important to note that the length of the polymer chain as well as the processing of the material are not negligible. As an example, Luxenhofer and co-workers investigated short (DP = 11) poly(2-*n*-nonyl-2-oxazoline) (P*n*NonOx) homopolymers and found significantly lower T_m of ~89 °C.[154] Furthermore, Bassiri *et al.* and Demirel *et al.* reported T_m for PMeOx and P*n*PrOx, respectively, which might originate from isothermal heating or prolonged processing times.[129,197] Due to their hindered alignment and the resulting decrease in packing density, the introduction of branched alkyl side chains results in completely amorphous POx with low T_g.[149,154,198]

In comparison to the T_g of POx, the T_g of the corresponding POzi is approximately 30 – 50 °C lower due to the additional methylene group which leads to an increased chain flexibility. Litt *et al.* reported a T_g of 16 °C and 30 °C for PMeOzi (DP = 200), the latter was reported for a polymer prepared under improved conditions, 8 °C for PEtOzi (DP = 200) and -16 °C for poly(2-*n*-pentyl-2-oxazine) (P*n*PenOzi) (DP = 200).[133] Poly(2-phenyl-2-oxazine) (PPhOzi) (DP = 2500) was found to be semicrystalline with a T_m at 165 °C and a T_g at 72 °C. Interestingly, unsubstituted POzi is partially crystalline with a T_m around 120 °C.[199] Very recently, Luxenhofer and co-workers extended this small library by investigating poly(2-*n*-nonyl-2-oxazine) (PNonOzi) (DP = 11) and poly(2-(3-ethylheptyl)-2-oxazine) (PEtHepOzi) (DP = 11).[154] Surprisingly, they did not observe a T_g for the latter in the investigated temperature range between -50 °C and 200 °C. Although this might be a first step to increase the insights into POzi, a direct combination with existing values is not advisable due to the very low DP.

To summarize, it was shown that small modification in the side chain as well as the slight elongation of the polymer backbone by one methylene group per repeat unit have significant influence on the thermal and solution properties. These can be adjusted over a brought range to perfectly suit almost any envisioned application. By taking POzi into account, it is easily conceivable that the T_g can be tuned by copolymerization of POx and POzi among each other and with each other.

2.2.4 Applications

Although it has been shown previously that a great variety of POx is easily accessible, only a few members of this polymer family have been investigated for potential applications. PEtOx with a broad molar mass distribution, which is commercially available under the trade name Aquazol®, is most widely used followed by the more hydrophilic PMeOx. A major drawback for the development of large-scale applications are the absence and the relatively high fabrication costs of large quantities of defined POx. Thus, the main focus of research lies still on the development of high added value POx based biomaterials, although some other interesting applications were reported recently.

2.2.4.1 Poly(2-oxazoline) Based Performance Materials

The rapid growth of the world population and a steady increase in prosperity go hand in hand with a growing energy demand. Polymer solar cells are considered to be a very promising alternative as they can be produced as flexible modules and enable high throughput. However, the power conversion efficiency with ~10% is still comparably low. Recently, Nam *et al.* used a PEtOx layer as alternative to poly(ethylene imine) (PEI) in polymer:fullerene solar cells.[200] By thermal annealing of the PEtOx coating a considerable improvement could be achieved. Chen *et al.* reported a performance increase from 9.01% to 14.52% by inserting a thin PEtOx layer into a perovskite solar cell.[201] Furthermore, PEtOx was introduced into near-infrared organometallic halide perovskite LEDs leading to ~70%-fold increment in quantum efficiency compared to a control device.[202]

Another interesting application of POx was reported by Jang and co-workers. The authors exploited the thermoresponsive behavior of POx to design and prepare a switchable multicolor emission material.[203] P*i*PrOx was coupled with three different dyes through a Cu(I)-catalyzed click reaction to cover the three primary colors (red, green and blue). Subsequently, the emission colors could be changed reversibly by modification of the temperature.

2.2.4.2 Poly(2-oxazoline) Based Biomaterials – A General Overview

This subchapter is a brief summary of the review article "Poly(2-oxazoline)s based Biomaterials: A comprehensive and critical update" by T. Lorson; M. M. Lübtow; E. Wegener; M. S. Haider; S. Borova; D. Nahm; R. Jordan; M. Sokolsky-Papkov; A. V. Kabanov and R. Luxenhofer published recently in Biomaterials.

In general, POx homopolymers have been established to exhibit excellent cyto- and hemocompatibility up to high polymer concentrations. However, mainly the hydrophilic PMeOx and PEtOx have been investigated[127,204,205] and often compared to PEG as they are considered as promising alternative[97,206]. It is therefore essential, to evaluate cyto- and hemocompatibility for POx with different compositions, end-groups or architectures. Furthermore, it is important to bear in mind that unreacted monomer can remain in the polymer and, therefore, may influence cell viability.[207] For many, if not most POx based biomaterials, copolymers are utilized which either comprise solely this polymer family, certainly with different side chains, or combine other polymers like PCL[208], polysarcosine (PSR)[209], PLA[210], or PEI[211]. Recently, many reports regarding the cyto- and hemocompatibility of POx based copolymers for biomedical applications have been published[212,213], corroborating the promising results obtained for homopolymers.

In addition to *in vitro* cytotoxicity test *in vivo* experiments are necessary to understand biodistribution mechanisms. In the late 1980s Goddard *et al.*[214] and later Gaertner *et al*.[215] reported rapid clearance from the blood pool. More recently, Wyffels *et al.* investigated the pharmacokinetic behavior of PEtOx and compared it with PEG.[216] Corroborating other studies, they found that both polymers were rapidly excreted via the kidneys, if the molar mass was below 20 kg/mol. Especially for larger polymers, the question of their removal and degradability needs to be kept in mind.

It is well known, that POx are amendable to acidic and basic hydrolysis at harsh conditions and thus can be used as a precursor for linear and defined PEI or partially hydrolyzed POx polymers[217] which can both be used for gene delivery[218]. However, at physiological conditions, no significant hydrolysis was observed in simulated stomach an intestine fluid.[213] Additionally, other possible degradation mechanisms like the degradation by reactive oxygen species[219] or enzymes[220] need to be taken into account.

In the last decade, the conjugation of POx with nanoparticles, carbohydrates, peptides, proteins[221], lipids, and drugs has been intensively investigated. The latter

forming a drug delivery system containing one or more drug(s) covalently attached to the polymer through functional groups. Very recently, the first clinical-trial of a POx-drug conjugate, initiated in 2015, was carried out with 20 participants. To address motor complications caused by dopaminergic drugs, administered against Parkinson's disease, Serina Therapeutics Inc. developed POx based rotigotine conjugates with three different release profiles.[222] Even though this study is ongoing and final results have not been published yet, the preliminary results appear promising.[137] Hopefully, the results will boost the development of new POx based biomaterials and serve as starting point for clinical trials of other promising materials like the ABA triblock copolymer PMeOx-P*n*BuOx-PMeOx, which provides outstanding solubilization capabilities for the important cancer chemotherapeutic Paclitaxel.[223]

2.2.4.3 Poly(2-oxazoline) Based Hydrogels

Taken together, the described properties and the diversity of POx makes them ideally suitable to be used as hydrogels for biomedical application. Although a detailed summary is already provided by some excellent recently published reviews[79,80,138] a brief summary will be given in the following.

Around the year 1990, Chujo and co-workers reported in a series of papers on POx based hydrogels.[78,224,225] On the one hand, they used irreversible chemical cross-linkers like diisocyanates or diacylchlorides, on the other hand reversible cross-linking was achieved by Diels-Alder reaction of pending furan and maleimide groups or by ionic interactions of bipyridyl with di- and trivalent ions. All the approaches mentioned here have in common that POx is hydrolyzed in a first step followed by subsequent introduction of functional side chains or cross-linkers at the resulting secondary amine (**Fig. 2.8 A**). However, the introduction of functional groups like double bonds or amines can also take place during polymerization if appropriate monomers are utilized.[226] In addition, two other main approaches towards POx hydrogels can be identified. Polymeric networks can either be formed *in situ* by the copolymerization of mono- and bis-functional monomers[220,227,228] (**Fig. 2.8 B**) what was also initially reported by Chujo *et al.*[225,229], or via the so called macro-monomer method[230] which utilizes α,ω-functionalized POx bearing polymerizable groups such as methacrylates (**Fig. 2.8 C**). Recently, Sedlacek *et al.* reported another approach which requires quite harsh conditions. They exposed PEtOx, PEG, PNiPAAm, poly(vinylpyrrolidone) and poly(hydroxylpropyl acrylamide) to β- and γ-irradiation and found formation of hydrogels above 2 kGy (β – irradiation) and 20 kGy (γ – irradiation),

respectively.[231] Finally, it is important to note, that even though POzi is mentioned in **Fig. 2.8** for the sake of completeness and because of the potential transferability of reactions from POx to POzi, no studies on such materials have been reported until today.

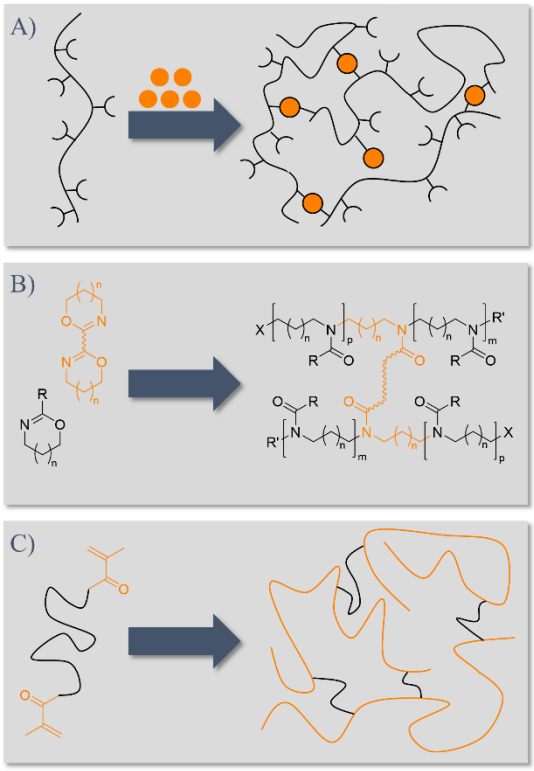

Fig. 2.8| Schematic representation of different approaches leading to chemical cross-linked POx (n = 0) or POzi (n = 1) hydrogels: (A) side chain functionalization, (B) *in situ* copolymerization, and (C) macro-monomer method.

In the recent years, research on biomedical applications of POx gels has pushed basic proof-of-principle studies more and more into the background. In order to promote cell adhesion Farrugia *et al.* incorporated RGD via UV-mediated thiol-ene reaction into the POx hydrogel.[232] They found significantly higher cell-attachment compared to corresponding control-groups. However, it is questionable if the usage of UV-light, which is necessary for the thiol-ene reaction, is appropriate in this context as cells can be damaged although they might appear alive. Shortly thereafter Schenk *et al.* presented a report on RGD-functionalized POx gels showing enhanced adhesion of $\alpha_v\beta_5$-expressing cancer cells *in vivo*.[228] Recently, Dargaville and co-workers combined Additive Manufacturing (AM) with POx based hydrogels to create micro-channels which could be flushed with fluorescent molecules.[233] Especially in the context of vascularization, which is of paramount importance for any artificial tissue, the use of a sacrificial template presents a promising approach. Another interesting field of research are POx micro- and nanogels for biomedical application which have been investigated in the recent years.[234]

Physically cross-linked POx gels are investigated much less frequently than their chemical counterparts, *inter alia* because of their unpredictable and rare occurrence. Wang *et al.* synthesized an ABA block copolymer containing PEtOx blocks attached to a PCL segment and observed temperature induced gelation between 15 °C and 30 °C. Unfortunately, no values for G' and G'' are provided. In a comparable approach Liu and co-workers synthesized a series of amphiphilic ABA copolymers with a poly(D,L-lactide)

segment and two flanking PEtOx blocks.[235] Although a sol-gel transition is reported around body temperature, G' does not form a plateau but rather goes through a maximum with a peak value of around 0.6 Pa. In spite of its similarities with PEG, no solely POx/POzi based equivalent to thermogelling Pluronic has been reported so far. Therefore, this will be the main focus of the present work.

2.2.5 Summary

Cyclic imino ethers bearing aryl or alkyl chains in 2-position function as monomers for the LCROP of poly(2-oxazoline)s and poly(2-oxazine)s. The living character allows good control over the molar mass and narrow dispersities are accessible. The polymerization is initialized by an electrophilic initiator and can proceed either by an ionic or covalent mechanism. Functional groups can be introduced at both chain ends and in the side chain by choosing suitable monomers which might be protected to prevent unwanted interference of the propagation. Furthermore, block- or random copolymers can be prepared. (Chapter 2.2.1 & Chapter 2.2.2)

The length of the side chain influences the physical properties like T_{CP} and T_G what allows their adjustment according to needs derived from specific applications. Amphiphilic copolymers further increase the accessible temperature range and can form aggregates like micelles, cylinders, vesicles, or lamellar structures in selective solvent. (Chapter 2.2.3)

Poly(2-oxazoline) based biomaterials are of great interest as POx exhibits good cyto- and hemocompatibility and can easily be attached to peptides, proteins, lipids and drugs with the aim to improve, stability, solubility, and catalytic activity as well as biodistribution and cellular uptake. In particular, the first in-human studies of a POx-drug conjugate are a milestone in the development into a serious alternative to PEG. (Chapter 2.2.4.2)

Chemically cross-linked hydrogels based on POx can be precisely designed with versatile physical, chemical, viscoelastic and biological properties due to the great synthetic variability. Furthermore, stimuli-responsive characteristics are readily-incorporated. Consequently, 3D cell culture, tissue engineering, and biofabrication seem to be perfect applications for POx based hydrogels. (Chapter 2.2.4.3)

2.3 Additive Manufacturing in the Context of Tissue Engineering and Regenerative Medicine

AM, also referred to as 3D printing was first introduced during the 1980s and comprises various technologies that allow the production of customized parts from ceramics, metals and polymers. The direct generation in a layer-by-layer fashion through computer-aided design (CAD) supersedes the use of molds or machining and enables a significantly higher degree of freedom compared to conventional formative and subtractive manufacturing techniques. Furthermore, fabrication of objects is no longer coupled to inflexible and controlled industrial mass production or even to any company as 3D printers are commercially available for less than 500 $ (e.g. fused deposition modelling (FDM)). As a result, AM in combination with the internet of things is often regarded as the next industrial or manufacturing revolution.[236] However, the transfer of AM from prototyping to manufacturing on a larger scale revealed that a number of challenges, mostly material related, have to be tackled beforehand.

The process related advantages of AM, namely a high degree of reproducibility and automation in conjunction with the precisely controlled deposition of different materials in a 3D model, render AM principally interesting for TE and regenerative medicine (RM). Initially, TE was described as interdisciplinary field that applies engineering principles and life science to develop biological substitutes that maintain, restore, or improve biological tissue function or a whole organ.[237] In addition, RM has been defined as the application of tissue science and TE to restore the function and structure of damaged tissue and organs.[238] To achieve these challenging goals, three main components (cells, growth factors, and prefabricated scaffolds) are combined to build a construct that can either be cultured *in vitro* to generate 3D tissue models or implanted with or without previous *in vitro* maturation (**Fig. 2.9**). Predominantly, AM techniques like FDM or melt electro writing (MEW)[239,240] have been utilized to generate scaffolds for seeding with cells for TE approaches.[241,242] However, cells are randomly distributed over the whole construct what does not reflect the complexity and the hierarchical layout of native tissue.[243] This might be the reason why for example in the field of orthopedic applications no real breakthrough could be achieved despite many years of extensive research.[244] Although MEW enables the possibility to decrease the fiber diameter to the sub-micron range[245], a direct printing of cells within a matrix remains impossible due to the elevated processing temperatures. Nevertheless,

MEW offers great potential for TE applications and will therefore be discussed in detail (chapter 2.3.1).

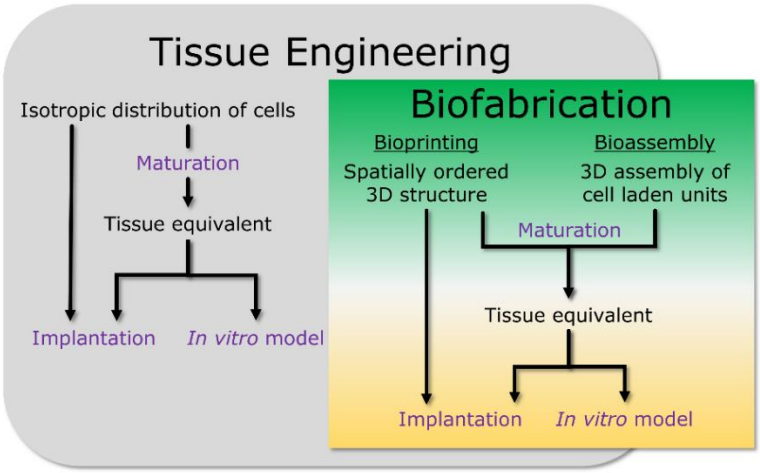

Figure 2.9| Biofabrication as new technology approach for tissue engineering, applying additive manufacturing technologies to directly create functional tissue equivalents that can either be used as implants or *in vitro* models.

One possibility to overcome limitations of TE is to fabricate spatially defined cell-laden constructs which can function as tissue equivalents. Consequently, biomaterials, cells, and bioactive components have to be processed together at cell-compatible conditions to prevent cell death during fabrication. Bearing in mind the opportunities available, AM technologies are regarded as method of choice to accomplish this.[246] The definition of the this relatively young but rapidly growing field termed biofabrication was recently revised by the International Society for Biofabrication.[247] Herein, biofabrication for TE and RM (**Fig. 2.9**) is defined as

"the automated generation of biologically functional products with structural organization from living cells, bioactive molecules, biomaterials, cell aggregates such as micro-tissue, or hybrid cell-material constructs, through Bioprinting or Bioassembly and subsequent tissue maturation process".[247]

The main hypothesis of biofabrication is to provide a more suitable starting situation for an optimized and faster development of printed construct towards biological structures for TE and basic cell biology studies. This also includes the incorporation of vessel-like structures which should ensure a sufficient oxygen and nutrient supply for embedded cells. In general, the bioprinting process places high demands on the printing devices as well as on the

utilized materials, mostly so-called bioinks (*vide infra)*. Temperature, pressure, solvent, and if necessary the cross-linking chemistry have to be precisely controlled to generate a cell-friendly environment. Regarding the used materials, both cytocompatibility as well as mechanical stability and durability of the 3D constructs need to be guaranteed. Accordingly, only a few 3D printing techniques and materials are worth considering. Predominantly, robotic dispensing, inkjet printing, and laser-induced forward transfer (LIFT) are used in the context of biofabrication and will therefore be discussed in the following (Chapter 2.3.2). Current developments in the field of biofabrication have very recently been addressed by several excellent reviews to which the interested reader is referred to.[18,248,249]

2.3.1 Melt Electro Writing

MEW combines the thin fiber diameters accessible via solution electro-spinning[250], that is not considered as AM approach, with the automated and precise control of FDM. This innovate technique (**Fig. 2.10**) enables the deposition of thin polymer fibers (0.8 µm – 30 µm) into 3D constructs with overall heights in the range of millimeters.[251] In contrast to FDM where the filament diameter is largely determined by the nozzle diameter, the polymer jet is electrostatically drawn during MEW, resulting in a considerable reduction of the final fiber diameter. Printing on a movable plane collector or on a rotating and translating mandrel enables the printing of flat scaffolds with square pores or triangular morphology and tubular scaffolds[252,253], respectively. PCL is the most commonly used material for MEW due to its low melting temperature, thermal stability, cytocompatibility, biodegradability, and good printing properties.[254] However, recently, other non-conductive polymers like water soluble PEtOx[240], polypropylene (PP)[255], PLA-PEG-PLA[256], photo-cross-linkable and biodegradable poly(L-lactide-*co*-

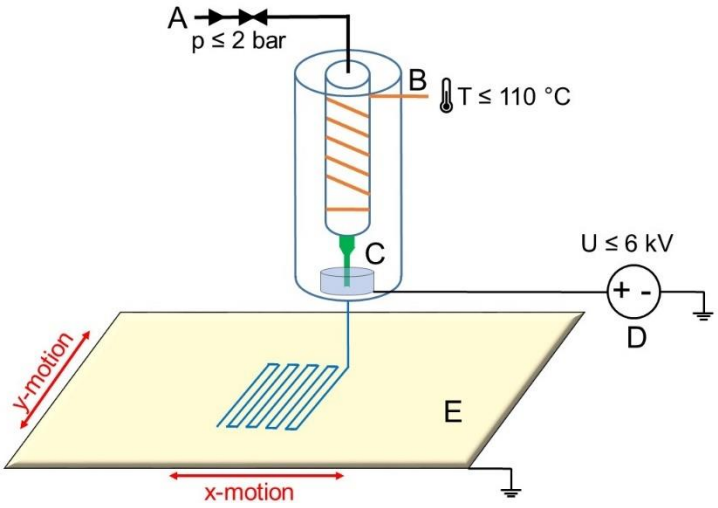

Fig. 2.10| Schematic representation of a MEW device with (A) pneumatically assisted feeding system, (B) electrical heating system, (C) syringe with molten polymer and needle tip with electrode, (D) high voltage source, and (E) computer-aided movable collector plate.

ε-caprolactone-*co*-acryloyl carbonate)[257], or thermoplastic elastomers (TPE)[258] have successfully been processed via MEW. Furthermore, PCL scaffolds fabricated with MEW were used to build up hydrogel composite materials[259] with outstanding mechanical properties, in one case similar to those of native articular cartilage[260]. In several reports it was demonstrated that MEW scaffolds (PCL) are readily penetrated by cells which then produce ECM.[252,261] Recently, Hochleitner *et al.* showed that recreating cellular dimensions by using sub-micron fibers is beneficial for the adhesion of primary human mesenchymal stromal cells (hMSCs).[245] Initial *in vivo* studies of MEW scaffolds which were recently reviewed by Youssef *et al.*, were exclusively performed in rodents and indicate that no chronic inflammation is induced by subcutaneous implantation.[262] However, at this point, it should also be mentioned that Woodward *et al.* reported fibrin deposition on the surface of implanted PCL segments.[263] The unspecific adsorption of proteins of the blood plasma may cause blood clotting and therefore drastically reduce biocompatibility. One possible approach to overcome this drawback is the usage of protective hydrogel coatings as already demonstrated for other polymers like polystyrene (PS).[264]

2.3.2 Bioprinting

The term bioprinting is strongly related to the field of biofabrication and has appeared for the first time in the title of a workshop held at the University of Manchester in 2004. As an effective differentiation between biofabrication and bioprinting is difficult they are often used interchangeably or inconsistently, resulting in the demand to develop new norms to unambiguously define both terms.[265] According to Guillemot *et al.* bioprinting uses AM techniques to assemble living and non-living materials with a prescribed 2D or 3D organization with the aim to generate bioengineered structures.[266] To be considered as appropriate printing technique it must be capable to fabricate complex 3D structures from hydrogels what excludes FDM or selective laser sintering. Two processes which both use light to induce spatially limited polymerization are stereolithography (SLA) and two-photon polymerization. The latter offers the possibility to fabricate arbitrary and precise 3D microstructures with spatial resolutions as small as 100 nm. However, the object size is limited to a few hundred microns.[267] In contrast, the layer-by-layer approach SLA allows the printing of hydrogel constructs with dimensions in the centimeter range but with lower resolution around 80 – 125 µm which is defined by the laser spot size.[242,268] Recently, DeSimone and co-workers developed a new version of the traditional top-down

SLA approach termed continuous liquid interface production (CLIP) which drastically reduces the manufacturing times.[269] By using liquid resins which additionally contain active pharmaceutical ingredients it was possible to fabricate biocompatible and drug-loaded devices which show different controlled release properties depending on the pore size and the resin formulations.[270] These study can be seen as a first step towards biomedical applications of CLIP. However, further studies need to carried out to investigate if cells can be directly included into the resin. Additionally, the number of commercially available photopolymerizable resins to produce biocompatible constructs is still very limited. For all light-induced techniques a special focus needs to be put on the cytotoxicity of the photoinitiator and its decomposition products, as well as on the influence of UV-light. Although UV-curing is generally accepted by many researches and no reports clearly prove a negative effect, it should be used with care and if possible replaced by more cell-friendly alternatives.

For bioprinting of 3D hydrogel constructs under cell-friendly conditions three techniques (LIFT, inkjet printing, and robotic dispensing) can be regarded as well-established at the moment (**Fig. 2.11**) and were therefore recently discussed in several review articles[18,268,271-273]. However, none of these approaches can be considered better

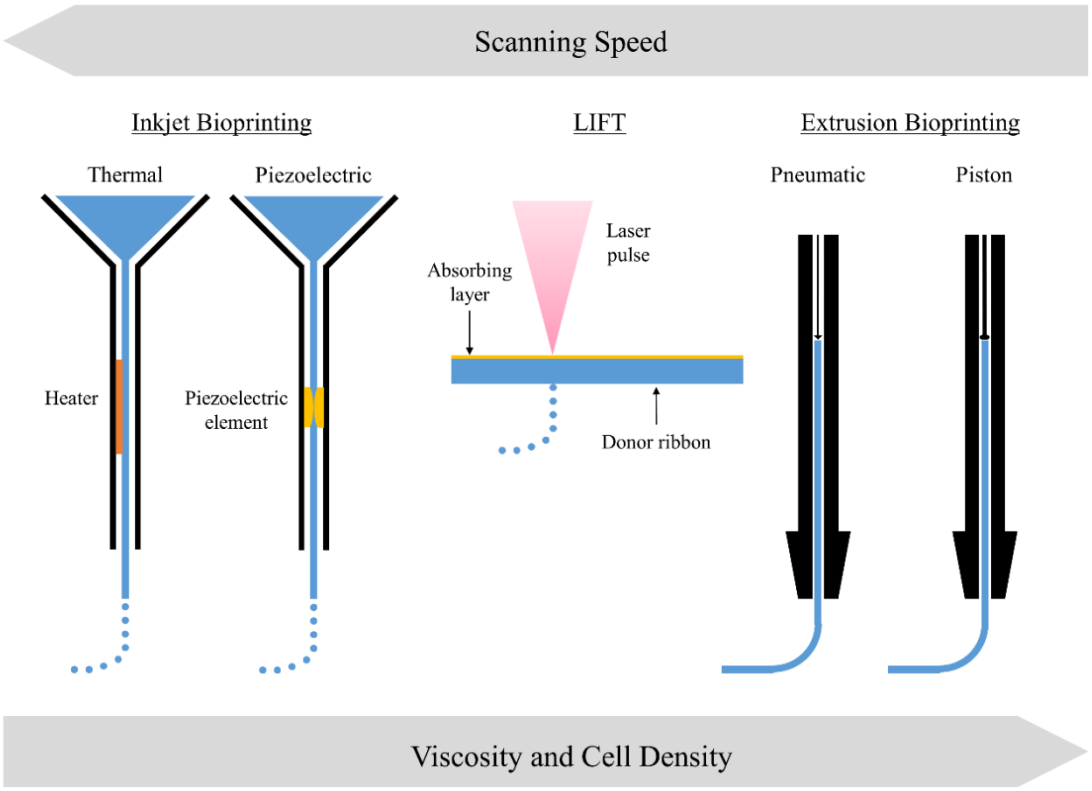

Fig. 2.11| Overview of the selected bioprinting approaches and according parameters crucial for printability of the material.

than the other as all exhibit specific advantages and disadvantages. Generally, the choice of the method depends on the designed construct (size, resolution, and architecture) and on the properties of the material that shall be printed. In the following sub-chapters these techniques will be described in detail and conclusively compared.

2.3.2.1 Laser-Induced Forward Transfer

LIFT also known as laser-assisted bioprinting is a laser direct-writing technique that allows for printing with high spatial resolution from a broad range of materials. Modifications of the initial LIFT technique, namely matrix-assisted pulsed laser evaporation direct writing (MAPLE-DW) and absorbing film-assisted laser-induced forward transfer (AFA-LIFT) are mostly applied for biomedical applications as comprehensively reviewed by Ringeisen *et al.* and Chrisey and co-workers.[274] Still, both systems have the same general setup in common which includes a pulsed laser that is focused and scanned over a donor substarte (ribbon) from which the bioink is propelled forward as a jet, and a CAD/CAM controlled receiving substrate. By controlling the movement of either the donor or the substrate it is possible to write 2D and also 3D constructs from material droplets.[275,276] The main difference can be found in the donor slide which consist of two (MAPLE-DW)[277] or three (AFA-LIFT, biological laser printing)[278,279] different layers. In the latter arrangement additionally to a laser transparent support layer and a layer with the deposition material, an energy conversion layer is added. On the one hand, this layer should protect the cells from the incident laser light which may cause DNA damage and on the other hand, ensure a more reproducible energy conversion which subsequently reduces the spot-to-spot variations. However, evaporation of the additional light-absorption layer may result in contamination of the printed material.[280] Although many studies mention no negative effects on the cell viability using MAPLE-DW[277,281], Xiong *et al.* recently reported the reduction of DNA double-strand breaks by ~50% when using gelatin as energy absorbing layer [282]. The print result is mainly influenced by the laser energy and laser pulse duration which both have to suit the respective material properties (surface tension, viscoelastic properties, etc.). Furthermore, the thickness of the deposition material layer as well as the air gap between the donor substrate and the collector platform need to be taken into account. A finely tuned process provides resolution in the range of 10 – 100 µm and is suitable for bioinks with a viscosity in the range from 1 up to 300 mPa·s and cell densities of ~10^8 cells per mL.[276,278,283]

2.3.2.2 Inkjet Bioprinting

Inkjet printers prevail in offices and private households and are used every day to prepare millions of 2D graphical printouts. For this, small droplets of ink are delivered on predefined locations of a paper sheet. Early attempts to employ inkjet printers for bioprinting used modified versions of commercially available printers originally produced for desktop applications.[284] Cartridges were thoroughly cleaned and refilled with a suitable bioink for instance on basis of sodium alginate which was then printed into $CaCl_2$ solution. In general, a distinction is made between continuous inkjet and drop-on-demand (DOD) bioprinting. The latter is preferred over the first-mentioned in the context of bioprinting as the generation of single droplets is more economical, and more suitable to pattern biologics.[285] The working principle of DOD printing is based on an actuator generating triggered pulses, leading to the dropwise ejection of material from the reservoir if the surface tension at the nozzle orifice is overcome. Xu *et al.* reported a decrease of surface tension with increasing cell concentration as more cells are adsorbed to the liquid-gas interface. Thus, the droplet size and velocity decrease.[286] Generally, the pressure pulses can be introduced either through means of a piezoelectric or a thermal actuator.[287,288] In thermal inkjet printers, pulses of pressure are generated by an electrical heater that is used to evaporate its surrounding bioink. Although, the temperature can reach about 300 °C, this does not affected cell viability or proliferation capacity as demonstrated by several groups.[289,290] It is believed that the short period of exposure of around 2 µs only leads to a negligible temperature increase of the bulk material. However, Saunders *et al.* rightly stress the need for further research on the influence of heat during bioprinting to establish thermal inkjet printing.[288] This might be the reason why piezoelectric DOD inkjet systems are primarily used by researches for biomedical applications. Here, the distortion of a piezoelectric crystal, which is induced by an applied voltage, produces acoustic waves leading to triggered ejection of material.[291,292] Based on the frequencies (15-25 kHz) used by piezoelectric inkjet bioprinters some concerns are raised as these have the potential to induce damage of the cell membrane and lysis.[293]

Although inkjet bioprinters are compatible with many biological materials and are successfully applied with a micrometer resolution (10 – 50 µm)[288,290,294] for the deposition of cells, it is difficult to achieve biologically relevant cell densities. Low cell concentrations ($<10^6$ cells/mL)[290] and low bioink viscosities (<12 mPa·s)[295] have to be used to avoid nozzle clogging, to reduce shear stress[292], and to facilitate droplet formation. Despite the

mentioned drawbacks, inkjet bioprinting offers great potential due to its simplicity, availability, high fabrication speed, and versatility with great control on the deposition pattern.

2.3.2.3 Extrusion Bioprinting

Perhaps the most common but still comparatively new method for the field of biofabrication is extrusion bioprinting, also termed microextrusion bioprinting or robotic dispensing.[19,111,296,297] Especially the possibility to rapidly fabricate 3D structures with sizes and dimensions which are relevant for biomedical applications, lead to the fast establishment of this technique. In contrast to LIFT and inkjet bioprinting, 3D constructs are mainly build up in a layer-by-layer fashion from continuously extruded filaments with diameters of approximately 150 – 400 µm.[41,298,299] The bioink is generally loaded into a reservoir and dispensed – either pneumatically or mechanically – through an easily replaceable nozzle on the movable build plate. Mechanically driven extrusion bioprinting is mainly piston- or screw-based. Especially for bioinks exhibiting a higher viscosity, screw-based deposition is favorable.[272,273] By rotation of the screw the bioink is transported to the nozzle, thus the material feed can be controlled by the rotation speed and additionally by the design of the screw comparable to industrially used screw extruders. However, due to the high shear stress generated during printing, screw-driven systems are the least applied approach in biofabrication. Piston-based systems provide the highest control over the flow of the bioink as the linear displacement of a plunger directly causes material ejection. However, the process is limited by the stability of the piston and the tightness of barrel. In the most frequent pneumatically driven setup, the valve triggering material ejection is located between the inlet of the pressurized gas and the bioink. Being able to accurately adjust the pressure over a broad range, enables the possibility to print a huge variety of bioinks exhibiting different viscosities ($30 – 6 \times 10^7$ mPa·s)[249] what makes this approach the most versatile among the introduced setups. This significant advantage is at the same time however a huge disadvantage as the sterile gas used for dispensing is compressible, what will cause a delay between the actual start/stop of dispensing and the start/stop of material flow.

All of the mentioned extrusion bioprinting systems have in common that the bioink is dispensed through a nozzle which determines the resolution of the process (100 µm – mm range)[19,26,300] and bears the potential risk of clogging inside the nozzle tip[297]. Nevertheless, it is possible to print with very high cell densities and even cell spheroids.[301]

During the printing process special attention must be paid to the deposition of the first layer as this interacts with the substrate. Insufficient wetting will result in huge damage of the construct or will even impede the whole printing process.

Recently, several groups replaced the build plate with a reservoir, containing a self-healing hydrogel in which a bioink can be printed.[110,302] Hinton *et al.* used a thermoresponsive support gel containing Ca^{2+} ions which act as cross-linker for the printed alginate.[303] After solidification of the printed material, the support gel can easily be removed by changing the temperature accordingly. Generally, this approach is termed gel-in-gel bioprinting and allows for the usage of mechanically weaker materials. Additionally, the printing of multiple materials and different cell types is possible and enables the fabrication of more complex structures.

2.3.2.4 Advantages and Disadvantages

After having introduced the three most important bioprinting techniques the main advantages and disadvantages with regard to the processing of physically cross-linked and shear-thinning hydrogels will be highlighted. A comparison of the fundamental differences of the printing methods reveals the broad range which can be addressed by thoughtful combination of bioink and suitable printing method (**Table 2.2**). From a structural and material point of view, extrusion bioprinting is the most versatile process. It enables printing of constructs from a wide range of material viscosities as the force leading to material extrusion can be precisely controlled. Although high cell densities are achievable, the influence of the shear stress during printing on cell viability must be taken into account. Furthermore, nozzle diameters can be simply adjusted by interchanging the utilized needle. In contrast to the other two processes, a continuous filament is extruded instead of single drops, significantly increasing the structural integrity of the printed object. However, regarding the resolution which is one of the most important aspects for many applications, extrusion bioprinting cannot keep up with modified LIFT processes and inkjet bioprinting. Especially when new materials are developed, only small quantities are synthesized on the laboratory scale. Therefore, the material requirement and throughput are crucial. With only several hundred nanoliters, LIFT-based processes require the least material what consequently limits the size of printable constructs significantly. Almost no size limitations are present for extrusion-based bioprinters, enabling the fabrication of constructs on the millimeter scale in an acceptable time. However, depending on the nozzle diameter the material consumption can account to milliliters per minute.

Tab. 2.2: Comparison of selected bioprinter systems.

	Modified LIFT	Inkjet Bioprinting	Extrusion Bioprinting
Working principle	Noncontact	Noncontact	Contact
Load volume	>500 nL	mL range	mL range
Bioink viscosity	1 – 300 mPa·s	3.5 – 12 mPa·s	30 – 6 x 10^7 mPa·s
Nozzle size	Nozzle free	20 – 150 µm	20 µm to mm range
Resolution	10 – 100 µm	10 – 50 µm	100 µm to mm range
Fabrication speed	Medium (200 – 1600 mm·s^{-1})	Fast (1 – 100000 droplets/s)	Slow (700 mm·s^{-1} – 10 µm·s^{-1}
Cell density	Medium, 10^8 cells/mL	Low, $<10^6$ cells/mL	High, cell spheroids
Commercially available	No	Yes	Yes
Costs for printer	High	Low	Low

Another key aspect is the production time including the preparation of the printer as well as the fabrication of the construct. For inkjet bioprinting and extrusion bioprinting, the preparation times are comparable low as it primarily consist of filling a reservoir. However, the ink preparation that can take several days is not taken into account here. In contrast, modified LIFT techniques require the preparation of a thin film that needs to be applied to the ribbon. As one ribbon only contains about several hundred nanoliters of material a new ribbon must be prepared when the material is used what leads to increasing preparation times.

Although commercially available systems that are specialized in material dispensing for biomedical applications are slightly more expensive than modified desktop inkjet printers or low-cost open source extrusion printer, they significantly contributed to the recent expansion of the field of biofabrication. Researchers, especially from academic disciplines with no engineering or physical background, have now the possibility to develop new bioink candidates and directly investigate their printability on user-friendly bench-top bioprinters. This might hopefully further accelerate the research as suitable bioinks are urgently needed.

2.3.3 Bioink – Requirements and Challenges

A hydrogel, already defined in chapter 2.1, has to fulfill several requirements to be considered as bioink. In general, it should meet the mechanical demands of the selected bioprinting process and at the same time ensure cell survival during printing.[304] Murphy and Atala identified five main categories to evaluate the suitability of hydrogels as bioink[249]:

- Printability

  Mainly influenced by rheological properties like viscosity, shear thinning behavior, and yield stress.

- Biocompatibility

  After implantation the bioink should not induce undesirable local or systemic responses from the host. Ideally, it should contribute controllably and actively to the biological and functional components of the construct. In this context, cytocompatibility of a bioink should always investigated in preparatory work as it is a crucial aspect.

- Degradation kinetics and byproducts

  As embedded cells secrete proteases and subsequently produce their own ECM, the bioink should degrade with comparable rate; of course it must be ensured that all byproducts are nontoxic, readily metabolized and rapidly cleared from the body.

- Structural and mechanical properties

  Depending on the required mechanical properties of the intended application stiffness, strength, and swelling properties need to be controlled.

- Material biomimicry

  Knowledge of tissue-specific endogenous material composition should be used to engineer desired functional and structural material properties.

From a rheological perspective, printing using nozzle-based systems can be regarded as material flow through a contraction followed by tube flow.[18] After ejection and deposition of the bioink onto the collector, the material must solidify rapidly to preserve the shape of the printed construct. An ideal ink shows physical gel formation before printing, prevents sedimentation of cells in the barrel and exhibits shear thinning (also known as pseudo-plasticity). This refers to the non-Newtonian behavior in which the

viscosity decreases as shear rate increases.[305] The applied shear stress induces reorganization of the polymer chains to a stretched conformation or disrupts aggregates, resulting in a lower viscosity. In this context, it is important to distinguish between shear thinning and thixotropic materials as there is a very distinct difference. Shear thinning is time-independent, whereas thixotropy is not. The latter behavior is unfavorable for the printing process and the shape fidelity and should therefore be excluded during ink development. After exiting the nozzle, a more or less pronounced increase of the jet diameter can be observed for elastic materials like polymer solutions.[306] This is known as Barus effect or extrudate swell. Especially, if utilizing extrusion bioprinting and striving for high resolutions, the ink should exhibit no or only little pronounced extrudate swell. Another aspect which is crucial for shape fidelity at high resolution of the printed construct is a rapid regelation. Therefore, the recovery rate to the initial viscosity or G' values must be investigated. The method of choice to assess printability is rheological analysis[307], which is still often underestimated in terms of hydrogel design for biomedical applications[308]. From the beginning of the development of potential bioink candidates, a minimum of rheological investigations should be taken into considerations. These include, determination of the shear-thinning region, yield stress, linear-viscoelastic (LVE-)range, and recovery after printing. The latter can be identified by alternating the shear rate. However, interlaboratory comparability is a major problem as characterization methods are multifarious and sensitive even to small parameter variations.

Although physical gels are ideal for printing, their comparatively poor mechanical properties as well as dissolution in aqueous environment[109] significantly impede handling and impair the overall performance. Furthermore, cell culture is typically limited as media exchange is only possible to a limited extent. Therefore, increasing attention is given to polymers that allow chemical cross-linking after printing to further stabilize the construct. Importantly, the selected method should be feasible under mild/physiological conditions to avoid damage of the living cells or bioactive proteins. Additionally, the formation of non-cytocompatible by-products has to be avoided as well as the usage of unsuitable chemicals. Well-established post-processing reactions are radical polymerizations[309] triggered by temperature or radiation[27,310], redox reactions, as well as reactions of complementary chemical groups (e.g., click chemistry[299,311], Michael addition[312], or enzymatic reactions[313]). Moreover, chemically cross-linking via peptide sequences which are substrates for matrix-remodeling enzymes – matrix metalloproteases – has been utilize to

generate hydrogels.[314] This allows the combination of tailored specific biodegradability with chemical cross-linking.

All hydrogels, briefly introduced in chapter 2.1, are at the moment discussed and investigated as potential bioink. It is currently impossible to estimate if one polymer, either naturally derived or synthetic, will prevail over the others or if a selection consisting of several polymers, each specialized in one specific application, will emerge. In any event, collaborative research at national and international levels will accelerate research in the field of biofabrication and particularly on bioinks as these are the fundament for further applications. Furthermore, basic research has to be conducted to better understand the influence of the printing process not only on cell viability but also on the proliferation and long term stability. Only if these fundamental issues can be answered, the envisioned long-term goals of biofabrication can be achieved.

3 Motivation

AM, more commonly referred to as 3D printing is currently extremely fashionable, and many people expect the next industrial revolution and discuss the potential of decentralized production. Already at an early stage, scientist and also the U.S. Defense Advanced Research Projects Agency[315] realized the huge potential of the combination of AM and biology resulting in the term biofabrication. Especially in the context of TE and RM biofabrication is very promising and rapidly growing field that creates hope and speculations about the possibility to be able print functional tissue that might serve as alternative to urgently needed donor organs in the near future.[316]

Despite many promising approaches and initial results, biofabrication faces some major issues which might slow down the development. As an example, the response of cells, in particular of human primary cells, during and after the printing process is only poorly understood. However, the major limitation at the moment is the shortage of suitable and versatile bioinks. These cytocompatible and printable materials must be regarded as key element as they are the basis of the whole process. Both naturally derived as well as synthetic polymers have to meet numerous of requirements to be considered as potential bioink candidate. From a chemical point of view, account should be taken, *inter alia*, to the synthetic variability, scalability of the synthesis, and controllability of the product. Furthermore, the monomers should be readily available in consistent quality as this is the first step in a production chain and therefore affects the final result (**Fig. 3.1**). Obviously, very low cytotoxicity up to high concentration is a mandatory biological requirement. But also the interaction with proteins as well as biodegradability and excretion from the body have to be considered. From a materials science point of view, the important factors are, gelation behavior, printability, along with shape fidelity, and structure recovery. For the adequate analysis new tools have to be developed or adapted accordingly to fit the needs of bioink development. To combine all requirements in only one polymer or to accordingly modify

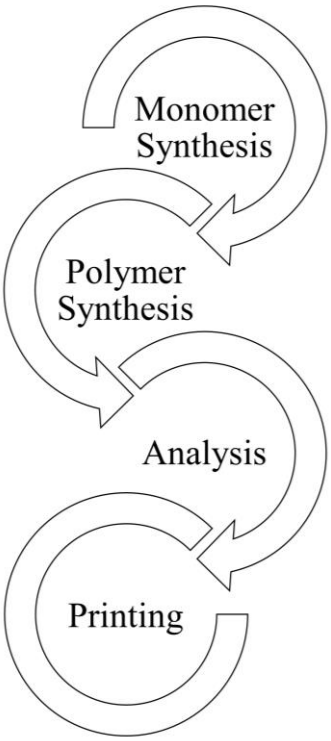

Fig. 3.1| Schematic representation of the production chain of a 3D printable polymer based hydrogel.

one material is a huge challenge for those engaged in research in the field of biofabrication and polymer chemistry.

In the context of this dissertation, a novel polymeric bioink platform was developed. Therefore, a polymer class that has seen a very significant increase in recent years, the poly(2-oxazoline)s as well as their almost forgotten higher homologues the poly(2-oxazine)s are investigated with regard to their suitability to be used as bioink.

As only little is known about the copolymerization capabilities of POx and POzi as well as about the properties of the resulting copolymers, the first part of the present work deals with the synthesis of block and random copolymers consisting of POx and POzi with varying alkyl side chain. Subsequently, thermal properties of the copolymers in bulk are analyzed. As a combination of PMeOx and P*n*PrOzi coincidentally reveals thermogelling properties while investigating the thermoresponsive viscosity of aqueous solutions of several copolymers, this exceptional diblock copolymer comes into focus. The major part of the present thesis deals with the thorough investigation of the formed hydrogels and their adjustability. Initially, the rheological properties are investigated to assess the printability in general. In this context, the influence of several parameters, such as the end groups or the used solvent is analyzed. In order to elucidate the microstructure of the formed gel SANS as well as DLS and static light scattering (SLS) are applied. Before finally 3D printing the developed bioink with and without living cells, the sterilizability and cytocompatibility of the polymer is investigated.

4 Results and Discussion

4.1 Synthesis of Amphiphilic and Thermoresponsive Poly(2-oxazoline)-*block*- Poly(2-oxazine) Copolymers

4.1.1 Up-scaling the Synthesis of 2-Oxazines and 2-Oxazolines

In preparation for up-scaling the polymer synthesis to several kilograms it was necessary to initially establish the synthesis of monomers in an adequate quantity while maintaining a high purity. Both, MeOx and 2-*n*-propyl-2-oxazine (*n*PrOzi) have been synthesized via the metal salt catalyzed reaction of nitriles with alkanolamines initially described by Witte and Seeliger.[148]

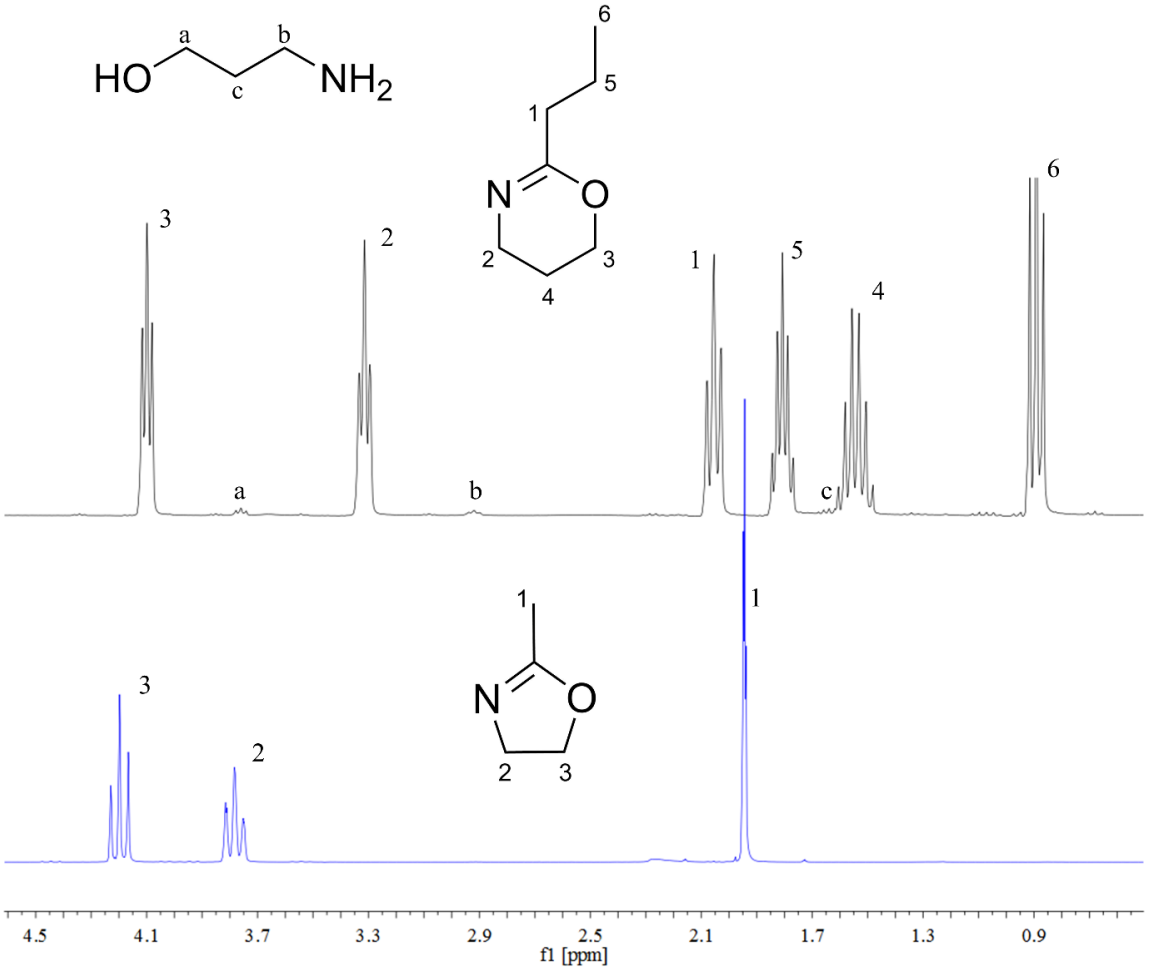

Fig. 4.1| ^{1}H NMR spectrum of 2-*n*-propyl-2-oxazine (top spectrum) with traces of propanolamine after distillation from the reactor and 2-methyl-2-oxazoline without traces of ethanolamine after direct distillation from the reactor.

Initially, *n*PrOzi was synthesized by an adapted standard procedure developed for smaller batch sizes with 1.2 eq of 3-aminopropanol.[151] After a first distillation step 3-aminopropanol was detectable in all fractions via ^{1}H NMR spectroscopy, whereby the

least amount could be found in the third fraction (**Fig. 4.1, top spectrum**). Nonetheless, further purification is inevitable as 3-aminopropanol is a nucleophile and therefore would interfere with the LCROP by causing uncontrolled early termination of propagating species. After repeated distillation and drying over CaH_2 the product could be obtained with a yield of 52% (**Tab. 4.1**). In order to ensure consumption of the respective alkanolamine to be as completely as possible during the reaction and to minimize the necessary purification steps 1.2 eq of acetonitrile (ACN) and 1 eq of ethanolamine were utilized for the synthesis of MeOx. No traces of ethanolamine (**Fig. 4.1, bottom spectrum**) could be detected in the fifth fraction of the first distillation directly from the reactor. The other fractions were partially combined and distillated for a second or third time adding up to total yield of 57% for MeOx (**Tab. 4.1**). The yield difference of 5% cannot be regarded as a significant improvement as the synthesis of the respective monomer was only carried out once. Still it might be an interesting approach to reduce the number of purification steps. For both reaction, the yields are comparable to smaller batch sizes, usually used on a laboratory scale (**Tab. 4.1**). At the beginning of the present work, small batches of MeOx have only been purified and not synthesized as it is commercially available. Thus, no direct comparison could be drawn with a small batch of MeOx.

Table 4.1| Yields and boiling points (bp) of the synthesized monomers either on laboratory scale or in a 5 L reactor.

Scale	Monomer	Abbreviation	Yield [%]	bp [°C]
5 L reactor	2-methyl-2-oxazoline	MeOx	57	65 (185 mbar)
	2-*n*-propyl-2-oxazine	*n*PrOzi	52	56 (12 mbar)
<1 L flask	2-methyl-2-oxazine	MeOzi	50	85 (200 mbar)
	2-ethyl-2-oxazine	EtOzi	65	84 (102 mbar)
	2-*n*-propyl-2-oxazine[1]	*n*PrOzi	42	40 (10 mbar)
	2-*iso*-propyl-2-oxazine[2]	*i*PrOzi	56	48 (15 mbar)
	2-*n*-butyl-2-oxazine[1]	*n*BuOzi	48	70 (10 mbar)

[1] kindly provided by Christian May; [2] kindly provided by Michael Lübtow

It is important to note, that an increasing demand of monomers makes the in-house synthesis economical. However, due to the larger volume of several liters, distillation is more time consuming at the moment as it is carried out with standard glass ware designed for laboratory scale, which needs to be considered when aiming for up-scaling of the

monomer synthesis. Ideally, distillation columns are directly connected to the 5 L reactor allowing for more efficient processing.

4.1.2 Synthesis of Di- and Triblock Copolymers

As outlined previously, the aim of the present work was to investigate the properties of thermoresponsive copolymers consisting solely of the poly(cyclic imino ether)s POx and POzi. Although the copolymerization of 2-oxazolines and 2-oxazines should be easy to implement as both are readily accessible via LCROP[135,152], only one single report by Kobayashi *et al.* dealing with surfactants can be found throughout the literature[165]. This is even more surprising as such copolymers can open up new material properties like thermogelation which were unachievable with pure POx based systems[190] until today.

Therefore, a small library of amphiphilic and thermoresponsive di- and triblock copolymers with varying compositions (DP = 50 – 200) comprising one or two oxazoline block(s) and one oxazine block have been synthesized by LCROP. In most cases methyl triflate (MeOTf) was used as initiator and ethyl-4-piperidinecarboxylate (EPC) as terminating agent (**Scheme 4.1**). Additionally, pure oxazoline based block copolymers as well as pure oxazine based block copolymers were synthesized to conduct control experiments. As higher temperatures are necessary for the LCROP of 2-oxazines, benzonitrile (PhCN) was chosen as solvent due to its higher boiling point compared to the

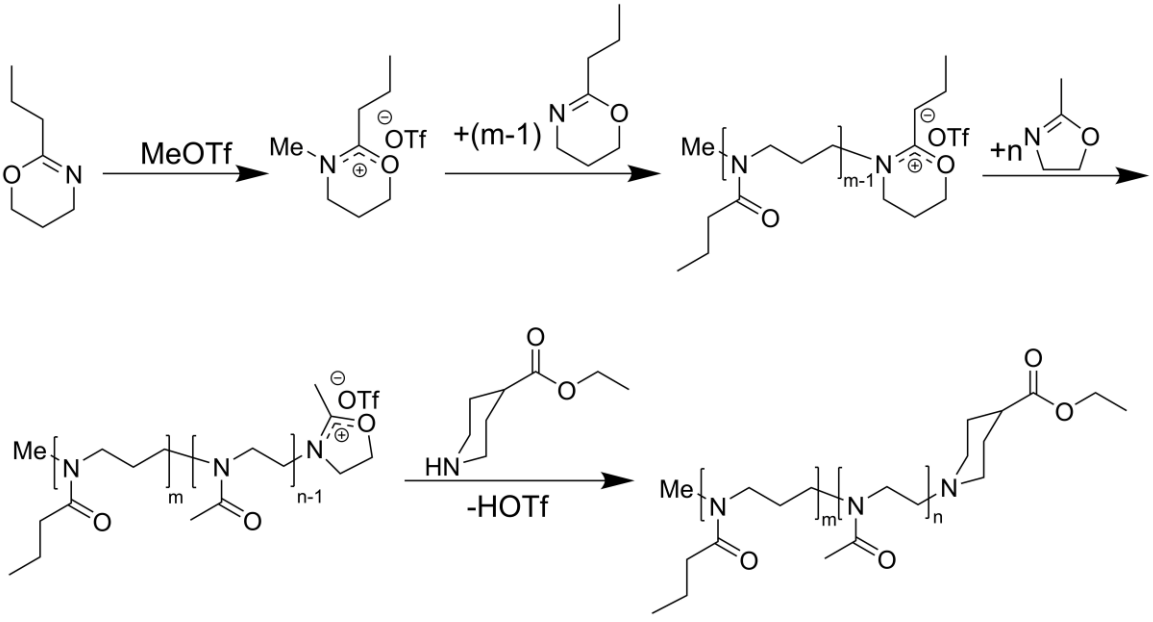

Scheme 4.1| Schematic presentation of one-pot two-stage copolymerization, exemplarily shown for 2-*n*-propyl-oxazine and 2-methyl-2-oxazoline monomers. Methyl triflate was used as initiator and ethyl-4-piperidinecarboxylate as terminating agent.

most commonly used solvent ACN. The monomer concentration was adjusted to 3 M, what has been reported to be in the optimal range for high molecular weight polymers.[173] In total, twenty different diblock copolymers (D1 – D20), one triblock copolymer (T1), and one random copolymer (R1) have been synthesized (**Tab. 4.2**). The theoretical polymer composition could be achieved for most of the synthesized block copolymers with a deviation of 10%, as determined by proton nuclear magnetic resonance (^{1}H NMR) spectroscopy.

In order to determine the polymer compositions and to evaluate the copolymerization suitability of 2-oxazolines and 2-oxazines, ^{1}H NMR spectroscopy and GPC have been utilized. It is important to note that the molar mass obtained by GPC is no absolute value, but is based on calibration with PEG standards and thus may deviate from the mass calculated by end group analysis from ^{1}H NMR spectroscopy. This difference becomes even larger when using HFIP instead of DMF as eluent (**Tab. 4.2**). Of course, ^{1}H NMR does also not directly give absolute values like for example matrix-assisted laser desorption/ionization time-of-flight mass spectrometry (MALDI-TOF MS) but allows for the calibration of the integrals to the signal of the initiator fragment (peaks h in **Fig. 4.2 A**). However, taking into account the low intensity already at a DP of 100, it is obvious that this calibration strongly depends on the quality and processing of the spectrum as well as the set limits of the integral and can easily lead to misinterpretations. The signal of the ester protection group (quartet i in **Fig. 4.2 A**) can also be considered as reference but should be treated cautiously, as the terminating agent was used in excess and traces not covalently attached to the polymer would distort the result. There is, however, another smaller problem visible in the spectrum. One signal of the POzi backbone (peak b in **Fig. 4.2 A**) overlaps with the methanol signals making a precise integration impossible. Although this issue might be resolved by using $CDCl_3$, MeOD was still used as NMR solvent as it is an unselective solvent which readily dissolve both blocks and appeared more suitable for the investigated diblock copolymers. Generally, the broad shape of the POx/POzi backbone is explained by cis/trans isomerism of the tertiary amide moiety.

Table 4.2| Polymer composition (PC), molar masses [kg/mol], and dispersities of synthesized di- and triblock copolymers and a statistical copolymer obtained via ^{1}H NMR and GPC with DMF or HFIP (*) as eluent.

ID	PC, theo.	PC, exp[a]	M_n[a]	M_n[b]	M_w[b]	Đ[b]
D1	Me-P*n*PrOzi$_{25}$-*b*-PMeOx$_{25}$-EPC	22/21	4.8	3.9	4.6	1.18
D2.1	Me-P*n*PrOzi$_{52}$-*b*-PMeOx$_{52}$-EPC	50/49	10.7	10.0	14.9	1.49
D3	Me-P*n*PrOzi$_{24}$-*b*-PMeOx$_{74}$-EPC	27/72	9.7	5.6	7.1	1.28
D4	Me-P*n*PrOzi$_{74}$-*b*-PMeOx$_{25}$-EPC	106/31	16.3	8.3	10.7	1.30
D5	Me-PMeOx$_{60}$-*b*-P*n*PrOzi$_{60}$-EPC	59/61	13.0	6.2*	7.5*	1.20*
D6	Me-PMeOx$_{80}$-*b*-P*n*PrOzi$_{80}$-EPC	85/85	18.2	7.9*	9.6*	1.22*
D7.1	Me-P*n*PrOzi$_{97}$-*b*-PMeOx$_{75}$-EPC	107/79	20.5	9.9	12.2	1.24
D8	Me-P*n*PrOzi$_{105}$-*b*-PMeOx$_{102}$-BOC	102/99	21.6	8.1*	11.5*	1.42*
D9	Propargyl-PMeOx$_{100}$-*b*-P*n*PrOzi$_{100}$-EPC	98/101	21.4	12.3	19.2	1.56
D10	Propargyl-PMeOx$_{100}$-*b*-P*n*PrOzi$_{100}$-MCP[c]	101/103	21.9	14.7	21.2	1.44
D11	Propargyl-PMeOx$_{100}$-*b*-P*n*PrOzi$_{100}$-OH	92/96	20.1	15.9	20.8	1.31
D12	Me-P*n*PrOzi$_{50}$-*b*-PEtOx$_{50}$-EPC	54/52	12.2	7.6	8.9	1.18
D13	Me-P*n*PrOx$_{52}$-*b*-PMeOzi$_{52}$-EPC	67/46	12.3	4.6	5.5	1.21
D14	Me-P*n*PrOx$_{49}$-*b*-PMeOx$_{49}$-EPC	48/48	9.7	5.4	6.6	1.22
D15	Me-PMeOzi$_{47}$-*b*-P*n*PrOzi$_{50}$-EPC	50/57	12.4	2.7*	4.9*	1.82*
D16	Me-P*n*BuOzi$_{38}$-*b*-PMeOx$_{38}$-EPC	39/40	9.1	6.2	7.2	1.15
D17	Me-P*i*PrOzi$_{100}$-*b*-PMeOx$_{100}$-EPC	103/100	21.8	6.3*	8.9*	1.43*
D18	Me-PMeOx$_{50}$-*b*-P[*n*PrOzi$_{45}$-*co*-*n*BuOzi$_{5}$]-EPC	57/51/5	12.2	6.5	7.3	1.12
D19	Me-PMeOx$_{99}$-*b*-P[*n*PrOzi$_{88}$-*co*-*n*BuOzi$_{10}$]-EPC	96/87/11	21.0	8.6*	10.5*	1.22*
D20	Me-PMeOx$_{101}$-*b*-P[*n*PrOzi$_{76}$-*co*-*n*BuOzi$_{25}$]-EPC	109/82/28	23.8	10.4*	13.2*	1.27*
T1	Me-PMeOx$_{24}$-*b*-P*n*PrOzi$_{49}$-*b*-PMeOx$_{24}$-EPC	25/50/24	10.7	6.8	7.8	1.15
R1	Me-P(*n*PrOzi$_{50}$-*co*-MeOx$_{50}$)-EPC	58/60	12.7	6.2	8.1	1.31

[a]Determined by end-group analysis (^{1}H NMR spectroscopy in MeOD-d_4 (300 MHz, 298 K)). [b]Determined from GPC in DMF with LiBr (1 g/L) or HFIP (*) with KTFA (3 g/L) at 313 K.[c]mercaptopropionate.

The dispersity Đ (M_w/M_n) obtained by GPC analysis is a measure of the distribution of molar mass of a polymer and therefore directly reflects the control over the polymerization. Consequently, Đ constitutes the easiest approach to evaluate the copolymerization capabilities of 2-oxazolines and 2-oxazines. The elugrams of selected di- and triblock copolymers (**Fig. 4.2 B**) appear essentially monomodal with only minor tailing to lower molar masses and reveal low to moderate dispersities (**Tab. 4.2 & 4.3, Đ < 1.3**). The absence of a second molar mass distribution in all elugrams indicates virtually

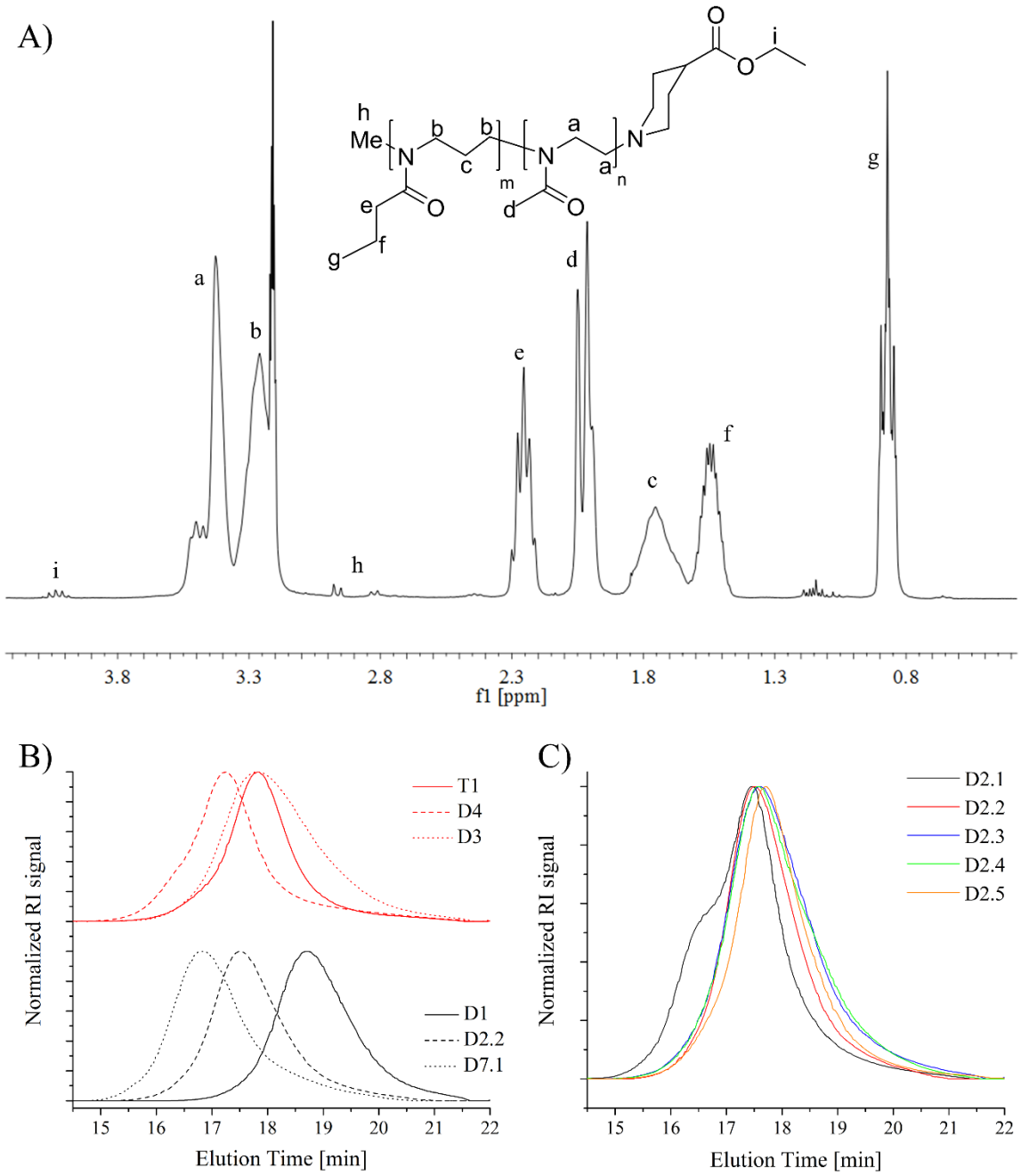

Fig. 4.2| A) ^{1}H NMR spectrum (300 MHz, 298 K) of Me-PMeOx$_{50}$-*b*-P*n*PrOzi$_{50}$-EPC in MeOD-d_4. B) Normalized GPC traces of di- and triblock copolymers with varying block length. For better visibility traces of T1, D4, and D3 were shifted by adding 1 to the calculated values. C) Normalized GPC traces of diblock copolymers D2.1 – D2.5.

quantitative initiation of the second or third block, respectively. It can therefore be assumed that a living chain end of POzi can function as macroinitiator for 2-oxazoline monomers. Doubling the chain length of each block (~25 (D1) → ~50 (D2.2) → ~100 (D7.1)) results in a clear shift of the peak to shorter elution times reflecting the increasing hydrodynamic volume what accompanies with higher molecular weight.

Table 4.3| Polymer composition (PC), molar masses [kg/mol], and dispersities of repeatedly synthesized di- and triblock copolymers obtained via ^{1}H NMR and GPC with DMF or HFIP (*) as eluent.

ID	PC, theo.	PC, exp[a]	M_n[a]	M_n[b]	M_w[b]	Đ[b]
D2.2	Me-P*n*PrOzi$_{50}$-*b*-PMeOx$_{50}$-EPC	57/55	12.1	7.3	8.5	1.17
D2.3	Me-P*n*PrOzi$_{50}$-*b*-PMeOx$_{50}$-EPC	51/51	10.9	6.3	8.1	1.29
D2.4	Me-P*n*PrOzi$_{50}$-*b*-PMeOx$_{58}$-EPC	55/50	11.4	6.4	8.2	1.28
D2.5	Me-P*n*PrOzi$_{50}$-*b*-PMeOx$_{50}$-EPC	45/44	9.6	6.5	8.0	1.22
D2.6	Me-PMeOx$_{50}$-*b*-P*n*PrOzi$_{51}$-EPC	51/53	11.3	5.4*	6.4*	1.19*
D7.2	Me-P*n*PrOzi$_{99}$-*b*-PMeOx$_{100}$-EPC	104/105	22.3	10.1 7.2*	13.4 9.4*	1.34 1.30*

[a]Determined by end-group analysis (^{1}H NMR spectroscopy in MeOD-d_4 (300 MHz, 298 K)). [b]Determined from GPC in DMF with LiBr (1 g/L) or HFIP (*) with KTFA (3 g/L) at 313 K.

During the course of this study, additionally, several batches of selected diblock copolymers (D2 and D7) were synthesized to investigate batch-to-batch variations and the resulting consequences on material properties, which is a crucial but frequently neglected aspect in the context of biomaterials research.[317] Furthermore, the batch size was increased up to 100 g for D7.2, which revealed no influence on the polymer quality. Comparing the elugrams obtained by GPC for five different batches of D2 (DP_{theo} = 50 for each block) revealed that D2.1 exhibits a significant shoulder at higher molar masses, and, accordingly, the highest dispersity (Đ = 1.49) (**Fig. 4.2 C, Tab. 4.3**). Furthermore, a more pronounced low molecular tailing was observed for D2.3 and D2.4, what will be discussed in more detail in context with the material properties (see chapter 4.3.1). Although there is a visible difference between the individual elugrams, in general the synthesis of diblock copolymers comprising ~50 units of P*n*PrOzi and ~50 units of PMeOx can be regard as reproducible, according to the GPC traces. Furthermore, exchanging the two blocks (D2.6) does not influence the dispersity of the resulting polymers (**Tab. 4.3**). This was surprising as there was reasonable evidence to assume that the living chain end of P*n*PrOzi would cause a slower initiation, consequently resulting in higher dispersities. However, to be able to draw a reliable conclusion, a detailed kinetic study should be conducted to investigate the initiation capabilities of the living POzi chain end for 2-oxazolines and *vice versa*. Unfortunately, a direct comparison of the GPC traces is not conclusive as D2.6 could only be measured in HFIP due to rearrangement of the analytical setup.

Slight variations between individual batches (D2.1 – D2.6) are inevitable as the polymerization is a statistical process that can only be controlled to a certain extent. At the moment the influence of dispersity on material properties is controversially discussed but initial results revealed a remarkable effect between discrete and disperse amphiphilic ABC-oligomers in bulk as well as in solution.[318] Unfortunately, the synthesis of discrete POx or POzi is not possible at the moment. However, polypeptoids[319], which are structural analogs to POx and are also considered as pseudo-polypeptides, are perfectly suitable to investigate the influence of dispersity. They can either be polymerized in solution[320] (disperse) or from solid supports (disperse)[321], or synthesized by solid phase submonomer synthesis (discrete)[322]. Especially when discussing structure-property relationships it is important to keep in mind that all polymers synthesized for this study exhibit a molar mass distribution which always entails a structural range instead of a single molecule.

4.1.3 Temperature Dependent Water Solubility of PMeOx-*block*-P*n*PrOzi Copolymers

As already outlined in chapter 2.2.3.1, POx as well POzi are well known for their thermoresponsive solubility behavior. Most of the homopolymers exhibit a T_{CP} above which the polymer precipitates in water. Of course this phenomena and its tunability was already investigated for a series of block copolymers. However, no reports on the water solubility of POx-*b*-POzi copolymers could be found in the literature. As the main focus of the present work is on diblock copolymers comprising PMeOx as hydrophilic and P*n*PrOzi as thermoresponsive block the temperature dependent water solubility of D2.2 and D7.2 was investigated at different concentrations and temperatures.

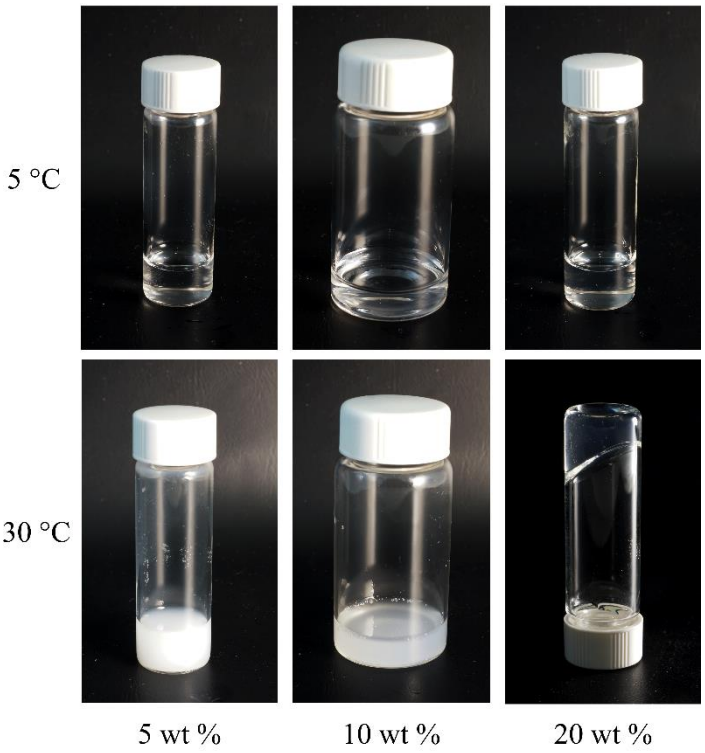

Fig. 4.3| Photographs of solutions of D7.2 at different concentrations and temperatures in MilliQ water.

Below the T_{CP} of P*n*PrOzi as homopolymer (approximately 13 °C)[152] transparent solutions were observed at all concentrations for D2.2 and D7.2 (**Fig. 4.3, upper row**). Interestingly, at 5 wt% and above the T_{CP} of P*n*PrOzi, the solutions became turbid which was again observed for either diblock copolymers. By contrast, in the case of D2.2, between 10 and 20 wt%, the solutions remained clear and liquid over the entire temperature range investigated (5 – 50 °C), while D7.2 turned turbid (**Fig. 4.3, bottom row**). It is important to note, that either diblock copolymer forms transparent physical hydrogels above a concentration of 20 wt% which will be thoroughly discussed in the remainder of the study. Still, I want to emphasize, that to the best of my knowledge, this is the first report of a thermogelling physical hydrogel solely based on POx and POzi.

In order to further investigate the water solubility, temperature dependent ^{1}H NMR spectroscopy was performed at concentrations of 5 and 20 wt% for D7.2 in D_2O (**Fig. 4.4**) in cooperation with Prof. Dr. Ann-Christin Pöppler. At 5 °C and 5 wt% both blocks are solubilized in D_2O as the signals of PMeOx and P*n*PrOzi are clearly visible (**Fig. 4.4 A&B**). Increasing the temperature to 10 °C leads to slight decrease of signal b, but still all signals are clearly visible. Additionally, a downfield shift of the whole spectrum can be observed. This might be caused by either hydrogen bonding or anisotropy effects. As expected, further increasing the temperature leads to strong attenuation of the signals attributed to the P*n*PrOzi block. Within the hydrophobic domain of the formed aggregate, the P*n*PrOzi block is strongly hindered in its mobility causing a broadening and disappearance of the correlating ^{1}H NMR signals (b, c, e, f, and g) by shortening its transverse relaxation time T_2 (spin-spin relaxation). The signals attributed to the PMeOx block (a and d) did not decrease and the fine structure remained unchanged (**Fig. 4.4 B**) what indicates that they are still surrounded by D_2O. At higher concentrations (**Fig. 4.4 C**) a considerable attenuation of the P*n*PrOzi signals occurs already at 10 °C indicating the formation of aggregates already below the T_{CP} of P*n*PrOzi. Between 10 °C and 15 °C the sol-gel transition (*vide infra*) takes place resulting in an almost complete disappearance of the signals attributed the P*n*PrOzi backbone (b and c). However, these findings do not allow any conclusion on the formed structure. With increasing temperature, the ratio between the signals of the POzi (signal b) and POx (signal a) backbone decreased and formed a plateau at approximately 0.2 above 17 °C (290 K) for either polymer concentration (**Fig. 4.4 D**). Interestingly, the obtained data at 5 wt% reveal a change of the hydrophobicity of the P*n*PrOzi block already at ~7 °C (280 K) which is approximately 6 °C below the T_{CP}

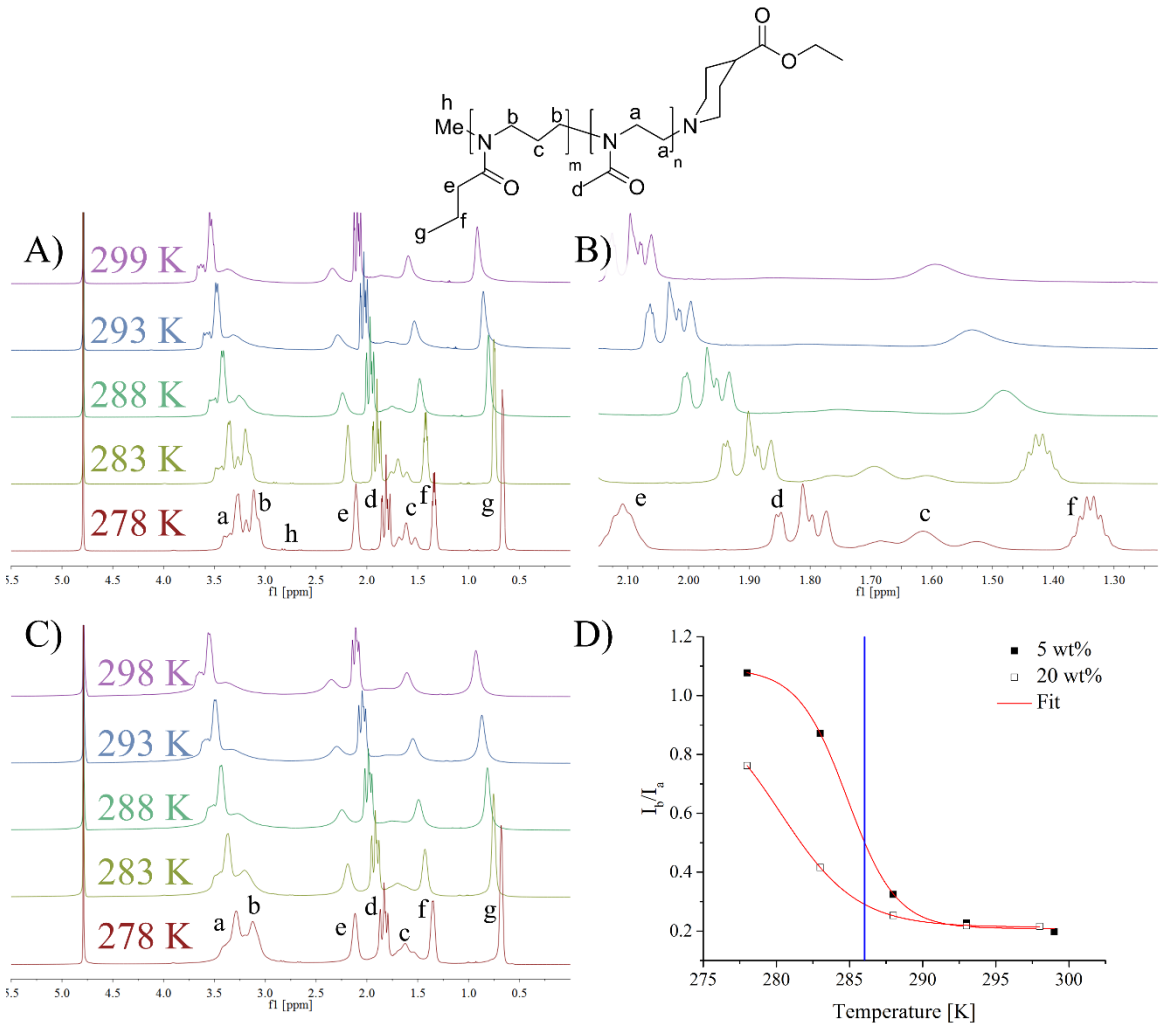

Fig. 4.4| Chemical structure and ^{1}H NMR spectra (600 MHz) of D7.2 in D_2O at different temperatures with signal assignments for all major polymer signals. A) Polymer concentration of 5 wt%; B) enlarged spectra of 5 wt% sample; C) Polymer concentration of 20 wt%. D) Ratio of the signal intensity of the POzi backbone (I_b) and the POx backbone (I_a) with increasing temperature. The blue vertical lines marks T_{CP} of P*n*PrOzi homopolymer. A Boltzmann function (red curve) was used to fit the data.

reported for the homopolymer (blue vertical line in **Fig. 4.4 D**). For a polymer concentration of 20 wt% it would be necessary to further decrease the temperature to investigate if the ratio of I_b and I_a reach values comparable to the ones found for a 5 wt% sample. Additionally, this would demonstrate if a plateau is formed at low temperatures as presumed by applying a Boltzmann fit function. A more detailed ^{1}H NMR study has the potential to further characterize the temperature induced phase transitions at different polymer concentrations and therefore help to gain fundamental understanding of the polymer system developed in the present thesis.

4.1.4 Conclusion

In summary, the copolymerization of 2-oxazolines and 2-oxazines bearing different alkyl side chains could be successfully demonstrated up to ~100 g per batch (D7.2). With very few exceptions, the resulting di- and triblock as well as random copolymers exhibited narrow molar mass distributions with moderate to low dispersities (Đ < 1.5). In order to ensure a high economic efficiency of the whole process, the monomer synthesis was up-scaled to a total reaction volume of 4.5 L resulting in 1.5 kg pure monomer with a yield of 57%. Aqueous solutions of a diblock copolymer comprising a hydrophilic PMeOx and a thermoresponsive P*n*PrOzi block showed a unique behavior by forming an optically clear thermoresponsive hydrogel at room temperature at 20 wt%. At lower concentrations a LCST behavior which is mainly caused by the P*n*PrOzi block could be observed visually and was further investigated by ^{1}H NMR spectroscopy.

4.2 Influence of the Copolymer Composition on the Physicochemical Properties

The possibility to influence material properties like solubility, glass transition or melting temperature, or T_{CP} by variation of the side chain, was already presented for POx and POzi homopolymers (see chapter 2.2.3). The accessible range can further be broadened by synthesizing block copolymers which can also be amphiphilic or thermoresponsive. Recently, Luxenhofer and co-workers published a communication investigating a small library of structurally similar amphiphilic triblock copolymers based on POx and POzi with regard to their solubilization capacity for curcumin and paclitaxel.[323] They reported significantly different solubilization capacities even if only a methylene group is exchanged between the polymer side chain and its backbone (POzi ↔ POx). This nicely illustrates that small changes of the polymer composition can tremendously effect the material properties. Inspired by thermoresponsive poloxamers, Zahoranová *et al.* synthesized a library of ABA and BAB triblock copolymers comprising PMeOx as hydrophilic and P*n*PrOx as thermoresponsive part.[190] Although no gelation could be observed in the investigated concentration (20 – 30 wt%) and temperature (10 – 50 °C) range, it was shown that the formation and size of the aggregates depends on the polymer structure. In the following, the thermal properties of selected diblock copolymers and a random copolymer will be comparatively discussed before thoroughly investigating the dependence of dynamic viscosity on the temperature.

4.2.1 Thermal Properties of Poly(2-oxazoline)/Poly(2-oxazine) Copolymers

Unfortunately, only little or no information can be found on the thermal properties of copolymers comprising POx and POzi. Very recently, we published a paper dealing with triblock copolymers consisting of two flanking PMeOx blocks and a hydrophobic core.[154] This was either realized by P*n*NonOx, P*n*NonOzi, PEtHepOx, or PEtHepOzi. Unexpectedly, all four triblock copolymers exhibited similar T_g values in the range of 54 °C to 61 °C, even though the thermal properties of the homopolymers strongly differed. It is important to note, that only one glass transition could be observed in the investigated temperature range (-50 – 200 °C), what indicates the formation of a homogeneous microstructure with no phase separation. Similar findings have been reported for triblock copolymers consisting of PMeOx and P*n*BuOx[324] or P*n*PrOzi[325], respectively. In order to set the correct temperature range for the characterization of diblock copolymers the T_g of a

P*n*PrOzi homopolymer (H5, DP = 50) was determined via differential scanning calorimetry (DSC) as to the best of my knowledge, this has not been reported before. Similar to the melting point, the glass transition point represents a broader range in which the transitions takes place. Nevertheless, for the present work the T_g is defined as the midpoint of the step in the heat curve which is characteristic for glass transition. In the second and third heating phase a distinct glass transition at ~5 °C could be observed for H5 (data not shown). This value nicely fits with the T_g reported for PEtOzi (~8 °C, DP = 200) by Levy and Litt[133] as a longer side chain should lead to a decrease of T_g. Compared to POx, for which the T_g can be adjusted within a range of almost 100 °C (C1 – C6 side chain)[134], the T_g range accessible with POzi is significantly smaller (~45 °C, C1 – C5 side chain)[133]. This is not surprising as the longer backbone results in a more flexible polymer chain and therefore mitigates the influence of the side chain on the T_g.

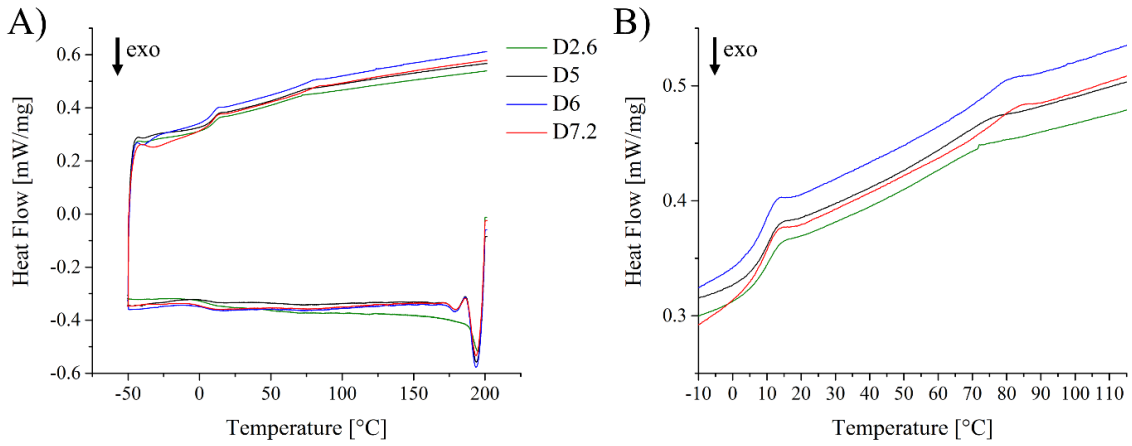

Fig. 4.5| A) Heat flow occurring during second heating and cooling cycle of differential scanning calorimetry (DSC) measurements of several P*n*PrOzi and PMeOx containing diblock copolymers with varying DP. B) Enlarged heat flow curves of the second heating cycle for better visibility of glass transition points. Samples were heated from -50 °C to 200 °C with a heating rate of 10 °C/min in nitrogen atmosphere.

In contrast to triblock copolymers based on POx, for which one T_g was reported, the heating curves recorded at a heating rate of 10 °C/min in a nitrogen atmosphere for diblock copolymers consisting of PMeOx and P*n*PrOzi with a DP ranging from 50 to 100 for each block (**Fig. 4.5 A**) appear significantly different. Two glass transition points (endothermic signals) can be found for all polymers, independent on DP. Compared to the heating cycle, they are shifted to lower temperatures in the cooling cycle. The rationale behind this hysteresis is the fact that the frozen movements thaw only at higher temperatures. Increasing the cooling rate would result in higher glass transition temperature. The first glass transition, which is more pronounced than the second one,

occurs at ~8 °C and thus can be attributed to P*n*PrOzi, although it is 3 °C above the value determined for the homopolymer (H5). For the second one, occurring between 65 °C and 75 °C, a stronger deviation between the individual polymers can be observed (**Fig. 4.5 B**). It appears that a higher DP results in a slightly more pronounced signal in the heat flow curves. Still this glass transition appears uncommon and might easily be misinterpreted as melting point. However, analyzing the first derivative as well as the tangents indicates the existence of a glass transition. Interestingly, the obtained values are only slightly lower than the value reported for PMeOx homopolymer (T_g = 75 °C), which is why the second glass transition is attributed to the hydrophilic block. Therefore, one can conclude that (micro)phase separation occurs in bulk demonstrating the immiscibility of the PMeOx block and the P*n*PrOzi block. Calculating the theoretical T_g according to the Fox equation (eq. 4.1), assuming that both blocks are miscible, gives a value of 29.3 °C. As expected, this is identical to the measured value (29.4 °C) for a random copolymer (R1) consisting of MeOx and *n*PrOzi (**Fig. 4.6 A**).

$$\frac{1}{T_{g,mix}} = \frac{w_1}{T_{g,1}} + \frac{w_2}{T_{g,2}} \qquad \text{(eq. 4.1)}$$

with $T_{g,mix}$ = T_g of the mixture in Kelvin; $T_{g,1}$ and $T_{g,2}$ are the T_g values of the corresponding compound; and w_1 and w_2 are the weight fractions of compound 1 and 2, respectively.

In order to investigate if phase separation only occurs for the combination of PMeOx and P*n*PrOzi several other diblock copolymers were analyzed via DSC. Qualitatively, the results can be broken down into two different phenotypes. Exchanging the hydrophilic PMeOx block with a PEtOx (T_g = 62 °C)[174] block also consisting of ~50 monomer units (D12) slightly reduces the hydrophilicity of this block. Although the block copolymer still exhibits amphiphilic character, only one glass transition at 23.6 °C is visible in the heat flow curve (**Fig. 4.6 A**) being almost in accordance with the calculated value (26.3 °C). Thus, the polymer exhibits a leathery appearance and could only be handled properly in the cold. Switching the backbones results in a diblock copolymer comprising a thermoresponsive P*n*PrOx (T_g = 35 °C)[134,193] block and a hydrophilic PMeOzi (T_g(Lit.) = 16 – 30 °C[133], T_g(H2) = 30 °C) block (D13). Due to the elongated backbone it is conceivable that PMeOzi also exhibits LCST behavior, however this has not been investigated and remains a presumption. A glass transition of the copolymer could be observed at ~25 °C which is slightly lower than the calculated value (27 °C) if using the lowest reported value for PMeOzi. As expected, a triblock copolymer (T1) containing a

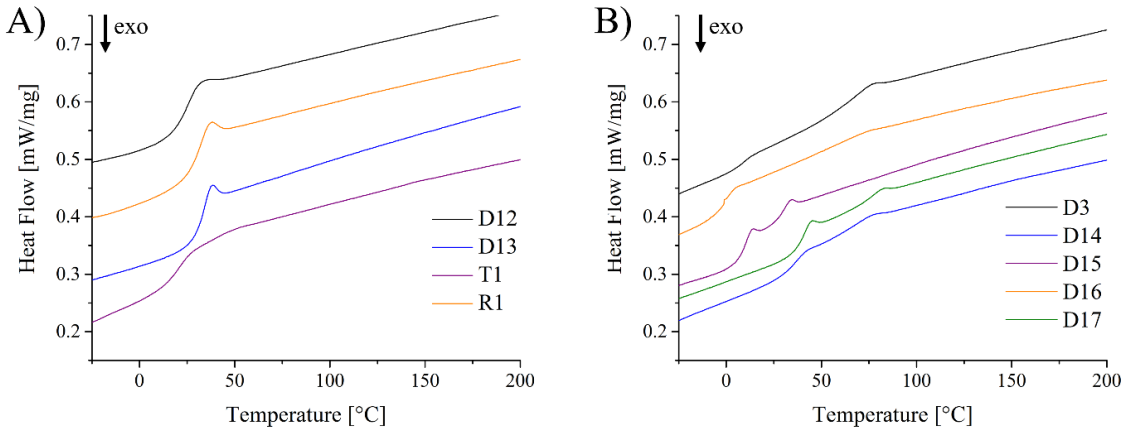

Fig. 4.6| Heat flow occurring during second heating cycle of DSC measurements of several diblock copolymers with varying composition. Samples were heated from -50 °C to 200 °C with a heating rate of 10 K/min in nitrogen atmosphere. A) P*n*PrOzi-*b*-PEtOx (D12), P*n*PrOx-*b*-PMeOzi (D13), PMeOx-b-P*n*PrOzi-*b*-PMeOx (T1), and P(MeOx-*co*-*n*PrOzi) (R1) exhibiting one glass transition which is in good agreement with the calculated values. D12 and R1 curves were shifted along the y-axis by 0.15 and 0.1, respectively. B) P*n*PrOzi-*b*-PMeOx (asym., D3), P*n*PrOx-*b*-PMeOx (D14), PMeOzi-*b*-P*n*PrOzi (D15), P*n*BuOzi-*b*-PMeOx (D16), and P*i*PrOzi-*b*-PMeOx (D17) with two visible glass transition point which can be attributed to the respective homopolymer. D3 and D16 curves were shifted along the y-axis by 0.2 and 0.15, respectively.

similar number of monomers as D2.6, exhibits only one glass transition point at ~26 °C which is slightly lower than the calculated value (~29 °C). However, the glass transition appears to be rather broad for this polymer. The observation of one T_g for T1 is in accordance with the results published by Lübtow *et al.* who observed also only one T_g (~50 °C) for an ABA triblock copolymer comprising a P*n*PrOzi core and PMeOx flanking blocks, however with a shorter hydrophobic core.[325] In this case the outer blocks probably prevent the formation of nanoscopic domains sufficient in size to cause two distinct glass transition points.

In case of D3, and D14 – D17 two more or less pronounced glass transition points could be detected which match with the values reported for the respective homopolymers in all cases (**Fig. 4.6 B**). In the heat flow curve of D3 the signal of the P*n*PrOzi block is only weakly defined as this is an asymmetrical copolymer in which the thermoresponsive block only accounts for ~25%. It is important to note that the result obtained for D14 must be regarded critically as GPC analysis revealed a bimodal molar mass distribution which also might influence the glass transitions. Synthesizing a diblock copolymer which is completely based on POzi (D15) with methyl and *n*-propyl side chains also clearly shows two glass transitions that are close to each other (T_g(PMeOzi) ~28 °C and T_g(P*n*PrOzi) ~9 °C). As a consequence of this narrow gap, a leathery material was obtained if the

polymer was stored at room temperature. Using P*n*BuOzi (D16) instead of P*n*PrOzi resulted in an expected decrease of the first glass transition point. Although, the T_g of the homopolymer (P*n*BuOzi) has not been reported yet a value of ~-1 °C fits with the temperatures discussed in chapter 2.2.3.2. Expectedly, changing the constitution of the propyl side chain results in an increase of the T_g (compare ~8 °C for P*n*PrOzi vs. ~39 °C for P*i*PrOzi) what is visible in the heating curve of D17. In comparison to POx, this increase by eightfold is considerably high. Toncheva *et al.* reported a T_g for P*i*PrOx between 52 °C and 68 °C depending on the chain length[326] which is less than twice the temperature found for P*n*PrOx. Consequently, changing the constitution of the POzi side chain leads to a more pronounced increase of rigidity of the formed structure. However, to clearly assign the glass transition at ~39 °C to P*i*PrOzi the T_g of the homopolymer (H6, DP = 11), which was synthesized by Daniela Lautz during a research internship, was determined (~20 °C). Although, the difference is quite large, it is important to keep in mind that depending on the DP the T_g converges against an asymptote, resulting to a strong chain-length dependency especially at low DPs.[327] Therefore, it is reasonable to attribute the first glass transition in the heating flow curve of D17 to the P*i*PrOzi block.

In conclusion, it appears that PMeOx, exhibiting the strongest hydrophilic character, is immiscible with P*n*PrOx, P*n*PrOzi, P*i*PrOzi, and P*n*BuOzi resulting in two glass transition points which correspond to the values obtained for the respective homopolymers. This is particularly interesting as triblock copolymers with a hydrophobic/thermoresponsive core and two flanking PMeOx blocks reveal a different behavior with no (micro)phase separation detectable. Decreasing the hydrophilicity by polymerizing EtOx instead of MeOx while keeping the thermoresponsive block (P*n*PrOzi) constant lead to an increase of the miscibility and consequently only one T_g could be observed. The fact that this value matches the result obtained by using the Fox equation corroborates the notion of miscibility of both blocks. The same applies for a diblock copolymer consisting of PMeOzi and P*n*PrOx as well as for a random copolymer of MeOx and P*n*PrOzi. The question therefore arises whether the heat flow curves, or to be more precise, the occurrence of two T_g allows for the prediction of thermogelling behavior. To investigate this issue, temperature dependency of dynamic viscosity is measured at different concentrations of a selection of aqueous solutions of diblock and triblock copolymers.

4.2.2 Temperature Dependent Viscosity of Aqueous Polymer Solutions

In general, the viscosity of a fluid, either a liquid or a gas, is the measure of its resistance to gradual deformation by stress. In simple terms, viscosity means friction between the molecules of fluid. The higher the viscosity, the lower is the flowability and *vice versa*. Usually, a distinction is made between the dynamic viscosity (η) [Pa•s] and the kinematic viscosity [m^2•s^{-1}], which is calculated by dividing η by the density of the fluid. In some cases, also the fluidity is mentioned, which is defined as the reciprocal value of the dynamic viscosity. To determine the viscosity of a liquid a viscometer is utilized. A falling ball viscometer also known as Höppler viscometer is commonly used for lower viscosities. Here, the liquid to be measured is filled into a measuring cylinder with the radius R. A ball with the radius r<R falls through the liquid and the constant velocity is measured. Thus, the dynamic viscosity can be calculated based on Stokes' law according to **eq. 4.2** as an equilibrium is formed between gravitational force, buoyant lift, and friction.

$$\eta = \frac{2gr^2}{9v}(\rho_B - \rho_L) \qquad \text{(eq. 4.2)}$$

with g being the gravity acceleration (9.81 m•s^{-2}), v is the constant falling velocity, and ρ_B and ρ_L are the densities of the ball and the liquid, respectively.

Without even noticing, our everyday life teaches us the phenomenon by which liquid viscosity tends to decrease as the temperature increases, for example when putting cooking oil in a hot frying pan. To describe this complex process, several empirical models have been developed for liquids and melts and are valid for a limited temperature range. However, some polymer solutions show the so-called reverse thermoresponsive phenomenon[328] which describes a viscosity increase upon heating. Examples like solutions of PNiPAAm or Pluronics as well as their LCST behavior have already been discussed in chapter 2.1.2. Regarding the temperature dependent viscosity of POx based amphiphilic block copolymers only one report by Zahoranová *et al.* dealing with ABA and BAB copolymers can be found.[190] This is surprising as the LCST behavior, which often correlates with changes of the dynamic viscosity, is thoroughly investigated in numerous publications. Based on the visual observation that aqueous solutions of D2.1, D2.2, D7.1, and D7.2 form thermoresponsive physical gels at concentrations above 20 wt% while turbidity is observed at lower concentrations, the viscosity of a series of solutions of D2.2 in MilliQ water with varying polymer content (5 wt% - 30 wt%) was measured depending

on the temperature (**Fig. 4.7 A**). Below the T_{cp} of P*n*PrOzi (blue vertical line) relatively low viscosities were observed for all concentrations. At 5 wt% the viscosity remained very low and decreased monotonously with temperature. For concentrations between 10 wt% and 20 wt% an increase of viscosity was observed, consistently starting around T_{CP} while the maximum of the viscosity goes through a plateau, the maximum of which shifts to higher temperatures with increasing polymer concentrations. At concentrations of 20 wt% and above, the solutions of D2.X gel. In this behavior these thermogelling polymers are quite distinct from F127 and P123, which also form gels at elevated temperature and/or concentration and are commonly used for gel plotting in biofabrication. Important for the prospective use as injectable hydrogel or as bioink, the viscosity of D2.2 is relatively low at low temperatures (10 °C), in particular compared to the viscosity of Pluronic block copolymers (compare 700 mPa•s (F127 at 10 wt%) vs. 7 mPa•s (D2.2 at 10 wt%)). Even at 30 wt%, a solution of D2.2 at 10 °C has a lower viscosity than a 10 wt% solution of F127, which does not form a gel at this concentration. From visual observations it can be inferred that a higher DP (D7.1) affects the viscosity of the polymer solution. While at lower concentration (5 wt% & 10 wt%) viscosity is of the same order of magnitude as for D2.2 (**Fig. 4.7 B**) a large increase to over 1000 mPa•s can be identified between 10 wt% and 15 wt%. Comparable to the progression of viscosity observed for D2.2, the viscosity of D7.1 also goes through a plateau before decreasing. However, the maxima are shifted to lower values (compare 23 °C for D2.2 vs. 15 °C for D7.1 at 10 wt%) what might indicate the formation of larger aggregates which are also responsible for the turbidity between 10 wt% and 20 wt% only visible at higher DP (chapter 4.1.3). D1 with a DP of ~20 for each block did not show thermogelation, however aqueous solutions are still thermoresponsive (**Fig. 4.7 C**). Interestingly, the increase of viscosity does not occur at the T_{CP} of P*n*PrOzi as for D2.X and D7.X. For solutions with a polymer concentration of 5 wt% and 10 wt% a slight increase occurs at 17.5 °C after an initial decrease with increasing temperature. This resembles the curve progression of aqueous solutions of ABA triblock copolymers with a high P*n*PrOx content and two flanking PMeOx blocks, recently reported by Zahoranová *et al*. However, it is important to note that these results were obtained at 20 wt% and therefore a direct comparison is not appropriate. Still the formed local maximum might be indicative for the formation of aggregates. Increasing the polymer concentration to 20 wt% causes a slightly higher viscosity between 10 mPa•s and 20 mPa•s which is comparable to 12.5 wt% solution of D2.2. At low temperature the viscosity decreases with increasing temperature until a local minimum is formed at 22 °C. After that, an increase to a local

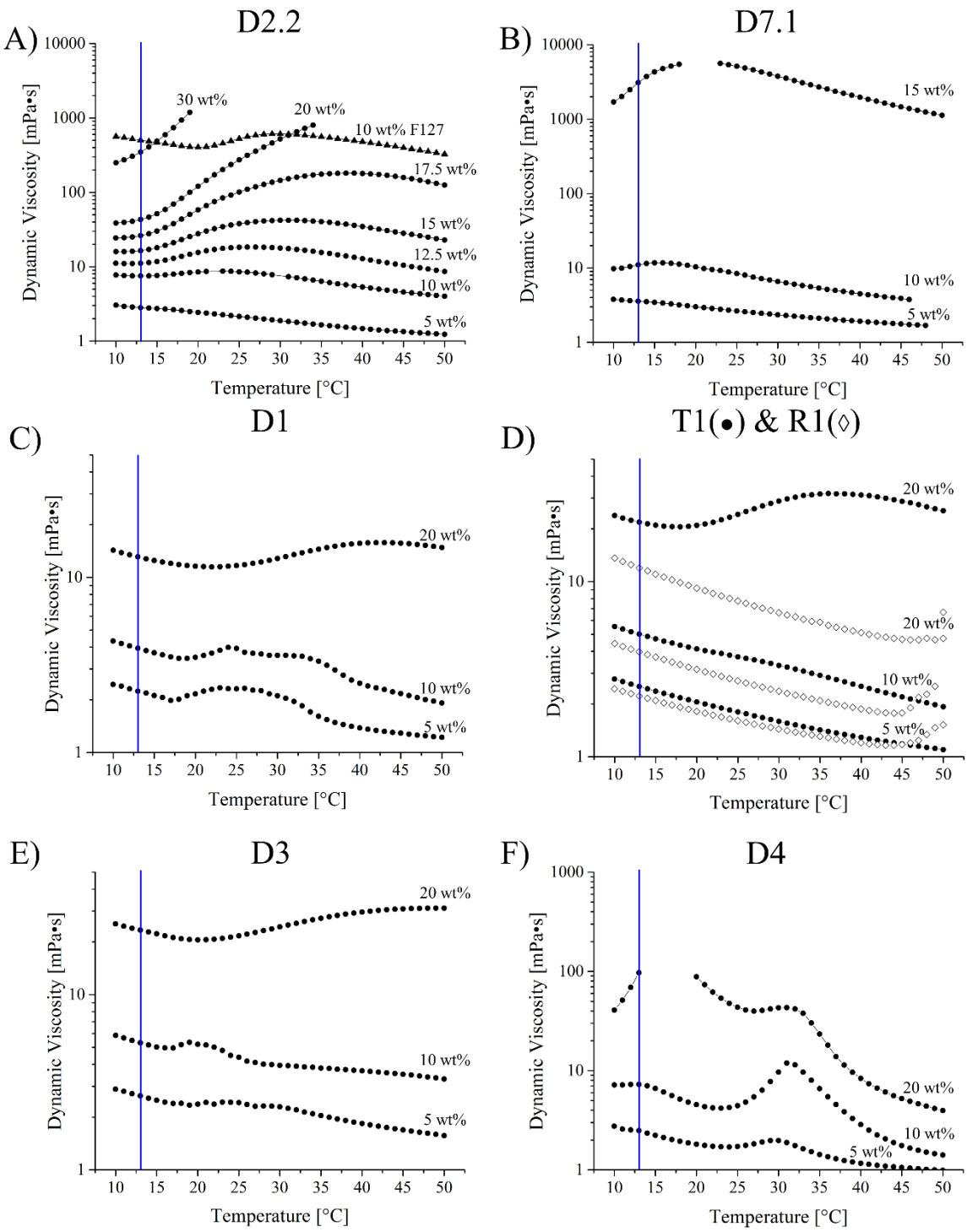

Fig. 4.7| Dependency of dynamic viscosity on temperature (5 – 50 °C) of aqueous solutions of di- and triblock copolymers in MilliQ water. The blue vertical lines marks T_{CP} of P*n*PrOzi homopolymer. A) D2.2 at 5 wt%, 10 wt%, 12.5 wt%, 15 wt%, 17.5 wt%, 20 wt% and 30 wt% compared to Pluronic F127 at 10 wt%, B) D7.1 at 5 wt%, 10 wt%, and 15 wt%, C) D1 at 5 wt%, 10 wt%, and 20 wt%, D) T1 at 5 wt%, 10 wt%, and 20 wt%, E) D3 at 5 wt%, 10 wt%, and 20 wt%, and F) D4 at 5 wt%, 10 wt%, and 20 wt%. Note that, although not ideal for direct comparison, the scaling of y-axis (logarithmic scale) had to be adjusted for better visibility but is equal for A) and B) as well as for C) to E).

maximum at 43 °C can be observed. Interestingly, Zahoranová *et al.* found a similar behavior for ABA (PMeOx-P*n*PrOx-PMeOx) block copolymers, albeit shifted to higher values (~factor 5) due to the significantly higher molar mass (compare D1 with 4.8 kg/mol

vs. P12 with 43.5 kg/mol[190]). Unexpectedly, a triblock copolymer comprising an almost identical quantity of monomer units than D2.2 with two flanking PMeOx blocks did not show thermogelation at concentration up to 20 wt%. The viscosity change with increasing temperature is comparable to D1 with the exception that no local maximum is formed at 5 wt% and 10 wt% (**Fig. 4.7 D**). Expectedly, the viscosity of all solutions of R1 monotonously decreases with increasing temperature until 45 °C as no aggregation should occur due to the missing or at least very weak amphiphilic character of a random copolymer. Above 45 °C a slight increase is observable, which might be indicative of a LCST. These findings demonstrate the tremendous influence of the polymer structure on the physicochemical properties and suggest that, although triblock copolymers comprising PMeOx and P*n*PrOx did not show thermogelation, it might be worth to investigate the related diblock copolymers. However, random copolymers will not further investigated in the present work as they are not regarded as potential candidate for thermoresponsive polymers.

Additionally, dependency of dynamic viscosity on temperature was investigated for asymmetrically designed diblock copolymers. Important to note, D7.1 is also slightly asymmetric but is discussed in the context of symmetrical diblock copolymer due to its thermogelling behavior and the smaller difference between both blocks in comparison to D3 and D4 for which the shorter block constitutes only around 25% with regard to the total number of monomers. D3 comprises a longer PMeOx block whereas D4 comprises a longer thermoresponsive block. The observed viscosity behavior for aqueous solutions of D3 (**Fig. 4.7 E**) differs only slightly from those obtained for D1 and T1. Only at the highest concentration the maximum occurs at higher temperatures and the dip seems to appear above the highest temperature investigated in the present study. However, a completely different curve progression was found for D4. At low concentrations (5 wt%) a first, albeit weakly defined maximum can be observed at 13 °C followed by a second one at 29 °C. Nevertheless, the overall trend of decreasing viscosity with increasing temperature is clearly visible. Increasing the concentration to 10 wt% lead to more pronounced increase of the viscosity at 13 °C and 31 °C. Surprisingly, the increase at 13 °C which might be attributed to an association of the *n*-propyl groups by hydrophobic bonding, is considerably lower than the second one. However, this changes at concentration of 20 wt% (**Fig. 4.7 F**). Already at low temperatures a steep increase of the viscosity from 40 mPa•s to 100 mPa•s is visible. Between 13 °C and 20 °C it was not possible to determine the viscosity via falling

ball viscosimetry as the fall time was too long. Tam *et al.* reported a less pronounced but similar steep increase of viscosity for a 1.5 wt% PNiPAAm solution.[329] They have argued that hydrophobic intermolecular associations which lead to an apparent increase of the molecular weight are responsible for the observed increase of viscosity. The subsequent decrease reflects the phase separation and formation of unstable colloidal particles. Therefore, the steep increase of viscosity should be attributed to the aggregation at the T_{CP} of P*n*PrOzi. Compared to all other solution with a concentration of 20 wt% D4 exhibits the lowest viscosity at 50 °C.

Combining the temperature dependent viscosity behavior with the previously discussed results obtained by DSC measurements allows an initial conclusion. The fact that aqueous solutions of D3 did not show thermogelation at reasonable polymer concentrations although two glass transition points could be identified in the heat flow curve contradicts the assumption that microphase separation in bulk is a necessary requirement or indicator for thermogelation in solution. However, to investigate if thermogelation can be excluded if only one glass transition appears in the heat flow curves and how a varying monomer composition influences the temperature dependent viscosity of diblock copolymers, aqueous solutions of D12, D14, and D17 were analyzed. Important to note, it was impossible to measure the viscosity of D13 which comprises a P*n*PrOx block and a PMeOzi block as the polymer precipitates in water at elevated temperatures even at 5 wt%. The same applies for D15, consisting of PMeOzi and P*n*PrOzi, which precipitated while storing at 3 °C. Therefore these two polymer composition were not further investigated as they appear unsuitable for the envisioned application as bioink. Nevertheless, this unusual and unexpected behavior warrants further investigation.

As discussed previously, substituting PMeOx by PEtOx and keeping the thermoresponsive block constant (D12) resulted in no (micro)phase separation according to DSC measurements. However, it must be taken into account that in case of D12 either blocks are thermoresponsive (see chapter 2.2.3.1). This fact is reflected in the curve progression of the viscosity especially at 20 wt% (**Fig. 4.8 A**). At around 13 °C an increase of the viscosity is observed resulting in values too high to be measured via falling ball viscosimetry between 18 °C and 35 °C. Up to 42 °C the decrease to almost initial values could be observed before a second increase is observable which can probably assigned to PEtOx, although its T_{CP} is reported to be at 60 °C. Probably, this increase can be interpreted as onset of precipitation of completely hydrophobic polymer what will apparently result in

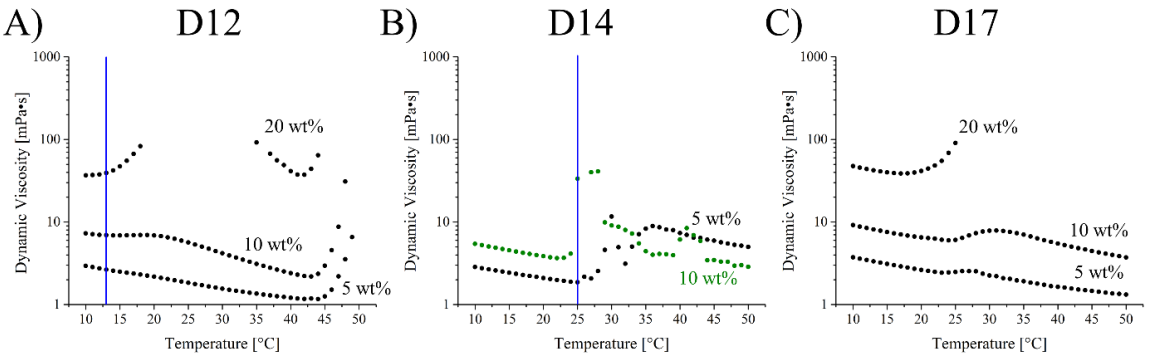

Fig. 4.8| Dependency of dynamic viscosity on temperature (5 – 50 °C) of aqueous solutions of dilock copolymers in MilliQ water. The blue vertical lines marks T_{CP} of P*n*PrOzi (A) or T_{CP} of *n*PrOx (B) homopolymer. A) P*n*PrOzi-*b*-PEtOx (D12) at 5 wt%, 10 wt%, and 20 wt%, B) P*n*PrOx-*b*-PMeOx (D14) at 5 wt% and 10 wt%, and C) P*i*PrOzi-*b*-PMeOx (D17) at 5 wt%, 10 wt%, and 20 wt%.

longer falling times. This may appear contradictory at first as the viscosity should decrease due to reduced polymer entanglement. However, the formed precipitate caused partial clogging of the used glass capillary and therefore affected the results. In general, precipitation during viscosimetry measurements will lead to misinterpretation and should therefore be avoided. At lower concentration the first increase is noticeably reduced whereby the increase over almost a decade at ~45 °C is still clearly visible, corroborating the assumption of starting precipitation. This could also be visually verified after the measurements.

Two other diblock copolymers which differ in composition from the gel forming D2.X and D7.X and did not precipitate were therefore also regarded as potential candidates. The first one, D14, consists of P*n*PrOx and PMeOx and reveals a quite unique temperature dependency of the dynamic viscosity with a sharp increase occurring at the T_{CP} of P*n*PrOx (blue line) followed by an abrupt decrease at 30 °C (**Fig. 4.8 B**). Unfortunately, it was unfeasible to measure a 20 wt% solution as the viscosity was too high over the whole temperature range. The second one, D17 consists of P*i*PrOzi and PMeOx (**Fig. 4.8 C**). No blue line, indicating the T_{CP} of the homopolymer is drawn in this case as the value is unknown for P*i*PrOzi. However, based on the T_{CP}s reported for P*i*PrOx and P*n*PrOx (see chapter 2.2.3.1), it is to be assumed that the T_{CP} of P*i*PrOzi is higher than the one reported for P*n*PrOzi. At ~22 °C a steep increase of dynamic viscosity is observable at 20 wt% what leads to exceedance of the measurable range at 25 °C. For concentrations of 5 wt% and 10 wt% a local maximum is identifiable at 27 °C and 31 °C, respectively. Interestingly, the curve progressions obtained for D17 rather resemble those of D2.2, although comprising approximately 100 monomer units of each block like D7.1. Nevertheless, curve progression

supports the supposition of potential gel formation, although not visible up to 37 °C in a glass vial.

All three polymers (D12, D14, D17) have in common that an aqueous solution with a polymer concentration of 20 wt% revealed a strong increase of dynamic viscosity which could partially not be measured, or not at all due to the high values. Therefore, temperature dependent rheological measurements were conducted to elucidate whether a gel is formed or not. For an aqueous solution of D2.2 with a concentration of 20 wt% a relatively sharp sol-gel transition at approximately 34 °C was observed (**Fig. 4.9 A**). In general, the gel point is defined as the intersection of G', representing the elastic properties of a material, and G'', representing the viscous properties of a material. If the elastic properties dominate the viscous properties (G' > G'') a gel exists.[330] Although D2.2 was used as benchmark

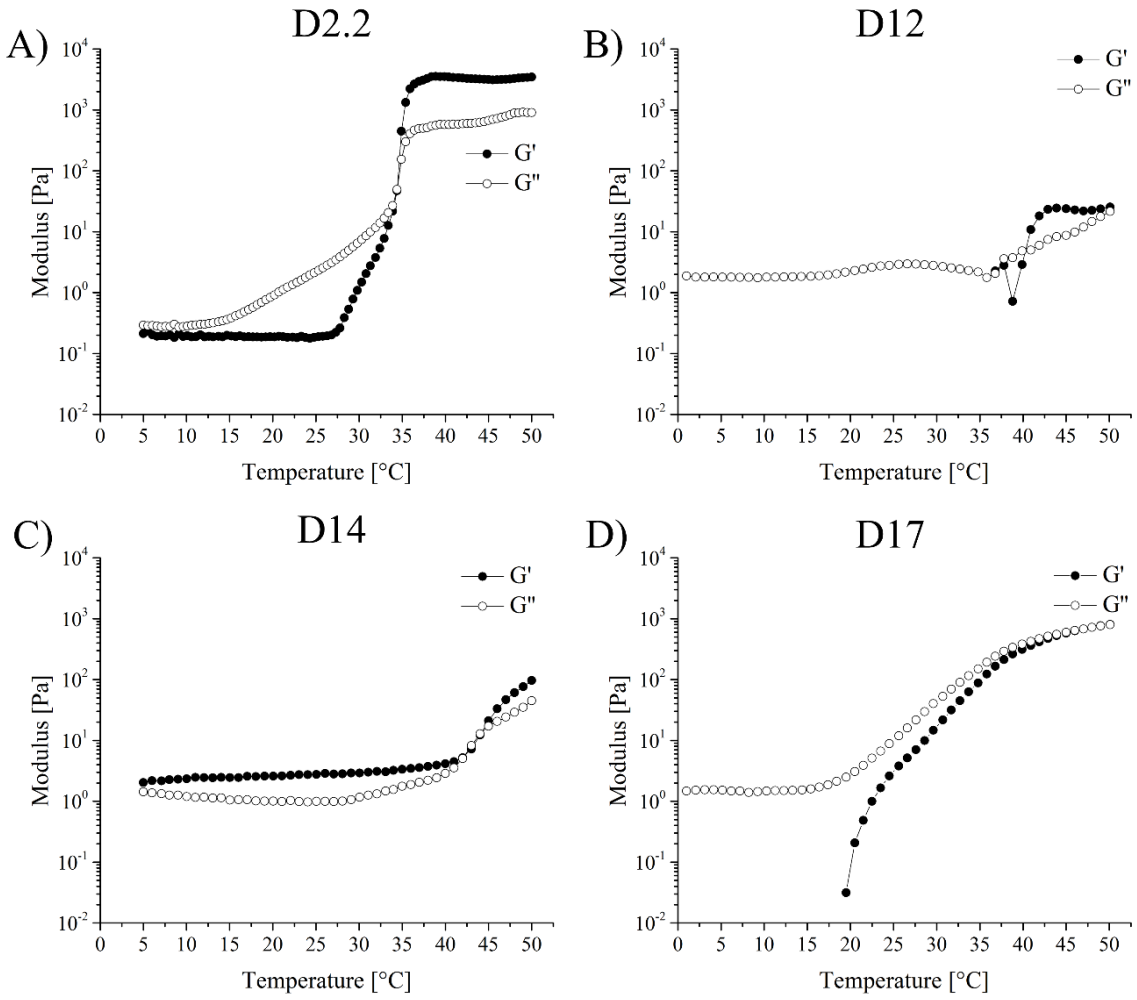

Fig. 4.9| Dependency of G' and G'' on temperature (5 – 50 °C) of aqueous solutions (20 wt%) of diblock copolymers in MilliQ water. A) P*n*PrOzi-*b*-PMeOx (D2.2), B) P*n*PrOzi-*b*-PEtOx (D12), C) P*n*PrOx-*b*-PMeOx (D14), and D) P*i*PrOzi-*b*-PMeOx (D17). Temperature was raised linearly with 0.66 K/min. The used angular frequency was 10 rad/s and the strain was adjusted to 1%.

for D12, D14, and D17 due to its ability to form stable macroscopic gel, the properties and gelation behavior will be thoroughly discussed in the following chapter. Oscillatory measurements revealed that an aqueous solution (20 wt%) of D12 formed a hydrogel albeit significantly weaker. Interestingly, no gelation could be observed in the range between 18 °C and 35 °C where dynamic viscosity could not be measured via falling ball viscosity due to too high values. However, gelation could be observed at ~40 °C which approximately corresponds with the onset of the second increase of dynamic viscosity (**Fig. 4.9 B**). Important to note, although rheology indicates the formation of a weak gel at very low shear rates, no macroscopic gel could be observed in a vial as the material probably flows under its own weight. Nevertheless, this debunks the hypothesis that the absence of micro phase separation in bulk can be exploited to predict the inability to form hydrogels. Of course the gelation process always depends on multiple factors which is why a general statement is extremely difficult to make. Unexpectedly, aqueous solutions of D14 appeared gel like over the whole temperature range investigated, except at 43 °C and 44 °C (**Fig. 4.9 C**). A temperature induced increase of G' and G'' occurs at ~40 °C which corresponds with the second increase of dynamic viscosity observed at 10 wt%. However, the formed gel was very weak and due to the absence of thermoresponsive sol-gel transition not usable as potential ink. Although, the largest increase of G' over approximately four decades is observable for D17 no clear gel point can be found as G' and G'' are almost equally above 40 °C (**Fig. 4.9 D**). None of the three polymer solutions exhibited properties comparable to solutions of D2.2 what is remarkable as only slight variations were made.

4.2.3 Conclusion

This comparative study of a small library of different di- and triblock copolymers consisting of POx and POzi nicely illustrates the importance of understanding and investigating structure-property relationships as slight variations can tremendously influence material performance. Obviously, this also applies to other properties than thermogelation and to other polymer classes than poly(cyclic imino ether)s. In the present study, the influence of the polymer composition on thermal properties (glass transition points), temperature dependent viscosities, and thermogelation was demonstrated and revealed particularity of symmetric P*n*PrOzi-*b*-PMeOx copolymers compared to other combinations of poly(2-alkyl-2-oxazoline)s and poly(2-alkyl-2-oxazine)s.

4.3 Characterization of Thermoresponsive Poly(2-oxazoline)-*block*-Poly(2-oxazine) Based Physical Hydrogels

Based on the results discussed in the previous chapter only the polymers D2.X and D7.X are regarded as suitable materials to be used as bioinks due to the gelation behavior of their aqueous solutions. Important to note, that does not mean that it can be generally excluded that any other POx or POzi based polymer either blocky, statistically, or gradient like does also form hydrogels. In fact, based on the small library investigated in the present study aqueous solutions of D2.X and D7.X exhibited properties never described before for polymers solely comprising POx or POzi which is why they were thoroughly investigated regarding their potential use as bioink platform. However, thermogelation is only a minor albeit very beneficial aspect for the printability of bioinks as already outlined previously (see chapter 2.3.3). In the following subchapters, initially, the rheological properties of the novel thermoresponsive hydrogel system will be examined in the context of extrusion based bioprinting. Thereafter, special attention will be paid to the elucidation of the micro- and nanostructure of the hydrogel by using SANS as well as DLS and static light scattering (SLS).

4.3.1 Rheological Properties and Assessment of Printability

Although bioinks are urgently needed to further develop biofabrication, only little attention has been paid to methods which allow a reliable prediction of printability.[331] In general, the term printability is only poorly defined in the literature. Very recently, Paxton *et al.* proposed a two-step method for the assessment of printability for which they characterized the yield point, shear thinning, and recovery behavior of four model inks.[307] Another systematic approach to assess printability was reported by Gao and Gillispie *et al.* who used gelatin and alginate as model hydrogels.[332] They investigated the influence of the loss factor ($G''/G' = \tan\delta$) on the printing outcome and defined a range between 0.25 and 0.45 as excellent compromise between extrusion uniformity and structural integrity. However, the authors also mention this does not necessarily apply to other bioinks as they found a different behavior for 40 wt% solution of Pluronic F127. This relativizes the relevance of the proposed method or at least shows the importance to define a model for every gel type. Ribeiro and Blokzijl *et al.* reported another interesting approach to assess bioink shape fidelity after extrusion-based bioprinting by testing the filament collapse on overhanging structures as well as the filament fusion of parallel printed hydrogel

strands.[333] Furthermore, they developed a theoretical model to relate the bioink yield stress with the filament collapse.

The following characterization of thermoresponsive hydrogels based on POx-*b*-POzi copolymers is in some points similar to the work published by Paxton *et al.*[307] which is why some obtained results are compared with their findings.

4.3.1.1 Thermogelation and Reproducibility

Initially, the aim was to examine if material properties can be achieved reproducibly as batch-to-batch variance is one of the major arguments which is brought up against hydrogels based on naturally derived polymers. As already mentioned in chapter 4.1.2 several batches of D2 were synthesized and the rheological properties of their aqueous solutions were investigated in dependence of the temperature. First, the LVE range was determined by performing an amplitude sweep at constant angular frequency which was set to 10 rad/s (exemplarily illustrated for D2.2 in **Fig. 4.10 A**). This test is crucial to ensure that only elastic and no plastic deformation occurs, which would lead to damage of the sample. The limit of the LVE range is generally defined as the onset of the decrease of G' (blue vertical line in **Fig. 4.10 A**). However, for some samples an early increase of the loss modulus can also be seen as indication for plastic deformation as it is often explained with the formation of micro fractures. An aqueous solution of D2.2 can be clearly identified as sol at 10 °C as G'<G'' applies. At the highest temperature used for the temperature sweep (50 °C) the existence of a gel is evident as G'>G'' with a limitation of the LVE range at around 3%. A relatively sharp sol-gel transition at approximately 27 °C and 34 °C was observed for D2.1 and D2.2, respectively (**Fig. 4.10 B**). It is noteworthy, that G' increases by 4 orders of magnitude within a narrow temperature window. Notably, G'' starts to increase at much lower temperature than G' (approximately 13 °C), which corresponds very well with the T_{CP} of P*n*PrOzi as homopolymer. After sol-gel transition a plateau is reached at about 4-5 kPa (G'). Therefore, these gels are surprisingly strong compared to many other thermogelling polymers, for which values <1 kPa are more commonly found in the literature.[39,334] A prominent exception are hydrogels of F127 (see chapter 2.1.2) at 20 wt% or higher which exhibit G' values of approximately 10 kPa. For this reason, the novel hydrogel system based on POx-*b*-POzi copolymers will be benchmarked against F127. Comparing the different batches (**Fig. 4.10 B**), it is obvious that at 20 wt% only D2.1, D2.2, D2.5, and D2.6 formed gels with a more elastic character ($\tan\delta \approx 0.1$ - 0.2).

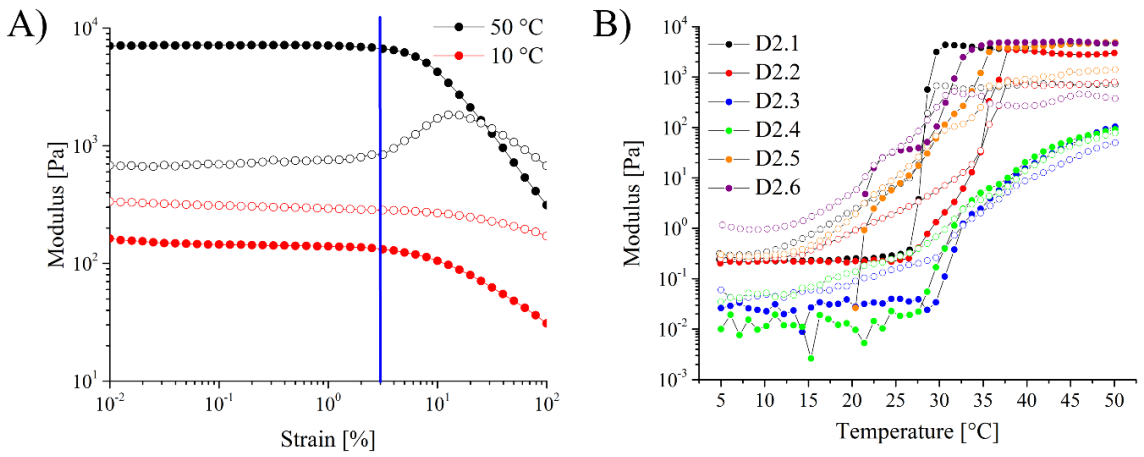

Fig. 4.10| Rheological characterization of aqueous polymer solutions with a concentration of 20wt%. A) Amplitude sweeps at constant angular frequency of 10 rad/s at 10 °C and 50 °C of D2.2. Vertical blue line marks the limit of the LVE range (γ_L). B) Temperature-dependent rheology of D2.1 – D2.6. Filled circles represent G', empty circles represent G''.

Furthermore, it could be proven that the order of the two blocks, which was changed for D2.6, does neither significantly influence the gelation temperature nor the plateau value of G'. However, the obtained values for G'' (purple empty circles in **Fig. 4.10 B**) are slightly lower in the plateau region resulting in values of ~0.1 for tan δ. In contrast, even though D2.3 and D2.4 formed gels as evidenced by G' > G'', these are more viscous in character (tan δ ≈ 1; G' < 0.1 kPa). This was surprising as all six batches, in particular D2.2 – D2.5, appeared very similar from ^{1}H NMR spectroscopy and GPC analysis. D2.3 and D2.4 only showed a somewhat more pronounced low-molecular tailing in the GPC elugrams (**Fig. 4.2 C**). Comparing all batches with respect to rheology and GPC elugrams, molar mass appeared to be a dominant factor for G' of the resulting hydrogels. While a higher molar mass did not negatively influence G' (D2.1) even a slightly higher content of lower molar mass components resulted in the formation of significantly weaker hydrogels (D2.3 and D2.4). This data underlines the importance of studying batch-to-batch variations in the context of biomaterials research.[317]

In contrast, the high molecular shoulder visible in the GPC elugram (D2.1) presumably leads to a shift of the gelation temperature to lower values. To investigate the dependency of the gelation temperature (T_{Gel}) on the DP, several diblock copolymers with varying chain length (PMeOx$_{51}$-*b*-P*n*PrOzi$_{53}$ (D2.6), PMeOx$_{59}$-*b*-P*n*PrOzi$_{61}$ (D5), PMeOx$_{85}$-*b*-P*n*PrOzi$_{85}$ (D6), and P*n*PrOzi$_{104}$-*b*-PMeOx$_{105}$ (D7.2)) were investigated and compared (**Fig. 4.11**). If several batches with more or less identical DP (D2.X and D7.X) were available the mean values and standard deviations (SD) of T_{Gel} were calculated.

Subsequently, the determined values (mean ± SD) were plotted against DP of each block (**Fig. 4.11, inset**). Here 10% was postulated as systematic bias for determination of the chain length via ^{1}H NMR spectroscopy. Apparently, increasing the DP of symmetric diblock copolymers leads to a decrease of T_{Gel} converging against approximately 13 °C (T_{CP} of P*n*PrOzi). In contrast, decreasing the chain length leads to a steep increase of T_{Gel} which pointed to the conclusion that below a certain block length no gelation can be observed. This is confirmed by the results obtained for aqueous solutions of D1 (DP ~21) which showed viscosity change dependent on the temperature but no thermogelation. Additionally, these findings corroborate the observation made during the comparison of the D2.X batches which revealed a strong influence of low molecular mass components. A correlation of the chain-length dependency of T_{Gel} with the critical overlap concentration would open up new insights into the gelation behavior and presumably allow prediction of T_{Gel}. However, therefore, a precise determination of the radius of gyration (R_g) is necessary. As in the present study R_g was only determined for D7.2 by SLS (*vide infra*) a comparison is not feasible at the moment but highly recommended for future investigations.

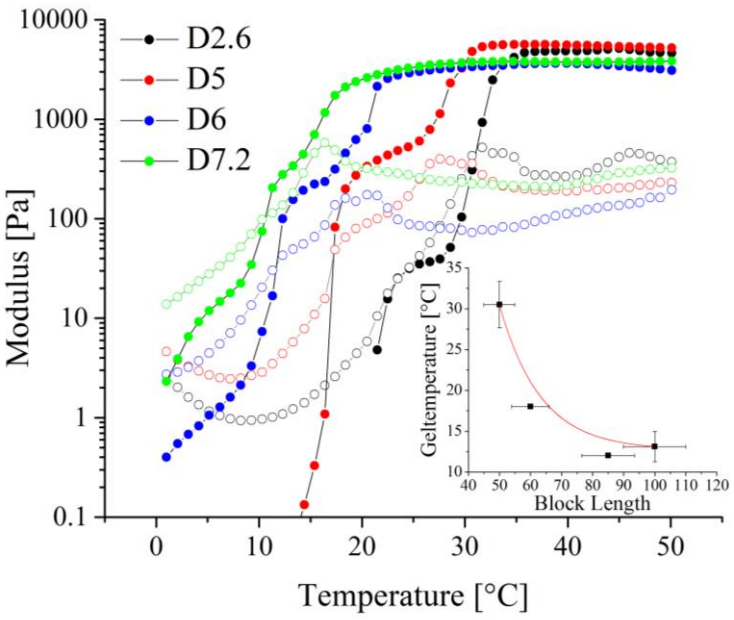

Fig. 4.11| Temperature-dependent rheology of D2.6, D5, D6, and D7.2 with increasing DP. Filled circles represent G', empty circles represent G''. Inset figure) Dependency of T_{Gel} (mean ± SD) on DP (± 10%). Red line is intended as a guide to the eye.

Besides the importance of being able to tune G' and G'', respectively, the straightforward adjustability of T_{Gel} is also important for the applicability of POx-POzi based hydrogels as bioink platform in the context of tissue engineering and 3D printing. The latter can easily be achieved by controlling the DP (**Fig. 4.11**). Depending on the demanded characteristics the gelation behavior can be adjusted to the customer's needs. The described findings are, however, not surprising as in publications dealing with other polymers similar findings have been reported. By investigating the sol-gel transition of

Pluronic P65, P85, and P105 Sun *et al.* were able to sketch a phase diagram illustrating that P105 with the highest molecular weight formed a gel at lower concentrations and temperatures than P65.[335] According to Constantinou and Georgiou who summarized more studies investigating the effect of molar mass on T_{Gel}, a high molar mass also enhances the mechanical properties.[99] This was also shown by Jiang *et al.* who managed to link several F127 molecules together using hexamethylene diisocynate.[336] The resulting multiblock copolymers revealed a drastic increase of viscosity and G'. However, in case of the developed POx-POzi based system, no correlation between DP and the plateau value of G' can be found at least in the investigated range of molar masses. The visible difference of around 900 Pa between D2.6 and D7.2 cannot be explained at the moment and might be attributed to surrounding parameters like humidity which could have influenced the measurements. However, this can only be addressed by performing the measurements as well as the synthesis multiple times. Important to note, it is necessary to synthesize more symmetric PMeOx-*b*-P*n*PrOzi copolymers with different DP to confirm the suggested chain length dependency of T_{Gel} and to gain a better understanding and a more reliable basis to be able to predict the behavior of a POx-POzi based hydrogel. In particular, with regard to a potential commercialization it is important to be able to reproducibly address a certain temperature range.

4.3.1.2 Effect of the Polymer End Group on Physicochemical Properties of Poly(2-oxazoline)-block-Poly(2-oxazine) Based Hydrogels

The influence of the polymer end group on material properties is often discussed, however, it is quite obvious that the impact will be significantly stronger the lower the molar mass of the polymer is. Due to the possibility to easily functionalize both α- as well as ω-chain ends with end groups of varying hydrophilicity and reactivity, POx and POzi are ideally suitable to investigate this effect. This interesting topic was recently reviewed by Weber *et al.* who compared biocompatible polymers based on PEG and POx.[178] Yu *et al.* studied end group effects on the macroscopic physical gelation of aqueous solutions of amphiphilic PLGA-*b*-PEG-*b*-PLGA copolymers capped with hydroxyl, acetate, propionate, or butyrate groups.[337] Surprisingly, only the copolymers end-capped with acetate and propionate groups caused the formation of turbid physical hydrogels above concentrations of 15 wt%. Important to note, both hydrogels were only stable in a temperature range of approximately 10 °C and liquefied again already below physiological temperature. In contrast, block copolymers capped with butyrate end groups did not form

a gel but precipitated in water. In conclusion, a drastic influence of the end group on the gelation properties could be demonstrated.

In order to investigate end group effects on the gelation properties of POx-POzi based hydrogels and to exclude that EPC which was mainly used as termination agent (D7.2) did cause the thermogelation, three other residues were introduced at the ω-chain end (**Scheme 4.2**). Furthermore, the α-chain end was also changed to a propargyl group for D9-D11 by using propargyl tosylate instead of MeOTf. Although alkyl tosylates are reported to cause slow initiation and it is recommended to only use methyl tosylate[157], it was possible to obtain diblock copolymers which exhibit a monomodal molar mass distribution as shown via GPC analysis (**Fig. 4.12 A**). Interestingly, although D9, D10, and D11 were synthesized as one batch and were only split just before adding the termination reagent the obtained dispersities showed a significant difference (compare Đ = 1.56 (D9), Đ = 1.44 (D10), Đ = 1.31 (D11)) which can probably attributed to the end group as all batches were treated equally and were measured on the same day. Especially for D9,

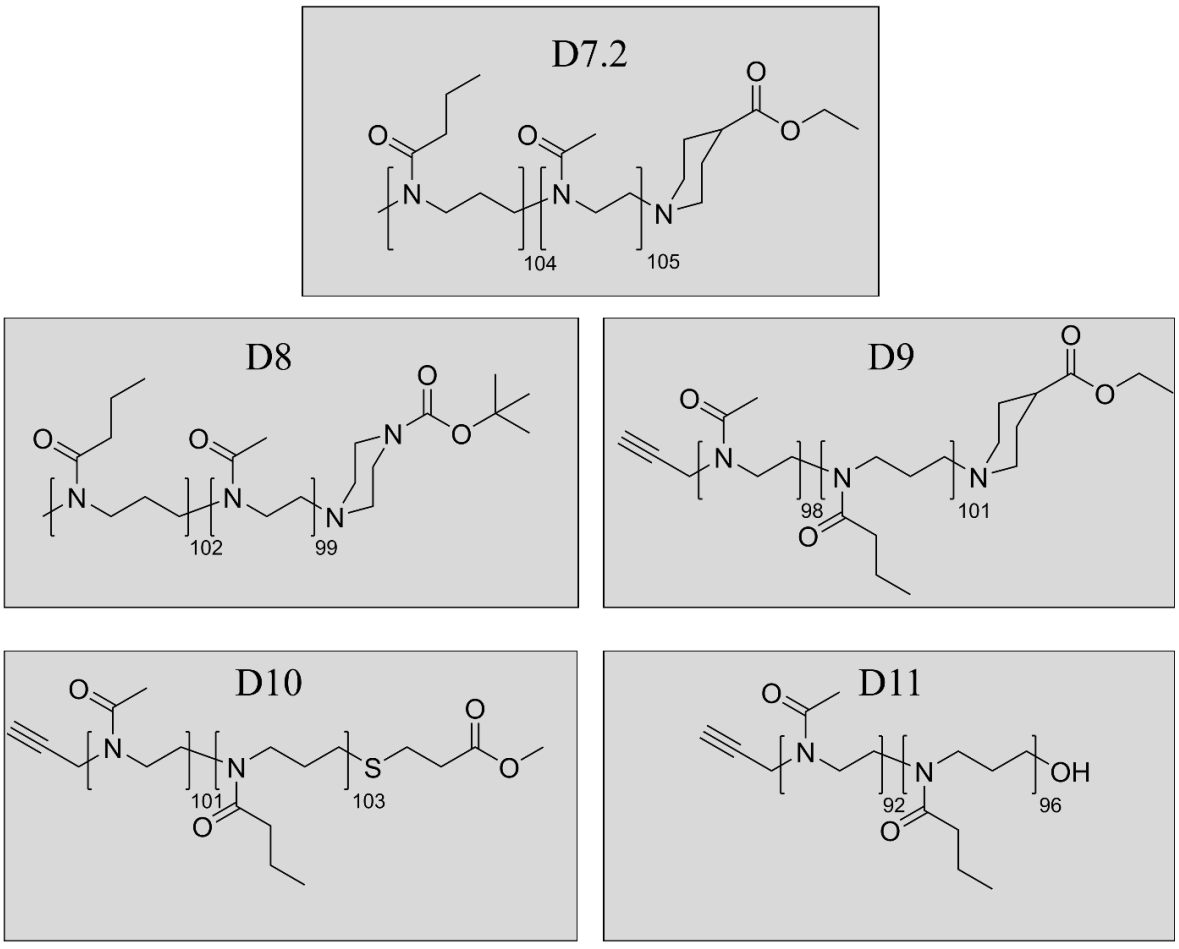

Scheme 4.2| Chemical structure of the investigated block copolymers. Given chain length was determined by ^{1}H NMR spectroscopy.

exhibiting the highest dispersity, a more pronounced low molecular tailing could be observed. Using propargyl tosylate instead of methyl triflate as initiator, did not influence the molar mass distribution (compare D7.2 vs. D9, D10, and D11) as the GPC elugrams of polymers initiated with propargyl tosylate are almost similar to the one obtained for D7.2. This could be expected as the chain lengths calculated from the respective ^{1}H NMR spectra are almost identical (**Scheme 4.2**). It remains unclear whether the shift to lower elution volumes, observed for D8, can be attributed to the BOC protection group of the utilized terminating agent and should therefore be investigated in future experiments.

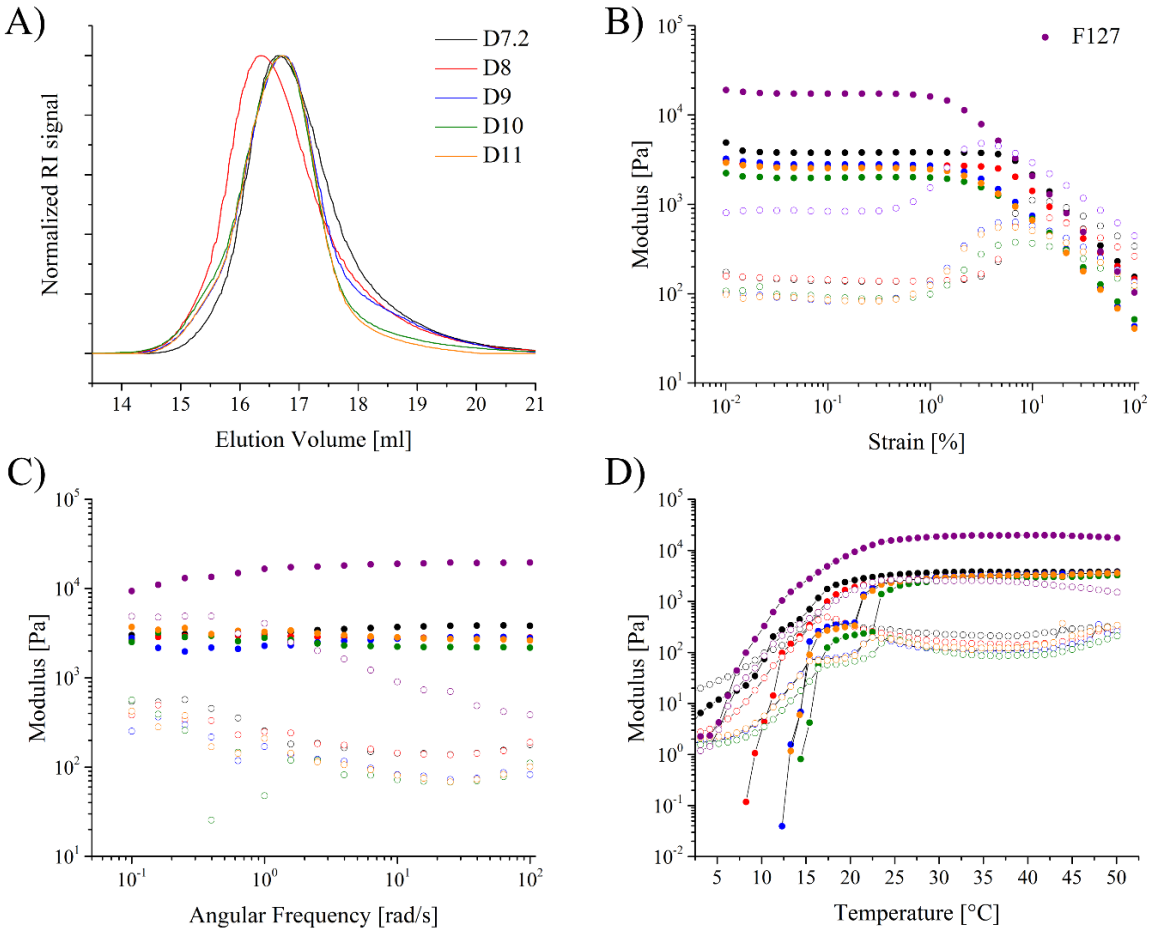

Fig. 4.12| A) Normalized GPC traces of diblock copolymers with varying end groups. B) Amplitude sweeps at constant angular frequency of 10 rad/s at 37 °C of POx-*b*-POzi copolymers and F127. Filled circles represent G', empty circles represent G''. C) Frequency sweeps at constant strain of 0.01% at 37 °C. D) Temperature-dependent rheology of block copolymers.

It is crucial, however, if the variation of the end groups influences the characteristics of the macroscopic hydrogel. Therefore, rheology constitutes the method of choice. In all cases a 20 wt% aqueous polymer solution was prepared, stored at 3 °C until the polymer was completely dissolved and measured directly after taking the solution out of the cooling

incubator. Prior to each temperature sweep, an amplitude as well as a frequency sweep were performed at 5 °C (data not shown) and 37 °C (**Fig. 4.12 B & C**) and revealed only minor variations between the individual batches. Interestingly, the limit of the LVE range (strain γ_L) is shifted from a strain of 3% (D7.2) to approximately 1% for D9 – D11 (**Tab. 4.4**), suggesting a weaker inner structure of the gel which might be caused by the propargyl group at the α-chain end. Although a more pronounced low molecular tailing is visible for D9, no adverse effects regarding the mechanical properties could be determined. Pluronic F127 was used as reference and exhibits significantly higher G' and G'' values at 37 °C and γ_L was found to occur at ~1%. Important to note, the described linearity limit (γ_L) cannot be equated to the yield point which is defined as lowest shear stress value and not the lowest strain above which a samples shows irreversible deformation of the structure. Furthermore, all POx-*b*-POzi samples investigated appeared gel like up to a strain of approximately 10%. In contrast the gel-sol transition for Pluronic F127 was found to be at lower amplitudes of ~7%. Apart from the fact that D7.2 and D10 exhibited slightly higher (3.8 kPa) and lower (2.0 kPa) G' values, respectively, no clear influence of the end group could be found during the amplitude sweep. These findings were further corroborated as no differences could be found during the performed frequency sweeps which revealed constant G' values between 3 kPa and 4 kPa over the whole range investigated. Regarding G'', a decrease occurring at 0.4 rad/s could be observed for all hydrogels resulting in smaller tan δ values (~0.03 – 0.05) at higher angular frequencies (100 rad/s). This represents an increasing stiffness at high dynamic stress. More importantly, no gel-sol transition was observable at very low frequencies, suggesting a stable gel at zero shear conditions. A similar frequency dependency of the viscoelastic properties has been reported for an aqueous solution of F127 (20 wt%) by Grassi and co-workers.[338] These findings could be confirmed and revealed a more pronounced increase of tan δ for F127 (compare 0.52 for F127 vs. 0.19 for D7.2 at 0.1 rad/s) at low frequencies compared to all POx-*b*-POzi samples (**Fig. 4.12 C**).

Finally, a temperature sweep was performed to investigate how the different end groups effect the thermogelling behavior (**Fig. 4.12 D and Tab. 4.4**). Although T_{Gel} of D8 increased by 1 °C compared to D7.2, no significant influence could be observed whether ethyl isonipecotate or 1-BOC-piperazine was used as termination agent. In contrast, T_{Gel} of D9 – D11 was found to be at 15 °C (D9 and D11) and 16 °C (D10), respectively, showing a negligible influence of the ω-chain end. As ^{1}H NMR spectroscopy revealed identical

block lengths of 100 ± 5 monomer units for each block, it is assumed that the propargyl group at the α-chain end influences T_{Gel}. In comparison to a methyl end group, a propargyl group is slightly more hydrophobic and therefore might hinder the formation of secondary structures which are presumably responsible for the formation of macroscopic hydrogels. Furthermore, progression of G' of D9 – D11 clearly showed two steps while increasing to the final plateau value which is reached between 20 °C and 25 °C for all five hydrogels. Likewise, the two steps were visible for D7.2 and D8 but were considerably less pronounced. Most probably, they originate from a phase transition occurring at this temperature which has a strengthening effect due to the formation of a more ordered structure. Obviously, the values obtained for F127 under identical conditions significantly exceed those of POx-*b*-POzi based hydrogels. However, according to the calculated tan δ values F127 gels appear to exhibit a more viscous character.

Table 4.4| Molar masses [kg/mol] of synthesized diblock copolymers with varying end groups obtained via GPC with DMF as eluent. $\gamma_{L\,[\%]}$, T_{Gel} [°C], $G'_{Plateau}$ [kPa], and tan δ obtained via rheological measurements in oscillatory mode.

ID	M_n	γ_L	T_{Gel}	$G'_{Plateau}$	tan δ
D7.2	10.1	3	11	3.8	0.06
D8	13.7	3	12	3.1	0.05
D9	12.3	1	15	3.3	0.04
D10	14.7	1	15	2.9	0.03
D11	15.9	1	16	3.2	0.04
F127	9.1[a]	1	<2.5	19.6	0.13

[a] sample appeared bimodal during GPC analysis

To conclude, it could be shown, that the end groups introduced in the present work on the α- and ω-chain end had only minor influence on the thermogelation as well as on the resulting mechanical properties as analyzed via amplitude and frequency sweeps. Therefore, it can be hypothesized that all polymers discussed in this subchapter are suitable for bioprinting. Although, the functional group, which attacks the propagating species was different (HN-, HO-, HS-), the end groups were quite similar with respect to their polarity which is why only slight variations were expected. Changing the polarity of the terminal moiety more drastically, e.g. by introducing a nonyl group as reported by Huber *et al.*[179] should have a more drastic effect which might impede or enhance formation of a physical hydrogel.

4.3.1.3 Influence of the Controlled Insertion of nBuOzi "Impurities" on the Thermogelling Behavior

To acquire the ability to further adjust the physicochemical properties of POx-*b*-POzi based hydrogels *n*BuOzi was used as thermoresponsive block (D16). However, a 20 wt% aqueous solution could not be prepared due to solubility issues at this concentration. Although, some undissolved polymer was visible an increase of viscosity could be observed but was not measured via viscosimetry or rheology as the obtained results would not have much validity due to the unknown polymer concentration. Another approach to increase the hydrophobicity of the POzi block and thus tuning the material properties was to copolymerize *n*PrOzi and *n*BuOzi. The *n*BuOzi contents aimed for (theo.) as well as the actual values (exp.) are summarized together with the basic results obtained via rheology (**Tab. 4.5**). All polymers appeared monomodal with low dispersities (< 1.3) and ^{1}H NMR confirmed the existence of a P(*n*PrOzi-*co*-*n*BuOzi) block in all polymers. It is assumed that *n*BuOzi is randomly distributed within the copolymer although no kinetic studies have been performed to exclude the existence of a gradient copolymer.

Table 4.5| Molar masses [kg/mol] of synthesized diblock copolymers with varying *n*BuOzi content, given as absolute and relative values [%], were obtained via GPC with HFIP as eluent and ^{1}H NMR spectroscopy, respectively. γ_L [%], T_{Gel} [°C], $G'_{Plateau}$ [kPa], and tan δ obtained via rheological measurements in oscillatory mode.

ID	*n*BuOzi$_{theo}$	*n*BuOzi$_{exp}$	*n*BuOzi†	M_n	γ_L	T_{Gel}	$G'_{Plateau}$	tan δ
D7.2	0	0	0	7.2	3	11	3.8	0.06
D18	5	5	9	6.5	1	9	8.4	0.03
D19	10	11	11	8.5	1	7	3.8	0.05
D20	25	28	25	10.4	1	6	0.5*	0.1

*No plateau was formed, instead the value at 37 °C was chosen for comparison. †*n*BuOzi content in percent relates to the total length of the thermoresponsive block.

For analyzing the rheological properties the already described diblock copolymer (D7.2) was used as reference. As frequency sweeps only showed an increase of elasticity with increasing angular frequency, as already described in the previous chapter the data are not shown in the following. More interestingly, copolymerizing *n*PrOzi and *n*BuOzi causes significant differences observable in the amplitude sweep (**Fig. 4.13 A**). First of all, gelation could be observed for all three block copolymers containing *n*BuOzi. Interestingly, D18 exhibits clearly higher G' values in the low strain area. A comparable increase of G'

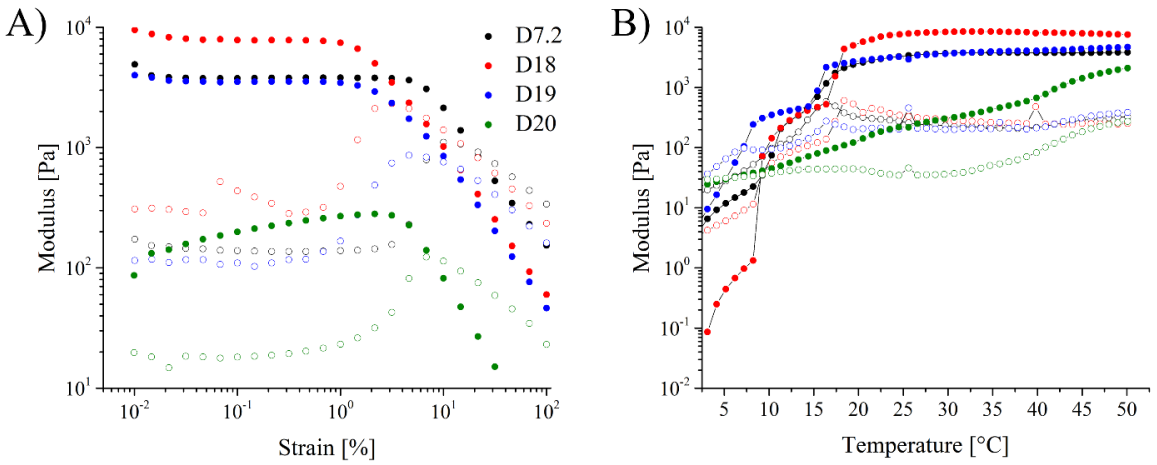

Fig. 4.13| A) Amplitude sweeps at constant angular frequency of 10 rad/s at 37 °C of POx-*b*-POzi copolymers containing a varying amount of *n*BuOzi copolymerized with *n*PrOzi. Filled circles represent G', empty circles represent G''. B) Temperature-dependent rheology of block copolymers.

could not be observed for D19 what is surprising as this block copolymer comprises also ~10% *n*BuOzi, however at a total block length of 98 compared to 56 (D18). Regarding the linearity limit of D18 and D19, γ_L was shifted to lower γ values of 1% or slightly lower, indicating disruption of the formed structure at lower shear stress compared to D7.2 which is used as reference. A similar effect was discussed in the previous chapter for D9 – D11 which were initiated with propargyl tosylate. Further increasing the *n*BuOzi content to 25% (D20) causes a significant decrease of the G' and G'' values to ~100 – 300 Pa and ~20 Pa, respectively. It should also be noted that G' does not form a plateau at low shear rates what might indicate a slow development of the structure.

Regarding the thermogelation, the controlled insertion of *n*BuOzi impurities shows a clear impact (**Fig. 4.13 B** and **Tab.4.5**). Usually for a diblock copolymer with ~50 monomer units per block T_{Gel} is expected around 30 °C (D2.X). Taking into account that the decrease of T_{Gel} with increasing chain length is very steep (**Fig. 4.11**) a minimal value of 20 °C should be expected for D18. However, T_{Gel} was observed at 9 °C which is 2 °C below the value found for D7.2 consisting of 100 monomer units of each block. Presumably, the observed shift could be attributed to the five *n*BuOzi units which increase the hydrophobicity of the thermoresponsive block and thus lead to a decrease of the LCST and the gelation temperature. Above 20 °C, after the second step in the G' curve, a plateau is reached at 8 kPa which is twice as high as the plateau formed by D7.2 and D19, however still not comparable to values found and reported for Pluronic F127 gels[112,338] (**Fig. 4.12 D** and **Tab. 4.4**). Increasing the chain length and keeping the *n*BuOzi content approximately

constant did not influence the G' value in the gel region (**Fig. 4.13 B** and **Tab. 4.5**). However, for D19 gelation occurs at 7 °C what is only a minor shift compared to shorter chain length. Although D20 exhibited the lowest T_{Gel} value obtained in the present study (6 °C) the gelation behavior is distinct from the other polymers. G' increases over the whole temperature range what is again indicative for the slow development of the nano- and microstructure. It is conceivable that the randomly distributed *n*BuOzi units disrupt the ordered structure which is formed by the PMeOx and P*n*PrOzi blocks.

To conclude, it was possible to influence T_{Gel} as well as the mechanical properties of the resulting gel by using a random copolymer consisting of *n*PrOzi and *n*BuOzi as thermoresponsive block of a diblock copolymer. A *n*BuOzi content of ~10% (D18 and D19) lead to a decrease of T_{Gel} and to a significant increase of G' in the case of D18. Why this effect could only observed for shorter diblock copolymers remains unclear at the moment and further research has to be conducted to elucidate this phenomena. Exceeding a critical value that seems to occur between 10% and 25%, has a negative effect on the mechanical properties of the gel. In general, it was ascertained that the insertion of *n*BuOzi leads to a decrease of γ_L which might be a problem for the envisioned application as bioink as γ_L correlates with the yield point. Still D18 and D19 are potential bioinks which allow the adjustment of low T_{Gel}, thus broadening the temperature range that can be covered by the new bioink platform.

4.3.1.4 Influence of the Solvent on the Rheological Properties

Usually, characterizations of physical hydrogels which are envisioned to be used as bioinks are carried out by using MilliQ or distilled water, or sometimes PBS as solvent for the respective polymer. However, this does not resemble reality. To print with living cells it is necessary to dissolve the polymer in cell culture medium which, in contrast to water, contains a mixture of inorganic salts, amino acids, vitamins, proteins and several other ingredients which have the ability to influence the gel properties. The so called Hofmeister Salts are well-known to effect the assembly of polymers in solution. Several groups investigated the effect of Hofmeister Salts on the LCST of POx[186,339] and found a significant influence. Very recently, Xue *et al.* published a thorough NMR study investigating how Hofmeister ions change the local environment around thermoresponsive polymers in aqueous solutions.[188] Therefore, the effect of salts and other ingredients should not be neglected during the development of bioinks, especially in the case of

physical gels. In the present study, D7.2 was chosen as model system to investigate the influence of cell culture medium on the rheological properties.

The initially performed amplitude sweep revealed a decrease of G' in the LVE range from 4 kPa in MilliQ water to approximately 2.7 kPa in cell culture medium (Dulbecco's Modified Eagle Medium (DMEM) high glucose containing 10% (v/v) heat inactivated FBS, 100 U/mL penicillin and 0.1 mg/mL streptomycin) (**Fig. 4.14 A**). Simultaneously, a small increase of G'' from 140 Pa to 171 Pa could be observed resulting in lower tan δ values, indicating a slightly more viscous character of the formed hydrogel if utilizing growth medium. No change could be observed regarding γ_L which remained constant at ~3%.

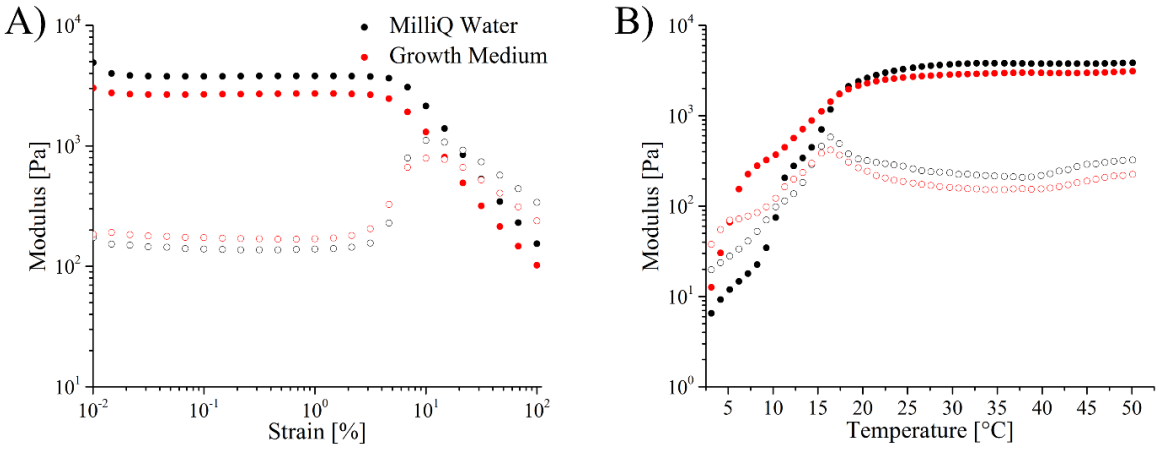

Fig. 4.14| | A) Amplitude sweeps at constant angular frequency of 10 rad/s at 37 °C of D7.2 in MilliQ water and cell culture medium (DMEM high glucose containing 10 % (v/v) heat inactivated FBS, 100 U/mL penicillin and 0.1 mg/mL streptomycin). Filled circles represent G', empty circles represent G''. B) Temperature-dependent rheology of D7.2 in MilliQ water and cell culture medium.

As expected from the amplitude sweep the obtained plateau values (**Fig. 4.14 B**) are lower if cell culture medium is used for hydrogel preparation (compare 3 kPa for growth medium *vs.* 3.8 kPa for MilliQ water at 37 °C). However, more interestingly, T_{Gel} shifted to lower values (~5 °C) if the hydrogel is prepared with growth medium. The obtained behavior can be compared to the salting out effect, causing a decrease of the LCST for homopolymers. Probably, the observed effect can be attributed to Cl^- ions which are one of the dominating anions present in the used growth medium and are known to cause salting out.

Although this experiment was kept deliberately simple, the results nicely illustrated that also the solvent can have an impact on the printability by influencing T_{Gel} and the mechanical properties. This should be kept in mind when evaluating the printability of a

material to avoid unpleasant surprises when finally working with cells which also might have an influence on the rheological properties. Consequently, rheology experiments should be performed on cell-laden hydrogels to mimic the printing process in the best possible way. However, this would require S1 certified laboratories equipped with a rheometer which are currently not available at the Julius-Maximilians-University, Wuerzburg.

4.3.1.5 Assessment of Printability

Based on the rheological characterization discussed in the previous chapter, it was reasonable to hypothesize that polymers D2.1, D2.2, D2.5, D2.6, D7.X – D11, D18, and D19 are suitable for bioprinting. As an example, and due to the fact that D2.2 and D7.2 could be regarded as basic model which have additionally been synthesized in larger quantity, crucial bioink parameters (see chapter 2.3.3) of these two diblock copolymers have been investigated. According to Paxton *et al.* three measurements are necessary for the rheological evaluation of bioinks.[307] All of them have in common that η, which is obtained via rheological measurements (rotational mode) is analyzed. Initially, η is investigated in dependency of the shear rate ($\dot{\gamma}$) to analyze the shear thinning behavior. Second, η is measured depending on the shear stress (τ) to determine the flow point. Finally, the structure recovery ability is investigated by recording η over time while changing $\dot{\gamma}$ stepwise. This allows for the assessment of post-printing recovery.

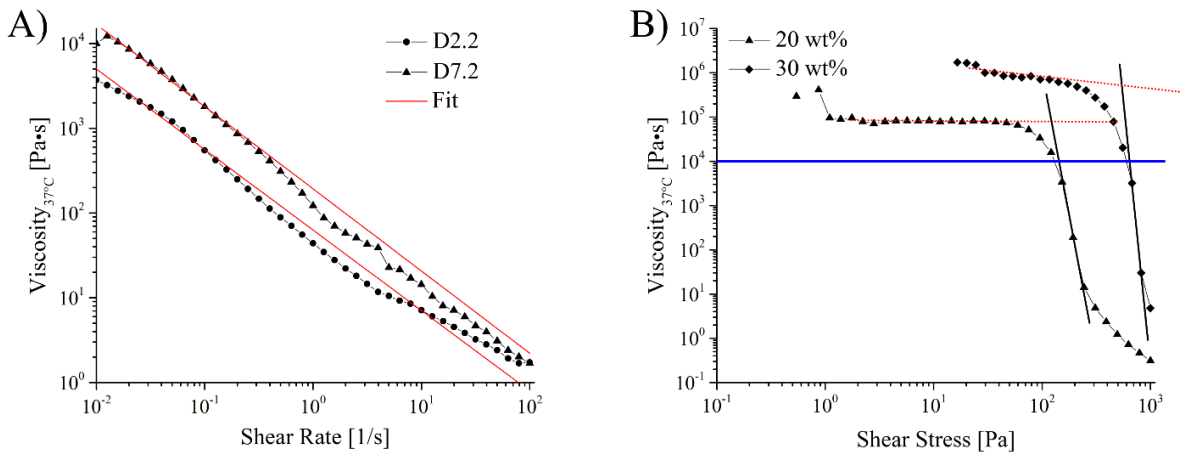

Fig. 4.15| A) Shear-viscosity results for D2.2 and D7.2, performed at 37 °C with the related fit. B) Shear stress ramp data for D7.2 at 20 wt% and 30 wt%, performed at 37 °C. Horizontal blue line marks a viscosity of 10 kPa•s. The intersection of the tangents is defined as yield point.

Regarding the shear thinning behavior of D2.2 and D7.2, a decrease from 4 kPa•s and 12 kPa•s, respectively, to 1 Pa•s could be observed while increasing the shear rate from

0.01 s^{-1} to 100 s^{-1} (**Fig. 4.15 A**). By fitting the linear region of the obtained data using the Ostwald-de Waele relationship (**eq. 4.3**) it was possible to extract the shear thinning coefficients which allowed for a direct comparison between D2.2, D7.2, Pluronic F127, and Nivea Crème (**Tab. 4.6**).

$$\eta = K\dot{\gamma}^{n-1} \quad \text{(eq. 4.3)}$$

with η the viscosity, $\dot{\gamma}$ the shear rate, K the flow consistency index, and n the flow behavior index. A Newtonian behavior results in n = 1 whereas n = 0.6 is defined as weakly shear thinning and n = 0.2 as highly shear thinning.[307]

Either POx-*b*-POzi copolymer based hydrogel exhibits a significantly lower flow behavior index (n) than Pluronic F127, indicating that they could possibly be extruded at lower pressure. Additionally, both K and n influence the flow profile in the nozzle which probably affects cell viability (*vide infra*). A direct correlation between the shear thinning coefficients and printability cannot be derived, as both F127 25 wt% and Nivea Crème are classified as printable[307], although exhibiting significantly different values.

Table 4.6| Values of shear thinning coefficients K[Pa•s^n] and n [dimensionless] for D2.2, D7.2, F127*, and Nivea Crème*.

ID	K	n
D2.2 20 wt%	63	0.05
D7.2 20 wt%	193	0.03
F127 20 wt%	222*	0.117*
F127 25 wt%	406*	0.127*
Nivea Crème	26*	0.552*

*Values were taken from Ref. [307]

In a next step, the yield point was analyzed by a shear stress sweep (**Fig. 4.15 B**). A logarithmic shear stress ramp offers a useful tool for the determination of the yield stress of hydrogels. By plotting η against τ, it is possible to approximately determine the viscosity of the hydrogel at rest. Additionally, the yield stress can be analyzed by using two tangents, one in the region where the viscosity drops and one in the plateau-region of the viscosity were the hydrogel is deformed elastically. Unfortunately, only D7.2 (20 wt% and 30 wt%) could be investigated because only from this batch enough material was present to perform all measurements and printing experiments. Important to note, all measurements were performed at 37 °C to ensure working in the gel state. For a 20 wt% polymer solution the

yield stress was determined at ~120 Pa which is slightly above the value of ~94 Pa[307] reported for a F127 solution with the same concentration. Increasing the polymer concentration to 30 wt% resulted in an increase of the yield stress to ~550 Pa (compared to ~350 Pa for 30 wt% F127). Below the determined τ values, the material behaves like a solid rather than a liquid. This allows for a rough estimation of the printability as materials without an observable or very low yield point flow even if no shear stress is applied. Paxton *et al.* found that for inks which they classified as printable a yield point viscosity above 10 kPa•s (**Fig. 4.15 B,** blue horizontal line**)** could be observed which is fulfilled by either investigated hydrogel. According to the mentioned requirements, it is assumed that D7.2 is a suitable bioink and could be used at 20 wt% as well as at 30 wt%.

However, the last crucial requirement – structural recovery ability – has to be investigated before considering printing with POx-*b*-POzi hydrogels. Here, too, only D7.2 was analyzed as the needed amount of polymer was available (**Fig. 4.16**). After an initial temperature equilibration step to 37 °C, the shear rate was stepwise changed between 0.1 s^{-1} and 100 s^{-1} to mimic the shear conditions during the printing process as well as at-rest conditions. For D7.2 as well as for Pluronic F127 an immediate recovery to almost initial values, which are similar for both polymers, could be observed within the first second after reducing the shear rate. This is crucial as otherwise the printed strand would not exhibit shape fidelity and would probably just spread on the substrate. The shear rate cycle was repeated 10-times, although it strongly depends on the architecture of the reservoir, the gel loading, and the printing process how often shear forces occur. A slight decrease of η in the low shear state was observable for either polymer solution over time, however more pronounced for F127. This might be attributed to drying effects which could not be prevented completely.

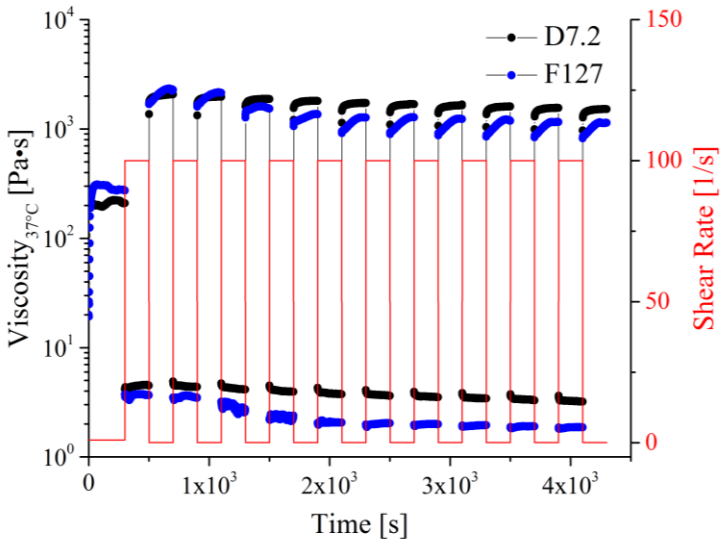

Fig. 4.16| Structure recovery testing performed at 37 °C with viscosity (black curve D7.2 20 wt% and blue curve F127 20 wt%) and applied shear rate (red curve).

4.3.2 Structure Elucidation of the Formed Hydrogel

4.3.2.1 Small Angle Neutron Scattering

SANS measurements were performed at the KWS-1 instrument in cooperation with Dr. Sebastian Jaksch from the Jülich Centre for Neutron Science JCNS at the Heinz Maier-Leibnitz Zentrum in Garching, Germany (Proposal No.: 13096).

As previously remarked, the viscosity profiles of POx-*b*-POzi based hydrogels are different compared to those based on Pluronic F127 and other polymers as reported in the literature. This is likely to be linked to the structure of polymer self-assemblies in water. For many, if not most thermogelling polymers, the gelation is explained through an aggregation of spherical micelles into a cubic lattice (see chapter 2.1.2). Therefore, D2.2 at 20 wt%[340] and D7.2 at different concentrations ranging from 0.01 wt% up to 20 wt% were studied using SANS at different temperatures. SANS was chosen as it offers a good contrast between polymer and solvent (scattering length density (SLD) polymer: $0.834 \cdot 10^{-6}$ Å^{-2}; SLD D_2O: $6.393 \cdot 10^{-6}$ Å^{-2}), while there is little contrast in the case of X-ray scattering (SLD polymer: $9.58 \cdot 10^{-6}$ Å^{-2}; SLD H_2O: $9.46 \cdot 10^{-6}$ Å^{-2}). For the 20 wt% sample of D2.2 a peak around q = 0.03 Å^{-1} with a plateau before the peak and a sharp decay afterwards could be observed (**Fig. 4.17 A**).[340] Initially, a cubic lattice of spherical micelles was assumed following the reports by Mortensen *et al*. on Pluronic based hydrogels[104]. However, unless employing a dispersity of 1, which appears to be physically nonsensical, this fit seemed unsuitable for the obtained SANS data. Instead, a model of a bicontinuous sponge-like structure as developed by Teubner *et al.*[341] described the experimental data very well. From the used model it was possible to extract ξ the correlation length and *d* the characteristic domain size (periodicity) ranging from 50 to 350 Å. Important to note, ξ is a cutoff length, above which correlations are no longer noticeable in the system. With increasing temperature, an increase of *d* and ξ was observed, the latter eventually exceeding the former at approximately 18 °C (**Fig. 4.17 B**). As this is well below T_{Gel} of D2.1 at 20 wt%; ξ apparently needs to exceed *d* considerably for a macroscopic rheological response from the system to occur. At temperatures slightly below 30 °C, the increase of ξ levels off what corresponds with the T_{Gel} at ~27 °C (**Fig. 4.10 B**). The shoulder which becomes visible at temperatures of 28 °C and above at approximately q = 0.05 Å^{-1} (**Fig. 4.17 A**, blue line) is indicative of an additional phase besides the bicontinuous hydrogel in the sample. Unfortunately, as the features of that curve are hidden by the predominant scattering of the bicontinuous phase, it could not be further investigated.

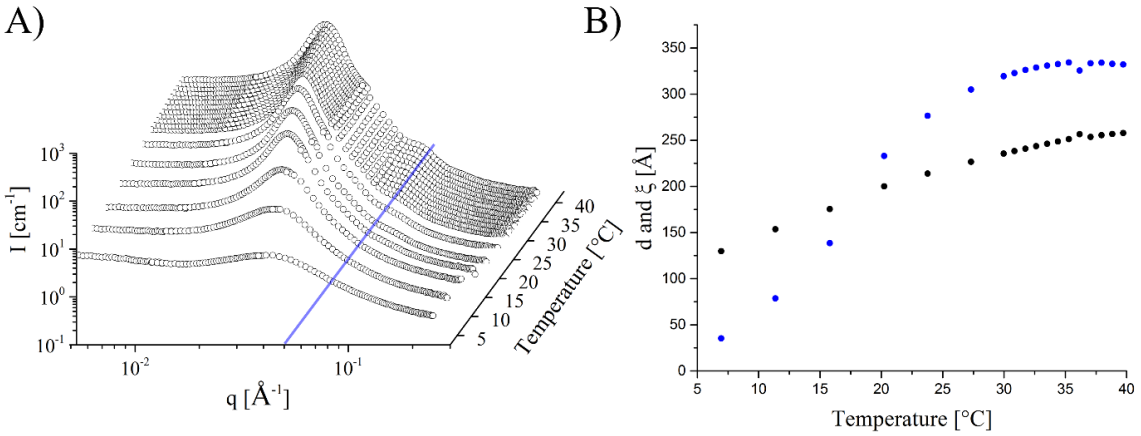

Fig. 4.17| A) SANS scattering data at varying temperatures of 20 wt% D2.1, with a blue line at 0.05 Å^{-1} which was added for better visibility of the second shoulder. B) Resulting correlation length ξ (blue dots) and characteristic domain size *d* (black dots) of an aqueous solution of 20 wt% D2.1.

To better understand the processes that cause the thermogelation, a more detailed study was conducted using D7.2 at different concentrations. Unfortunately, 24 °C was the highest temperature investigated in these experiments due to an unplanned reactor shut down during allocated beam time. A direct comparison of D2.1 and D7.2, both at 20 wt%, revealed some similarities but also significant differences which were possibly caused by the different chain length. As described for D2.1, a peak around q = 0.02 Å^{-1} with a plateau before the peak and a sharp decay afterward could be observed for D7.2 (**Fig. 4.18 A**). While the SANS scattering data of D2.1 showed an isotropic structure over the whole temperature range, a transition from an isotropic to an anisotropic structure occurs for D7.2 at ~15 °C (**Fig. 4.18 A – C**). This coincides with the second increase of G' observed via rheological experiments (**Fig. 4.12 B**). The anisotropic structure leads to an unsymmetrical 2D scattering image (**Fig. 4.18 B**) whereas the isotropic structure which occurred below 15 °C leads to a homogenous circular 2D scattering image (**Fig. 4.18 C**). It is assumed that a gyroid structure is formed although the characteristic 10-spot pattern which was reported by Vigild *et al.* under shear conditions[342] could not be clearly observed. Important to note, all SANS experiments discussed in the present work were performed under static conditions and therefore no shear alignment could be performed. Unfortunately, no fit model for a gyroid was available for the established SANS evaluation software, thus only a qualitative analysis was possible at the moment. Nevertheless, it was possible to sketch a phase diagram based on the obtained data. At low concentrations (0.5 wt%) temperature induced aggregation of D7.2 in water can be observed as single Gaussian chains were present up to

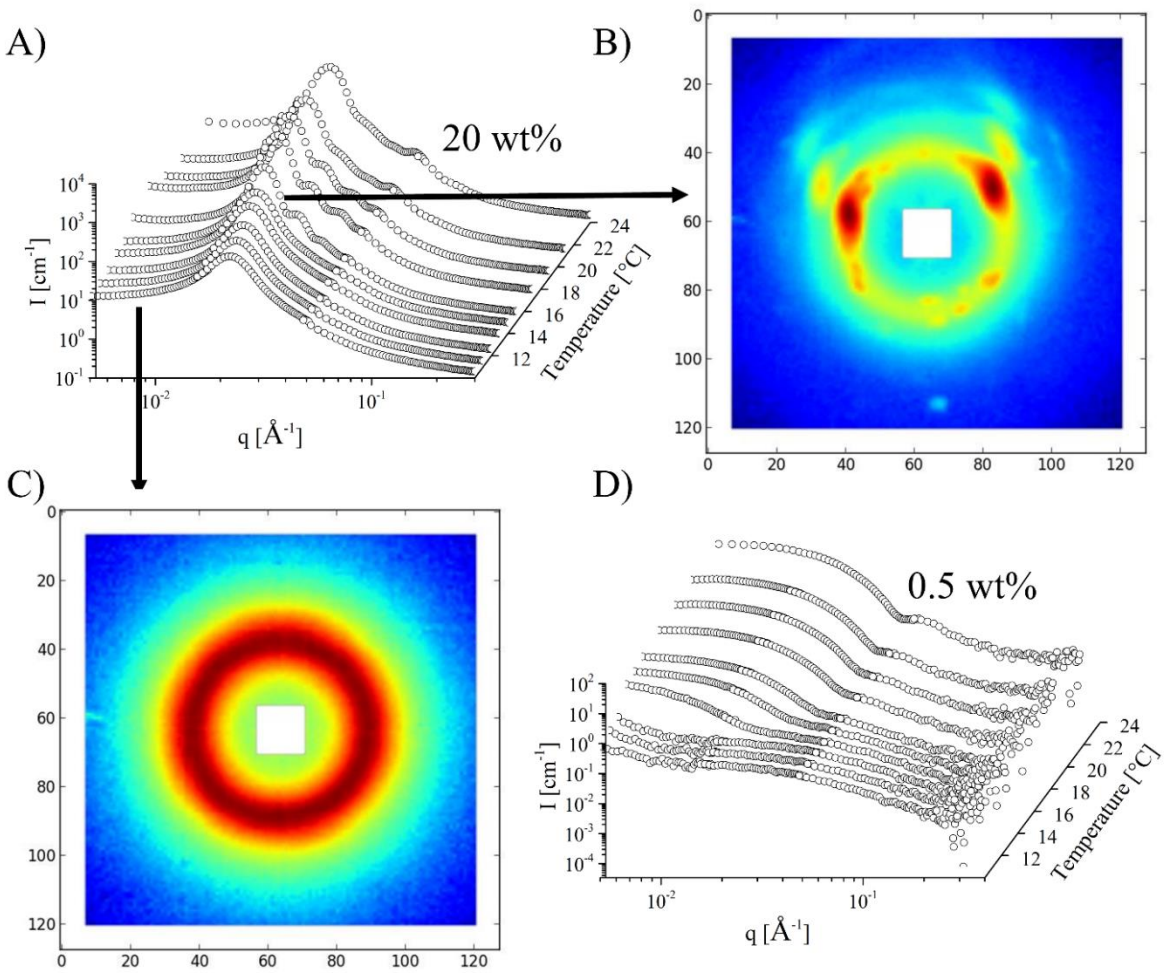

Fig. 4.18| A) SANS scattering data at varying temperatures of 20 wt% D7.2, B) 2D scattering image at a sample-detector distance (SDD) of 7.61 m at 15 °C, C) 2D scattering image at a SDD of 7.61 m at 10 °C, and D) SANS scattering data at varying temperatures of 0.5 wt% D7.2. All SANS experiments were conducted under static conditions.

12 °C (first three temperatures measured) while formation of presumable spherical aggregates occurred above 13 °C (**Fig. 4.18 D**). This corresponds to the T_{CP} of P*n*PrOzi as homopolymer as already mentioned previously.

In summary, four different phases could be identified via SANS experiments (**Fig. 4.19**). These depend on the polymer concentration as well as on the temperature. At low polymer concentrations and low temperatures single chains could be identified. Increasing the hydrophilic contrast be either increasing temperature or polymer concentration caused aggregation. Even higher concentrations resulted in the formation of a bicontinuous sponge-like structure which was already identified for D2.1 at 20 wt%. This structure is already formed at concentrations (e.g. 10 wt%) which did not cause macroscopic gelation but a turbid liquid. Therefore, formation of a sponge-like structure

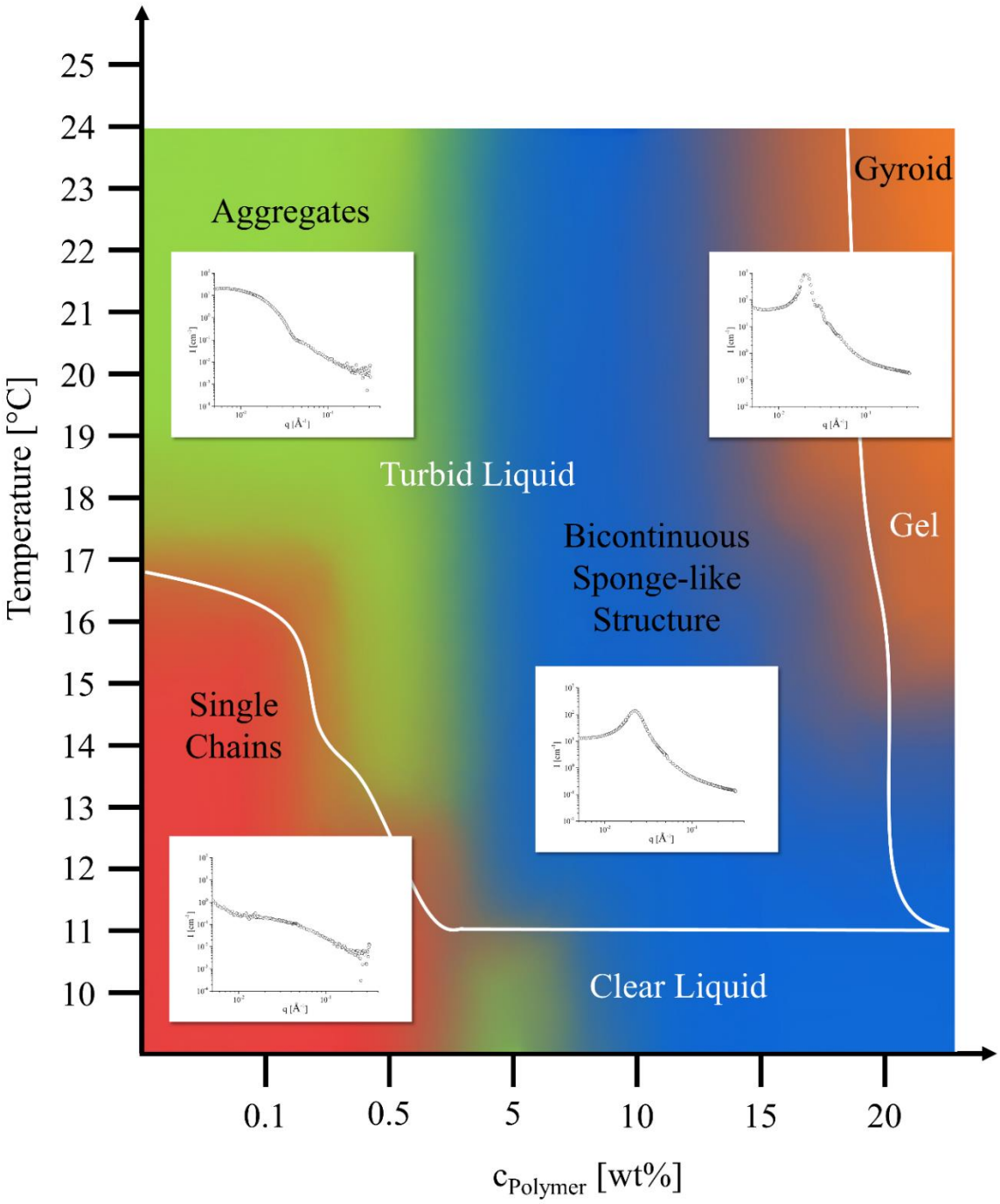

Fig. 4.19| Phase diagram of D7.2 in water deduced from SANS data at different concentrations (0.1 wt% - 20 wt%) and temperatures (10 – 24 °C). Depicted scattering data are representative for the respective phase (black lettering). The physical appearance of the aqueous polymer solution is delineated and lettered in white.

can be interpreted as formation of small domains with a gel like character. However, the correlation length of these nanogels is too small to induce the formation of a macroscopic gel. At concentrations above 20 wt% macroscopic gels are formed at 11 °C which exhibit a sponge-like structure below 15 °C and transform into a more ordered gyroid structure at

higher temperatures. Further phase transitions which probably occur at higher temperatures have not been investigated in the course of the present study.

Based on the sponge-like or gyroid structure it is conceivable that liquids and small molecules can freely move through the channels of the interpenetrating network which is beneficial for the supply of embedded cells with e.g. nutrients. This assumption is corroborated by DOSY experiments which were performed in cooperation with Dr. Matthias Grüne from the Julius-Maximilians University, Wuerzburg. It was possible to show that the diffusion coefficient of HDO decreased only slightly (compare HDO in gel: $1.29 \cdot 10^{-9}$ $m^2 \cdot s^{-1}$ vs. 1% HDO in D_2O: $1.91 \cdot 10^{-9}$ $m^2 \cdot s^{-1}$) in the hydrogel (20 wt% D7.2, 25 °C). A quick estimation of the average diffusion distance according to the Einstein-Smoluchowksi-equation (**eq. 4.4**) revealed values of approximately 11 µm during the measurement time of 50 ms.

$$\Delta x = \sqrt{2 * D * t_{\Delta x}} \qquad \text{(eq. 4.4)}$$

with Δx the diffusion distance, D the diffusion coefficient, and $t_{\Delta x}$ the diffusion time.

There is strong evidence that HDO is not trapped inside pores but can rather freely diffuse through the sponge-like structure. However, it is important to determine the cut-off size above which diffusion processes are significantly slowed down by the microstructure of the gel. This can either be done by DOSY NMR spectroscopy or by fluorescence recovery after photobleaching. For the latter, dextranes with different molecular weight coupled to a fluorescent molecule such as fluorescein isothiocyanate could be utilized.

Another indication for the formation of a sponge-like structure was provided via SEM which was performed on lyophilized samples and revealed a highly porous structure (**Fig. 4.20 A**). However, these results have to be treated with caution as sample preparation including lyophilization is not ideally suitable due to the thermoresponsive character of the gels and can therefore influence the visible structure. Nevertheless, a direct comparison with an equally prepared F127 specimen (**Fig. 4.20 B**) showed significant differences as no pores could be detected. Important to note, the displayed sections are representative for the whole samples as several parts have been investigated. To be able to draw a trustworthy conclusion based on SEM it is crucial to implement proper sample preparation and to perform cryo-SEM experiments in combination with focused ion beam. This would allow

the imaging of the hydrogel structure in high resolution and 3D and could finally prove the proposed structure based on SANS.

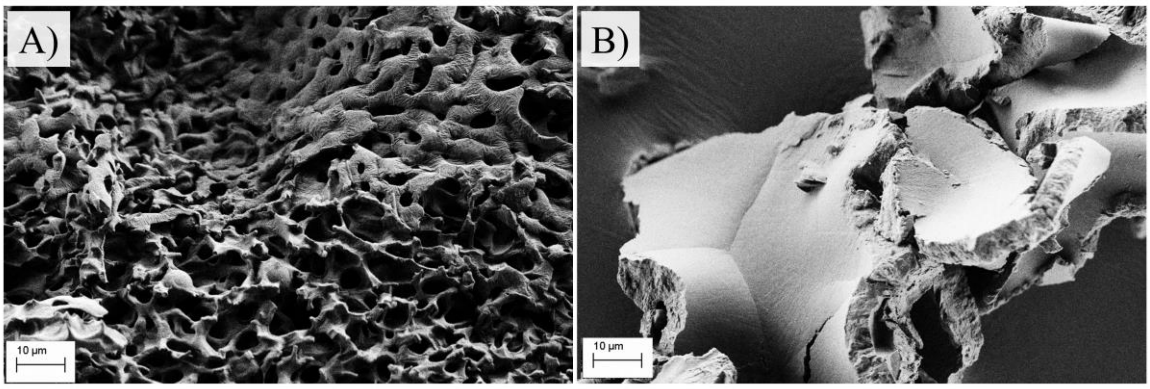

Fig. 4.20| SEM images of A) D7.2 and B) Pluronic F127. SEM: Magnification 1000 X at 2.00 kV and working distance 2.0 mm for both samples.

4.3.2.2 Dynamic and Static Light Scattering

To further characterize the block copolymers, elucidate the structure of the formed gel and to better understand the gelation process, SLS and DLS were performed in cooperation with Dr. Karl Fischer from the Johannes-Guthenberg-University in Mainz. However, before performing light scattering on physical cross-linked POx-*b*-POzi gels in a selective solvent e.g. water, it is necessary, to characterize the single molecule in an overall good solvent and to gain a basic understanding of what is actually happening at low concentrations in water as a selective solvent, where the occurrence of aggregation is to be expected. Therefore, initially, the solutions of D2.6 (20 g/L) and D7.2 (10 g/L) in methanol were investigated. Methanol is the solvent of choice, as it is a thermodynamically good solvent for both block copolymer constituent homopolymers. Furthermore due to a nearly identical refractive index compared to water, it allows further structural insight and conclusion of the aggregates formed in aqueous medium (*vide infra*).

In order to remove contaminations both samples were filtered through Millipore Millex-LG (hydrophilic PTFE, 200 nm pore size) syringe filters. Subsequently, angular dependent DLS measurements were performed of the solutions of D2.6 and D7.2 in MeOH. Since small angles are particularly sensitive for larger particles and scatter orders of magnitude more light as compared to larger angles, the correlation function $g_1(t)$ is plotted at the scattering angle $\Theta = 30°$ in order to investigate the isolated solutions of both unimers (**Fig. 4.21**).[343] The observed monoexponential decay is strong evidence for the presence of molecular dissolved unimers of D2.6 and D7.2, respectively. Fitting a regression line in

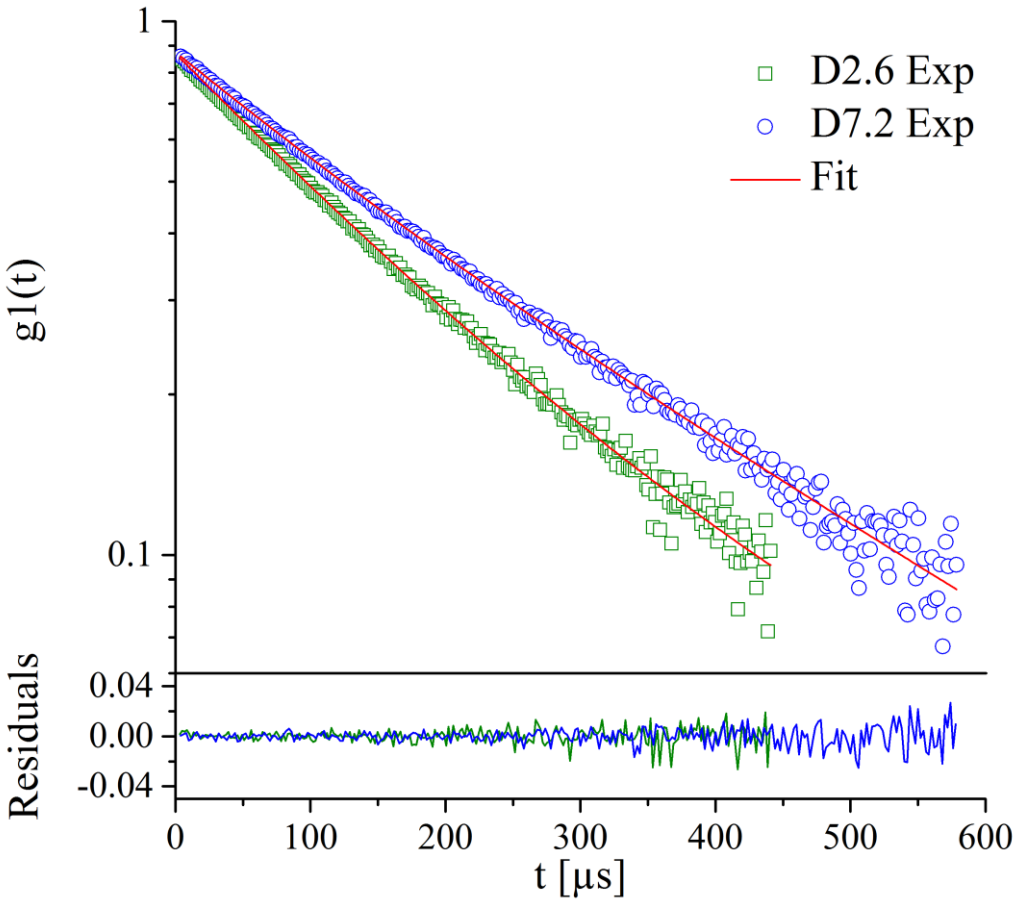

Fig. 4.21| Correlation function $g_1(t)$ at the scattering angle $\Theta = 30°$ for isolated solutions of polymer D2.6 (green square, 20 g/L) and D7.2 (blue circle, 10 g/L) in methanol and regression line (red). The residuals of the single fits are depicted at the bottom.

the $\ln(g_1(t))$ versus t plot yields a slope of q^2D (with D the Brownian diffusion coefficient). D is then translated into a hydrodynamic radius R_h by using the Stokes-Einstein equation (**eq. 4.5**) and yields $R_h = 2.8$ nm for D2.6 and $R_h = 3.7$ nm for D7.2, respectively. The values are both in the range expected for molecularly dissolved random coil polymers with a molar mass of 11.3 kg/mol and 22.3 kg/mol.

$$D = \frac{k_B T}{6\pi\eta R} \qquad \text{(eq. 4.5)}$$

Afterwards, highly diluted polymer solutions of D7.2 in methanol (1 g/L) and MilliQ water (6 mg/L) were measured via SLS at the angles starting from 30 ° to 150 ° in 5 ° steps. As expected, no angle dependency could be determined for the methanol sample as both blocks are readily dissolved and no aggregates are formed (data not shown). Data obtained for the water sample were analyzed via Berry Plot (**Fig. 4.22 A)** as a Zimm plot

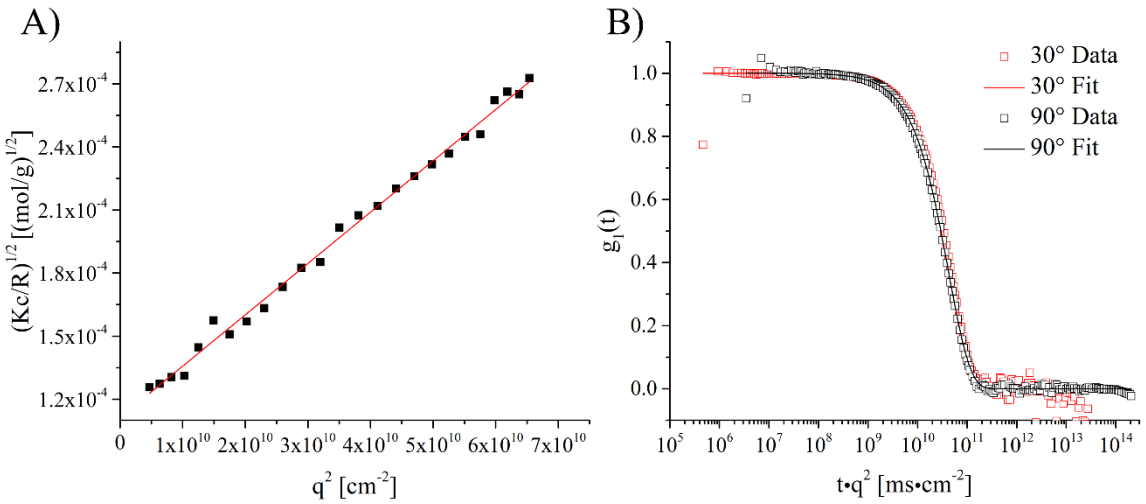

Fig. 4.22| A) Berry plot (black squares) and linear regression (red; slope (s) = 2.44E-15 $\frac{\sqrt{\frac{mol}{g}}}{cm^{-2}}$, axis intercept (a) = 1.11E-4 $\sqrt{\frac{mol}{g}}$) for a solution of D7.2 (6 mg/L) in MilliQ water. B) Experimental (Θ = 30°, red squares, and Θ = 90°, black squares) and fitted autocorrelation functions (red and black lines) for a solution of D7.2 (6 mg/L) in MilliQ water.

was bended upwards what is indicative for spherical aggregates of limited polydispersity. According to **eq. 4.6**, the apparent weight-average molar mass is given as reciprocal value of the square of the axial intercept obtained by extrapolation (**Tab. 4.7**). Here, the second viral coefficient A_2 is neglected due to heavy dilution.

$$\sqrt{\frac{Kc}{R_\theta}} = \sqrt{\frac{1}{M_W}} * \left(1 + \frac{1}{6}\langle R_G^2\rangle q^2 + \ldots\right) \qquad \text{(eq. 4.6)}$$

The refractive index increment (dn/dc) which has not been explicitly determined for the polymer solutions, is rather similar for water (1.333) and methanol (1.3288) and therefore the aggregation number is given by the ratio of the axis intercepts (**Tab. 4.7**).Furthermore, SLS also yields the radius of gyration R_g (**Tab. 4.7**) which can by calculated from the slope (s) and axis intercept (a) according to **eq. 4.7** (**Fig. 4.22 A**).

$$R_g = \sqrt{\frac{6 * s}{a}} \qquad \text{(eq. 4.7)}$$

Table 4.7| Characterization of aggregates of D7.2 in MilliQ water via dynamic and static light scattering.

ID	M_{unimer}[a] [kg/mol]	M_{app}[b] [kg/mol]	N_{agg}[b]	R_g[b] [nm]	R_h[c] [nm]	ρ-ratio	Apparent polymer density in the vesicle shell [g/cm³]
D7.2	22.3	80640	~1500	115	116	0.99	0.036

[a] obtained by ^{1}H NMR spectroscopy; [b] obtained by static light scattering; [c] obtained by dynamic light scattering

Additionally, DLS experiments were performed on the same highly diluted sample and revealed no scattering angle dependency (**Fig. 4.22 B**). Plotting the D values obtained for angles from 30 ° to 158 ° in 17 ° steps versus q^2 and extrapolating against zero yields an apparent diffusion coefficient (D_{app} = 1.86•10^{-8} cm^2•s^{-1}) which is again converted into R_h (**Tab. 4.7**) by using the Stokes-Einstein equation.

The so-called ρ-ratio is an experimental quantity derived from combining the particle size characteristics determined from static (R_g) and dynamic light scattering (R_h) measurements. For a vesicle (with limited shell thickness compared to size e.g. infinitesimally thin), which can also be described as hollow sphere, the ρ-ratio equals 1 whereas for homogenous spheres a value of 0.775 is theoretically expected and reported.[344] The ρ-ratio calculated for D7.2 (**Tab. 4.7)** perfectly fits the value for hollow spheres what suggest their existence at very low polymer concentrations. To examine if this is a physically meaningful conclusion the apparent polymer density in the vesicle shell was calculated according to **eq. 4.8**. It is assumed, that the shell of the vesicle is approximately as thick as twice the R_h of one unimer (~3.7 nm). In the interest of simplification, a shell thickness of 10 nm was assumed. With a CMC around 1 mg/L (**Fig. 4.23 A**), the concentration of freely dissolved diblock copolymer is negligible on molar mass determination of the aggregate; a lower limit density of 0.036 g/cc and an upper limit of 0.07 g/cc occurs to be realistic for a vesicle shell and further corroborates the theory of their formation.

$$\rho = \frac{M}{V} = \frac{\frac{N_{Agg} * M_{Unimer}}{N_A}}{\left(\frac{4}{3} * \pi * (R_1^3 - R_2^3)\right)} \qquad \text{(eq. 4.8)}$$

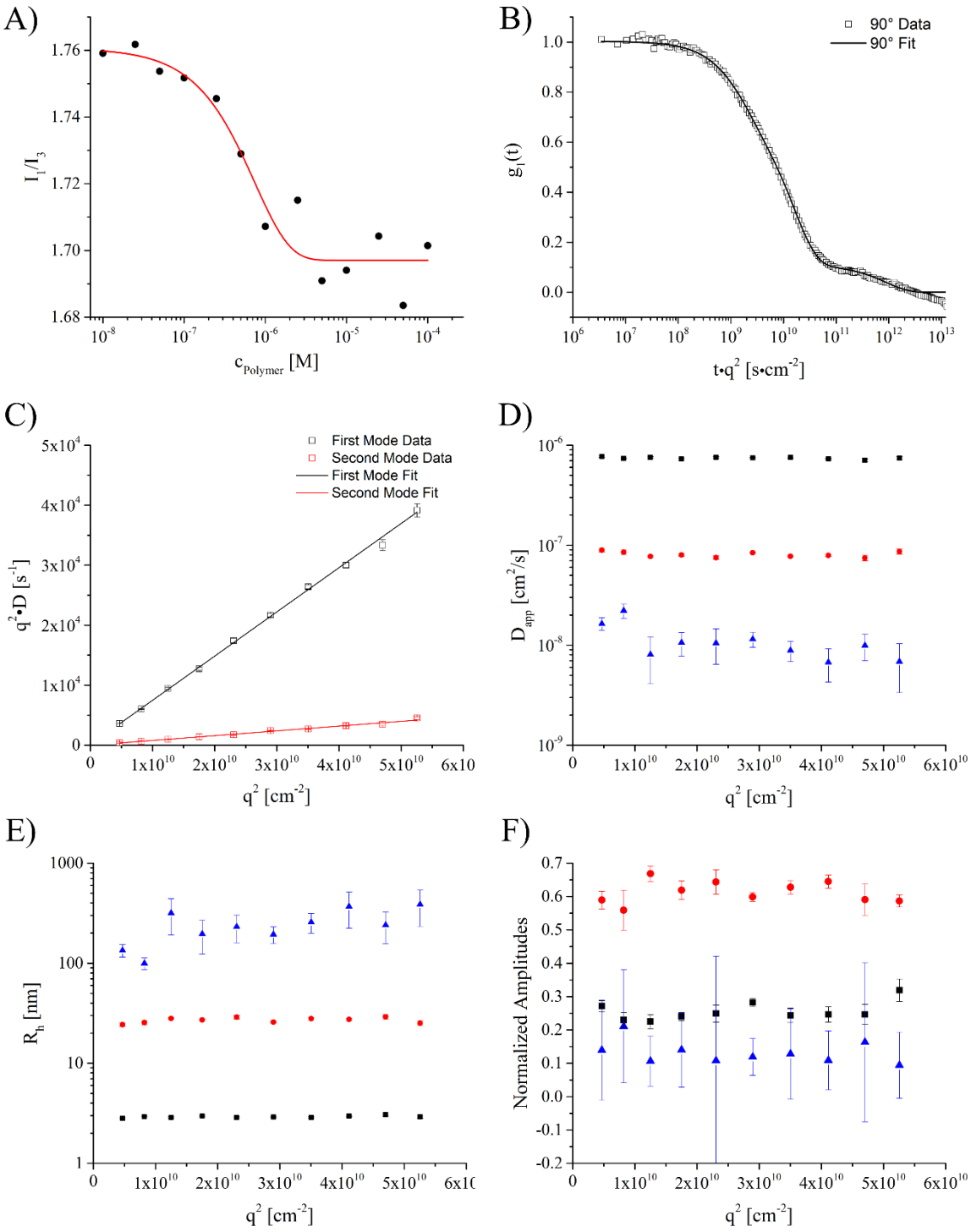

Fig. 4.23| A) I_1/I_3 ratio (pyrene assay) in dependence of the diblock copolymer (D7.2) concentration with corresponding fit (Boltzmann function). B) Experimental (Θ = 90°, black squares) and fitted autocorrelation function (black line) for a solution of P7.2 (250 g/L) in MilliQ at 25 °C in the gel state. C) q^2•D versus q^2 for the first and second mode for D7.2 based hydrogel (250 g/L). D) D_{app} versus q^2 for three modes of D7.2 in MilliQ water. E) Hydrodynamic correlation length (R_h) calculated from the diffusion coefficients for three modes as a function of q^2. F) Normalized amplitudes versus q^2 for three modes of D7.2 in MilliQ water. Values are presented as means ± SD (n = 10).

These findings complete the phase diagram developed on SANS data in the previous chapter as vesicles with a R_h of approximately ~116 nm are too large to detectable in the SANS experiments.

Unfortunately, it was not possible to perform a comparable in-depth study with solutions of D2.6. Even at very low concentrations a colloidal precipitation was observed resulting in metastable aggregates with a size of several µm. For this purpose, no meaningful light scattering experiments could be conducted. These observation might be attributed to the lower DP of the hydrophilic chain which might be too short to ensure a proper stabilization of the formed aggregates. However, it is interesting that the D2.X polymers still form hydrogels at a concentration of 20 wt% which exhibit comparable mechanical properties and form the same micro- and nano-structure then gels formed by D7.X polymers.

Based on the results described above, 2 mL of hydrogel were prepared by dissolving 500 mg of D7.2 in MilliQ water which was filtered through a Millipore Millex VV (hydrophilic PVDF, 100 nm pore size) syringe filter prior to use. Due to its higher viscosity even at low temperatures the polymer solution could not be filtered and was used without further purification. Thus, it was necessary to manually exclude the existence of scatter centers like air bubbles or small dust particles before every measurement. DLS was measured at the angles starting from 30° to 120° in 10° steps. For each angle 10 auto correlation functions (ACF) were recorded (exemplarily shown at 90°, **Fig. 4.23 B**) whereby the cuvette was slightly turned after every measurement. Subsequently, the obtained data were fitted with a triexponential function as described in chapter 7.1.2 and the mean value as well as the standard deviation of the diffusion coefficients for all three modes were calculated. The product of D and q^2 is plotted versus q^2 in order to verify the diffusivity of the individual processes (**Fig. 4.23 C**). The resulting straight line through the origin for the first and second mode is strong evidence for the diffusive character of these processes. The third mode did not show a linear correlation and was therefore excluded from **Fig. 4.23 C**. As described previously, the diffusion coefficient (**Fig. 4.23 D**) was converted into R_h and yields R_h = 3 nm and R_h = 24 nm for the first and second mode, respectively (**Fig. 4.23 E**). However, it is important to note that in the context of hydrogels R_h cannot be regarded as a hydrodynamic radius of an equivalent sphere. Indeed, it must be considered as hydrodynamic correlation length. As the hydrodynamic correlation length of 3 nm is slightly smaller than the coil size determined for unimers of D7.2 this mode can

potentially be attributed to the external hydrophilic PMeOx block which is present on the inner surface of the gyroid and might be moving in water. The second mode with a hydrodynamic correlation length of 24 nm could be assigned to several structures not allowing for a definite statement. However, it corresponds quite well to the values found via SANS for the correlation length (30 – 35 nm) of a hydrogel formed by D2.2. Apart from that, it might also be attributed to the double layer although the values appear slightly too large.

The angle independency of the normalized amplitudes (**Fig. 4.23 F**) verifies the correctness of the chosen fitting approach as it is consistent over the whole q^2 range. The middle mode (red dots) was the strongest with a share of 60%. For the slowest mode (blue triangles) one would expect an increasing of D_{app} and a decrease of the amplitude with q^2. However, with a contribution of approximately 10% this was too small to be detected. Theoretically, it should be also possible to perform SLS experiments on the discussed hydrogels to further elucidate the micro- and nanostructure. However, the slowest mode is highly problematical for SLS experiments as small amplitudes do have a very strong effect on static heterogeneities.

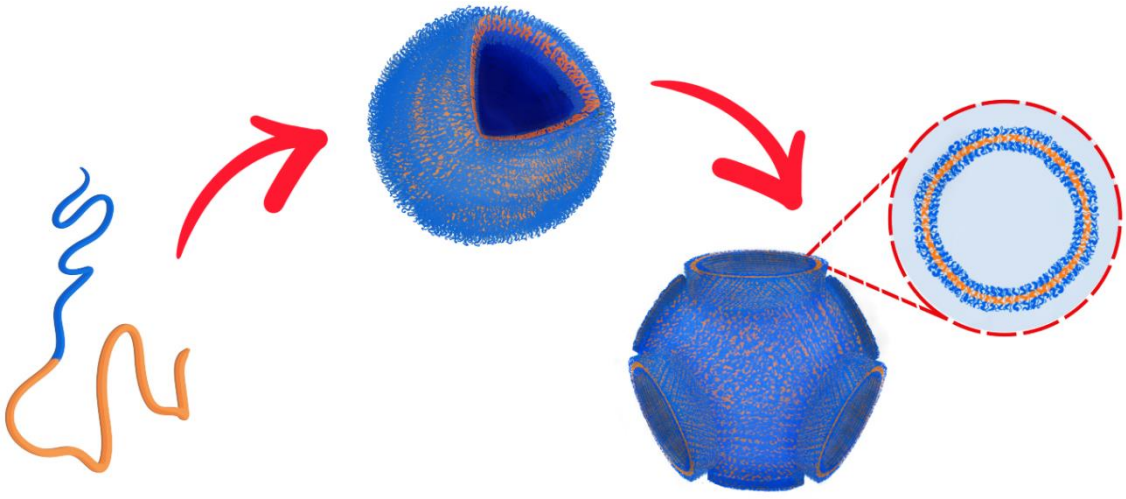

Fig. 4.24| Schematic presentation of the transition from a dissolved amphiphilic diblock copolymer into polymersomes which might cause the formation of a bicontinuous network at higher concentration. The detail of the bicontinuous network shows the tubular connection to neighboring polymersomes.

In conclusion, by performing dynamic and static light scattering it was possible to further elucidate the nanostructure of the POx-*b*-POzi based hydrogel and to corroborate findings made by SANS. Furthermore, investigating diluted polymer solutions in MeOH and MilliQ water revealed the size of the unimers of polymers D2.6 and D7.2 and the highly

probable formation of vesicles what complements the phase diagram (**Fig. 4.19**) at lower concentrations at 20 °C. Based on these findings, it is possible propose a hypothesis for the formation of a gyroid structure at higher polymer concentrations (**Fig. 4.24**). The formation of a lamellar structure already at low concentrations forms the basis. These hollow spheres grow and probably stick together with increasing concentration. At a certain point a transition probably occurs where the vesicles break and the bicontinuous network is formed. Obviously, to confirm this hypothesis, a multiplicity of light scattering experiments have to be conducted under controlled conditions. In this context it would be crucial to ensure the synthesis to be light scattering suitable from the very first step of synthesis.

4.3.3 Conclusion

To conclude, it could be demonstrated that aqueous solutions of PMeOx-*b*-P*n*PrOzi copolymers show temperature induced gelation above a polymer concentration of 20 wt%. By changing the DP it was possible to adjust T_{Gel} what is beneficial when aiming for a broad field of applications. Additionally, it could be shown that variations of the end group did not significantly influence the gelation behavior what allows for the introduction of functional groups like alkynes. In contrast, using cell culture medium instead of MilliQ water revealed an influence on T_{Gel} indicating the importance of working as close as possible to real conditions in the evaluation experiments. Furthermore, POx-*b*-POzi based hydrogels exhibited a highly shear thinning character in combination with an excellent recovery behavior both indicating printability. The yield point, determined by shear stress sweep, was found to be higher than for Pluronic F127 solutions with equal polymer concentrations which is another evidence for the printability of the material.

SANS, DLS, and SLS have been applied to resolve the structure of the formed hydrogel and to understand the phase transitions occurring in aqueous solution depending on polymer concentration and temperature. Taken together, it was possible to:

- estimate the size of the unimers by using a non-selective solvent,
- determine the formation of a bicontinuous sponge-like structure above 5 wt% and 11 °C,
- and the development of a gyroid phase at 15 wt% and 17 °C or 20 wt% and 14 °C, respectively.

DOSY experiments performed in the gel state revealed only a slight decrease of the diffusion coefficient of HDO compared to HDO in D_2O, indicating that water can move almost unimpeded in a macroscopic solid gel.

According to the classifications proposed by Flory or Russo (chapter 2.1) it is reasonable to regard the investigated POx-*b*-POzi based hydrogels as Flory-Type I gels or so-called *Lattice gels*, respectively.

4.4 Applicability of Poly(2-oxazoline)-block-Poly(2-oxazine) Based Hydrogels as a Biomaterial

Another major requirement for bioinks, identified by Murphy and Atala (see chapter 2.3.3) is biocompatibility. Although one might argue about the usefulness of the term and a clear definition strongly depends on the field, the assertion behind that term summarizes many aspects. A very important, however in the context of hydrogels sometimes neglected one, is the sterilization process. Regarding medical devices which are used every day in the clinic, sterilizability is only a minor issue, especially for metal and glass objects as they are more resistant to heat compared to the most polymers. Another very important aspect that should addressed very early during the bioink development process is cytotoxicity, as low cytocompatibility naturally is an exclusion criteria for the use in biofabrication.

4.4.1 Sterilizability

Several sterilization processes like, heat sterilization, gas sterilization, chemical sterilization, or radiation are generally available. However, sterilization is known to potentially change the physicochemical and mechanical properties of polymers and hydrogels, e.g. by inducing cross-linking or, in contrast, degradation. Sterile filtration, which is frequently used for diluted polymer solutions is not directly applicable here as the high polymer concentration would cause clogging of the filter. Therefore, two different sterilization techniques, namely γ-irradiation at a radiation dose of 25 kGy and autoclaving were applied to D7.2 and the effects were analyzed via GPC and rheology.

Although, a monomodal molar mass distribution could be observed in the GPC elugram after autoclaving and after γ-irradiation, a significantly different progression was detected (**Fig. 4.25 A**). The elugram obtained after autoclaving was virtually congruent with the one measured before sterilization causing only minor deviation of the extracted values for M_n and Đ (**Tab. 4.8**). In contrast, the elugram obtained after γ-sterilization revealed a significantly more pronounced low molecular tailing (higher elution volumes) resulting in a broader molar mass distribution translating into a lower M_n (4.7 kg/mol) as well as a higher dispersity (Đ = 1.80). These findings correlate with other studies dealing with γ-irradiation of polymers. For example, Lee *et al.* investigated the influence of γ-rays in the dose range of 10-500 kGy on aqueous solution of alginate, a commonly used material for the preparation of bioinks.[345] They also found a decrease in molecular weight, and as a result a decrease of viscosity. Furthermore, an exponential increase in degradation even at

the lowest radiation dose investigated was reported. Very recently, Sedlacek *et al.* reported a decrease of molar mass accompanying with an increase of dispersity for PEtOx (20 kDa) if irradiated with γ-rays (up to 50 kGy) in bulk.[231]

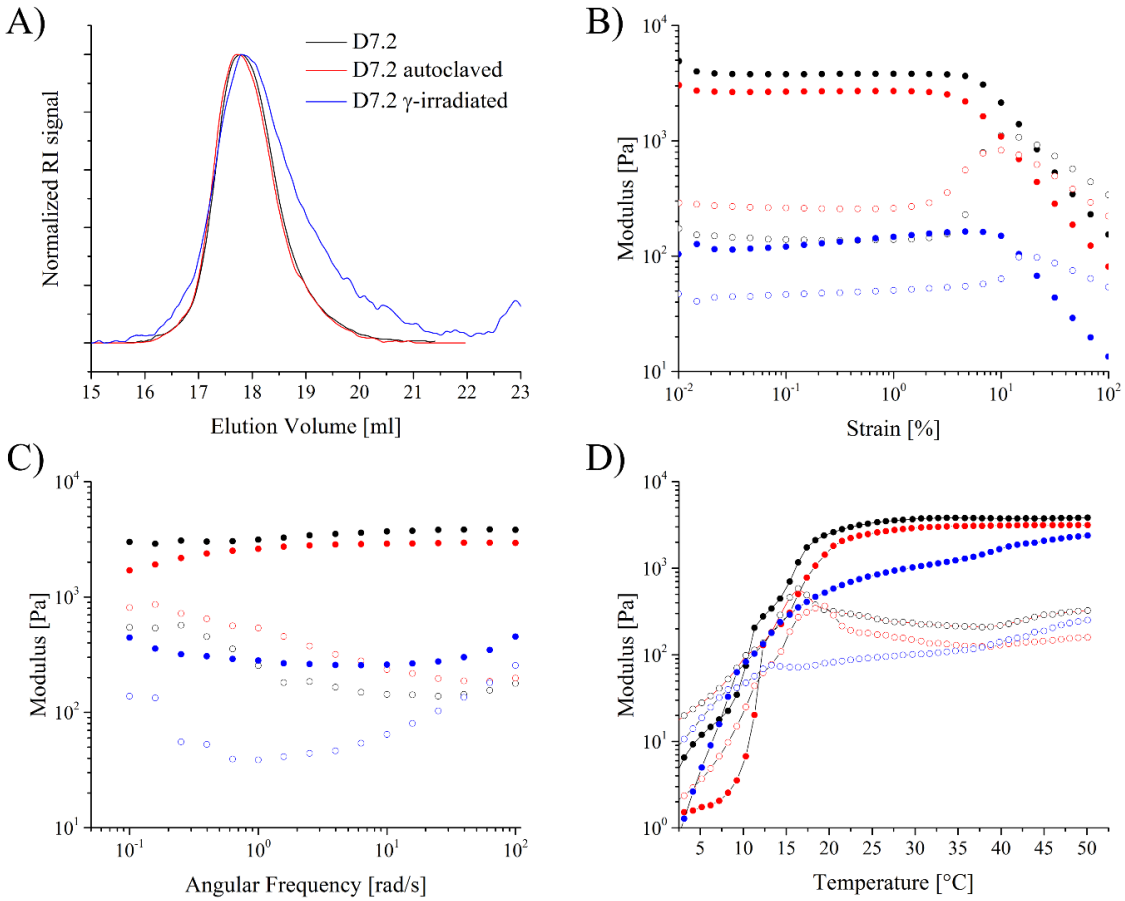

Fig. 4.25| A) Normalized GPC traces of D7.2 after synthesis and after sterilization by autoclaving and γ-irradiation. B) Amplitude sweeps at constant angular frequency of 10 rad/s at 37 °C of D7.2 before and after sterilization. Filled circles represent G', empty circles represent G''. C) Frequency sweeps at constant strain of 0.01% at 37 °C. D) Temperature-dependent rheology of D7.2.

Table 4.8| Molar masses [kg/mol] and Đ of D7.2 after synthesis and after sterilization by autoclaving and γ-irradiation obtained via GPC with HFIP as eluent. $\gamma_{L\ [\%]}$, T_{Gel} [°C], $G'_{Plateau}$ [kPa], and tan δ obtained via rheological measurements in oscillatory mode.

ID	M_n	Đ	γ_L	T_{Gel}	$G'_{Plateau}$	tan δ
D7.2	7.2	1.30	3	11	3.8	0.06
D7.2 autoclaved	7.6	1.28	2	12	3.1	0.04
D7.2 γ-irradiated	4.7	1.80	7	8.5	1.4	0.09

To finally prove the unsuitability of γ-rays for the sterilization of POx-*b*-POzi copolymers the effect on the mechanical properties was investigated via rheological measurements. The performed amplitude sweep (**Fig. 4.25 B**) revealed the formation of a gel at 37 °C but a significantly reduced G' value (compare 3.8 kPa for P7.2 vs. 0.1 kPa for D7.2 γ-irradiated) in the LVE region. In contrast, an increase of γ_L to approximately 7% was observed. Surprisingly, for the autoclaved sample a decrease of G' accompanied by an increase of G'' was observed which was not expected based on the almost identical GPC elugrams. Although, the formed gels appear slightly more viscous in character it is assumed that no difference would be noticed during handling.

The performed frequency sweep after autoclaving showed the expected behavior apart from the decrease of G' at low angular frequencies which was not observable for D7.2 (**Fig. 4.25 C**). This might indicate a lower structure strength at rest, but no creep is estimated as G'>G'' is still fulfilled. After γ-irradiation of D7.2 a different behavior was observed. G' and G'' form a minimum at intermediate angular frequencies (~4 rad/s and ~1 rad/s, respectively) but increase both at higher frequencies. Here a tan δ of 0.6 was calculated which is significantly larger than the values obtained for the untreated and autoclaved polymer (~0.05 and ~0.07, respectively), indicating a very weakly cross-linked gel with a higher amount of unlinked molecules which can move freely. This is in accordance with the low molecular weight tailing found via GPC analysis, as these molecules do probably not contribute to the gel forming structure and act as softeners.

The observation already discussed are reflected by the temperature sweep performed similar to those discussed in chapter 4.3.1. Thermoreversible gelation was observable after either sterilization method, however with significant differences (**Fig. 4.25 D**). Although no clear plateau was formed by G' after γ-sterilization, a steady increase with increasing temperature was visible resulting in hydrogels with acceptable mechanical properties. Autoclaving D7.2 caused a minor decrease of G' but due to the simultaneous decrease of G'' tan δ values are below those of unsterilized D7.2 indicating a slightly more elastic character of the formed gel. However, the changes are so small that they would probably not influence the visual appearance and applicability. Regarding T_{Gel}, γ-sterilization causes a decrease to 8.5 °C whereas autoclaving causes a minor increase by 1 °C, which is probably negligible (**Tab. 4.8**). Consequently, the use of γ-sterilization has to be seen critically as major changes of the chemical structure occurred which resulted in weaker gels which are probably not capable to fulfill the expected requirements.

4.4.2 Cytocompatibility – A Crucial Requirement for Bioinks

Some reports demonstrating the excellent cytocompatibility of POx homo- and copolymers have already been discussed in the course of this study (chapter 2.2.4.2). However, as block copolymers consisting of POx and POzi have never thoroughly been investigated as biomaterial before, their cytocompatibility as well as the cytocompatibility of POzi was unknown.

4.4.2.1 Cytotoxicity of PMeOzi and PEtOzi

This study was performed in cooperation with Zuzana Kroneková from the Polymer Institute in Bratislava, Slovakia, who performed the cell experiments. These data were recently published as a preprint on ChemRxiv (DOI: 10.26434/chemrxiv.5793990.v1)[346] and thus will only be briefly summarized in the following.

Table 4.9| DP obtained by ^{1}H NMR spectroscopy in MeOH-*d*$_4$. Molar masses [kg/mol] and Đ of H1, H3, and H4 obtained via GPC with HFIP as eluent, and IC_{50} after incubation for 24 h with varying polymer concentration ranging from 0.001 g/L up to 100 g/L.

ID	DP	M_n	Đ	IC_{50}
H1	50	2.4	1.32	~70 g/L
H3	50	2.8	1.21	~70 g/L
H4	205	3.1	1.64	~20 g/L

Homopolymers H1, H3, and H4 are water soluble and therefore evaluated with respect to their cytotoxicity against 3T3 mouse fibroblasts subsequent to standard polymer characterization via GPC analysis and ^{1}H NMR spectroscopy (**Tab. 4.9**). The homopolymers were tested at varying concentrations ranging from 0.001 up to 100 g/L for 24 h. Polymers with similar DP but different side chains (H1 and H3) revealed comparable cytotoxicity profiles and IC_{50} values (**Tab. 4.9**). In contrast the two homopolymers with the identical side chain but different DP (H3 (DP = 50) and H4 (DP = 205) showed significantly different cytotoxicity profiles and thus IC_{50} values. The observation that H4 appears more cytotoxic than H3 differs from results for PMeOx and PEtOx for which a decreasing cytotoxicity with increasing molar mass of the polymers was reported.[127,347] However, it is important to note that in all cases, the observed IC_{50} (**Tab. 4.9**) are comparably high and comparable with or several orders of magnitude higher than those of other hydrophilic polymers which are termed non-cytotoxic in the literature. Unfortunately,

it was not possible to investigate the cytotoxicity of *n*PrOzi due to its low T_{CP} (~13 °C) which would have caused precipitation under cell culture conditions.

4.4.2.2 Cytotoxicity of Diblock Copolymers Consisting of PMeOx and PnPrOzi

To gain a first insight into the cytocompatibility of diblock copolymers comprising hydrophilic PMeOx and thermoresponsive P*n*PrOzi cell culture studies were conducted in cooperation with PD Dr. Tessa Lühmann and Marco Saedtler from the Department of Pharmacy and Food Chemistry, Chair for Drug Formulation and Delivery, Julius-Maximilians University, Wuerzburg who performed the cell culture experiments discussed in the following and provided the raw data. On the one hand, murine NIH 3T3 fibroblasts and on the other hand human immortalized keratinocytes (HaCat cells) were cultured at different nongelling concentrations up to 100 g/L for 24 h before using the WST-1-assay to determine cell viability (**Fig. 4.26 A – C**). D2.2 was used for murine fibroblast whereas

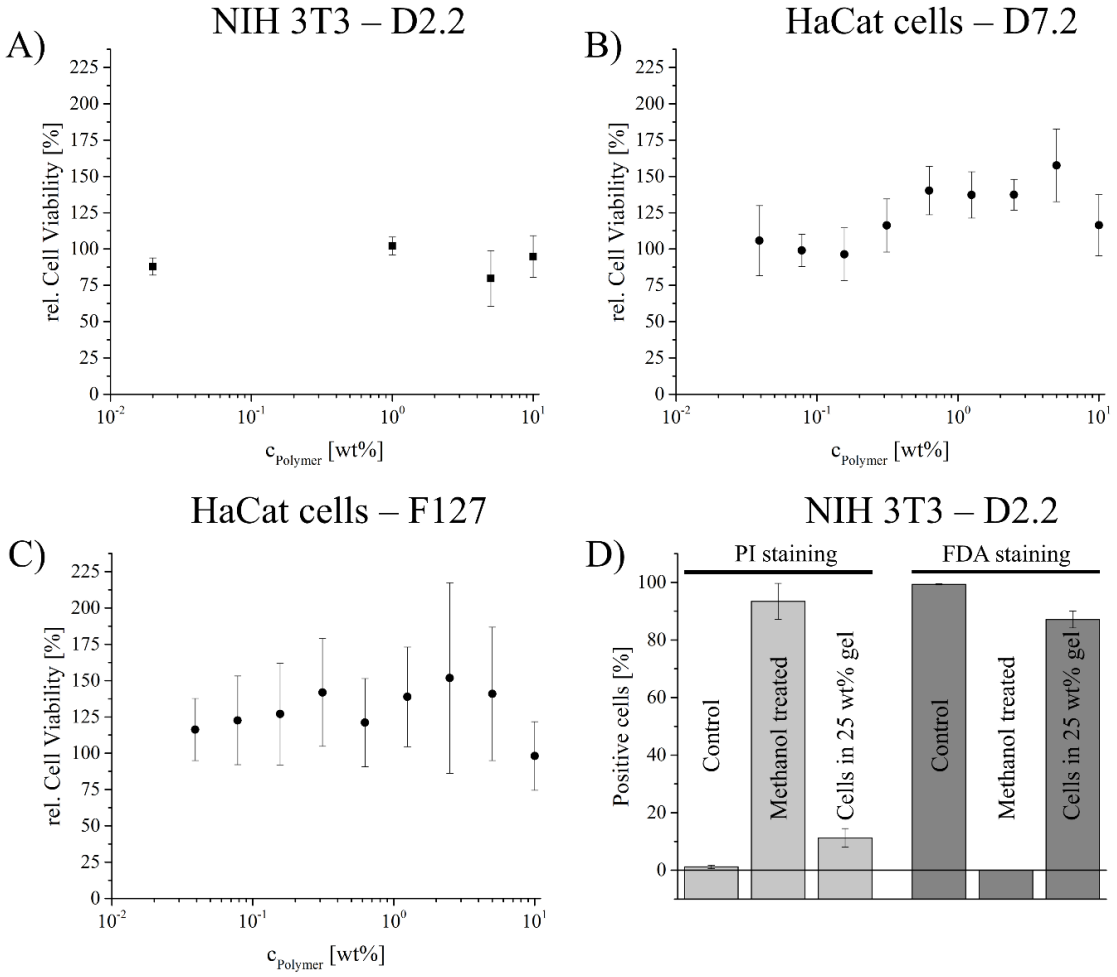

Fig. 4.26| A) Cell viability of NIH 3T3 fibroblasts at nongelling polymer concentrations, B) and C) cell viability of human immortalized keratinocytes (HaCat cells), and D) cell viability of NIH 3T3 fibroblast at polymer concentrations of 25 wt%. Incubation was carried out for 24 h at 37 °C.

D7.2 and Pluronic F127 were used for HaCat cells. No dose-dependent cytotoxicity in murine fibroblasts could observed for D2.2. This is remarkable, as Schubert and co-workers found cytotoxicity well below this concentrations for POx homopolymers.[127,204] Regarding the HaCat cells, again no dose-dependent cytotoxicity could be observed neither for D7.2 nor for F127 up to 10 wt%. However, it is noteworthy that the obtained values showed a relatively strong variation for either polymer. Important to note, the relatively short incubation time of 24 h does not allow for a definitive conclusion regarding the cytotoxicity. For example, Roberts and co-workers observed a significant cytotoxicity of F127 in human liver carcinoma cells[348], however only on the third day of incubation. Furthermore, unpublished data obtained in the working group of Prof. Luxenhofer suggested cytotoxicity of F127 at least in some cell types. These results clearly emphasizes that cytocompatibility of a material can never be derived from cell test with only one cell type. Consequently, the results regarding cytotoxicity obtained for POx-*b*-POzi diblock copolymers have to be regarded as preliminary as extended time periods as well as different cells types have to be investigated to be able to draw a definite conclusion.

Nevertheless, a higher polymer concentration (D2.2, 25 wt%) which caused gelation of the aqueous polymer solution has been investigated against NIH 3T3 fibroblast by using fluorescence-activated cell sorting (FACS). After incubation for 24 h at 37 °C, the temperature was reduced, which resulted into liquefaction of the hydrogel, and cells could be easily retrieved for analysis. Important to note, cells did not sediment during incubation as evidenced by a z-stack analysis of the cell loaded hydrogel.[340] This is beneficial for extrusion based bioprinting (*vide infra*) as a homogenous cell distribution can be ensured even at extended printing times. Also under these conditions, the polymers/gels exhibited very good cytocompatibility. Although a small fraction (11.2 ± 3.2%) was positive for propidium iodide (PI) staining (**Fig. 4.26 D**), the vast majority (87.1 ± 2.9% fluorescein diacetate (FDA) positive) of cells were metabolically active. Important to note, at this point, the bioink does not contain bioinstructive cues such as peptide or sugar moieties; however, these can easily be introduced using the rich polymer analogue modifications available for POx and POzi.[349]

4.4.3 Conclusion

To conclude, it was possible to show that sterilization of POx-*b*-POzi copolymers is generally possible and allows their use as biomaterial, e.g. as bioink. Two sterilization

processes, namely autoclaving and γ-sterilization, have been applied and their influence on the molecular structure as well as on the mechanical properties of the formed gels has been investigated. In this process, it became apparent that γ-sterilization is not ideally suitable as it caused polymer degradation and significantly influenced the mechanical properties as demonstrated by rheological measurements. In contrast, autoclaving had no influence on the molecular structure as evidenced by GPC analysis. Although minor changes of the mechanical properties appeared, no significant influence on the material performance is expected.

In initial cell culture experiments it was shown, for the first time, that PMeOzi and PEtOzi homopolymers appear highly cytocompatible at low DP. PEtOzi with a moderate molecular weight exhibited a lower IC_{50} as the low molecular weight polymer bearing the identical side chain. Regarding the diblock copolymers comprising PMeOx and P*n*PrOzi (D2.2 and D7.2) no dose-dependent cytotoxicity could be observed at nongelling concentrations up to 100 g/L against murine fibroblasts and HaCat cells after incubation for 24 h. Furthermore, cells did not sediment when incubated in the hydrogel and revealed very good cytocompatibility after 24 h.

4.5 Printing of Poly(2-oxazoline)-*block*-Poly(2-oxazine) Based Hydrogels

Due to their shear thinning properties, their recovery behavior, and their very good cytocompatibility, the hydrogels developed in the present work, seemed highly suitable for printing via extrusion-based bioprinting. To be able to work at room temperature without risking unwanted liquefaction, the printing experiments were conducted with batch D7.2 which exhibited a relatively low T_{Gel} (11 °C) and reached a plateau of constant G' values at ~20 °C.

4.5.1 Printing of Cell-free Gels in 2D and 3D

2D experiments were conducted in cooperation with Tomasz Jüngst from the Department for Functional Materials in Medicine and Dentistry, Julius-Maximilians University, Wuerzburg, who was responsible for the used 3DDiscovery bioprinter and provided the G-codes used within the scope of this work.

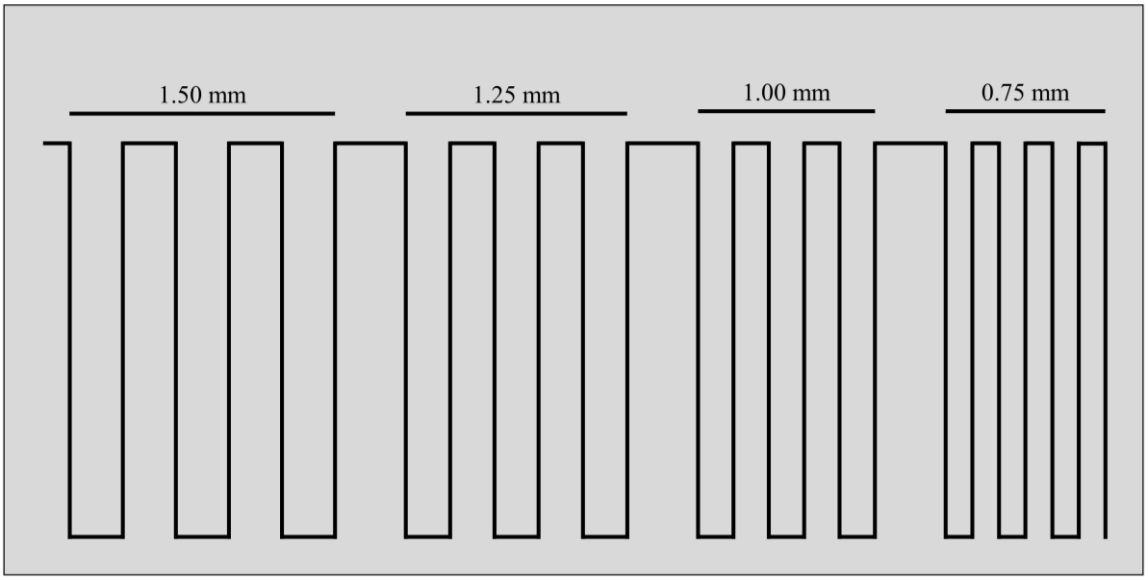

Fig. 4.27| 2D pattern which was printed from right to left to evaluate shape fidelity and minimal printable strand-to-strand distance for cell-free hydrogels. Given distance represents the strand-to-strand distance in the marked region.

During the first experiments which were conducted at room temperature with a 20 wt% solution of D7.2, a restoring force leading to droplet formation could be observed directly after extruding a free hanging hydrogel fiber. To investigate, if this behavior could be suppressed and if it is detrimental for the shape of the printed hydrogel strands, the temperature of the reservoir was varied between 12 °C, thus close above T_{Gel} of D7.2, and

25 °C, while the collector temperature was set to 30 °C. For evaluation, a pattern with stepwise increasing strand-to-strand distance (0.75 mm → 1.0 mm → 1.25 mm → 1.5 mm) was used (**Fig. 4.27**) which allowed determination of the lowest strand distance printable before causing fusion of the single hydrogel strands. A needle with an inner diameter 0.25 mm (25G) was utilized and the pressure was adjusted to 1.2 bar. It was observable that no strand was formed at the needle at 12 °C and only droplets appeared at the tip of the needle. However, it was possible to print the prescribed structure with good shape fidelity at a strand-to-strand distance of 1.25 mm and above (**Fig. 4.28**). Below 1.25 mm the single strands fuse into each other and form a more or less continuous surface. Although the result of the printing process did not significantly change at 13 °C and 14 °C, strand formation followed by droplet formation due to restoring forces on the nozzle could be observed at a reservoir temperature of 14 °C. Further increasing the temperature resulted in an increasing length of the formed hydrogel strand at the nozzle, however droplet formation still occurred. Interestingly, the strand-to-strand distance which could be printed decreased further as the formation of a continuous surface already occurred at 1.25 mm strand distance. From rheological experiments and SANS measurement it is known that at 15 °C a phase transition occurs what results in the second increase of G' that might influence the

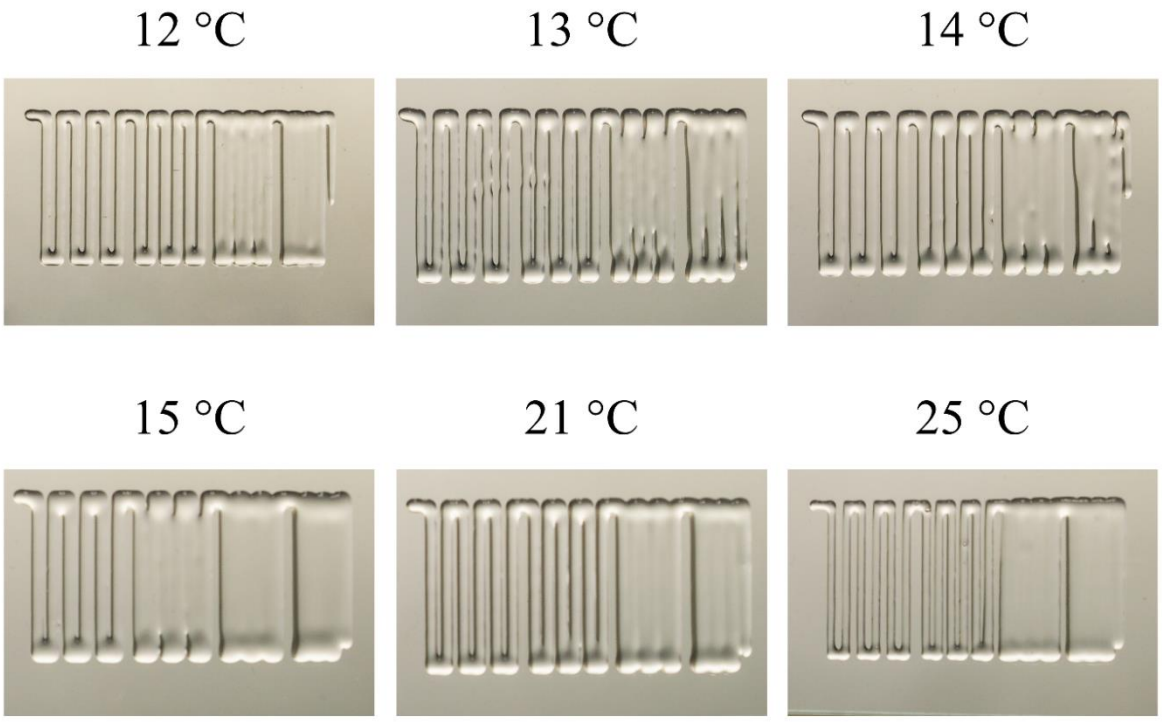

Fig. 4.28| 2D printed pattern for assessing minimal strand-to-strand distance and shape fidelity at different reservoir temperatures. For all experiments the collector plate was heated to 30 °C and the pattern was printed onto glass microscope slides. Pictures were taken 1 min after removing the microscope from the collector plate in an upright position.

recovery behavior of the hydrogel when printed at this specific temperature. However, it is highly speculative to directly correlate these findings with each other. Higher temperatures of 21 °C and 25 °C showed a clear separation of the individual strands at distance of 1.25 mm comparable to results obtained at 12 °C, although contraction of the free-hanging hydrogel fiber (several cm) could still be observed. Therefore, it is assumed that the droplet formation due to contraction of the fiber did not significantly influence the result of the printing process. However, the reason for this behavior remains unknown and was not further investigated. Presumably, it is caused by the micro- and nanostructure of the hydrogel in aqueous solution as Pluronic F127 exhibits a different gelation mechanism and did not show any contraction. In contrast, it is also conceivable that the polymer concentration and, accordingly the yield point, were too low to stabilize the formed fiber and minimization of surface energy is the driving force of droplet formation. More precisely, the appearing surface tension causes a restoring force.

Based on the results obtained for one layer, constructs with a base area of 12 x 12 mm^2 were printed by orthogonally stacking two layers onto each other (**Fig. 4.29**). It has turned out that a larger fiber spacing of 3 mm is more suitable as the individual strands as well as the resulting pores are clearly visible. Obviously, stacking multiple layers on top of each other is not reasonable at this point as the material would fuse together. This could already be observed at the intersection of the two layers which did not allow a distinction between the individual strands and caused the formation of round corners. Nevertheless, the printed construct exhibited good overall shape fidelity and did not flow even when the microscopy slide on which the construct was printed, was tilted by almost 90°. To the best of my knowledge, this was the first time printing a thermoreversible hydrogel solely based on POx or POzi by using AM techniques.

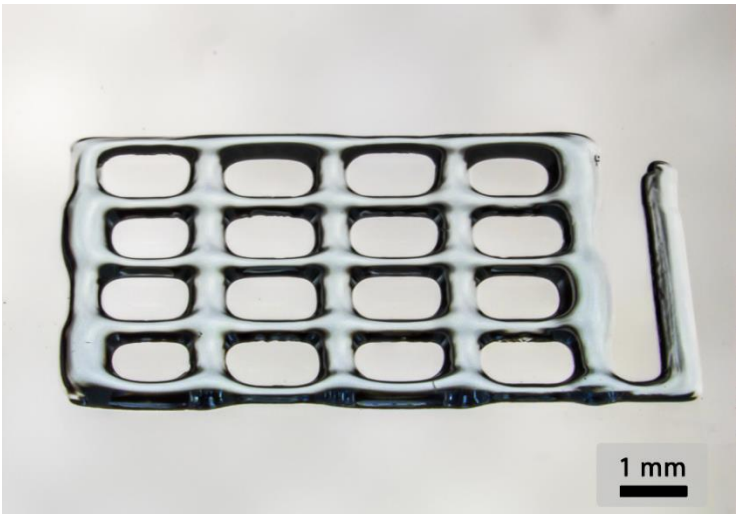

Fig. 4.29| Light microscope image of a printed construct composed of orthogonal stacks of hydrogel strands with a base area of 12 x 12 mm^2 and a strand-center to strand-center distance of 3mm.

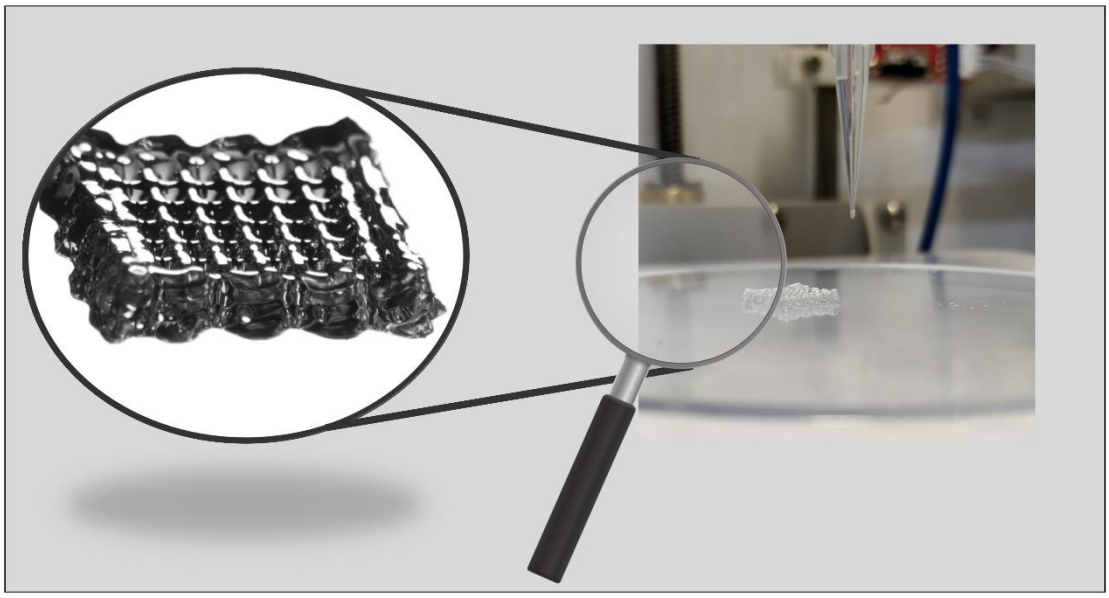

Fig. 4.30| Picture and light microscope image of a printed construct composed of 8 orthogonal stacks of hydrogel strands with a base area of 12 x 12 mm^2.

Although it was a success to be able to process the developed hydrogel by 3D printing techniques, the obtained results were unsatisfactory because printing a 3D construct was not possible with a 20 wt% solution of D7.2. However, according to the conducted rheological measurements (see chapter 4.3.1) increasing the polymer concentration should result in a higher flow point and consequently affect strand formation and shape fidelity of the printed construct. For this purpose, a 30 wt% polymer solution was used for the following experiments which were conducted on an INKREDIBLE 3D bioprinter. Initial tests revealed that no droplet formation occurred at the tip (0.20 mm inner diameter, 27G) and a filament with a length of several centimeters sustaining its own weight could be extruded if the pressure was adjusted to 1.1 bar. Subsequently a rectangular structure with a base area of 12 x 12 mm^2 and 8 layers (4 in 0° direction and 4 in 90° direction) was successfully printed and showed excellent shape fidelity (**Fig. 4.30**). In the light microscopy image, it was possible to distinguish between the individual strands on the outside of the construct what can be regarded as evidence for the first 3D printed POx based hydrogel construct.

Especially for the establishment of a bioink platform with a broad field of application, the adjustability of the printing properties is another benefit alongside with variable T_{Gel} and excellent cytocompatibility. However, the final proof, that POx-*b*-POzi

copolymers are a serious bioink candidate and can be processed with cells, what is per definition a major requirement, will be discussed in the following chapter.

4.5.2 3D-Bioprinting

3D-biopriting experiments were conducted in cooperation with Tomasz Jüngst and PD Dr. Tessa Lühmann.[340] Based on the excellent cytocompatibility results obtained at 25 wt% we decided to use a 20 wt% polymer solution for bioprinting although multilayer constructs are not printable at this concentration. However, the aim was to investigate cell viability during the printing and therefore 3D constructs were not essential. Nevertheless,

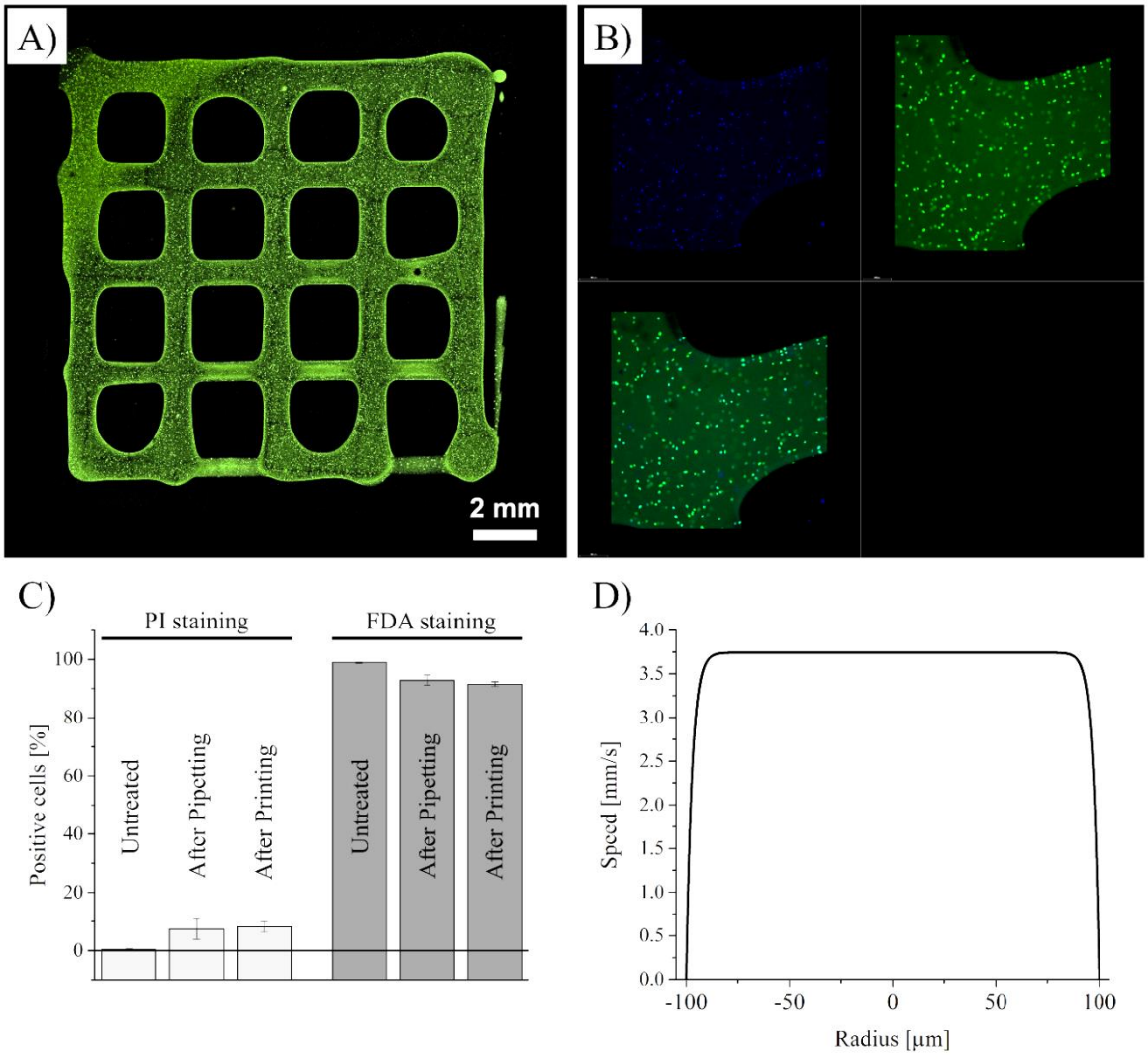

Fig. 4.31| A) 3D printed cell loaded construct, B) detailed view showing cell nucleus stained with Hoechst dye (top left), fluorescein diacetate (FDA) stained cells (top right), and an overlay image (bottom left), C) results of FACS analysis on the influence of the printing process on the viability of NIH 3T3 fibroblasts. While the untreated control represents cells in medium, the control represents cells that were redispersed in the bioink but not printed, and D) simulated plug-flow inside a circular needle with a diameter of 200 µm based on the shear thinning experiments conducted on a plate-plate rheometer.

it is crucial to investigate cell viability when printing at higher polymer concentrations up to 40 wt% for future research and development.

By mixing 1.0 million/mL NIH-3T3 fibroblasts into the polymer which was dissolved in cell culture medium, cell-loaded constructs could be generated at room temperature (**Fig. 4.31 A**). It could be shown, that the incorporated cells did not influence the printability of the material, and the same settings as for cell free inks could be applied to process the bioink (see chapter 4.5.1). Nevertheless, it would be instructive to perform rheology experiments with cell-laden inks as already outlined previously. The cell distribution within the construct was homogenous throughout the entire construct (**Fig. 4.31 B**). The homogeneous cell distribution was facilitated due to the thermoresponsive properties of the material. At low temperatures (ice bath), the ink has a very low viscosity and cells are readily distributed within the material via repeated mixing by pipetting. Once taken off the ice, the immediate, temperature-driven viscosity increase preserved the homogeneous distribution within the ink until the material was dispensed. As noted by Mouser *et al.*, it can be challenging to homogeneously distribute cells in highly viscous bioinks due to various issues (air bubbles, difficult pipetting/handling).[350] To investigate whether dispensing had a negative effect on cell viability, NIH 3T3 cells included in biofabricated scaffolds were further investigated via FACS analysis (**Fig. 4.31 C**). This revealed similar levels of cell viability (91.5% ± 0.8%) compared to cells incorporated into the material without further processing (92.8% ± 1.7%) and untreated cells (98.9% ± 0.2%). Therefore, the printing process seems to have no effect on the cell viability when using the bioink developed in the present work. Presumably, the high cell survival rate can be attributed to the flow profile which occurs in the needle. According to calculations, performed on basis of the shear thinning data (see chapter 4.3.1.5) by Prof. Dr. Gekle and his PhD student Christian Bächer a clear plug flow occurred in the cylindrical needle (d = 0.20 mm) during extrusion based bioprinting at a constant flow rate of 400 µL/h (**Fig. 4.31 D**). Consequently, only a small amount of cells which were located directly next to the wall of the needle (~10 µm) suffered from high shear stress caused by the larger speed difference. It is reasonable to assume that the plug flow does not change when increasing the needle diameter to 0.25 mm which was the case for cell printing experiments.

4.5.3 Conclusion

To conclude, the printability of D7.2 was successfully shown at two different concentrations. At 20 wt% only 2 layers could be stack on top of each other as the strands fused into each other on the intersections. Nevertheless, printing with cells was possible at this polymer concentration and revealed excellent cell survival after incubation for 24 h post printing. No significant difference could be found if compared to cells which were only pipetted as usual. Increasing the polymer concentration to 30 wt% enabled the possibility to print 3D constructs with 8 layers orthogonally stacked on top of each other. Important to note, the hydrogels are only physically cross-linked what limits the field of applications at the moment. As an example, long-term cytotoxicity studies in 3D could not be performed as addition of fresh media would have dissolved the printed structure. Future studies have to be conduct to develop a strategy for cell-friendly cross-linking after printing.

5 | Summary and Outlook

Motivated by the great potential which is offered by the combination of additive manufacturing and tissue engineering, a novel polymeric bioink platform based on poly(2-oxazoline)s was developed which might help to further advance the young and upcoming field of biofabrication.

In the present thesis, the synthesis as well as the characteristics of several diblock copolymers consisting of POx and POzi have been investigated with a special focus on their suitability as bioinks.

Synthesis

In general, the copolymerization of 2-oxazolines and 2-oxazines bearing different alkyl side chains was demonstrated to yield polymers in good agreement with the DP aimed for and moderate to low dispersities. Triggered by the large amount of polymer needed for significant printing results and biological testing, the polymer synthesis was performed in batches up to 100 g. Thus monomer synthesis was also up-scaled to several kilograms to satisfy the needs. The next step should be to establish polymer synthesis in the 5 L reactor to be able to produce several kilograms of one batch. However, in advance some obstacles have to be overcome to ensure a safe reaction and high quality of the product. Especially initiation might be critical due to heat development which is not a problem on laboratory scale due to the small amount. This problem might be overcome be using an initiator salt which could be produced in several small batches and then combined. Furthermore, purification of the synthesized polymers might be more challenging when working with several kilograms as the current approach is not reasonable due to at least one dialysis step. Precipitation, which is the standard approach for hydrophilic polymers appears also unsuitable due to the high amount of precipitating agent. Spray drying directly from PhCN or after solvent exchange appears most promising for purification of such larger polymer batches at the moment.

Influence of the Copolymer Composition on the Physicochemical Properties

Based on their thermal properties in bulk, diblock copolymers investigated in the present study can principally divided into two groups. Polymers which are part of the first group exhibited only one glass transition within the investigated range (-50 – 200 °C)

whereas polymers which belong to the second group exhibited two glass transitions which could be assigned to the corresponding homopolymers. Interestingly, the polymer architecture influences the glass transition as a triblock copolymer exhibited only one glass point whereas a diblock copolymer with the identical amount of monomers revealed two glass transitions. In the present thesis, the different hydrophilicity of the blocks was used to explain the observed behavior, however this is just a very rough estimation. To be more precise and to be able to draw a clear conclusion it would be necessary to calculate the Flory-Huggins parameter which can be estimated from the Hansen solubility parameters.

For every diblock copolymer synthesized during the present study, a more or less pronounced dependency of the dynamic viscosity on temperature could be demonstrated. However, thermal properties in bulk do not allow any conclusion on the thermoresponsive behavior in aqueous solution. Diblock copolymers comprising a hydrophilic PMeOx block and a thermoresponsive P*n*PrOzi block showed temperature induced gelation above a DP of 50 and a polymer concentration of 20 wt%. Such a behavior has never been described before for copolymers solely consisting of poly(cyclic imino ether)s.

POx-*b*-POzi based Thermoresponsive Hydrogels

Physically cross-linked hydrogels based on POx-*b*-POzi copolymers exhibit reverse thermal gelation properties like described for solutions of PNiPAAm and Pluronic F127. However, by applying SANS, DLS, and SLS it could be demonstrated that the underlying gel formation mechanism is different for POx-*b*-POzi based hydrogels. While gelation is explained through an aggregation of spherical micelles into a cubic lattice for Pluronic F127, POx-*b*-POzi based hydrogels show a unique mechanism. It appears that polymersomes with low polydispersity are formed already at very low polymer concentrations of 6 mg/L. Increasing the concentration resulted in the formation of a bicontinuous sponge like structure which might be formed due to the merger of several vesicles. For longer polymer chains a phase transition into a gyroid structure was postulated and corresponds well with the observed rheological data. Future SANS studies based on the accepted proposal (Heinz Maier-Leibnitz Zentrum, ID: 14755) of the author of the present thesis, will allow an even more detailed insight on the structural changes occurring during shear thinning and structure recovery as RheoSANS will be performed during the next reactor cycle. Furthermore, this might allow for the unequivocal detection of the

gyroid phase as shear alignment can be performed as described by Viglid *et al.* The shortcoming of an insufficient contrast between the PMeOx block and the P*n*PrOzi block may be alleviated in future experiments by selective deuteration of one block to improve the contrast conditions and thus allow a detailed analysis. As already outlined, an in-depth light scattering study would require a large synthetic effort that is time consuming but might be very helpful to enable a better understanding. Based on the preliminary DOSY data suggesting almost unimpeded diffusion of HDO, it would be recommendable to perform an extensive study with several model molecules which allow for an estimation of the structure. This study should be complemented by FRAP experiments to ensure consistency of the results. Understanding and being able to predict diffusion process inside the hydrogel after 3D printing would be a huge benefit for the further development of the presented bioink platform as well as for the whole field of biofabrication.

Stable hydrogels with an unusually high mechanical strength (G' ~ 4 kPa) have been formed above T_{Gel} which could be adjusted over a range of 20 °C by changing DP if maintaining the symmetric polymer architecture. Variations of the chain ends revealed only a minor influence on T_{Gel} whereas the influence of the solvent should not be neglected as shown by a comparison of cell culture medium and MilliQ water. Modification of the polymer by incorporation of a third monomer (*n*BuOzi) which is randomly copolymerized with the thermoresponsive block revealed significant increase of the mechanical strength and caused a decrease of T_{Gel} for short diblock copolymers (DP ≈ 50). This observation is a great starting point for future variations of the linear diblock copolymer with the aim to be able to further adjust mechanical properties and T_{Gel}. In this context, also 2-oxazolines and 2-oxazines with branched or aromatic side chains should be considered. In contrast to the present study, modification of the hydrophilic block constitutes another possibility, especially for increasing T_{Gel} by increasing the hydrophobicity

Rotationally as well as oscillatory rheological measurements revealed a high suitability for printing as POx-*b*-POzi based hydrogels exhibit strong shear thinning behavior in combination with outstanding recovery properties after high shear stress. The yield point was found to be higher compared to Pluronic F127 gels with equal polymer concentration which is beneficial for the shape fidelity after printing and ensures the absence of flow at rest. Developing a model that allows prediction of the print result based on the parameters accessible via rheology would be highly beneficial for further

developments as many experiments would be superfluous in the future. In this context the use of machine learning might be highly interesting.

Finally, the manifold synthetic possibilities provided by POx and POzi should be used to investigate their influence on the material properties. Here, in particular, the polymer architecture should be varied by synthesizing star-shaped polymers or polymer brushes. Furthermore, by blending several polymer architectures together might result in unexpected material properties which were unachievable before. However, it should also be considered to link several linear diblock copolymers together as this resulted in outstanding mechanical properties for Pluronic F127. The basis for these future investigations, certainly is the establishment of the reproducible polymer synthesis in large amounts up to several kilogram.

Sterilizability and Cytocompatibility

A major requirement for a material to be considered as biomaterial is a very low cytotoxicity. Furthermore, sterilizability is important as sterile filtration is inapplicable at high polymer concentrations. Therefore, two sterilization process, namely autoclaving and γ-irradiation have been applied and investigated with regard to changes of the material properties. Corroborating other studies, it could be shown that γ-irradiation causes degradation of the polymer resulting in significantly higher Đ and low molecular tailing. This was also reflected in the rheological investigations as the gelation process was significantly slowed down and the mechanical properties were impaired. In contrast, autoclaving had no influence on the molar mass distribution and caused only minor changes of the mechanical properties.

Cell viability assays (WST-1) of PMeOx-*b*-P*n*PrOzi copolymers against NIH 3T3 fibroblasts and HaCat cells indicated that the polymers were well tolerated by the cells as no dose-dependent cytotoxicity could be observed after 24 h at non-gelling concentrations up to 100 g/L. Even when incubated in the gel stated (25 wt%) the polymers/gels exhibited very good cytocompatibility (87.1 ± 2.9 % FDA positive).

Due to its thermoresponsive character cells could be easily retrieved after incubation by reducing the temperature. This might become especially interesting after introducing bioinstructive cues such as peptide or sugar moieties. These can easily be

introduced using the rich polymer analogue modifications available of POx and POzi. However, incubation time is still limited as medium exchange would cause dissolution of the gel. Introducing cross-linking sites, which can be easily done and would allow for longer incubation up to several weeks, would rule out the thermoresponsive behavior and therefore the possibility to retrieve the cells. Again, the manifold possibilities allow an adjustment of the gel according to the needs of the envisioned application.

Future studies should focus on finding the maximal polymer concentration tolerated by NIH 3T3 fibroblasts as these cells constitute a good starting point. Subsequently, further cell studies *in vitro* have to be conducted to prepare *in vivo* tests which will reveal the potential, but also the limits of this new and promising bioink candidate.

2D Printing and 3D Bioprinting

In the last section of the present thesis, the polymers identified as most suitable for bioink formation have been printed in 2D and 3D with and without cells. Initially, a 2D pattern was printed to identify the minimal strand-to-strand distance at which the fibers did not fuse into each other. Subsequently, a simple two layered mesh was printed using a 20 wt% polymer solution but revealed insufficient fiber stability as fibers fused together at the intersection. Nevertheless, it was possible to print a cell-laden construct at room temperature. Cell distribution was found to be homogeneous throughout the whole construct. No negative effect on cell viability could be identified as cell viability (91.5 % ± 0.8 %) was similar compared to cell incorporated into the material without further processing.

Increasing the polymer concentration enabled the generation of 3D constructs with multiple layers which could be clearly distinguished under the light microscope.

As already mentioned in the context of cell culture for longer time periods, it would be essential to establish a second chemical cross-linking mechanism that allows curing directly after extruding the physical gel. This would allow the generation of large constructs with a height of several centimeters and also prevent drying of the hydrogel as the printed construct can easily soaked with water as it is chemically cross-linked. However, it must be kept in mind that the chemical cross-linking mechanism must not harm the cells and has to be quick on the other hand. In this context, Diels-Alder reactions appear ideally suitable.

As already demonstrated by Chujo *et al.* neither a catalyst or initiator nor UV-activation is necessary to obtain hydrogels.

The future development of the bioink platform developed in the present dissertation will be carried out within the framework of the collaborative research center SFB TRR 225 project A03. However, further applications are imaginable. For example, a combination with ABA triblock copolymers with outstanding solubilization properties for poorly water soluble drugs would allow for the creation of subcutaneous drug depots. Apart from that, the hydrogel could also be used to controllably place cells on any surface by printing and subsequent sedimentation of cells initiated by decreasing the temperature.

In summary, copolymers consisting of POx and POzi significantly increased the accessible range of properties of POx based materials. In particular thermogelation of aqueous solutions of diblock copolymers comprising PMeOx and P*n*PrOzi was never described before for any copolymer consisting solely of POx or POzi. In combination with other characteristics, e.g. very good cytocompatibility at high polymer concentrations and comparably high mechanical strength, the formed hydrogels could be successfully used for 3D bioprinting. Although the results appear promising and the developed hydrogel is a serious bioink candidate, competition is tough and it remains an open question which system or systems will be used in the future.

6|Zusammenfassung und Ausblick

Motiviert durch das große Potential, das die Kombination aus additiver Fertigung und künstlicher Geweberegeneration bietet, wurde eine neuartige polymerbasierte Biotintenplattform auf Basis von Poly(2-oxazolin)en entwickelt. Diese soll zukünftig dazu beitragen das noch junge, aber aufstrebende Forschungsfeld der Biofabrikation weiterzuentwickeln.

In der vorliegenden Arbeit wurden die Synthese sowie die Eigenschaften von mehreren Diblock Copolymeren, bestehend aus POx und POzi, untersucht, wobei der Hauptfokus auf deren Eignung als Biotinte lag.

Synthese

Grundsätzlich konnte gezeigt werden, dass Copolymeren, bestehend aus 2-Oxazolinen und 2-Oxazinen, die unterschiedliche Alkylseitenketten besitzen, synthetisiert werden können. Dabei lagen die ermittelten Polymerisationsgrade nahe am zuvor errechneten Wert. Die Polymere wiesen mittlere bis niedrigere Dispersitäten auf. Aufgrund der Tatsache, dass für eine ausführliche Materialcharakterisierung und insbesondere für Druckversuche größere Mengen Polymer benötigt wurden, wurde die Ansatzgröße der durchgeführten Synthesen auf bis zu 100 g erhöht. Aus diesem Grund wurde die Monomersynthese auf den Kilogramm-Maßstab erhöht. Der nächste Schritt sollte darin bestehen die Polymersynthese in 5 L Reaktoren durchzuführen und so die Ausbeute eines Ansatzes auf mehrere Kilogramm zu erhöhen. Allerdings müssen im Vorfeld einige Hindernisse adressiert werden, um eine sichere Reaktionsdurchführung und ein qualitativ hochwertiges Produkt zu gewährleisten. Insbesondere die Initiation kann, aufgrund der Hitzentwicklung, die im Labormaßstab vernachlässigbar ist, zu Problemen führen. Durch die Verwendung von geeigneten Initiatorsalzen, die in mehreren kleinen Chargen hergestellt und anschließend vereinigt werden können, ist es möglich, dieses Problem zu lösen. Die Reinigung größerer Polymermengen ist jedoch anspruchsvoller, da die aktuelle Vorgehensweise aufgrund der durchgeführten Dialyse nicht angemessen erscheint. Ausfällen, das Standardprozedere für hydrophile Polymere, erscheint aufgrund des hohen Bedarfs an Fällungsreagenz ebenfalls nicht sinnvoll. Am vielversprechendsten wäre es, größere Mengen des synthetisierten Block Copolymers entweder direkt aus PhCN sprühzutrocknen oder gegebenenfalls im Vorfeld einen Lösemittelwechsel durchzuführen.

Einfluss der Copolymerzusammensetzung auf die physikochemischen Eigenschaften

Basierend auf den thermischen Eigenschaften der Polymere ist es möglich, diese in zwei Gruppen zu unterteilen. Diejenigen, die der ersten Gruppe zugeordnet werden können, weisen nur einen Glasübergangspunkt im untersuchten Temperaturbereich (-50 – 200 °C) auf, wohingegen Polymere, die zur zweiten Gruppen gehören zwei Glasübergänge besitzen. Diese konnten den jeweiligen Homopolymeren zugeordnet werden. Interessanterweise beeinflusst die Polymerarchitektur das Auftreten von Glasübergangspunkten. Ein Triblock Copolymer, weist bei identischer Anzahl an Wiederholeinheiten im Vergleich zu einem Diblock Copolymer lediglich einen Glasübergang auf. In der vorliegenden Arbeit wurden die gemachten Beobachtungen mit Hilfe der unterschiedlichen Hydrophilie der Blöcke begründet. Dies ist allerdings nur eine sehr grobe Abschätzung. Um genauere Aussagen treffen zu können, ist es notwendig die Flory-Huggins Parameter der jeweiligen Homopolymere zu berechnen. Dies kann mit Hilfe der Hansen Löslichkeitsparameter erfolgen.

Für jedes der im Rahmen der vorliegenden Arbeit synthetisierten Diblock Copolymere konnte eine mehr oder weniger starke Abhängigkeit der dynamischen Viskosität von der Temperatur gezeigt werden. Allerdings ist es nicht möglich, aus den thermischen Eigenschaften des Bulkmaterials Rückschlüsse auf das temperaturabhängige Verhalten in Lösung zu ziehen. Diblock Copolymere mit einem hydrophilen PMeOx Block und einem thermoresponsiven P*n*PrOzi Block bildeten oberhalb einer Kettenlänge von 50 Einheiten und einer Polymerkonzentration von 20 Gew% ein physikalisches Gel. Solch ein Verhalten wurde bisher noch nicht für Copolymere, die ausschließlich auf POx oder seinen höheren Homologen basieren, beschrieben.

POx-*b*-POzi basierte thermoresponsive Hydrogele

Physikalische Hydrogele, basierend auf POx-*b*-POzi Copolymeren, weisen eine umgekehrte thermische Gelierung wie auch wässrige Lösungen von PNiPAAm und Pluronic F127 auf. Allerdings konnte durch die komplementäre Verwendung von SANS, DLS und SLS gezeigt werden, dass sich der zugrundeliegende Gelbildungsmechanismus für POx-*b*-POzi basierte Hydrogele deutlich von den beiden zuvor genannten unterscheidet. Während die Bildung für die meisten physikalischen Gele durch die Aggregation sphärischer Mizellen in einem kubischen Gitter erklärt wird, zeigen die in dieser Arbeit entwickelten Hydrogele einen anderen Mechanismus. Es wird davon ausgegangen, dass

sich zunächst bei einer sehr geringen Polymerkonzentration von 6 mg/L Vesikel mit geringer Polydispersität ausbilden. Eine Erhöhung der Konzentration resultiert in der Ausbildung eines bikontinuierlichen Netzwerks mit schwammartiger Struktur. Dieses bildet sich vermutlich durch die Fusion mehrerer Vesikel. Des Weiteren wird für höhere Polymerisationsgrade ein Phasenübergang zu einer gyroidalen Struktur postuliert der sich sehr gut mit den gewonnenen rheologischen Daten deckt. Weitere SANS Untersuchungen, basierend auf einem angenommenen Messzeitantrag (Heinz Maier-Leibnitz Zentrum, ID: 14755) des Autors der vorliegenden Arbeit, ermöglichen eine detailliertere Analyse der strukturellen Änderung während der Scherung und der Strukturerholung, da RheoSANS Experimente geplant sind. Auch könnte so die gyroidale Phase eindeutig nachgewiesen werden, da eine scherinduzierte Ausrichtung der Phasen, wie von Viglid *et al.* beschrieben, durchgeführt werden kann.

Das bisherige Defizit eines geringen Kontrasts zwischen den beiden Blöcken könnte in Zukunft durch die selektive Deuterierung eines Blocks gelöst werden. Dies hätte eine deutliche Steigerung des Kontrasts zur Folge und würde eine detaillierte Analyse der gebildeten Struktur erlauben. Eine ausführliche Lichtstreustudie wäre mit erheblichem synthetischem Aufwand verbunden. Dies wäre sehr zeitintensiv, aber gleichzeitig äußerst hilfreich beim Versuch den Gelprozess besser zu verstehen.

Basierend auf ersten DOSY Messungen, die eine nahezu ungehinderte Diffusion von HDO im Hydrogel zeigen, wäre es empfehlenswert eine umfangreiche Studie zu planen. Hierbei können unterschiedliche Modellmoleküle eingesetzt werden, um so eine Abschätzung der gebildeten Struktur zu ermöglichen. Um die Aussagekraft der Ergebnisse zu prüfen, sollten ebenfalls FRAP Experimente durchgeführt werden.

Die Fähigkeit, die Diffusionsprozesse innerhalb des Gels zu verstehen und vorhersagen zu können, wäre von essentiellem Nutzen für die weitere Entwicklung der hier vorgestellten Biotinten Plattform aber auch für das gesamte Feld der Biofabrikation.

Stabile Hydrogele mit außergewöhnlich hoher mechanischer Stärke (G‘ ≈ 4kPa) bildeten sich oberhalb der T_{gel}, die über eine Temperaturspanne von 20 °C durch Änderung des Polymerisationsgrades eingestellt werden konnte. Veränderung der Kettenenden zeigten nur einen geringen Einfluss auf die T_{Gel}, wobei der Einfluss des verwendeten Lösemittels nicht unterschätzt werden sollte. Dies konnte durch den direkten Vergleich von MilliQ Wasser und Zellkulturmedium gezeigt werden. Eine weitere

Modifikationsmöglichkeit stellt die Zusammensetzung der Polymere dar. Durch das Einbringen eines dritten Monomers, welches zufällig verteilt in den thermoresponsiven Block einpolymerisiert wurde, konnte eine Steigerung der mechanischen Festigkeit sowie ein Herabsetzen der T_{Gel} bei kürzeren Polymeren ($DP \approx 50$) erreicht werden. Diese Beobachtung ist ein hervorragender Ausgangspunkt für weitere Variationen des linearen Diblock Copolymers, mit dem Ziel die mechanischen und thermischen Eigenschaften der Hydrogele noch besser anpassen zu können. In diesem Zusammenhang sollten auch 2-Oxazoline und 2-Oxazine mit verzweigten Seitenketten und aromatischen Seitenketten in Betracht gezogen werden. Im Gegensatz zu den in der vorliegenden Arbeit gemachten Änderungen, stellen Modifikationen des hydrophilen Blocks eine gute Möglichkeit zur Erhöhung von T_{Gel} dar.

Rheologische Untersuchungen, die sowohl im rotierenden als auch im oszillierenden Modus durchgeführt wurden, zeigten eine gute Eignung der POx-*b*-POzi basierten Hydrogele für Extrusion basierte Druckverfahren. Insbesondere aufgrund des stark ausgeprägten scherverdünnenden Verhaltens und der ausgezeichneten Strukturerholung nach hoher Scherbelastung sollten gute Druckergebnisse erzielbar sein. Der Fließpunkt liegt leicht oberhalb von Pluronic F127 Gelen bei gleicher Polymerkonzentration, was vorteilhaft für die Formtreue des gedruckten Konstrukts ist. Die Entwicklung eines zuverlässigen Models, das basierend auf den rheologisch bestimmten Parametern Vorhersagen über das Druckergebnis erlaubt, wäre von großem Vorteil für die zukünftige Entwicklung, da zahlreiche Experimente überflüssig wären. In diesem Zusammenhang wäre auch der Ansatz des maschinellen Lernens denkbar.

Abschließend sollten die vielfältigen synthetischen Möglichkeiten der POx und POzi genutzt werden, um deren Einfluss auf die Materialeigenschaften zu untersuchen. Hierbei sollte insbesondere die Polymerarchitektur durch die Synthese von sternförmigen Polymeren oder Bürstenpolymeren variiert werden. Des Weiteren ist es sehr gut vorstellbar, dass Mischungen verschiedener Polymerarchitekturen in bisher ungeahnten und unerreichbaren Materialeigenschaften resultieren. Zusätzlich sollte auch in Betracht gezogen werden mehrere Diblock Copolymere aneinander zu koppeln, da dies im Falle von Pluronic F127 Gelen zu ausgezeichneten mechanischen Festigkeiten geführt hat. Die Basis für alle zukünftigen Entwicklungen ist allerdings die Etablierung einer reproduzierbaren Polymersynthese im Technikumsmaßstab.

Sterilisierbarkeit und Zytokompatibilität

Eine sehr geringe Zytotoxizität ist eine Hauptvoraussetzung für ein Material, um als Biomaterial in Betracht gezogen zu werden. Darüber hinaus ist die Sterilisierbarkeit ein wichtiger Faktor, da die Polymerlösungen, aufgrund der hohen Polymerkonzentration, nicht steril filtriert werden können. Aus diesem Grund wurden die zwei Sterilisationsverfahren – Autoklavieren und γ-Sterilisieren – angewandt und deren Auswirkungen auf die Materialeigenschaften untersucht. Hierbei konnte, im Einklang mit bestehenden Studien, gezeigt werden, dass γ-Strahlen zur Degradation des Polymers führen, was in einer deutlich gesteigerten Dispersität und einem stark ausgeprägten niedermolekularen Auslaufen des GPC Elugramms sichtbar wurde. Dies spiegelt sich ebenfalls in rheologischen Untersuchungen wieder. Die Gelbildung verlief deutlich langsamer und die mechanische Festigkeit war beeinträchtigt. Im Gegensatz dazu konnte nach dem Autoklavieren keine Änderung der Molmassenverteilung festgestellt werden. Allerdings zeigte sich eine minimale Verschlechterung der mechanischen Festigkeit.

Zellviabilität-Assays (WST-1) von PMeOx-*b*-P*n*PrOzi Copolymeren an NIH 3T3 Fibroblasten und HaCat-Zellen zeigten, dass die Polymere bei Konzentrationen von bis zu 100 g/L und Inkubationszeiten von 24 h keine dosisabhängige Zytotoxizität besitzen. Sogar nach der Inkubation für 24 h im Hydrogel (25 Gew%) weisen die Polymere bzw. Gele eine sehr gute Zytokompatibilität (87.1 ± 2.9 % FDA positiv) auf.

Aufgrund des thermoresponsiven Charakters der Hydrogele war es möglich, die inkubierten Zellen durch Absenken der Temperatur einfach zurückzugewinnen. Dies ist insbesondere nach dem Einbringen von bioinstruktiven Signalen wie beispielsweise Peptiden oder Zuckern interessant. Diese können durch die vielfältigen polymeranalogen Modifikationen, die sowohl für POx als auch POzi bekannt sind, einfach integriert werden. Allerdings ist die Inkubationszeit limitiert, da kein Medienwechsel durchgeführt werden kann ohne das gebildete Gel aufzulösen. Das Vernetzen der Polymere sollte einfach umzusetzen sein und längere Inkubationszeiten ermöglichen, was aber den Verlust des thermoresponsiven Charakters der Hydrogele und somit auch die Möglichkeit der Rückgewinnung der Zellen zur Folge hat. Resümierend lässt sich sagen, dass die vielfältigen Möglichkeiten es erlauben, das Gel so anzupassen, dass es den jeweiligen Anforderungen der geplanten Anwendung entspricht.

In zukünftigen Studien sollte zunächst die maximale Polymerkonzentration, welche von NIH 3T3 Fibroblasten toleriert wird, bestimmt werden. Anschließend müssen weitere Zellstudien *in vitro* durchgeführt werden, um mögliche *in vivo* Versuche vorzubereiten. Diese werden das wahre Potential offenbaren, aber auch die Grenzen dieses vielversprechenden Biotinten Kandidaten aufzeigen.

2D Druck und 3D Biodruck

Im letzten Teil der vorliegenden Arbeit wurden die Polymere, die sich als am besten geeignet für die Bildung von Biotinten erwiesen hatten, in 2D und 3D mit und ohne Zellen gedruckt. Zunächst wurde ein 2D Muster gedruckt, um den minimalen Strang-zu-Strang Abstand, der ohne ein Ineinanderfließen der einzelnen Hydrogelstränge gedruckt werden kann, zu bestimmen. Mit einer 20 Gew% Polymerlösung wurde anschließend ein einfach zweilagiges Netz gedruckt. Hierbei zeigte sich eine geringe Stabilität der Stränge, da diese an den Kreuzungspunkten miteinander verschmolzen. Trotzdem war es möglich ein mit Zellen beladenes Netz bei Raumtemperatur zu drucken. Die Verteilung der Zellen war im gesamten Konstrukt homogen. Mittels FACS Analyse konnte gezeigt werden, dass der Druckprozess keinen negativen Einfluss auf die Viabilität der Zellen hat. Es konnte kein signifikanter Unterschied im Vergleich zu nichtgedruckten, aber im Gel kultivierten Zellen nachgewiesen werden.

Durch die Erhöhung der Polymerkonzentration war es möglich, wirkliche 3D Konstrukte aus mehreren Schichten, die klar voneinander unterscheidbar waren, zu drucken.

Wie bereits im Zusammenhang mit einer Verlängerung der Inkubationszeiten erwähnt, ist es notwendig einen zweiten, chemischen Vernetzungsmechanismus, der eine Vernetzung direkt nach dem Drucken des physikalischen Gels erlaubt, zu etablieren. Dies würde einerseits das Drucken von größeren Konstrukten mit einer Höhe von mehreren Zentimetern erlauben und ein Austrocknen des Konstrukts verhindern, da dieses mit Wasser getränkt werden könnte. Bei der Entwicklung muss allerdings berücksichtigt werden, dass die chemische Vernetzung einerseits keinen negativen Einfluss auf die Zellen haben darf und andererseits sehr schnell ablaufen muss. In Bezug darauf scheinen Diels-Alder Reaktionen ideal geeignet. Wie bereits von Chujo *et al.* gezeigt wurde, ist für diese

Reaktionen weder ein Katalysator oder Initiator notwendig noch muss die Reaktion durch UV-Licht initiiert werden, um Hydrogele zu bilden.

Die zukünftige Entwicklung der in der vorliegenden Arbeit entwickelten Biotinten Plattform wird im Rahmen des Sonderforschungsbereichs SFB TRR 225 im Projekt A03 fortgeführt. Ferner sind auch noch weitere Anwendungen denkbar. Beispielsweise kann aus einer Kombination mit ABA Triblock Copolymeren, welche sich hervorragend zur Solubilisierung von schwer wasserlöslichen Arzneimitteln eignen, ein subkutanes Medikamentendepot entwickelt werden. Des Weiteren könnte das Hydrogel genutzt werden, um Zellen kontrolliert auf Oberflächen zu platzieren. Zunächst müssten einzelne Tropfen extrudiert werden, um anschließend die Sedimentation der Zellen durch eine Verringerung der Temperatur zu initiieren.

Zusammenfassend kann festgehalten werden, dass die Copolymerisation von POx und POzi den verfügbaren Eigenschaftsbereich von POx basierten Materialien deutlich vergrößert hat. Insbesondere die temperaturinduzierte Gelierung von wässrigen Polymerlösungen wurde noch nie zuvor für ein anderes Copolymer auf Basis von POx und POzi beschrieben. Aufgrund ihrer herausragenden Eigenschaften, wozu unter anderem eine sehr gute Zytokompatibilität bei hohen Polymerkonzentrationen und eine vergleichsweise hohe mechanische Festigkeit zählen, konnten die entwickelten Hydrogele erfolgreich für den 3D Biodruck verwendet werden. Obwohl die beschriebenen Ergebnisse sehr vielversprechend sind und die entwickelte Hydrogelplattform folglich als ernstzunehmender Biotintenkandidat angesehen werden sollte, ist die Konkurrenz sehr groß und es bleibt abzuwarten, welche Tinte bzw. Tinten in Zukunft zum Einsatz kommen.

7 |Experimental

7.1 Equipment & Methods of Measurement

7.1.1 Equipment

Glovebox

A *LabMaster 130* (*MBraun,* Garching, Germany) comprising nitrogen atmosphere (5.0, *Linde AG,* Germany) was used to store chemicals and to initiate polymerizations under inert conditions.

Infrared (IR) Spectroscopy

IR spectra were recorded on a *FT/IR-4100* spectrometer (*JASCO,* Groß-Umstadt, Germany) equipped with PIKE MIRacle single reflection attenuated total reflection sampling accessory (ZnSe crystal, *PIKE Technologies,* Madison, Wisconsin, USA) and a deuterated triglycine sulfate detector. The corresponding *JASCO spectra manager V.2.07.00* software was used to evaluate the obtained spectra.

Nuclear Magnetic Resonance (NMR) Spectroscopy

NMR spectra were recorded on a *Fourier 300* spectrometer (^{1}H; 300.12 MHz and ^{13}C{^{1}H}; 75.48 MHz; *Bruker Biospin;* Rheinstetten, Germany) at a temperature of 298 K and evaluated using *MestReNova V.6.0.2-5475* software (*Mestrelab Research,* Santiago de Compostela, Spain). Diffusion-ordered spectroscopy (DOSY) experiments as well as temperature dependent experiments were recorded on an *Avance III HD 600* spectrometer (^{1}H; 600 MHz; *Bruker Biospin;* Rheinstetten, Germany). The chemical shift of the signals is indicated in ppm. Spectra were calibrated using residual solvent signals (D_2O 4.67 ppm, MeOD 3.31 ppm, and $CDCl_3$ 7.26 ppm). Multiplicities of signals are categorized as follows: singlet (s), doublet (d), triplet (t), quartet (q), quintet (quin), multiplet (m), or broad (br).

Gel Permeation Chromatography (GPC)

Depending on the solvent, GPC measurement was performed on one of the three systems described below.

DMF GPC was conducted on a *Polymer Standard Service SECurity* (*PSS*, Mainz, Germany) system (pump mod. 1260 infinity, MDS RI detector mod. 1260 infinity (*Agilent Technologies*, Santa Clara, California, USA), precolumn PSS GRAM 10 µm (50 x 8 mm), PSS GRAM 30 Å 10 µm (300 x 8 mm) and PSS GRAM 1000 Å 10 µm (300 x 8 mm)) at 313 K. DMF was supplemented with 1 g/L lithium bromide and the flow rate was adjusted to 1 mL/min. Prior to each measurement, the samples were filtered through a 0.2 µm Teflon filter (*Thermo Scientific, Schwerte*, Germany) to remove particles. The systems was calibrated against PEG standards with molar masses ranging from 106 g/mol to 100 kg/mol. Data were processed using *WinGPC Unichrom V.8.20 Build 5350* software.

HFIP GPC was performed on the same *Polymer Standard Service SECurity* (*PSS*, Mainz, Germany) system (pump mod. 1260 infinity, MDS RI detector mod. 1260 infinity (*Agilent Technologies*, Santa Clara, California, USA), precolumn PSS PFG linear M 7 µm (50 x 8 mm), PSS PFG linear M; 2 columns: 7 µm (300 x 8 mm)) at 313 K. HFIP was supplemented with 3 g/L potassium triflate and the flow rate was adjusted to 0.7 mL/min. Calibration was performed using PEG standards with molar masses ranging from 200 g/mol to 100 kg/mol. Sample preparation and evaluation was performed as described for the DMF GPC.

Rheology

Rheology experiments were performed using a *Physica MCR 301* (*Anton Paar*, Graz, Austria) equipped with a *Toolmaster*^{TM} measuring cell and measuring system as well as with a peltier element. A plate-plate geometry with a diameter of 25 mm and a cone-plate geometry with a diameter of 60 mm and an angle of 0.5 ° were utilized. Data were processed using *Physica RheoPlus V.3.40* software (*Anton Paar*, Graz, Austria).

Densimetry & Viscometry

Dynamic viscosity was measured on a *LOVIS 2000M* microviscometer (*Anton Paar*, Graz, Austria) using a *LOVIS 1.8* capillary equipped with a steel ball (Mat. No. 73109, diameter 1.5 mm, steel 1.4125). Prior to this, the density was determined using a *DMA 4100 M* density meter (*Anton Paar*, Graz, Austria) working on the flexural resonator concept.

Small Angle Neutron Scattering (SANS)

The SANS measurements were performed at the KWS-1 instrument at the Jülich Centre for Neutron Science (JCNS) at Heinz Maier-Leibnitz Zentrum (MLZ) in Garching, Germany.[351] In all cases a wavelength of $\lambda = 7$ Å was used. The sample-detector distances (SDD) of 1.61, 7.61 and 19.61 m were used to cover the complete q range ($q = 4 \cdot \pi \cdot \sin\left(\frac{\theta}{2}\right)/\lambda$ is the momentum transfer with θ the scattering angle). The wavelength resolution was set to $\Delta\lambda/\lambda = 10\%$.

In KWS-1 the detector is a ^{6}Li-glass detector with an active area of 60 x 60 cm^2. The sample was filled into a Hellma cuvette with a light path of 1 mm. This cuvette was placed into a Julabo temperature controlled oven (*Julabo*, Seelbach, Germany). Dark current correction was carried out using boron carbide. The scattering of the empty cell was subtracted from the sample scattering, taking the transmissions into account. Poly(methyl methacrylate) was used to bring the data to absolute scale and to determine the detector sensitivity. The resulting intensities were azimuthally averaged. Good agreement was found in the overlap regions of the curves measured at different SDDs. All data reduction steps were performed with the software QtiKWS provided by JCNS. Subsequent data treatment was carried out with NIST NCNR SANS package for IGOR Pro and procedures written by Dr. Sebastian Jaksch.

Dynamic and Static Light Scattering (DLS and SLS)

Dynamic light scattering (DLS) experiments were conducted by either of the three instruments: Apparatus 1 consist of a HeNe laser (22 mW, $\lambda = 632.8$ nm), an ALV-CGS-3 goniometer equipped with eight simultaneously working APD Avalanche photodiode fiber optical detectors. Apparatus 2 operates with a HeNe laser (25 mW, $\lambda = 632.8$ nm), an ALV-CGS 8F SLS/DLS 5022F goniometer equipped with eight simultaneously working ALV 7004 correlators connected to eight ALV High QE APD Avalanche photodiode fiber optical detectors. Apparatus 3 consist of a HeNe laser (22 mW, $\lambda = 632.8$ nm), an ALV-SP86 goniometer equipped with an ALV 3000 correlator and an ALV High QE APD Avalanche photodiode fiber optical detection system. For Apparatus 1 & 2 the detectors were separated by 17 °. All samples were tempered in a cell with temperature stability of ± 0.1 °C. Prior to each measurement, samples were filtered either through regenerated cellulose filters (*Rotilabo*, Karlsruhe, Germany) with varying pore size or through 0.2 µm

PTFE Millex-LG filters (*Merck KGaA*, Darmstadt, Germany). The MilliQ water used for sample preparation (0.1 g/L – 250 g/L) was filtered through 0.1 µm PVDF Millex-VV filters (*Merck KGaA*, Darmstadt, Germany). Data was analyzed using *HDRC – V6.3.1* software developed by O. Nirschl and kindly provided by Prof. Schmidt from the Johannes-Guthenberg-University in Mainz.

Thermogravimetric Analysis (TGA)

Thermogravimetric analysis of the polymers was performed on a *TG 209F1 IRIS* (*NETZSCH*, Selb, Germany). The samples (5 – 10 mg) were added to aluminum oxide crucibles (*NETZSCH*, Selb, Germany) and heated under synthetic air from 30 °C to 900 °C with a heating rate of 10 K/min while detecting the mass loss. The corresponding *NETZSCH Proteus – Thermal Analysis – V.5.2.1* software was used to evaluate the obtained spectra.

Dynamic Scanning Calorimetry (DSC)

Differential scanning calorimetry (DSC) was performed on a *DSC 204F1 Phoenix* (*NETZSCH*, Selb, Germany) under N_2-atmosphere (20.0 mL/min). The samples were placed in aluminum pans with crimped-on lids, cooled to -50 °C (10 K/min) and subsequently heated 200 °C (10 K/min). The samples were heated/cooled two additional times from -50 °C to 200 °C (10 K/min). Sample evaluation was performed as described for the TGA.

Fluorescence Spectroscopy

Fluorescence spectra were recorded on a *FP-8300* spectrofluorometer (*JASCO*, Gross-Umstadt, Germany) equipped with a Peltier element for temperature regulation. The corresponding *JASCO spectra manager V.2.07.00* software was used to evaluate the obtained spectra.

Stereomicroscopy

Printed and coated constructs were analyzed with the stereomicroscope *SteREO Discovery.V20* (*Carl Zeiss Microscopy*, Jena, Germany) equipped with a Zeiss icc 5 color

camera (5 MP, 12 bit), two lenses (0.63x and 1.5x Plan Apo) and a zoom range up to 20:1. Pictures were processed with the corresponding *Zen2012 pro* software.

Confocal Laser Scanning Microscopy

Stained and printed cell-laden constructs were analyzed with a confocal laser scanning microscope *TCS SP8* (*Leica*, Wetzlar, Germany). The motorized stage in combination with the *LASX* software enabled 3D reconstruction of the constructs via tiles and z-stacks.

Scanning Electron Microscopy (SEM)

SEM was carried out with a *ZEISS Supra 25 SEM* (*Carl Zeiss Microscopy GmbH*, Jena, Germany).

3D Bioprinting

For bioprinting a 3D bioprinter *3DDiscovery* (*regenHU*, Switzerland) working on the principle of an extrusion-based printer was used. It was equipped with a pneumatic driven print head (syringe dispenser, DD-135N) and a 0.25 mm inner diameter precision needle (precision tip, *Nordson EFD*, Germany) was used as nozzle. The pressure was set to 1.2 bars and a print speed of 20 mm/min was applied for printing. Printing was performed at room temperature. In case of cell-laden inks, the NIH 3T3 fibroblasts were stained with Hoechst and FDA (as described for the cell viability tests) and gently mixed with the cold D7.2 20 wt% solution at 4 °C). A final concentration of 1.0 million cells/mL was prepared and the ink was transferred to a 3 cm^3 barrel (*Nordson EFD*, Germany). The barrel was placed in an incubator at 37 °C to prevent sedimentation of cells. Before printing the ink was cooled to room temperature and processed.

Alternatively, hydrogels were printed using a compact bench-top 3D bioprinter (*Inkredible*, *Cellink*, Sweden) working on the principle of an extrusion-based printer. After dissolving the polymer in water, the ink was transferred to a 3 cm^3 barrel (*Nordson EFD*, Germany) and stored at room temperature for at least 15 minutes. A 0.20 mm inner diameter precision tip (*Nordson EFD*, Germany) was used as nozzle and the pressure was adjusted to ~1.2 bar depending on the polymer concentration. Printing was performed at room temperature.

Water Determination according to Karl Fischer

Water content of the applied solvents was determined by coulometric titration using a *TitroLine 7500 KF trace (SI analytics,* Mainz, Germany) with HYDRANAL® - Coulomat E as reagent. .

7.1.2 Methods of Measurement

Rheology

Samples for rheological analysis were freshly prepared in 15 ml centrifuge tubes and dissolved at 3 °C by continuously shaking. The MilliQ water was filtered through 0.2 µm Teflon filter (*Thermo Scientific, Schwerte,* Germany) to remove particles. By default, 0.45 ml polymer solution were applied to the bottom plate which was kept at 25 °C. After moving the upper plate to the trim position excess material was removed with a spatula to avoid interference during the measurements. Finally, a solvent trap was attached to minimize solvent vaporization.

The program used by default consist of an amplitude (0.01% - 100%) and frequency sweep (0.1 rad/s – 100 rad/s) at 5 °C and 37 °C followed by a temperature sweep and an oscillatory recovery experiment. Finally, the amplitude and frequency sweeps are repeated to determine if any changes occurred during the measurements. Every time a new temperature was set, the system was given 600 s to equilibrate. Rotational recovery experiments (10 cycles) and yield point determinations were carried out in independent measurements.

Viscosimetry

Sample preparation was performed as described for rheology measurements. Prior to viscosimetry the density at the lowest and highest temperature were determined in triplicate. The mean value were used for viscosimetry. For samples with a low polymer concentration a measuring angle of 20° was set manually while the auto angle function was switched on for solutions with higher polymer content.

Dynamic Light Scattering

The decay of the electric field-time autocorrelation function (ACF) $g_1(t)$ was fitted by a triexponential function (eq. 7.1), as described in more detail by Rausch *et al.* as well

as by Fischer and Schmidt with the amplitudes $a_i(q)$ and the decay times $\tau_i(q) = \left(q^2 \cdot D_{i,app}(q)\right)^{-1}$, with $D_{i,app}$ the apparent Brownian diffusion coefficient of the respective mode i, and q being the absolute value of the scattering vector.[343,352]

$$g_1(t) = a_1(q) \cdot e^{-\frac{t}{\tau_1}} + a_2(q) \cdot e^{-\frac{t}{\tau_2}} + a_2(q) \cdot e^{-\frac{t}{\tau_3}}$$

Cell culture (performed by PD Dr. Tessa Lühmann and Marco Saedtler)

Murine NIH 3T3 fibroblasts (ATCC-Number CRL-1658, ATCC, Manassas, VA) and human immortalized keratinocytes (HaCat cells) were maintained in 100 mm culture dishes in culture medium (Dulbecco's Modified Eagle Medium (DMEM) high glucose containing 10% (vol%) heat inactivated FBS, 100 U/mL penicillin and 0.1 mg/mL streptomycin) at 37 °C and 5% CO_2. After thawing, HaCat cells were passaged three times in 1:5 – 1:10 ratios before usage, to develop their phenotype.

Cell viability

The lyophilized polymer was dissolved in culture medium (DMEM high glucose containing 10% (vol%) heat inactivated FBS, 100 U/mL penicillin and 0.1 mg/mL streptomycin) at 30 wt%. $2 \cdot 10^4$ NIH 3T3 fibroblasts dispersed in media were incorporated into the polymer stock-solution by gentile mixing with an Eppendorf pipette on ice to yield a 100 µL solution, in which the final polymer concentration was 25 wt%. The solution was subsequently added to one well of a preheated (37 °C) 8-well LabTek chambers slide. After incubation for 24 h at 37 °C and 5% CO_2, cells were suspended with ice-cold PBS and equally divided in two parts for staining with either 0.01 µg/100 cells FDA or 0.003 µg/100 cells PI dissolved in PBS for 3 min at room temperature.[353] FDA as non-fluorescent substrate is a viability marker for enzymatic activity and cell-membrane integrity after active conversion to fluorescein (λ_{ex} = 492 nm, λ_{em} = 517 nm) by intracellular esterases in living cells. In contrast, PI (λ_{ex} = 540 nm, λ_{em} = 608 nm) does not penetrate intact membranes and intercalates stoichiometrically with nucleic acids in dead cells.[354] The cells were subsequently analyzed by flow cytometry on a FACS Calibur system. For detection, a 488 nm laser was chosen with the emission channel FL2 (585 nm / ± 21 nm) for PI or the emission channel FL1 (530 nm / ± 15 nm) for FDA, respectively. A total number of $5 \cdot 10^3$ events were counted with BD CellQuest™ Pro and the geometric mean

fluorescence intensity was determined for each condition using Flowing Software (version 2.5.1; Turku Bioimaging).

Distribution of NIH-3T3 cells

To visualize cells within the thermoreversible gel, the cell pellet of NIH 3T3 fibroblasts was FDA-stained and $2•10^4$ cells were incorporated into a 25 wt% polymer solution and added into 37 °C preheated 8-well LabTek chambers slides as described above. Subsequently, FDA stained cells were analyzed with a Zeiss Observer Z1 epi-fluorescence microscope (*Zeiss*, Oberkochen, Germany) equipped with a 37 °C incubation chamber. 3D stacks with 1 µm z-stack intervals were taken. Acquired 3D stacks were analyzed with the ZEN Imaging Software (*Zeiss*, Oberkochen, Germany).

WST-1 proliferation assay

$2•10^3$ NIH 3T3 fibroblasts per well were seeded in growth medium in a 96-well-format and incubated overnight at 37 °C and 5% CO_2. Dilution concentrations of the 30 wt% polymer stock solution were prepared (final polymer concentrations: 10 wt%, 5 wt%, 1 wt%, and 0.02 wt%) in growth medium on ice and added to the cells. Cell growth was stimulated for 48 h at 37 °C and 5% CO_2. Before analysis, the cell medium was carefully exchanged and replaced by fresh growth medium. The cells were incubated with WST-1 for 3 h at 37 °C according to the manufacturer's instructions. The absorbance of the soluble formazan product was determined at 570 nm using a Spectramax 250 microplate reader from *Molecular Devices* (Sunnyvale, USA).

To determine the cytotoxicity of the compounds a WST-1 proliferation assay was performed using HaCat cells of passage 47 – 50. Briefly, cells were suspended in culture medium and 100 µL were transferred into each well of 96-well plates ($5•10^4$ cells/mL). Negative control was 100 µL culture medium w/o cells. These plates were incubated overnight and further processed on the next day. 20 wt% polymer stock solutions of both compounds (D7.2 and Pluronic F127) were prepared in culture medium and cooled to 4 °C. A serial dilution with culture medium at 4 °C was performed and 100 µL of the dilutions were transferred into each well yielding a tested concentration range of 10 – 0.02 wt%. Positive control was untreated cells in culture medium. Treated plates were incubated for 24 h. After cooling the plates to 4 °C the medium was aspirated and each well was washed

with 200 µL PBS, which was aspirated immediately. Following the manufacturer instructions WST-1 proliferation dye was diluted 1:20 in culture medium and 200 µL were transferred into each well. The plates were incubated for 120 min and absorption was measured at 450 and 630 nm with a SpectraMax 250 microplate reader from *Molecular Devices* (San José, CA, USA). The absorption was corrected (Abs.(Corr.) = Abs.(450 nm)-Abs.(630 nm)) and normalized to the positive control (untreated cells + WST-1 proliferation dye) and negative control (culture medium + WST-1 proliferation dye). Experiments were performed in quadruplet (n = 4). Results were given as mean ± standard deviation.

Critical Micelle Concentration (CMC)

Pyrene features an emission spectrum with 5 distinct peaks between 360 and 400 nm.[355] The ratio of I_1/I_3 (i.e. the first and third peak of five) can be utilized to determine changes in the polarity of the microenvironment surrounding pyrene which occur for example after encapsulation into polymeric aggregates.[356] Pyrene solutions (24 µM, 5.0 mg/L in acetone) were added to glass vials and the solvent was removed by a gentle stream of argon. Subsequently, various amounts of polymer stock solutions were added and the solutions were diluted with MilliQ water to yield a final pyrene concentration of $5 \cdot 10^{-7}$ M. The samples were stored overnight at ambient temperature under the exclusion of light. Pyrene fluorescence was recorded from 360 – 400 nm (λ_{ex} = 333 nm) at 25 °C. The CMC was determined as the concentration at which the fitted I_1/I_3 ratio decreased by 10% of its total decrease.

7.2 Reagents and Solvents

All chemicals and solvents used in the scope of this work were purchased from *Sigma-Aldrich* (Steinheim, Germany), *Acros Organics* (Geel, Belgium), *abcr* (Karlsruhe, Germany), *Fluka* (Steinheim, Germany), or *Carl Roth* (Karlsruhe, Germany) and used as received unless otherwise stated. 2-*n*-propyl-oxazoline was prepared previously in the group by Christian May. Dulbecco's Modified Eagle Medium (DMEM), fluorescein diacetate (FDA) and propidium iodide (PI) were purchased from *Sigma-Aldrich* (Schnelldorf, Germany). Penicillin G and streptomycin solution were purchased from *Biochrom AG* (Berlin, Germany). Fetal bovine serum (FBS) was from *Gibco* (Darmstadt, Germany). 8-well LabTek chamber slides were from *Nunc* (Thermo Fisher Scientific, Schwerte, Germany). 96-well plates and 100 mm culture dishes were from *Greiner Bio One* (Frickenhausen, Germany). Water-soluble tetrazolium (WST-1) was from *Roche* (Basel, Switzerland). Methyl trifluoromethylsulfonate (MeOTf), propargyl tosylate, and all monomers were dried by refluxing over CaH_2, benzonitrile (PhCN) over P_2O_5, under dry argon atmosphere and subsequent distillation prior to use. Afterwards, all chemicals were stored under dry and inert conditions in a *MBRaun* (Garching, Germany) LABmaster 130 glovebox.

7.3 Methods

7.3.1 Monomer Synthesis, General Synthetic Procedure, GSP 1

1 eq of the respective nitrile, 0.8 – 1.2 eq of alkanolamine and 0.025 eq of zinc acetate dihydrate were added to a nitrogen flushed flask and heated to a maximum of 130 °C under reflux for at least 72 h until the reaction mixture turned dark brown. Reaction progress was controlled by Fourier-transform infrared (FTIR) – and ^{1}H NMR spectroscopy. Subsequently, the raw product was distilled via fractional vacuum distillation. The colorless distillate was stirred with CaH_2 before vacuum distillation was repeated. If traces of the respective educts were still present, distillation was repeated and the final product was stored under dry nitrogen atmosphere.

2-Methyl-2-Oxazoline, Up-scaling

1.56 kg (38.0 mol, 1.2 eq) acetonitrile, 1.93 kg (31.7 mol, 1.0 eq) ethanolamine and 173 g (792 mmol, 0.025 eq) zinc acetate dihydrate were synthesized according to GSP 1. After 94 h and 117 h in each case 109 g (2.66 mol) acetonitrile were added.

Lab notebook-ID: BUS01

Yield: 1.54 kg (18.09 mol, 57%)

M = 85.11 g/mol

bp = 65 °C (185 mbar)

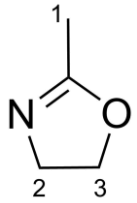

^{1}H NMR (300 MHz, 298.15 K, $CDCl_3$): δ [ppm] = 4.16 (t, 2H, H^3); 3.74 (t, 2H, H^2); 1.90 (t, 3H, H^1)

2-Methyl-2-Oxazine

117 g (2.85 mol, 1.0 eq) acetonitrile, 256.9 g (3.4 mol, 1.2 eq) 3-aminopropanol and 15.7 g (71 mmol, 0.025 eq) zinc acetate dihydrate were synthesized according to GSP 1.

Lab notebook-ID: GRM_MeOzi

Yield: 139.5 g (1.41 mol, 49.5%)

M = 99.13 g/mol

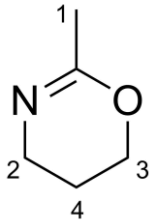

bp = 85 °C (200 mbar)

^{1}H NMR (300 MHz, 298.15 K, $CDCl_3$): δ [ppm] = 4.04 (t, 2H, H^3); 3.24 (t, 2H, H^2); 1.77 (t, 3H, H^1); 1.75 (quint, 2H, H^4)

2-Ethyl-2-Oxazin

195.0 g (3.54 mol, 1.0 eq) propionitrile, 319.1 g (4.25 mol, 1.2 eq) 3-aminopropanol and 19.4 g (99 mmol, 0.025 eq) zinc acetate dihydrate were synthesized according to GSP 1.

Lab notebook-ID: GRM_EtOzi

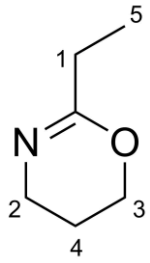

Yield: 260.4 g (2.30 mol, 65.0%)

M = 113.16 g/mol

bp = 84 °C (102 mbar)

^{1}H NMR (300 MHz, 298.15 K, $CDCl_3$): δ [ppm] = 4.08 (t, 2H, H^3); 3.30 (t, 2H, H^2); 2.08 (q, 2H, H^1); 1.79 (quint, 2H, H^4); 1.03 (t, 3H, H^5)

2-*n*-Propyl-2-Oxazin, Up-scaling

1.20 kg (17.36 mol, 1.0 eq) butyronitrile, 1.56 kg (20.83 mol, 1.2 eq) 3-aminopropanol and 95.3 g (434 mmol, 0.025 eq) zinc acetate dihydrate were synthesized according to GSP 1.

Lab notebook-ID: LRT029

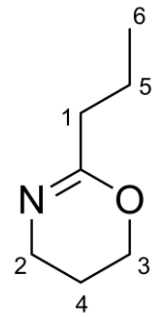

Yield: 1.15 kg (9.0 mol, 52%)

M = 127.19 g/mol

bp = 56 °C (12 mbar)

^{1}H NMR (300 MHz, 298.15 K, $CDCl_3$): δ [ppm] = 4.09 (t, 2H, H^3); 3.31 (t, 2H, H^2); 2.05 (t, 2H, H^1); 1.80 (quint, 2H, H^4); 1.53 (sext, 2H, H^5); 0.89 (t, 3H, H^6)

7.3.2 Polymer Synthesis

7.3.2.1 LCROP of 2-Oxazolines and 2-Oxazines, General Synthetic Procedure, GSP 2

Unless otherwise stated, all polymerizations were carried out according to the following procedure.

The initiator and the monomer(s) of the first block were dissolved in dry PhCN at room temperature under dry and inert conditions in a flame-dried flask. The reaction mixture was placed in an oil bath and heated to a maximum of 130 °C for 2-oxazines or 120 °C for 2-oxazolines, respectively. Full monomer conversion was verified by FTIR- and ^{1}H NMR spectroscopy before addition of the monomer(s) of the second block or third block. Termination was carried out with 3 eq with respect to the initiator for at least 10 h at 40 °C. After cooling to room temperature, an excess of potassium carbonate was added and the mixture was stirred for at least 4 h. If viscosity was not too high, K_2CO_3 was removed by centrifugation. The solvent was removed at reduced pressure and the flask was placed in a vacuum drying oven at 40 °C and < 10 mbar for at least 1 day. The product was dissolved in deionized water, dialyzed overnight using a membrane (regenerated cellulose) with a molecular weight cut-off of 1 kDa, 4 kDa, or 8 kDa, respectively, and freeze-dried.

7.3.2.2 Homopolymers

PMeOzi$_{50}$, H1

Under dry and inert conditions, 160.0 mg MeOTf (0.97 mmol, 1.0 eq) and 4.83 g MeOzi (48.8 mmol, 50.8 eq) were dissolved in 11 ml dry PhCN at RT. The reaction mixture was stirred at 130 °C for 24 h before the full monomer consumption was determined by FTIR-spectroscopy. For termination, the flask was placed in an ice bath and 459.8 mg (2.9 mmol, 3.0 eq) EPC were added. The reaction mixture was stirred at 40 °C over night. An excess of potassium carbonate was added, and the mixture was stirred for 4 h. After centrifugation the supernatant was precipitated in cold diethylether (10-20 fold of volume of polymer solution). After repeated centrifugation the remaining diethylether was removed under reduced pressure and the polymer was dissolved in a mixture of chloroform and methanol (1:2, vol%) and precipitated again. The residual was dissolved in deionized water and freeze-dried. A yellowish leather like material was obtain.

Lab notebook-ID: GRM001

Yield:	4.52 g (0.88 mmol, 92%)
M =	5127.89 g/mol
GPC (DMF):	M_n = 2.7 kg/mol, Đ = 1.53
GPC (HFIP):	M_n = 2.4 kg/mol, Đ = 1.32

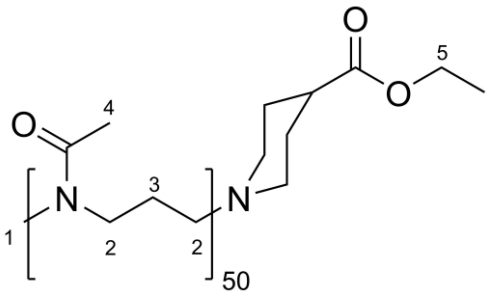

^{1}H NMR (300 MHz, 298.15 K, $CDCl_3$): δ [ppm] = 4.14 (q, 2H, H^5); 3.30 (br, 199H, H^2); 3.02 (br, 3H, H^1); 2.08 (br, 147H, H^4); 1.79 (br, 116H, H^3)

PMeOzi$_{62}$, H2

Synthesis was conducted by Jonas Herrmann in the course of his bachelor thesis according to GSP 2.

Initiation:	MeOTf	0.32 g (1.95 mmol, 1.0 eq)
Monomer:	MeOzi	9.67 g (97.5 mmol, 50 eq)
Termination:	EPC	0.92 g (5.85 mmol, 3.0 eq)
Reaction time:		24 h
Solvent:	PhCN	22.5 g
Lab notebook-ID:	HRJ006	
Yield:	7.89 g (1.25 mmol, 64%)	
M =	6317.49 g/mol	
GPC (HFIP):	M_n = 2.9 kg/mol, Đ = 1.36	
T_g (DSC) =	30.7 °C	

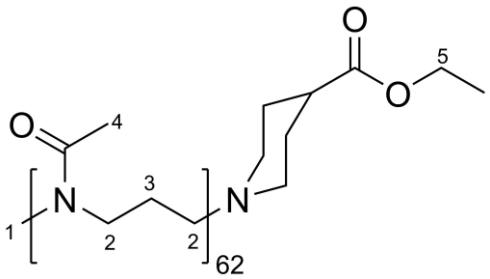

^{1}H NMR (300 MHz, 298.15 K, MeOD-d_4): δ [ppm] = 4.17 (q, 2H, H^5); 3.30 (br, 247H, H^2); 3.11-2.95 (br, 3H, H^1); 2.15 (br, 183H, H^4); 1.91 (br, 129H, H^3)

PEtOzi$_{50}$, H3

Synthesis was conducted as described for H1.

Initiation:	MeOTf	0.14 g (0.85 mmol, 1.0 eq)
Monomer:	EtOzi	4.85 g (42.9 mmol, 50 eq)
Termination:	EPC	0.41 g (2.61 mmol, 3.1 eq)
Reaction time:		6 h
Solvent:	PhCN	9.5 g
Lab notebook-ID:	GRM004	
Yield:	4.08 g (0.70 mmol, 81%)	
M =	5829.24 g/mol	
GPC (DMF):	M_n = 3.8 kg/mol, Đ = 1.34	
GPC (HFIP):	M_n = 2.9 kg/mol, Đ = 1.21	

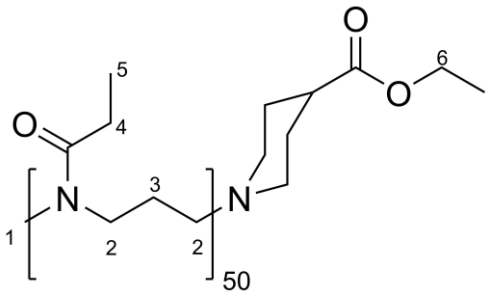

^{1}H NMR (300 MHz, 298.15 K, MeOD-*d*$_4$): δ [ppm] = 4.12 (b, 2H, H^6); 3.36 (br, 190H, H^2); 3.06 (br, 3H, H^1); 2.39 (br, 99H, H^4); 1.85 (br, 101H, H^3); 1.12 (br, 151H, H^5)

PEtOzi$_{205}$, H4

Synthesis was conducted as described for H1.

Initiation:	MeOTf	0.048 g (0.29 mmol, 1.0 eq)
Monomer:	EtOzi	4.95 g (43.7 mmol, 150 eq)
Termination:	EPC	0.138 g (0.88 mmol, 3.0 eq)
Reaction time:		4.5 h
Solvent:	PhCN	9.6 g
Lab notebook-ID:	GRM005	
Yield:	4.07 g (0.17 mmol, 60%)	
M =	23369.04 g/mol	
GPC (DMF):	M_n = 4.1 kg/mol, Đ = 2.06	
GPC (HFIP):	M_n = 3.1 kg/mol, Đ = 1.64	

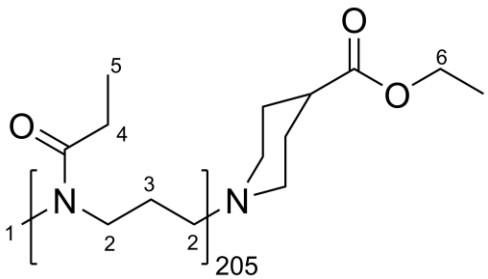

^{1}H NMR	(300 MHz, 298.15 K, MeOD-d_4): δ [ppm] = 4.12 (b, 1.6H, H^6); 3.36 (br, 802H, H^2); 3.06 (br, 3H, H^1); 2.39 (br, 410H, H^4); 1.85 (br, 411H, H^3); 1.12 (br, 622H, H^5)	

P*n*PrOzi$_{50}$, H5

Synthesis was conducted by Jonas Herrmann in the course of his bachelor thesis according to GSP 2 with slight variations. After removal of PhCN the polymer was dissolved in a mixture of deionized water and ethanol (1:1, v/v) and dialyzed and lyophilized as described.

Initiation:	MeOTf	0.23 g (1.40 mmol, 1.0 eq)
Monomer:	*n*PrOzi	9.87 g (77.6 mmol, 55 eq)
Termination:	EPC	0.258 g (1.64 mmol, 1.2 eq)
Reaction time:		20 h
Solvent:	PhCN	17.8 g
Lab notebook-ID:	HRJ001	
Yield:	7.01 g (1.07 mmol, 77%)	
M =	6530.59 g/mol	
GPC (HFIP):	M_n = 4.5 kg/mol, Đ = 1.08	
T_g (DSC) =	5.1 °C	
MALDI-TOF-MS:	M_p = 7066.6 m/z; Đ = 1.02	
^{1}H NMR	(300 MHz, 298.15 K, MeOD-d_4): δ [ppm] = 4.14 (q, 2H, H^7); 3.36 (br, 199H, H^2); 3.08-2.91 (br, 3H, H^1); 2.36 (br, 100H, H^4); 1.85 (br, 100H, H^3); 1.65 (br, 102H, H^5); 0.97 (br, 150H, H^6)	

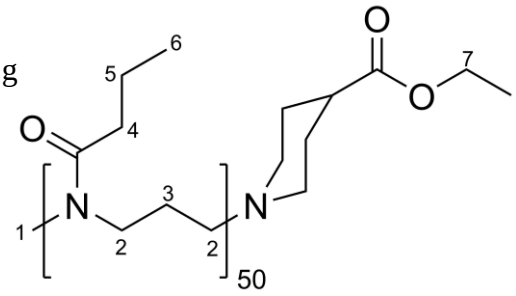

P*i*PrOzi$_{19}$, H6

Synthesis was conducted by Daniela Lautz in the course of her internship according to GSP 2 with slight variations. K_2CO_3 was removed by centrifugation before removing PhCN under reduced pressure. Then, the homopolymer was dissolved in chloroform and washed with acidified water for three times to remove unreacted 1-BOC-piperazine (BOC-Pip). Na_2S was added to the organic phase to remove remaining water before filtration. Subsequently, chloroform was removed under reduced pressure to obtain a yellowish leathery material.

Initiation:	MeOTf	0.12 g (0.73 mmol, 1.0 eq)
Monomer:	*i*PrOzi	1.85 g (14.5 mmol, 20 eq)
Termination:	BOC-Pip	0.27 g (1.44 mmol, 2.0 eq)
Reaction time:		16 h
Solvent:	PhCN	2 g
Lab notebook-ID:	LUD05	
Yield:	1.09 g (0.416 mmol, 57%)	
M =	2616.84 g/mol	
GPC (HFIP):	M_n = 1.0 kg/mol, Đ = 1.09	
T_g (DSC) =	20.3 °C	
^{1}H NMR	(300 MHz, 298.15 K, $CDCl_3$): δ [ppm] = 3.29 (br, 78H, H^2); 3.05-3.03 (br, 3H, H^1); 2.69 (br, 17H, H^4); 1.76 (br, 37H, H^3); 1.44 (br, 9H, H^6); 1.10 (br, 116H, H^5)	

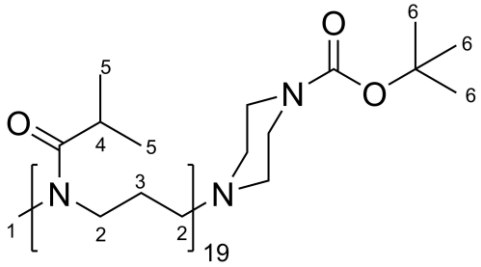

7.3.2.3 Diblock Copolymers

Me-P*n*PrOzi$_{22}$-*b*-PMeOx$_{21}$-EPC, D1

Synthesis was conducted according to GSP 2.

Initiation:	MeOTf	0.153 g (0.93 mmol, 1.0 eq)
Monomer 1st block:	*n*PrOzi	2.96 g (23.3 mmol, 25 eq)
Monomer 2nd block:	MeOx	1.98 g (23.2 mmol, 25 eq)
Termination:	EPC	0.426 g (2.71 mmol, 2.9 eq)
Reaction time (1./2.):		4.0 h / 1.5 h
Solvent:	PhCN	10.5 g
Lab notebook-ID:	LRT017	
Yield:	not determined	
M =	4756.58 g/mol	
GPC (DMF):	M_n = 3.9 kg/mol, Đ = 1.18	
^{1}H NMR	(300 MHz, 298.15 K, MeOD-d_4): δ [ppm] = 4.14 (q, 2H, H^9); 3.53 (br, 81H, H^7); 3.36 (br, 85H, H^2); 3.08-2.91 (br, 3H, H^1); 2.36 (br,	

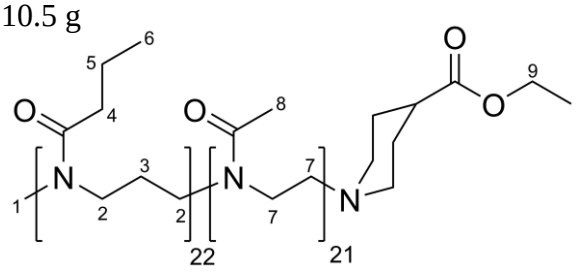

44H, H^4); 2.11 (br, 64H, H^8); 1.85 (br, 46H, H^3); 1.65 (br, 45H, H^5); 0.97 (br, 66H, H^6)

Me-P*n*PrOzi$_{50}$-*b*-PMeOx$_{49}$-EPC, D2.1

Synthesis was conducted according to GSP 2.

Initiation:	MeOTf	0.156 g (0.95 mmol, 1.0 eq)
Monomer 1st block:	*n*PrOzi	6.30 g (50 mmol, 52 eq)
Monomer 2nd block:	MeOx	4.17 g (49 mmol, 52 eq)
Termination:	EPC	0.480 g (3.1 mmol, 3.2 eq)
Reaction time (1./2.):		3.5 h / 1.5 h
Solvent:	PhCN	22 g
Lab notebook-ID:	HRA007	
Yield:	not determined	
M =	10700.78 g/mol	

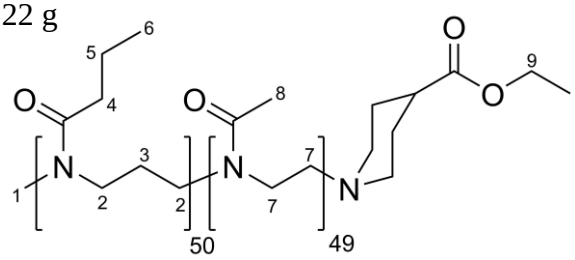

GPC (DMF): M_n = 10.0 kg/mol, Đ = 1.49

^{1}H NMR (300 MHz, 298.15 K, MeOD-d_4): δ [ppm] = 4.14 (q, 2H, H^9); 3.53 (br, 193H, H^7); 3.36 (br, 198H, H^2); 3.08-2.91 (br, 3H, H^1); 2.36 (br, 100H, H^4); 2.11 (br, 152H, H^8); 1.85 (br, 103H, H^3); 1.65 (br, 103H, H^5); 0.97 (br, 150H, H^6)

Me-P*n*PrOzi$_{57}$-*b*-PMeOx$_{55}$-EPC, D2.2

Synthesis was conducted according to GSP 2.

Initiation:	MeOTf	0.276 g (1.68 mmol, 1.0 eq)
Monomer 1st block:	*n*PrOzi	10.7 g (84 mmol, 50 eq)
Monomer 2nd block:	MeOx	7.15 g (84 mmol, 50 eq)
Termination:	EPC	0.85 g (5.4 mmol, 3.2 eq)
Reaction time (1./2.):		5.5 h / 12 h
Solvent:	PhCN	28 g

Lab notebook-ID: LRT011

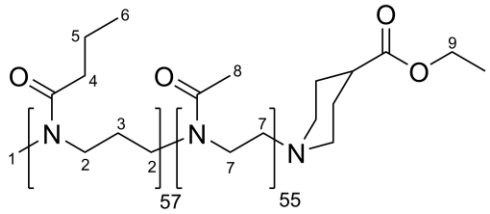

Yield: 18.35 g (1.5 mmol, 90%)

M = 12101.73 g/mol

GPC (DMF): M_n = 7.3 kg/mol, Đ = 1.17

^{1}H NMR (300 MHz, 298.15 K, MeOD-*d*$_4$): δ [ppm] = 4.14 (q, 3H, H^9); 3.53 (br, 216H, H^7); 3.36 (br, 214H, H^2); 3.08-2.91 (br, 3H, H^1); 2.36 (br, 112H, H^4); 2.11 (br, 170H, H^8); 1.85 (br, 115H, H^3); 1.65 (br, 116H, H^5); 0.97 (br, 168H, H^6)

Me-P*n*PrOzi$_{51}$-*b*-PMeOx$_{51}$-EPC, D2.3

Synthesis was conducted according to GSP 2.

Initiation:	MeOTf	0.228 g (1.39 mmol, 1.0 eq)
Monomer 1st block:	*n*PrOzi	8.84 g (69 mmol, 50 eq)
Monomer 2nd block:	MeOx	5.92 g (69 mmol, 50 eq)
Termination:	EPC	0.76 g (4.8 mmol, 3.5 eq)
Reaction time (1./2.):		6 h / 5 h
Solvent:	PhCN	35 g

Lab notebook-ID: BUB003

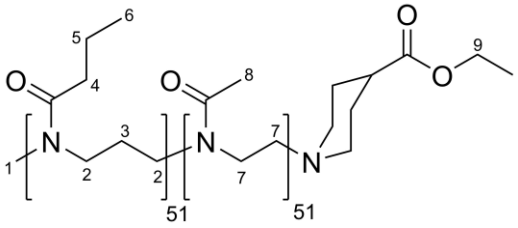

Yield: 12.15 g (1.1 mmol, 80%)

M = 10998.18 g/mol

GPC (DMF): M_n = 6.3 kg/mol, Đ = 1.29

^{1}H NMR (300 MHz, 298.15 K, MeOD-*d*$_4$): δ [ppm] = 4.14 (q, 1H, H^9); 3.52 (br, 203H, H^7); 3.36 (br, 201H, H^2); 3.08-2.91 (br, 3H, H^1); 2.36 (br, 108H, H^4); 2.11 (br, 160H, H^8); 1.86 (br, 110H, H^3); 1.65 (br, 111H, H^5); 0.97 (br, 162H, H^6)

Me-P*n*PrOzi$_{55}$-*b*-PMeOx$_{50}$-EPC, D2.4

Synthesis was conducted according to GSP 2.

Initiation:	MeOTf	0.0684 g (0.42 mmol, 1.0 eq)
Monomer 1st block:	*n*PrOzi	2.65 g (21 mmol, 50 eq)

Monomer 2nd block:	MeOx	2.07 g (24 mmol, 58 eq)
Termination:	EPC	0.22 g (1.4 mmol, 3.3 eq)
Reaction time (1./2.):		7 h / 12 h
Solvent:	PhCN	10 g
Lab notebook-ID:	BUB010	
Yield:	2.10 g (0.18 mmol, 44%)	
M =	11421.83 g/mol	

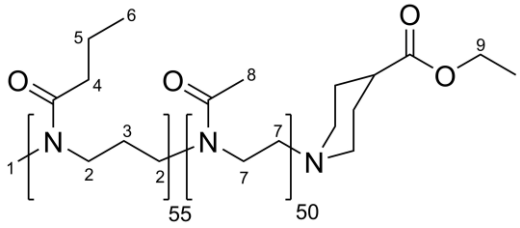

GPC (DMF):	M_n = 6.4 kg/mol, Đ = 1.28
^{1}H NMR	(300 MHz, 298.15 K, MeOD-*d*$_4$): δ [ppm] = 4.14 (q, 2H, H^9); 3.53 (br, 195H, H^7); 3.36 (br, 215H, H^2); 3.08-2.91 (br, 3H, H^1); 2.36 (br, 109H, H^4); 2.11 (br, 151H, H^8); 1.85 (br, 112H, H^3); 1.65 (br, 114H, H^5); 0.97 (br, 167H, H^6)

Me-P*n*PrOzi$_{45}$-*b*-PMeOx$_{44}$-EPC, D2.5

Synthesis was conducted according to GSP 2.

Initiation:	MeOTf	0.080 g (0.49 mmol, 1.0 eq)
Monomer 1st block:	*n*PrOzi	3.12 g (24.5 mmol, 50 eq)
Monomer 2nd block:	MeOx	2.08 g (24.4 mmol, 50 eq)
Termination:	EPC	0.28 g (1.8 mmol, 3.7 eq)
Reaction time (1./2.):		19 h / 2 h
Solvent:	PhCN	11 g
Lab notebook-ID:	MTA004	
Yield:	4.25 g (0.44 mmol, 90%)	
M =	9639.32 g/mol	

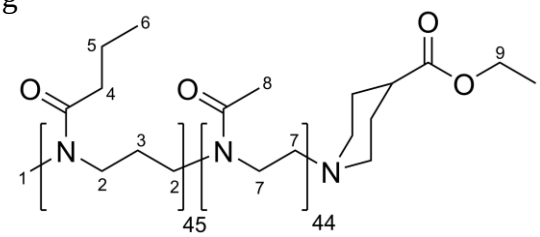

GPC (DMF):	M_n = 6.5 kg/mol, Đ = 1.22
^{1}H NMR	(300 MHz, 298.15 K, MeOD-*d*$_4$): δ [ppm] = 4.14 (q, 1H, H^9); 3.53 (br, 172H, H^7); 3.36 (br, 181H, H^2); 3.08-2.91 (br, 3H, H^1); 2.35 (br, 90H, H^4); 2.11 (br, 133H, H^8); 1.86 (br, 90H, H^3); 1.65 (br, 92H, H^5); 0.97 (br, 135H, H^6)

Me-PMeOx$_{51}$-*b*-P*n*PrOzi$_{53}$-EPC, D2.6

Synthesis was conducted according to GSP 2.

Initiation:	MeOTf	0.156 g (0.95 mmol, 1.0 eq)
Monomer 1st block:	MeOx	4.04 g (47.5 mmol, 50 eq)
Monomer 2nd block:	*n*PrOzi	6.17 g (48.5 mmol, 51 eq)
Termination:	EPC	0.46 g (2.9 mmol, 3.1 eq)
Reaction time (1./2.):		9 h / 15 h
Solvent:	PhCN	21 g
Lab notebook-ID:	LRT030	
Yield:	10.3 g (0.92 mmol, 96%)	
M =	11252.56 g/mol	
GPC (HFIP):	M_n = 5.4 kg/mol, Đ = 1.19	
T_g (DSC) =	8.6 °C, 69.0 °C	
^{1}H NMR	(300 MHz, 298.15 K, MeOD-d_4): δ [ppm] = 4.14 (q, 2H, H^9); 3.53 (br, 202H, H^7); 3.36 (br, 199H, H^2); 3.11-2.95 (br, 3H, H^1); 2.36 (br, 108H, H^4); 2.12 (br, 155H, H^8); 1.85 (br, 110H, H^3); 1.65 (br, 109H, H^5); 0.97 (br, 157H, H^6)	

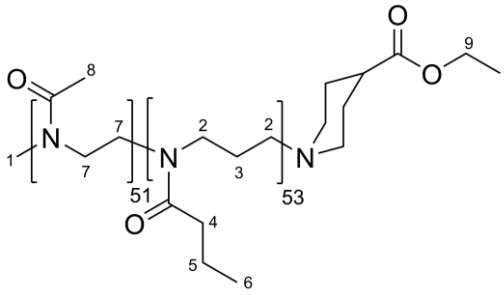

Me-P*n*PrOzi$_{27}$-*b*-PMeOx$_{72}$-EPC, D3

Synthesis was conducted according to GSP 2.

Initiation:	MeOTf	0.085 g (0.52 mmol, 1.0 eq)
Monomer 1st block:	*n*PrOzi	1.63 g (12.8 mmol, 24 eq)
Monomer 2nd block:	MeOx	3.27g (38.4 mmol, 74 eq)
Termination:	EPC	0.24 g (1.5 mmol, 2.9 eq)
Reaction time (1./2.):		4 h / 15 h
Solvent:	PhCN	12.5 g
Lab notebook-ID:	LRT016	
Yield:	not determined	
M =	9732.92 g/mol	

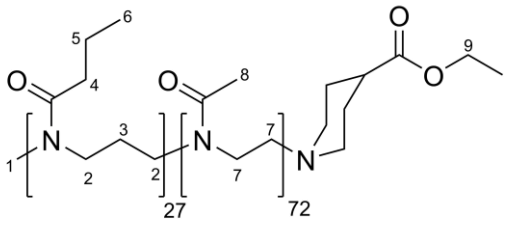

GPC (DMF): M_n = 5.6 kg/mol, Đ = 1.28

^{1}H NMR (300 MHz, 298.15 K, MeOD-d_4): δ [ppm] = 4.14 (q, 2H, H^9); 3.53 (br, 278H, H^7); 3.36 (br, 110H, H^2); 3.08-2.91 (br, 3H, H^1); 2.36 (br, 52H, H^4); 2.11 (br, 217H, H^8); 1.85 (br, 55H, H^3); 1.65 (br, 54H, H^5); 0.97 (br, 77H, H^6)

Me-P*n*PrOzi$_{106}$-*b*-PMeOx$_{31}$-EPC, D4

Synthesis was conducted according to GSP 2.

Initiation:	MeOTf	0.070 g (0.43 mmol, 1.0 eq)
Monomer 1st block:	*n*PrOzi	4.03 g (31.7 mmol, 74 eq)
Monomer 2nd block:	MeOx	0.90 g (10.6 mmol, 25 eq)
Termination:	EPC	0.20 g (1.3 mmol, 3.0 eq)
Reaction time (1./2.):		15 h / 4 h
Solvent:	PhCN	10 g
Lab notebook-ID:	LRT015	
Yield:	not determined	
M =	16291.35 g/mol	

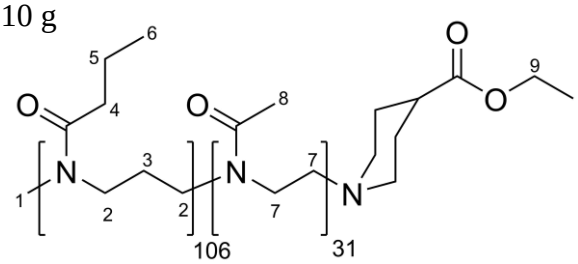

GPC (DMF): M_n = 8.3 kg/mol, Đ = 1.30

^{1}H NMR (300 MHz, 298.15 K, MeOD-d_4): δ [ppm] = 4.14 (q, 3H, H^9); 3.53 (br, 119H, H^7); 3.36 (br, 416H, H^2); 3.08-2.91 (br, 3H, H^1); 2.36 (br, 211H, H^4); 2.11 (br, 94H, H^8); 1.85 (br, 213H, H^3); 1.65 (br, 214H, H^5); 0.97 (br, 323H, H^6)

Me-PMeOx$_{59}$-*b*-P*n*PrOzi$_{61}$-EPC, D5

Synthesis was conducted according to GSP 2.

Initiation:	MeOTf	0.134 g (0.82 mmol, 1.0 eq)
Monomer 1st block:	MeOx	4.18 g (49.1 mmol, 60 eq)
Monomer 2nd block:	*n*PrOzi	6.21 g (48.8 mmol, 60 eq)
Termination:	EPC	0.463 g (2.95 mmol, 3.6 eq)
Reaction time (1./2.):		6 h / 12 h
Solvent:	PhCN	22 g

Lab notebook-ID:	LRT031
Yield:	9.92 g (0.766 mmol, 93%)
M =	12950.90 g/mol
GPC (HFIP):	M_n = 6.2 kg/mol, Đ = 1.20
T_g (DSC) =	8.1 °C, 68.7 °C
^{1}H NMR	(300 MHz, 298.15 K, MeOD-*d*$_4$): δ [ppm] = 4.14 (q, 2H, H^9); 3.53 (br, 232H, H^7); 3.36 (br, 235H, H^2); 3.10-2.92 (br, 3H, H^1); 2.36 (br, 124H, H^4); 2.12 (br, 181H, H^8); 1.86 (br, 125H, H^3); 1.65 (br, 125H, H^5); 0.97 (br, 182H, H^6)

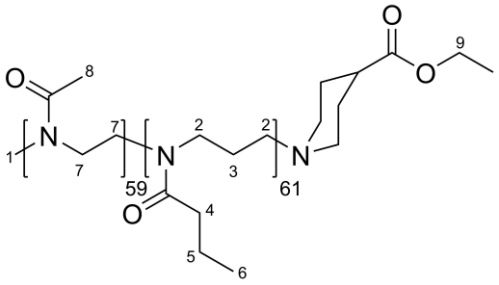

Me-PMeOx$_{85}$-*b*-P*n*PrOzi$_{85}$-EPC, D6

Synthesis was conducted according to GSP 2.

Initiation:	MeOTf	0.096 g (0.59 mmol, 1.0 eq)
Monomer 1st block:	MeOx	3.98 g (46.7 mmol, 80 eq)
Monomer 2nd block:	*n*PrOzi	5.98 g (47.0 mmol, 80 eq)
Termination:	EPC	0.282 g (1.79 mmol, 3.0 eq)
Reaction time (1./2.):		7 h / 20 h
Solvent:	PhCN	21 g
Lab notebook-ID:	LRT033	
Yield:	8.52 g (0.469 mmol, 80%)	
M =	18216.15 g/mol	
GPC (HFIP):	M_n = 7.9 kg/mol, Đ = 1.22	
T_g (DSC) =	7.5 °C, 72.7 °C	
^{1}H NMR	(300 MHz, 298.15 K, MeOD-*d*$_4$): δ [ppm] = 4.14 (q, 2H, H^9); 3.53 (br, 344H, H^7); 3.36 (br, 341H, H^2); 3.10-2.95 (br, 3H, H^1); 2.35 (br, 179H, H^4); 2.11 (br, 261H, H^8); 1.85 (br, 177H, H^3); 1.65 (br, 178H, H^5); 0.97 (br, 266H, H^6)	

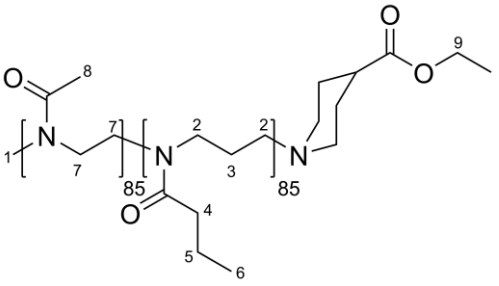

Me-P*n*PrOzi$_{107}$-*b*-PMeOx$_{79}$-EPC, D7.1

Synthesis was conducted according to GSP 2.

Initiation:	MeOTf	0.0567 g (0.35 mmol, 1.0 eq)
Monomer 1st block:	*n*PrOzi	4.266 g (33.5 mmol, 97 eq)

Monomer 2nd block:	MeOx	2.21 g (26.0 mmol, 75 eq)
Termination:	EPC	0.16 g (1.0 mmol, 2.9 eq)
Reaction time (1./2.):		5.5 h / 2 h
Solvent:	PhCN	13 g
Lab notebook-ID:	LRT012	
Yield:	6.5 g (0.32 mmol, 91%)	
M =	20503.62 g/mol	

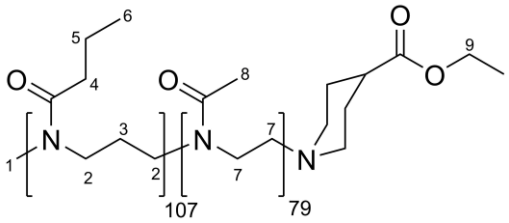

GPC (DMF):	M_n = 9.9 kg/mol, Đ = 1.24
^{1}H NMR	(300 MHz, 298.15 K, MeOD-*d*$_4$): δ [ppm] = 4.14 (q, 4H, H^9); 3.53 (br, 305H, H^7); 3.36 (br, 420H, H^2); 3.08-2.91 (br, 3H, H^1); 2.36 (br, 214H, H^4); 2.11 (br, 245H, H^8); 1.85 (br, 216H, H^3); 1.65 (br, 218H, H^5); 0.97 (br, 324H, H^6)

Me-P*n*PrOzi$_{104}$-*b*-PMeOx$_{105}$-EPC, D7.2

Synthesis was conducted according to GSP 2.

Initiation:	MeOTf	0.775 g (4.72 mmol, 1.0 eq)
Monomer 1st block:	*n*PrOzi	59.4 g (467.0 mmol, 99 eq)
Monomer 2nd block:	MeOx	40.2 g (472.4 mmol, 100 eq)
Termination:	EPC	2.28 g (14.5 mmol, 3.1 eq)
Reaction time (1./2.):		15 h / 4 h
Solvent:	PhCN	212 g
Lab notebook-ID:	MTA009	
Yield:	82.1 g (3.68 mmol, 78%)	
M =	22334.82 g/mol	

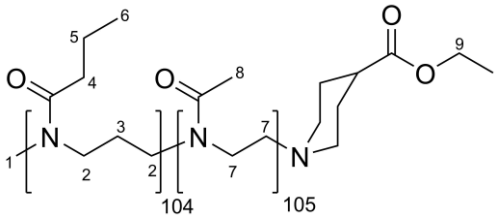

GPC (DMF):	M_n = 10.1 kg/mol, Đ = 1.34
GPC (HFIP):	M_n = 7.2 kg/mol, Đ = 1.30
T_g (DSC) =	8.1 °C, 71.7 °C
^{1}H NMR	(300 MHz, 298.15 K, MeOD-*d*$_4$): δ [ppm] = 4.14 (q, 2H, H^9); 3.53 (br, 422H, H^7); 3.36 (br, 414H, H^2); 3.08-2.91 (br, 3H, H^1); 2.36 (br, 225H, H^4); 2.11 (br, 324H, H^8); 1.85 (br, 227H, H^3); 1.65 (br, 230H, H^5); 0.97 (br, 334H, H^6)

Me-P*n*PrOzi$_{102}$-*b*-PMeOx$_{99}$-BOC, D8

Synthesis was conducted according to GSP 2.

Initiation:	MeOTf	0.0775 g (0.47 mmol, 1.0 eq)
Monomer 1st block:	*n*PrOzi	6.28 g (49.3 mmol, 105 eq)
Monomer 2nd block:	MeOx	4.11 g (48.3 mmol, 102 eq)
Termination:	BOC-Pip	0.293 g (1.57 mmol, 3.3 eq)
Reaction time (1./2.):		19.5 h / 4 h
Solvent:	PhCN	15 g
Lab notebook-ID:	MtC03	
Yield:	8.9 g (0.41 mmol, 87%)	
M =	21598.85 g/mol	

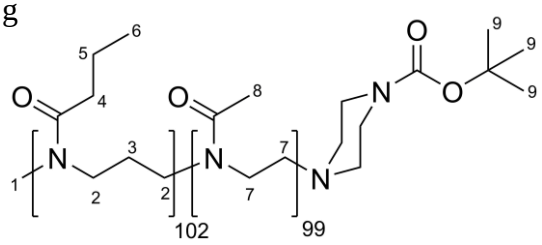

GPC (DMF):	M_n = 12.8 kg/mol, Đ = 1.66
GPC (HFIP):	M_n = 8.1 kg/mol, Đ = 1.42
^{1}H NMR	(300 MHz, 298.15 K, MeOD-*d*$_4$): δ [ppm] = 3.53 (br, 391H, H^7); 3.36 (br, 390H, H^2); 3.08-2.91 (br, 3H, H^1); 2.36 (br, 205H, H^4); 2.11 (br, 303H, H^8); 1.85 (br, 207H, H^3); 1.65 (br, 212H, H^5); 1.46 (s, 9H, H^9); 0.97 (br, 310H, H^6)

Propargyl-PMeOx$_{100}$-*b*-P*n*PrOzi$_{100}$-EPC/Thio/OH, D9/D10/D11

Synthesis was conducted according to GSP 2 with slight variations. In order to investigate end-group effects on the physicochemical properties of the resulting material, one batch was synthesized and equally divided into three batches before termination with EPC, methyl 3-mercaptopropionate (MMCP) and aqueous K_2CO_3 (D9 – D11). Subsequently each batch was treated as described in GSP 2. For reasons of clarity, in the following, a distinction will be made in the list after stating the amount of solvent used for this experiment.

Initiation:	Propargyl-OTs	0.160 g (0.76 mmol, 1.0 eq)
Monomer 1st block:	MeOx	6.484 g (76.2 mmol, 100 eq)
Monomer 2nd block:	*n*PrOzi	9.695 g (76.2 mmol, 100 eq)
Termination (D9):	EPC	0.230 g (1.46 mmol, 1.9 eq)
Termination (D10):	MMCP	0.165 g (1.37 mmol, 1.8 eq)
Termination (D11):	basic H_20	200 µL

Reaction time (1./2.): 4 h / 17.5 h

Solvent: PhCN 33 g

Lab notebook-ID: LEK003-I

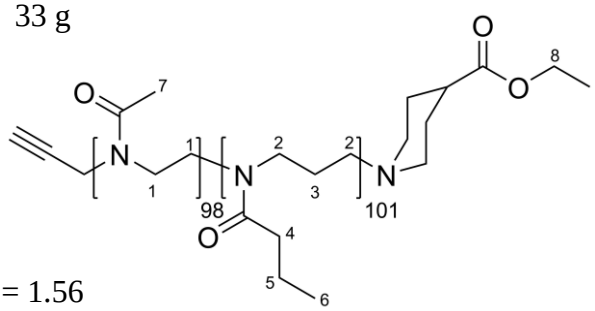

Yield: not determined

M = 21381.54 g/mol

GPC (DMF): M_n = 12.3 kg/mol, Đ = 1.56

^{1}H NMR (300 MHz, 298.15 K, MeOD-*d*$_4$): δ [ppm] = 4.14 (q, 2H, H^8); 3.52 (br, 392H, H^1); 3.36 (br, 397H, H^2); 2.35 (br, 202H, H^4); 2.11 (br, 294H, H^7); 1.85 (br, 205H, H^3); 1.65 (br, 203H, H^5); 0.97 (br, 300H, H^6)

Lab notebook-ID: LEK003-II

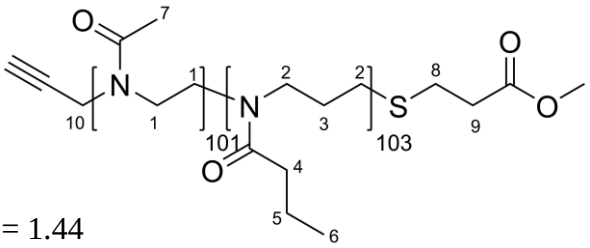

Yield: not determined

M = 21854.18 g/mol

GPC (DMF): M_n = 14.7 kg/mol, Đ = 1.44

^{1}H NMR (300 MHz, 298.15 K, MeOD-*d*$_4$): δ [ppm] = 4.12 (br, 2H, H^{10}); 3.53 (br, 405H, H^1); 3.36 (br, 406H, H^2); 2.90 (br, 2H, H^8), 2.57 (t, 2H, H^9); 2.36 (br, 207H, H^4); 2.11 (br, 302H, H^7); 1.85 (br, 209H, H^3); 1.63 (br, 210H, H^5); 0.97 (br, 307H, H^6)

Lab notebook-ID: LEK003-III

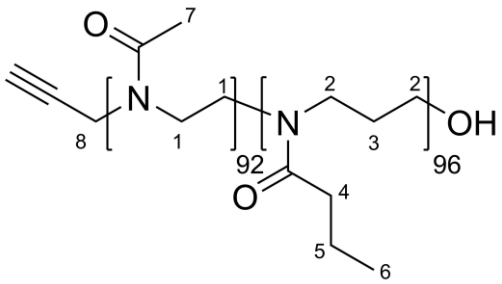

Yield: not determined

M = 20095.77 g/mol

GPC (DMF): M_n = 15.9 kg/mol, Đ = 1.31

^{1}H NMR (300 MHz, 298.15 K, MeOD-*d*$_4$): δ [ppm] = 4.15 (br, 2H, H^8); 3.52 (br, 372H, H^1); 3.36 (br, 380H, H^2); 2.35 (br, 192H, H^4); 2.11 (br, 273H, H^7); 1.85 (br, 197H, H^3); 1.64 (br, 192H, H^5); 0.97 (br, 279H, H^6)

Me-P*n*PrOzi$_{54}$-*b*-PEtOx$_{52}$-EPC, D12

Synthesis was conducted according to GSP 2.

Initiation:	MeOTf	0.0722 g (0.44 mmol, 1.0 eq)
Monomer 1st block:	*n*PrOzi	2.77 g (21.8 mmol, 50 eq)
Monomer 2nd block:	EtOx	2.16 g (21.8 mmol, 50 eq)
Termination:	EPC	0.22 g (1.42 mmol, 3.2 eq)
Reaction time (1./2.):		18 h / 5 h
Solvent:	PhCN	9 g
Lab notebook-ID:	LRT023	
Yield:	4.5 g (0.37 mmol, 84%)	
M =	12194.25 g/mol	
GPC (DMF):	M_n = 7.6 kg/mol, Đ = 1.18	
T_g (DSC) =	23.6 °C	

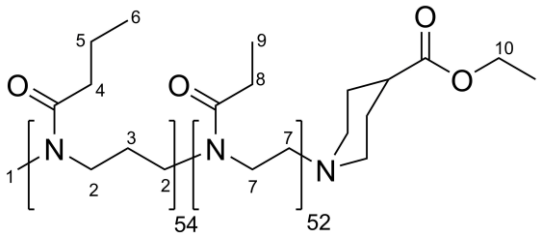

^{1}H NMR (300 MHz, 298.15 K, MeOD-*d*$_4$): δ [ppm] = 4.14 (q, 2H, H^{10}); 3.53 (br, 203H, H^7); 3.36 (br, 199H, H^2); 3.08-2.91 (br, 3H, H^1); 2.36 (br, 221H, H^4 & H^8); 1.85 (br, 114H, H^3); 1.65 (br, 119H, H^5); 1.11 (br, 161H, H^9) 0.97 (br, 175H, H^6)

Me-P*n*PrOx$_{67}$-*b*-PMeOzi$_{46}$-EPC, D13

Synthesis was conducted according to GSP 2.

Initiation:	MeOTf	0.0761 g (0.46 mmol, 1.0 eq)
Monomer 1st block:	*n*PrOx	2.71 g (23.9 mmol, 52 eq)
Monomer 2nd block:	MeOzi	2.37 g (23.9 mmol, 52 eq)
Termination:	EPC	0.25 g (1.59 mmol, 3.5 eq)
Reaction time (1./2.):		3 h / 19 h
Solvent:	PhCN	10.5 g
Lab notebook-ID:	MTA005	
Yield:	3.9 g (0.32 mmol, 68%)	
M =	12313.08 g/mol	
GPC (DMF):	M_n = 4.6 kg/mol, Đ = 1.21	

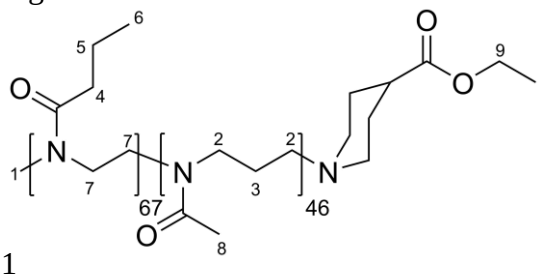

T_g (DSC) =	31.5 °C
^{1}H NMR	(300 MHz, 298.15 K, MeOD-d_4): δ [ppm] = 3.51 (br, 265H, H^7); 3.36 (br, 189H, H^2); 3.10-2.96 (br, 3H, H^1); 2.39 (br, 129H, H^4); 2.11 (br, 127H, H^8); 1.87 (br, 95H, H^3); 1.62 (br, 137H, H^5); 0.97 (br, 206H, H^6)

Me-P*n*PrOx$_{48}$-*b*-PMeOx$_{48}$-EPC, D14

Synthesis was conducted according to GSP 2.

Initiation:	MeOTf	0.0827 g (0.50 mmol, 1.0 eq)
Monomer 1st block:	*n*PrOx	2.82 g (24.9 mmol, 49 eq)
Monomer 2nd block:	MeOx	2.11 g (24.8 mmol, 49 eq)
Termination:	EPC	0.27 g (1.72 mmol, 3.4 eq)
Reaction time (1./2.):		4 h / 3 h
Solvent:	PhCN	11.5 g
Lab notebook-ID:	LRT024	
Yield:	4.2 g (0.43 mmol, 86%)	
M =	9688.01 g/mol	

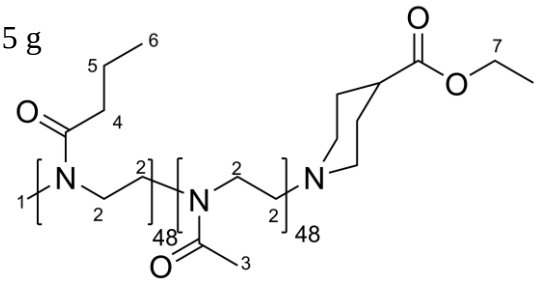

GPC (DMF):	bimodal, M_n = 5.4 kg/mol, Đ = 1.22
T_g (DSC) =	23.6 °C
^{1}H NMR	(300 MHz, 298.15 K, MeOD-d_4): δ [ppm] = 4.14 (q, 2H, H^7); 3.52 (br, 366H, H^2); 3.10-2.91 (br, 3H, H^1); 2.39 (br, 95H, H^4); 2.11 (br, 142H, H^3); 1.62 (br, 96H, H^5); 0.97 (br, 143H, H^6)

Me-PMeOzi$_{50}$-*b*-P*n*PrOzi$_{57}$-EPC, D15

Synthesis was conducted according to GSP 2.

Initiation:	MeOTf	0.0762 g (0.46 mmol, 1.0 eq)
Monomer 1st block:	MeOzi	2.18 g (22.0 mmol, 47 eq)
Monomer 2nd block:	*n*PrOzi	2.93 g (23.0 mmol, 50 eq)
Termination:	EPC	0.19 g (1.21 mmol, 2.6 eq)
Reaction time (1./2.):		47 h / 6 h
Solvent:	PhCN	10 g
Lab notebook-ID:	GRM006	

Yield:	4.2 g (0.36 mmol, 78%)
M =	12376.56 g/mol
GPC (HFIP):	M_n = 2.7 kg/mol, Đ = 1.82
T_g (DSC) =	9.7 °C, 27.4 °C

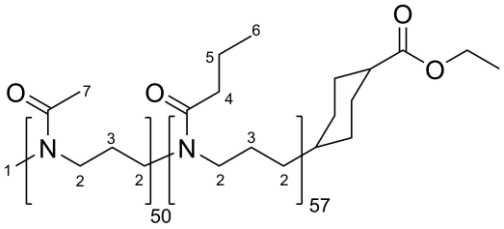

^{1}H NMR (300 MHz, 298.15 K, MeOD-*d*$_4$): δ [ppm] =3.36 (br, 389H, H^2); 3.08-2.91 (br, 3H, H^1); 2.36 (br, 113H, H^4); 2.11 (br, 151H, H^7); 1.86 (br, 189H, H^3); 1.65 (br, 119H, H^5); 0.97 (br, 170H, H^6)

Me-P*n*BuOzi$_{39}$-*b*-PMeOx$_{40}$-EPC, D16

Synthesis was conducted according to GSP 2 with slight variations. After centrifugation the supernatant was precipitated in cold diethyl ether and allowed to sediment overnight. The precipitate was filtered and dried under reduced pressure before dialysis was carried out as described in GSP 2.

Initiation:	MeOTf	0.220 g (1.34 mmol, 1.0 eq)
Monomer 1st block:	*n*BuOzi	7.09 g (50.2 mmol, 38 eq)
Monomer 2nd block:	MeOx	4.28 g (50.3 mmol, 38 eq)
Termination:	EPC	0.645 g (4.10 mmol, 3.1 eq)
Reaction time (1./2.):		2 h / 2 h
Solvent:	PhCN	20 g
Lab notebook-ID:	HRA008	
Yield:	not determined	
M =	9082.83 g/mol	

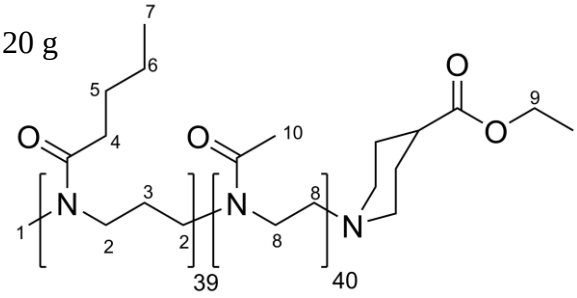

GPC (DMF):	M_n = 6.2 kg/mol, Đ = 1.15
T_g (DSC) =	-1.1 °C, 82.0 °C

^{1}H NMR (300 MHz, 298.15 K, MeOD-*d*$_4$): δ [ppm] = 4.14 (q, 2H, H^9) 3.53(br, 159H, H^8); 3.35 (br, 141H, H^2); 3.08-2.91 (br, 3H, H^1); 2.37 (br, 78H, H^4); 2.11 (br, 122H, H^{10}); 1.85 (br, 198H, H^3); 1.60 (br, 78H, H^5); 1.39 (br, 81H, H^6); 0.95 (br, 121H, H^7)

Me-P*i*PrOzi$_{103}$-*b*-PMeOx$_{100}$-EPC, D17

Synthesis was conducted according to GSP 2.

Initiation:	MeOTf	0.072 g (0.44 mmol, 1.0 eq)
Monomer 1st block:	*i*PrOzi	5.58 g (43.9 mmol, 100 eq)
Monomer 2nd block:	MeOx	3.74 g (43.9 mmol, 100 eq)
Termination:	EPC	0.307 g (1.95 mmol, 4.4 eq)
Reaction time (1./2.):		93 h / 8 h
Solvent:	PhCN	19 g
Lab notebook-ID:	LRT025	
Yield:	7.53 g (0.35 mmol, 79%)	
M =	21782.10 g/mol	
GPC (HFIP):	M_n = 6.3 kg/mol, Đ = 1.43	
T_g (DSC) =	39.0 °C, 75.8 °C	
^{1}H NMR	(300 MHz, 298.15 K, MeOD-d_4): δ [ppm] = 4.14 (q, 2H, H^6) 3.53(br, 395H, H^7); 3.36 (br, 393H, H^2); 3.12-3.08 (br, 2.4H, H^1); 2.86 (br, 103H, H^4); 2.11 (br, 307H, H^8); 1.84 (br, 213H, H^3); 1.11 (br, 617H, H^5)	

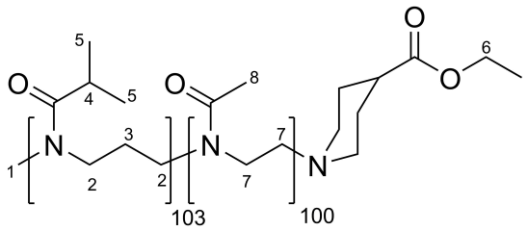

Me-PMeOx$_{57}$-*b*-P[*n*PrOzi$_{51}$-*co*-*n*BuOzi$_5$]-BOC, D18

Synthesis was conducted by a group of students during a practical laboratory course within the lecture “Polymere II” supervised by M.Sc. Niklas Gangloff according to GSP 2.

Initiation:	MeOTf	0.087 g (0.53 mmol, 1.0 eq)
Monomer 1st block:	MeOx	2.25 g (26.4 mmol, 50 eq)
Monomer 2nd block:	*n*PrOzi	3.03 g (23.8 mmol, 45 eq)
Monomer 2nd block:	*n*BuOzi	0.38 g (2.7 mmol, 5 eq)
Termination:	BOC-Pip	0.298 g (1.6 mmol, 3.0 eq)
Reaction time (1./2.):		3.5 h / 19 h
Solvent:	PhCN	17.6 g
Yield:	5.1 g (0.42 mmol, 79%)	
M =	12243.93 g/mol	
GPC (HFIP):	M_n = 6.5 kg/mol, Đ = 1.12	

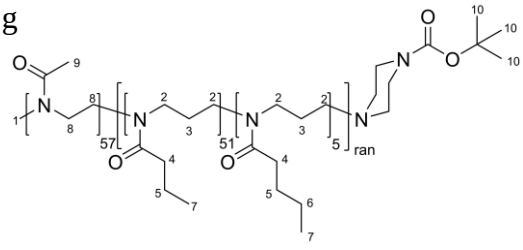

^{1}H NMR	(300 MHz, 298.15 K, MeOD-d_4): δ [ppm] = 3.52(br, 230H, H^8); 3.36 (br, 216H, H^2); 3.10-2.95 (br, 3H, H^1); 2.35 (br, 117H, H^4); 2.11 (br, 169H, H^9); 1.85 (br, 108H, H^3); 1.64 (br, 114H, H^5); 1.46 (s, 9H, H^{10}); 1.37 (br, 11H, H^6); 0.97 (br, 173H, H^7)

Me-PMeOx$_{96}$-*b*-P[*n*PrOzi$_{87}$-*co*-*n*BuOzi$_{11}$]-EPC, D19

Synthesis was conducted according to GSP 2.

Initiation:	MeOTf	0.077 g (0.47 mmol, 1.0 eq)
Monomer 1st block:	MeOx	3.95 g (46.4 mmol, 99 eq)
Monomer 2nd block:	*n*PrOzi	5.21 g (41.0 mmol, 88 eq)
Monomer 2nd block:	*n*BuOzi	0.65 g (4.6 mmol, 10 eq)
Termination:	EPC	0.352 g (2.24 mmol, 4.8 eq)
Reaction time (1./2.):		6 h / 15 h
Solvent:	PhCN	22 g
Lab notebook-ID:	LRT027	
Yield:	9.4 g (0.448 mmol, 96%)	
M =	20960.04 g/mol	
GPC (HFIP):	M_n = 8.6 kg/mol, Đ = 1.22	

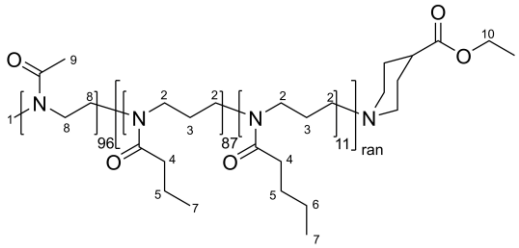

^{1}H NMR	(300 MHz, 298.15 K, MeOD-d_4): δ [ppm] = 4.14 (q, 2H, H^{10}) 3.53(br, 379H, H^8); 3.36 (br, 385H, H^2); 3.11-2.95 (br, 3H, H^1); 2.36 (br, 196H, H^4); 2.11 (br, 292H, H^9); 1.85 (br, 198H, H^3); 1.65 (br, 199H, H^5); 1.39 (br, 22H, H^6); 0.97 (br, 292H, H^7)

Me-PMeOx$_{109}$-*b*-P[*n*PrOzi$_{82}$-*co*-*n*BuOzi$_{28}$]-EPC, D20

Synthesis was conducted according to GSP 2.

Initiation:	MeOTf	0.075 g (0.46 mmol, 1.0 eq)
Monomer 1st block:	MeOx	3.92 g (46.1 mmol, 101 eq)
Monomer 2nd block:	*n*PrOzi	4.44 g (34.9 mmol, 76 eq)
Monomer 2nd block:	*n*BuOzi	1.63 g (11.5 mmol, 25 eq)
Termination:	EPC	0.246 g (1.56 mmol, 3.4 eq)
Reaction time (1./2.):		5 h / 17 h

Solvent:	PhCN	22 g
Lab notebook-ID:	LRT028	
Yield:	9.1 g (0.382mmol, 84%)	
M =	23815.28 g/mol	
GPC (HFIP):	M_n = 10.4 kg/mol, Đ = 1.27	
^{1}H NMR	(300 MHz, 298.15 K, MeOD-d_4): δ [ppm] = 4.14 (q, 2H, H^{10}) 3.53(br, 436H, H^8); 3.36 (br, 432H, H^2); 3.11-2.95 (br, 3H, H^1); 2.36 (br, 222H, H^4); 2.12 (br, 327H, H^9); 1.85 (br, 216H, H^3); 1.64 (br, 225H, H^5); 1.39 (br, 57H, H^6); 0.97 (br, 338H, H^7)	

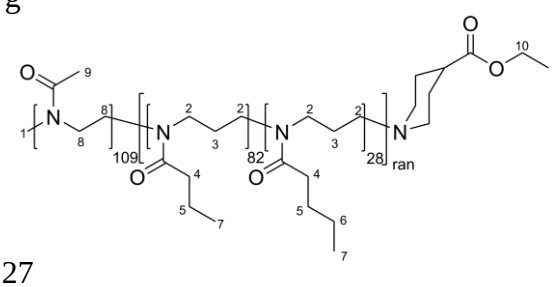

7.3.2.4 Triblock Copolymer

Me-PMeOx$_{25}$-*b*-P*n*PrOzi$_{50}$-*b*-PMeOx$_{24}$-EPC, T1

Synthesis was conducted according to GSP 2.

Initiation:	MeOTf	0.169 g (1.04 mmol, 1.0 eq)
Monomer 1st block:	MeOx	2.12 g (24.9 mmol, 24 eq)
Monomer 2nd block:	*n*PrOzi	6.47 g (50.9 mmol, 49 eq)
Monomer 3rd block:	MeOx	2.10 g (24.6 mmol, 24 eq)
Termination:	EPC	0.512 g (3.26 mmol, 3.1 eq)
Reaction time (1./2./3.):		3 h / 5 h / 3.5 h
Solvent:	PhCN	22 g
Lab notebook-ID:	GRM009	
Yield:	7.5 g (0.70 mmol, 68%)	
M =	10700.78 g/mol	
GPC (DMF):	M_n = 6.8 kg/mol, Đ = 1.15	
^{1}H NMR	(300 MHz, 298.15 K, $CDCl_3$): δ [ppm] = 4.13 (q, 2H, H^9); 3.46 (br, 189H, H^7); 3.30 (br, 196H, H^2); 3.04-2.95 (br, 3H, H^1); 2.26 (br, 100H, H^4); 2.14 (br, 151H, H^8); 1.78 (br, 104H, H^3); 1.63 (br, 106H, H^5); 0.94 (br, 147H, H^6)	

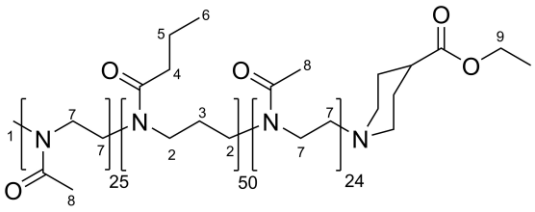

7.3.2.5 Random Copolymer

Me-P(*n*PrOzi$_{58}$-*co*-MeOx$_{60}$)$_{ran}$-EPC, R1

Synthesis was conducted according to GSP 2 with slight differences. In order to obtain a random copolymer both monomers were added simultaneously to the initiator dissolved in PhCN.

Initiation:	MeOTf	0.152 g (0.93 mmol, 1.0 eq)
1st Monomer:	*n*PrOzi	5.90 g (46.4 mmol, 50 eq)
2nd Monomer	MeOx	3.96 g (46.5 mmol, 50 eq)
Termination:	EPC	0.44 g (2.80 mmol, 3.0 eq)
Reaction time:		10 h
Solvent:	PhCN	21 g
Lab notebook-ID:	LRT014	
Yield:	8.7 g (0.69 mmol, 74%)	
M =	12654.45 g/mol	
GPC (DMF):	M_n = 6.2 kg/mol, Đ = 1.31	
T_g (DSC) =	29.4 °C	
^{1}H NMR	(300 MHz, 298.15 K, MeOD-d_4): δ [ppm] = 4.14 (q, 3H, H^9); 3.52 (br, 234H, H^7); 3.37 (br, 223H, H^2); 3.08-2.91 (br, 3H, H^1); 2.36 (br, 115H, H^4); 2.11 (br, 183H, H^8); 1.86 (br, 119H, H^3); 1.63 (br, 120H, H^5); 0.97 (br, 177H, H^6)	

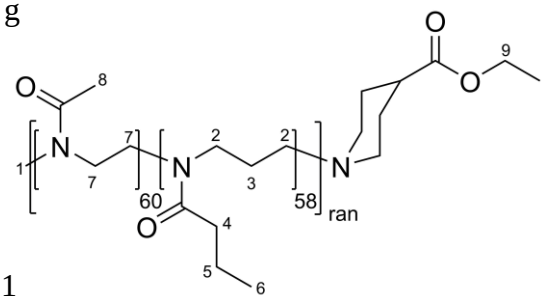

Bibliography

[1] J. Osterhammel, *Die Verwandlung der Welt. Eine Geschichte des 19. Jahrhunderts*, Verlag C. H. Beck oHG, München, **2016**.
[2] M. Gurven, H. Kaplan, *Popul. Dev. Rev.* **2007**, *33*, 321.
[3] The World Factbook 2018. Washington, DC: Central Intelligence Agency, **2018**. https://www.cia.gov/library/publications/the-world-factbook/index.html [Accessed 09th october 2018].
[4] NASA, https://www.nasa.gov/feature/vascular-tissue-challenge, [Accessed 09th october 2018].
[5] J. M. Bemmelen, *Zeitschr f Chem und Ind der Kolloide* **1907**, *1*, 213.
[6] P. J. Flory, *Faraday Discuss. Chem. Soc.* **1974**, *57*, 7.
[7] M. Rubinstein, R. H. Colby, *Polymer physics*, Oxford Univ. Press, Oxford, **2010**.
[8] P. S. Russo in *ACS Symposium Series, Vol. 350* (Ed.: P. S. Russo), American Chemical Soc, Washington, DC, **1987**, pp. 1–21.
[9] J. E. Babensee, J. M. Anderson, L. V. McIntire, A. G. Mikos, *Adv. Drug Deliv. Rev.* **1998**, *33*, 111.
[10] R. D. Harkness, *Biol. Rev.* **1961**, *36*, 399.
[11] C. H. Lee, A. Singla, Y. Lee, *Int. J. Pharm.* **2001**, *221*, 1.
[12] H. Furthmayr, R. Timpl in *International Review of Connective Tissue Research* (Eds.: D. A. Hall, D. S. Jackson), Elsevier Science, Burlington, **1976**, pp. 61–99.
[13] A. S. Craig, M. J. Birtles, J. F. Conway, D. A.D. Parry, *Connect. Tissue Res.* **2009**, *19*, 51.
[14] S. R. Caliari, J. A. Burdick, *Nat. Methods* **2016**, *13*, 405.
[15] B. D. Walters, J. P. Stegemann, *Acta Biomater.* **2014**, *10*, 1488.
[16] S. Gomes, I. B. Leonor, J. F. Mano, R. L. Reis, D. L. Kaplan, *Prog. Polym. Sci.* **2012**, *37*, 1.
[17] a) R. Parenteau-Bareil, R. Gauvin, F. Berthod, *Materials* **2010**, *3*, 1863; b) E. M. Noah, J. Chen, X. Jiao, I. Heschel, N. Pallua, *Biomaterials* **2002**, *23*, 2855.
[18] T. Jüngst, W. Smolan, K. Schacht, T. Scheibel, J. Groll, *Chem. Rev.* **2016**, *116*, 1496.
[19] C. M. Smith, A. L. Stone, R. L. Parkhill, R. L. Stewart, M. W. Simpkins, A. M. Kachurin, W. L. Warren, S. K. Williams, *Tissue Eng.* **2004**, *10*, 1566.
[20] a) V. Charulatha, *Biomaterials* **2003**, *24*, 759; b) L.-P. Yan, Y.-J. Wang, L. Ren, G. Wu, S. G. Caridade, J.-B. Fan, L.-Y. Wang, P.-H. Ji, J. M. Oliveira, J. T. Oliveira et al., *J. Biomed. Mater. Res. A* **2010**, *95*, 465; c) I. V. Yannas, J. F. Burke, *J. Biomed. Mater. Res.* **1980**, *14*, 65; d) P. Angele, J. Abke, R. Kujat, H. Faltermeier, D. Schumann, M. Nerlich, B. Kinner, C. Englert, Z. Ruszczak, R. Mehrl et al., *Biomaterials* **2004**, *25*, 2831; e) D. Y. S. Chau, R. J. Collighan, E. A. M. Verderio, V. L. Addy, M. Griffin, *Biomaterials* **2005**, *26*, 6518; f) S. Mizuno, J. Glowacki, *Biomaterials* **1996**, *17*, 1819.
[21] a) Arthur Veis, *The Macromolecular Chemistry of Gelatin*, Academic Press, New York & London, **1964**; b) L. Bozec, M. Odlyha, *Biophysical journal* **2011**, *101*, 228.
[22] C. Michon, G. Cuvelier, B. Launay, *Rheol. Acta* **1993**, *32*, 94.
[23] a) M. Nikkhah, N. Eshak, P. Zorlutuna, N. Annabi, M. Castello, K. Kim, A. Dolatshahi-Pirouz, F. Edalat, H. Bae, Y. Yang et al., *Biomaterials* **2012**, *33*, 9009; b)

J. Ramón-Azcón, S. Ahadian, R. Obregón, G. Camci-Unal, S. Ostrovidov, V. Hosseini, H. Kaji, K. Ino, H. Shiku, A. Khademhosseini et al., *Lab Chip* **2012**, *12*, 2959.

[24] a) J. W. Nichol, S. T. Koshy, H. Bae, C. M. Hwang, S. Yamanlar, A. Khademhosseini, *Biomaterials* **2010**, *31*, 5536; b) Y.-C. Chen, R.-Z. Lin, H. Qi, Y. Yang, H. Bae, J. M. Melero-Martin, A. Khademhosseini, *Adv. Funct. Mater.* **2012**, *22*, 2027.

[25] a) W. Schuurman, P. A. Levett, M. W. Pot, P. R. van Weeren, W. J. A. Dhert, D. W. Hutmacher, F. P. W. Melchels, T. J. Klein, J. Malda, *Macromol. Biosci.* **2013**, *13*, 551; b) R. Levato, W. R. Webb, I. A. Otto, A. Mensinga, Y. Zhang, M. van Rijen, R. van Weeren, I. M. Khan, J. Malda, *Acta Biomater.* **2017**, *61*, 41.

[26] F. P. W. Melchels, W. J. A. Dhert, D. W. Hutmacher, J. Malda, *J. Mater. Chem. B* **2014**, *2*, 2282.

[27] T. Billiet, E. Gevaert, T. de Schryver, M. Cornelissen, P. Dubruel, *Biomaterials* **2014**, *35*, 49.

[28] a) H. K. Kleinman, G. R. Martin, *Semin. Cancer Biol.* **2005**, *15*, 378; b) H. K. Kleinman, M. L. McGarvey, J. R. Hassell, V. L. Star, F. B. Cannon, G. W. Laurie, G. R. Martin, *Biochemistry* **1986**, *25*, 312.

[29] R. Fridman, G. Giaccone, T. Kanemoto, G. R. Martin, A. F. Gazdar, J. L. Mulshine, *Proc. Natl. Acad. Sci. U.S.A.* **1990**, *87*, 6698.

[30] J. W. Weisel, R. I. Litvinov, *Blood* **2013**, *121*, 1712.

[31] a) J. Liu, Y. Tan, H. Zhang, Y. Zhang, P. Xu, J. Chen, Y.-C. Poh, K. Tang, N. Wang, B. Huang, *Nat. Mater. (Nature Materials)* **2012**, *11*, 734; b) E. Sproul, S. Nandi, A. Brown in *Peptides and Proteins as Biomaterials for Tissue Regeneration and Repair* (Ed.: M. Barbosa), WOODHEAD, S.l., **2017**, pp. 151–173.

[32] D. Eyrich, F. Brandl, B. Appel, H. Wiese, G. Maier, M. Wenzel, R. Staudenmaier, A. Goepferich, T. Blunk, *Biomaterials* **2007**, *28*, 55.

[33] P. A. Janmey, J. P. Winer, J. W. Weisel, *J. R. Soc. Interface* **2009**, *6*, 1.

[34] a) A. C. Brown, T. H. Barker, *Acta Biomater.* **2014**, *10*, 1502; b) W. Zhao, X. Jin, Y. Cong, Y. Liu, J. Fu, *J. Chem. Technol. Biotechnol.* **2013**, *88*, 327; c) G. F. Smith, *Biochem. J.* **1980**, *185*, 1.

[35] S. L. Rowe, S. Lee, J. P. Stegemann, *Acta Biomater.* **2007**, *3*, 59.

[36] W. Ho, B. Tawil, J. C.Y. Dunn, B. M. Wu, *Tissue Eng.* **2006**, *12*, 1587.

[37] D. A. Cheresh, S. A. Berliner, V. Vicente, Z. M. Ruggeri, *Cell* **1989**, *58*, 945.

[38] Y.-B. Lee, S. Polio, W. Lee, G. Dai, L. Menon, R. S. Carroll, S.-S. Yoo, *Exp. Neurol.* **2010**, *223*, 645.

[39] C. Storm, J. J. Pastore, F. C. MacKintosh, T. C. Lubensky, P. A. Janmey, *Nature* **2005**, *435*, 191.

[40] a) A. Heidebrecht, T. Scheibel, *Adv. Appl. Microbiol.* **2013**, *82*, 115; b) J. A. Kluge, O. Rabotyagova, G. G. Leisk, D. L. Kaplan, *Trends Biotechnol.* **2008**, *26*, 244; c) J. M. Gosline, M.E. DeMont, M. W. Denny, *Endeavour* **1986**, *10*, 37.

[41] K. Schacht, T. Jüngst, M. Schweinlin, A. Ewald, J. Groll, T. Scheibel, *Angew. Chem., Int. Ed.* **2015**, *54*, 2816.

[42] a) K. Schacht, T. Scheibel, *Biomacromolecules* **2011**, *12*, 2488; b) K. Schacht, T. Scheibel, *Curr. Opin. Biotechnol.* **2014**, *29*, 62; c) K. Schacht, J. Vogt, T. Scheibel,

ACS Biomater. Sci. Eng. **2016**; d) G. H. Altman, F. Diaz, C. Jakuba, T. Calabro, R. L. Horan, J. Chen, H. Lu, J. Richmond, D. L. Kaplan, *Biomaterials* **2003**, *24*, 401; e) A. Leal-Egaña, T. Scheibel, *Biotechnol. Appl. Biochem.* **2010**, *55*, 155; f) L.-D. Koh, Y. Cheng, C.-P. Teng, Y.-W. Khin, X.-J. Loh, S.-Y. Tee, M. Low, E. Ye, H.-D. Yu, Y.-W. Zhang et al., *Prog. Polym. Sci.* **2015**, *46*, 86; g) L. T. Saldin, M. C. Cramer, S. S. Velankar, L. J. White, S. F. Badylak, *Acta Biomater.* **2017**, *49*, 1.

[43] a) F. Pati, J. Jang, D.-H. Ha, S. Won Kim, J.-W. Rhie, J.-H. Shim, D.-H. Kim, D.-W. Cho, *Nat. Commun.* **2014**, *5*, 3935; b) J. Jang, H.-J. Park, S.-W. Kim, H. Kim, J. Y. Park, S. J. Na, H. J. Kim, M. N. Park, S. H. Choi, S. H. Park et al., *Biomaterials* **2017**, *112*, 264.

[44] A. O. Brightman, B. P. Rajwa, J. E. Sturgis, M. E. McCallister, J. P. Robinson, S. L. Voytik-Harbin, *Biopolymers* **2000**, *54*, 222.

[45] M. T. Spang, K. L. Christman, *Acta Biomater.* **2018**, *68*, 1.

[46] R. Langer, D. A. Tirrell, *Nature* **2004**, *428*, 487.

[47] K. Meyer, J. W. Palmer, *J. Biol. Chem.* **1934**, *107*, 629.

[48] B. P. Toole, *Nat. Rev. Cancer* **2004**, *4*, 528.

[49] J. R. E. Fraser, T. C. Laurent, U. B. G. Laurent, *J. Intern. Med.* **1997**, *242*, 27.

[50] J. A. Burdick, G. D. Prestwich, *Adv. Mater.* **2011**, *23*, H41-56.

[51] M. George, T. E. Abraham, *J. Control. Release* **2006**, *114*, 1.

[52] a) K. I. Draget, B. T. Stokke, Y. Yuguchi, H. Urakawa, K. Kajiwara, *Biomacromolecules* **2003**, *4*, 1661; b) K. I. Draget, G. Skjåk Bræk, O. Smidrød, *Carbohydr. Pol.* **1994**, *25*, 31.

[53] a) G. T. Grant, E. R. Morris, D. A. Rees, P. J.C. Smith, D. Thom, *FEBS Letters* **1973**, *32*, 195; b) W. Mackie, S. Perez, R. Rizzo, F. Taravel, M. Vignon, *Int. J. Biol. Macromol.* **1983**, *5*, 329.

[54] R. A. A. Muzzarelli, *Cell. Mol. Life. Sci.* **1997**, *53*, 131.

[55] L. Vachoud, N. Zydowicz, A. Domard, *Carbohydr. Res.* **1997**, *302*, 169.

[56] A. Chenite, *Carbohydr. Pol.* **2001**, *46*, 39.

[57] R. Jin, L. S. Moreira Teixeira, P. J. Dijkstra, M. Karperien, C. A. van Blitterswijk, Z. Y. Zhong, J. Feijen, *Biomaterials* **2009**, *30*, 2544.

[58] D.-y. Teng, Z.-m. Wu, X.-g. Zhang, Y.-x. Wang, C. Zheng, Z. Wang, C.-x. Li, *Polymer* **2010**, *51*, 639.

[59] S. Arnott, A. Fulmer, W. E. Scott, I.C.M. Dea, R. Moorhouse, D. A. Rees, *J. Mol. Bio.* **1974**, *90*, 269.

[60] D. Velasco, E. Tumarkin, E. Kumacheva, *Small* **2012**, *8*, 1633.

[61] V. Normand, D. L. Lootens, E. Amici, K. P. Plucknett, P. Aymard, *Biomacromolecules* **2000**, *1*, 730.

[62] a) Y. Yamada, K. Hozumi, A. Aso, A. Hotta, K. Toma, F. Katagiri, Y. Kikkawa, M. Nomizu, *Biomaterials* **2012**, *33*, 4118; b) T. A. Ulrich, A. Jain, K. Tanner, J. L. MacKay, S. Kumar, *Biomaterials* **2010**, *31*, 1875; c) Q. Chen, L. Zhu, H. Chen, H. Yan, L. Huang, J. Yang, J. Zheng, *Adv. Funct. Mater.* **2015**, *25*, 1598; d) X. Yu, G. P. Dillon, R. B. Bellamkonda, *Tissue Eng.* **1999**, *5*, 291; e) E. Schuh, S. Hofmann, K. Stok, H. Notbohm, R. Müller, N. Rotter, *J. Biomed. Mater. Res. A* **2012**, *100*, 38.

[63] A. M. Fialho, L. M. Moreira, A. T. Granja, A. O. Popescu, K. Hoffmann, I. Sá-Correia, *Appl. Microbiol. Biotechnol.* **2008**, *79*, 889.

[64] F. Freitas, V. D. Alves, M. A. M. Reis, *Trends Biotechnol.* **2011**, *29*, 388.

[65] a) P.-E. Jansson, B. Lindberg, P. A. Sandford, *Carbohydr. Res.* **1983**, *124*, 135; b) M. A. O'Neill, R. R. Selvendran, V. J. Morris, *Carbohydr. Res.* **1983**, *124*, 123.

[66] S. Ikeda, Y. Nitta, B. S. Kim, T. Temsiripong, R. Pongsawatmanit, K. Nishinari, *Food Hydrocolloids* **2004**, *18*, 669.

[67] E. Miyoshi, T. Takaya, K. Nishinari, *Food Hydrocolloids* **1994**, *8*, 505.

[68] J. F. Mano, G. A. Silva, H. S. Azevedo, P. B. Malafaya, R. A. Sousa, S. S. Silva, L. F. Boesel, J. M. Oliveira, T. C. Santos, A. P. Marques et al., *J. R. Soc. Interface* **2007**, *4*, 999.

[69] O. Wichterle, D. Lim, *Nature* **1960**, *185*, 117.

[70] a) J. E. Elliott, M. Macdonald, J. Nie, C. N. Bowman, *Polymer* **2004**, *45*, 1503; b) M. T. Am Ende, N. A. Peppas, *J. Control. Release* **1997**, *48*, 47; c) M.-J. Yin, M. Yao, S. Gao, A. P. Zhang, H.-Y. Tam, P.-K. A. Wai, *Adv. Mater.* **2016**, *28*, 1394; d) S. L. Lim, C.-W. Ooi, W. S. Tan, E.-S. Chan, K. L. Ho, B. T. Tey, *Sens. Actuator B: Chem.* **2017**, *252*, 409.

[71] a) V. Kozlovskaya, E. Kharlampieva, M. L. Mansfield, S. A. Sukhishvili, *Chem. Mater.* **2006**, *18*, 328; b) C. Robin, C. Lorthioir, C. Amiel, A. Fall, G. Ovarlez, C. Le Cœur, *Macromolecules* **2017**, *50*, 700.

[72] a) L. H. Christensen, V. B. Breiting, A. Aasted, A. Jørgensen, I. Kebuladze, *Plast. Reconstr. Surg.* **2003**, *111*, 1883; b) W.-H. Chen, W.-C. Liao, Y. S. Sohn, M. Fadeev, A. Cecconello, R. Nechushtai, I. Willner, *Adv. Funct. Mater.* **2018**, *28*, 1705137.

[73] a) W. Zhang, P. Jiang, J. Chen, C. Zhu, Z. Mao, C. Gao, *J. Colloid Interface Sci.* **2017**, *490*, 181; b) H.-P. Cong, J.-H. Qiu, S.-H. Yu, *Small* **2015**, *11*, 1165; c) D. Sivakumaran, E. Mueller, T. Hoare, *Soft Matter* **2017**, *13*, 9060.

[74] a) M. Kobayashi, Y.-S. Chang, M. Oka, *Biomaterials* **2005**, *26*, 3243; b) N. Alexandre, J. Ribeiro, A. Gärtner, T. Pereira, I. Amorim, J. Fragoso, A. Lopes, J. Fernandes, E. Costa, A. Santos-Silva et al., *J. Biomed. Mater. Res. A* **2014**, *102*, 4262; c) R. H. Schmedlen, K. S. Masters, J. L. West, *Biomaterials* **2002**, *23*, 4325; d) M. I. Baker, S. P. Walsh, Z. Schwartz, B. D. Boyan, *J. Biomed. Mater. Res. B* **2012**, *100*, 1451.

[75] a) C. Li, A. Faulkner-Jones, A. R. Dun, J. Jin, P. Chen, Y. Xing, Z. Yang, Z. Li, W. Shu, D. Liu et al., *Angew. Chem., Int. Ed.* **2015**, *54*, 3957; b) Y. Loo, A. Lakshmanan, M. Ni, L. L. Toh, S. Wang, C. A. E. Hauser, *Nano Lett.* **2015**, *15*, 6919; c) L. Haines-Butterick, K. Rajagopal, M. Branco, D. Salick, R. Rughani, M. Pilarz, M. S. Lamm, D. J. Pochan, J. P. Schneider, *Proc. Natl. Acad. Sci. U.S.A.* **2007**, *104*, 7791; d) C. Yan, A. Altunbas, T. Yucel, R. P. Nagarkar, J. P. Schneider, D. J. Pochan, *Soft Matter* **2010**, *6*, 5143.

[76] a) Z. Huang, X. Liu, S. Chen, Q. Lu, G. Sun, *Polym. Chem.* **2015**, *6*, 143; b) C. Chun, S. M. Lee, C. W. Kim, K.-Y. Hong, S. Y. Kim, H. K. Yang, S.-C. Song, *Biomaterials* **2009**, *30*, 4752.

[77] a) E. A. Phelps, N. O. Enemchukwu, V. F. Fiore, J. C. Sy, N. Murthy, T. A. Sulchek, T. H. Barker, A. J. García, *Adv. Mater.* **2012**, *24*, 64-70, 2; b) A. V. Salvekar, W. M.

Huang, R. Xiao, Y. S. Wong, S. S. Venkatraman, K. H. Tay, Z. X. Shen, *Accounts of chemical research* **2017**, *50*, 141.

[78] Y. Chujo, K. Sada, T. Saegusa, *Macromolecules* **1990**, *23*, 2636.

[79] M. Hartlieb, K. Kempe, U. S. Schubert, *J. Mater. Chem. B* **2015**, *3*, 526.

[80] A. M. Kelly, F. Wiesbrock, *Macromol. Rapid Commun.* **2012**, *33*, 1632.

[81] a) A. S. Sawhney, C. P. Pathak, J. A. Hubbell, *Macromolecules* **1993**, *26*, 581; b) A. Metters, *Polymer* **2000**, *41*, 3993; c) M. A. Rice, K. S. Anseth, *Tissue Eng.* **2007**, *13*, 683; d) P. Gentile, V. Chiono, I. Carmagnola, P. V. Hatton, *Int. J. Mol. Sci.* **2014**, *15*, 3640.

[82] a) E.H. Sprecht, A. Neumann, H.T. Neher, U.S. Pat. 2,773,063, **1956**; b) N. H. Shearer Jr., H. W. Coover, U.S. Pat. 2,790,744, **1957**.

[83] a) H. G. Schild, *Prog. Polym. Sci.* **1992**, *17*, 163; b) X.-Z. Zhang, Y.-Y. Yang, T.-S. Chung, K.-X. Ma, *Langmuir* **2001**, *17*, 6094.

[84] S. Fujishige, K. Kubota, I. Ando, *J. Phys. Chem.* **1989**, *93*, 3311.

[85] J. Eliassaf, *J. Appl. Polym. Sci.* **1978**, *22*, 873.

[86] H. Feil, Y. H. Bae, J. Feijen, S. W. Kim, *Macromolecules* **1993**, *26*, 2496.

[87] a) D. J. Siegwart, S. A. Bencherif, A. Srinivasan, J. O. Hollinger, K. Matyjaszewski, *J. Biomed. Mater. Res. A* **2008**, *87*, 345; b) J. Gan, X. Guan, J. Zheng, H. Guo, K. Wu, L. Liang, M. Lu, *RSC Adv.* **2016**, *6*, 32967; c) D. Das, P. Ghosh, A. Ghosh, C. Haldar, S. Dhara, A. B. Panda, S. Pal, *ACS Appl. Mater. Interfaces* **2015**, *7*, 14338.

[88] T. Gan, Y. Zhang, Y. Guan, *Biomacromolecules* **2009**, *10*, 1410.

[89] a) A. Alexander, Ajazuddin, J. Khan, S. Saraf, S. Saraf, *Eur. J. Pharm Biopharm.* **2014**, *88*, 575; b) H.-H. Lin, Y.-L. Cheng, *Macromolecules* **2001**, *34*, 3710; c) J. Spěváček, R. Konefał, J. Dybal, E. Čadová, J. Kovářová, *Eur. Polym. J.* **2017**, *94*, 471.

[90] S. Ibusuki, Y. Fujii, Y. Iwamoto, T. Matsuda, *Tissue Eng.* **2003**, *9*, 371.

[91] a) D. I. Ha, S. B. Lee, M. S. Chong, Y. M. Lee, S. Y. Kim, Y. H. Park, *Macromol. Res.* **2006**, *14*, 87; b) R. Egbu, S. Brocchini, P. T. Khaw, S. Awwad, *Eur. J. Pharm Biopharm.* **2018**, *124*, 95; c) S. Ohya, Y. Nakayama, T. Matsuda, *Biomacromolecules* **2001**, *2*, 856.

[92] a) S. B. Lee, D. I. Ha, S. K. Cho, S. J. Kim, Y. M. Lee, *J. Appl. Polym. Sci.* **2004**, *92*, 2612; b) P.-Y. Chou, S.-H. Chen, C.-H. Chen, S.-H. Chen, Y. T. Fong, J.-P. Chen, *Acta Biomater.* **2017**, *63*, 85; c) D. Štular, I. Jerman, B. Simončič, B. Tomšič, *Carbohydr. Pol.* **2017**, *174*, 677; d) A. Mellati, S. Dai, J. Bi, B. Jin, H. Zhang, *RSC Adv.* **2014**, *4*, 63951.

[93] H. Cheng, L. Shen, C. Wu, *Macromolecules* **2006**, *39*, 2325.

[94] K. van Durme, G. van Assche, B. van Mele, *Macromolecules* **2004**, *37*, 9596.

[95] M. Glassner, K. Lava, V. R. de La Rosa, R. Hoogenboom, *J. Polym. Sci. A Polym. Chem.* **2014**, *52*, 3118.

[96] a) K. Knop, R. Hoogenboom, D. Fischer, U. S. Schubert, *Angew. Chem., Int. Ed.* **2010**, *49*, 6288; b) R. P. Garay, R. El-Gewely, J. K. Armstrong, G. Garratty, P. Richette, *Expert opinion on drug delivery* **2012**, *9*, 1319; c) J. J. F. Verhoef, T. J. Anchordoquy, *Drug Deliv. and Transl. Res.* **2013**, *3*, 499; d) H. Hatakeyama, H. Akita, H. Harashima, *Biol. Pharm. Bulletin* **2013**, *36*, 892.

[97] M. Barz, R. Luxenhofer, R. Zentel, M. J. Vicent, *Polym. Chem.* **2011**, *2*, 1900.

[98] W. Zhang, K. Gilstrap, L. Wu, R. B. K C, M. A. Moss, Q. Wang, X. Lu, X. He, *ACS Nano* **2010**, *4*, 6747.

[99] A. P. Constantinou, T. K. Georgiou, *Eur. Polym. J.* **2016**.

[100] P. Alexandridis, J. F. Holzwarth, T. A. Hatton, *Macromolecules* **1994**, *27*, 2414.

[101] a) Z. Zhou, B. Chu, *J. Colloid Interface Sci.* **1988**, *126*, 171; b) Bohorquez, Koch, Trygstad, Pandit, *J. Colloid Interface Sci.* **1999**, *216*, 34.

[102] K. Mortensen, *J. Phys.: Condens. Matter* **1996**, *8*, A103-A124.

[103] L. C. P. Trong, M. Djabourov, A. Ponton, *J. Colloid Interface Sci.* **2008**, *328*, 278.

[104] K. Mortensen, Y. Talmon, *Macromolecules* **1995**, *28*, 8829.

[105] A. Cabana, A. Aït-Kadi, J. Juhász, *J. Colloid Interface Sci.* **1997**, *190*, 307.

[106] a) G. Dumortier, J. L. Grossiord, F. Agnely, J. C. Chaumeil, *Pharm. Res.* **2006**, *23*, 2709; b) W. K. Bae, M. S. Park, J. H. Lee, J. E. Hwang, H. J. Shim, S. H. Cho, D.-E. Kim, H. M. Ko, C.-S. Cho, I.-K. Park et al., *Biomaterials* **2013**, *34*, 1433; c) A. Paavola, *Int. J. Pharm.* **2000**, *199*, 85; d) J. Qin, I. Asempah, S. Laurent, A. Fornara, R. N. Muller, M. Muhammed, *Adv. Mater.* **2009**, *21*, 1354; e) S. H. Kwon, S. Y. Kim, K. W. Ha, M. J. Kang, J. S. Huh, Im Tae Jong, Y. M. Kim, Y. M. Park, K. H. Kang, S. Lee et al., *Arc.h Pharm. Res.* **2007**, *30*, 1138.

[107] a) J. Barichello, *Int. J. Pharm.* **1999**, *184*, 189; b) T. P. Johnston, M. A. Punjabi, C. J. Froelich, *Pharm. Res.* **1992**, *09*, 425.

[108] a) Y. Shachaf, M. Gonen-Wadmany, D. Seliktar, *Biomaterials* **2010**, *31*, 2836; b) L. C. Gonçalves, A. B. Seabra, M. T. Pelegrino, D. R. de Araujo, J. S. Bernardes, P. S. Haddad, *RSC Adv.* **2017**, *7*, 14496; c) B. Pradines, M. Djabourov, C. Vauthier, P. M. Loiseau, G. Ponchel, K. Bouchemal, *Colloids Surf. B* **2015**, *135*, 669.

[109] E. Gioffredi, M. Boffito, S. Calzone, S. M. Giannitelli, A. Rainer, M. Trombetta, P. Mozetic, V. Chiono, *Procedia CIRP* **2016**, *49*, 125.

[110] D. B. Kolesky, R. L. Truby, A. S. Gladman, T. A. Busbee, K. A. Homan, J. A. Lewis, *Adv. Mater.* **2014**, *26*, 3124.

[111] C. C. Chang, E. D. Boland, S. K. Williams, J. B. Hoying, *J. Biomed. Mater. Res. B* **2011**, *98*, 160.

[112] M. Müller, J. Becher, M. Schnabelrauch, M. Zenobi-Wong, *Biofabrication* **2015**, *7*, 35006.

[113] Z. G. M. Wout, E. A. Pec, J. A. Maggiore, R. H. Williams, P. Palicharla, T. P. Johnston, *J. Pharm. Sci. Technol.* **1992**, *46*, 192.

[114] a) C. Li, W.K. Palmer, T.P. Johnston, *J. Pharm. Biomed. Anal.* **1996**, *14*, 659; b) W. K. Palmer, E. E. Emeson, T. P. Johnston, *Atherosclerosis* **1998**, *136*, 115.

[115] Z. Liu, D. Liu, L. Wang, J. Zhang, N. Zhang, *Int. J. Mol. Sci.* **2011**, *12*, 1684.

[116] Y.-S. Hwang, P.-R. Chiang, W.-H. Hong, C.-C. Chiao, I.-M. Chu, G.-H. Hsiue, C.-R. Shen, *PLOS ONE* **2013**, *8*, e67495.

[117] J. R. Thonhoff, D. I. Lou, P. M. Jordan, X. Zhao, P. Wu, *Brain Res.* **2008**, *1187*, 42.

[118] a) H. Yoshioka, M. Mikami, Y. Mori, E. Tsuchida, *J. Macromol. Sci., Pure Appl. Chem.* **1994**, *31*, 113; b) H. Yoshioka, M. Mikami, Y. Mori, E. Tsuchida, *J. Macromol. Sci., Pure Appl. Chem.* **1994**, *31*, 121; c) H. Yoshioka, Y. Mori, J. A. Cushman, *Polym. Adv. Technol.* **1994**, *5*, 122; d) H. Yoshioka, M. Mikami, Y. Mori, E. Tsuchida, *J. Macromol. Sci., Pure Appl. Chem.* **1994**, *31*, 109.

[119] T. Arai, T. Joki, M. Akiyama, M. Agawa, Y. Mori, H. Yoshioka, T. Abe, *J. Neurooncol.* **2006**, *77*, 9.

[120] H. Yoshioka, Y. Mori, S. Kubota, *Jpn. J. Artif. Organs*, *1998*, 503.

[121] a) A. Yasuda, K. Kojima, K. W. Tinsley, H. Yoshioka, Y. Mori, C. A. Vacanti, *Tissue Eng.* **2006**, *12*, 1237; b) K. Hishikawa, S. Miura, T. Marumo, H. Yoshioka, Y. Mori, T. Takato, T. Fujita, *Biochem. Biophys. Res. Commun.* **2004**, *317*, 1103; c) C. Mino, T. Iwata, T. Kawata, *J. Oral Sci.* **2017**, *59*, 365; d) M. M. Adil, D. V. Schaffer, *Curr. Protoc. Stem Cell Biol.* **2018**, *44*, 2D.21.1-2D.21.17; e) K. Kataoka, N. Huh, *J. Stem Cells Regen. Med.* **2010**, *6*, 10.

[122] C. R. Ramesh, D. F. Kirk in *Drugs and the pharmaceutical sciences, Vol. 184* (Ed.: M. J. Rathbone), Informa Healthcare, London, **2008**, pp. 171–181.

[123] S. Jo, J. Kim, S. W. Kim, *Macromol. Biosci.* **2006**, *6*, 923.

[124] T. R. R. Singh, G. Laverty, R. F. Donnelly, *Hydrogels. Design, synthesis and application in drug delivery and regenerative medicine*, CRC Press/Taylor & Francis Group, Boca Raton, FL, **2018**.

[125] a) R. Luxenhofer, G. Sahay, A. Schulz, D. Alakhova, T. K. Bronich, R. Jordan, A. V. Kabanov, *J. Control. Release* **2011**, *153*, 73; b) T. X. Viegas, Z. Fang, K. Yoon, R. Weimer, B. Dizman in *Woodhead Publishing series in biomaterials* (Ed.: A. Parambath), Woodhead Publishing, an imprint of Elsevier, Duxford, United Kingdom, **2018**, pp. 173–198; c) V. V. Khutoryanskiy, *Adv. Drug Deliv. Rev.* **2018**, *124*, 140.

[126] E. Vlassi, A. Papagiannopoulos, S. Pispas, *Eur. Polym. J.* **2017**, *88*, 516.

[127] M. Bauer, C. Lautenschlaeger, K. Kempe, L. Tauhardt, U. S. Schubert, D. Fischer, *Macromol. Biosci.* **2012**, *12*, 986.

[128] D. A. Tomalia, D. P. Sheetz, *J. Polym. Sci. A-1 Polym. Chem.* **1966**, *4*, 2253.

[129] T. G. Bassiri, A. Levy, M. Litt, *J. Polym. Sci., Part B: Polym. Lett.* **1967**, *5*, 871.

[130] T. Kagiya, S. Narisawa, T. Maeda, K. Fukui, *J. Polym. Sci., Part B: Polym. Lett.* **1966**, *4*, 441.

[131] W. Seeliger, E. Aufderhaar, W. Diepers, R. Feinauer, R. Nehring, W. Thier, H. Hellmann, *Angew. Chem., Int. Ed.* **1966**, *5*, 875.

[132] K. Aoi, H. Suzuki, M. Okada, *Macromolecules* **1992**, *25*, 7073.

[133] A. Levy, M. Litt, *J. Polym. Sci., Part B: Polym. Lett.* **1967**, *5*, 881.

[134] M. Glassner, M. Vergaelen, R. Hoogenboom, *Polym. Int.* **2018**, *67*, 32.

[135] B. Verbraeken, B. D. Monnery, K. Lava, R. Hoogenboom, *Eur. Polym. J.* **2017**, *88*, 451.

[136] a) G. Morgese, E. M. Benetti, *Eur. Polym. J.* **2017**, *88*, 470; b) P. Wilson, P. C. Ke, T. P. Davis, K. Kempe, *Eur. Polym. J.* **2017**, *88*, 486; c) R. Hoogenboom, H. Schlaad, *Polym. Chem.* **2017**, *8*, 24; d) Y. Jung, W.-D. Jang, *Supramol. Chem.* **2017**, *29*, 714; e) T. Lorson, M. M. Lübtow, E. Wegener, M. S. Haider, S. Borova, D. Nahm, R. Jordan, M. Sokolski-Papkov, A. V. Kabanov, R. Luxenhofer, *Biomaterials* **2018**, *178*, 204.

[137] R. W. Moreadith, T. X. Viegas, M. D. Bentley, J. M. Harris, Z. Fang, K. Yoon, B. Dizman, R. Weimer, B. P. Rae, X. Li et al., *Eur. Polym. J.* **2017**, *88*, 524.

[138] T. R. Dargaville, J.-R. Park, R. Hoogenboom, *Macromol. Biosci.* **2018**, e1800070.

[139] S. Gabriel, *Ber. Dtsch. Chem. Ges.* **1889**, *22*, 1139.

[140] A. I. Meyers, D. L. Temple, R. L. Nolen, E. D. Mihelich, *J. Org. Chem.* **1974**, *39*, 2778.
[141] A. Sakakura, S. Umemura, K. Ishihara, *Chem. Commun.* **2008**, 3561.
[142] H.-Q. Do, E. R. R. Chandrashekar, G. C. Fu, *J. Am. Chem. Soc.* **2013**, *135*, 16288.
[143] K. Aoi, M. Okada, *Prog. Polym. Sci.* **1996**, *21*, 151.
[144] B. M. Culbertson, *Prog. Polym. Sci.* **2002**, *27*, 579.
[145] M. Beck, P. Birnbrich, U. Eicken, H. Fischer, W. E. Fristad, B. Hase, H.-J. Krause, *Angew. Makromol. Chemie* **1994**, *223*, 217.
[146] R. Sharma, S. K. Vadivel, R. I. Duclos, A. Makriyannis, *Tetrahedron Lett.* **2009**, *50*, 5780.
[147] a) H. Wenker, *J. Am. Chem. Soc.* **1935**, *57*, 1079; b) H. Wenker, *J. Am. Chem. Soc.* **1938**, *60*, 2152; c) F. Franco, J. M. Muchowski, *J. Heterocycl. Chem.* **1980**, *17*, 1613.
[148] H. Witte, W. Seeliger, *Justus Liebigs Ann. Chem.* **1974**, *1974*, 996.
[149] K. Kempe, S. Jacobs, H. M. L. Lambermont-Thijs, M. M. W. M. Fijten, R. Hoogenboom, U. S. Schubert, *Macromolecules* **2010**, *43*, 4098.
[150] a) C. Taubmann, R. Luxenhofer, S. Cesana, R. Jordan, *Macromol. Biosci.* **2005**, *5*, 603; b) T. R. Dargaville, K. Lava, B. Verbraeken, R. Hoogenboom, *Macromolecules* **2016**, *49*, 4774.
[151] S. Sinnwell, H. Ritter, *Macromol. Rapid Commun.* **2006**, *27*, 1335.
[152] M. M. Bloksma, R. M. Paulus, van Kuringen, Huub P C, F. van der Woerdt, H. M. L. Lambermont-Thijs, U. S. Schubert, R. Hoogenboom, *Macromol. Rapid Commun.* **2012**, *33*, 92.
[153] H. M. L. Lambermont-Thijs, M. W. M. Fijten, A. J. van der Linden, B. M. van Lankvelt, M. M. Bloksma, U. S. Schubert, R. Hoogenboom, *Macromolecules* **2011**, *44*, 4320.
[154] M. M. Lübtow, L. Keßler, A. Appelt-Menzel, T. Lorson, N. Gangloff, M. Kirsch, S. Dahms, R. Luxenhofer, *Macromol. Biosci.* **2018**, *13*, 1800155.
[155] R. Luxenhofer, S. Huber, J. Hytry, J. Tong, A. V. Kabanov, R. Jordan, *J. Polym. Sci. A Polym. Chem.* **2013**, *51*, 732.
[156] a) R. M. Paulus, C. R. Becer, R. Hoogenboom, U. S. Schubert, *Macromol. Chem. Phys.* **2008**, *209*, 794; b) V. V. Jerca, F. A. Nicolescu, D. S. Vasilescu, D. M. Vuluga, *Polym. Bull.* **2011**, *66*, 785.
[157] M. Glassner, D. R. D'hooge, J. Young Park, P. H.M. van Steenberge, B. D. Monnery, M.-F. Reyniers, R. Hoogenboom, *Eur. Polym. J.* **2015**, *65*, 298.
[158] S. Kobayashi, H. Uyama, *J. Polym. Sci., Part A: Polym. Chem.* **2002**, *40*, 192.
[159] a) B. Guillerm, S. Monge, V. Lapinte, J.-J. Robin, *Macromol. Rapid Commun.* **2012**, *33*, 1600; b) S. Kobayashi, M. Kaku, S. Sawada, T. Saegusa, *Polym. Bull.* **1985**, *13*, 447; c) T. Bartz, M. Klapper, K. Müllen, *Macromol. Chem. Phys.* **1994**, *195*, 1097; d) Y. Chujo, E. Ihara, H. Ihara, T. Saegusa, *Macromolecules* **1989**, *22*, 2040.
[160] a) R. Hoogenboom, M. W. M. Fijten, U. S. Schubert, *J. Polym. Sci. A Polym. Chem.* **2004**, *42*, 1830; b) M. Miyamoto, K. Aoi, T. Saegusa, *Macromolecules* **1988**, *21*, 1880; c) M. Miyamoto, K. Aoi, T. Saegusa, *Macromolecules* **1991**, *24*, 11.
[161] M. W. M. Fijten, R. Hoogenboom, U. S. Schubert, *J. Polym. Sci. A Polym. Chem.* **2008**, *46*, 4804.

[162] T. Saegusa, H. Ikeda, *Macromolecules* **1973**, *6*, 808.
[163] S. Penczek, P. Kubisa, K. Matyjaszewski (Eds.) *Advances in Polymer Science*, *68/69*, Springer, Berlin, Heidelberg, **1985**.
[164] J. S. Hrkach, K. Matyjaszewski, *Macromolecules* **1992**, *25*, 2070.
[165] S. Kobayashi, T. Igarashi, Y. Moriuchi, T. Saegusa, *Macromolecules* **1986**, *19*, 535.
[166] a) S. Osawa, T. Ishii, H. Takemoto, K. Osada, K. Kataoka, *Eur. Polym. J.* **2017**, *88*, 553; b) J. F. Nawroth, J. R. McDaniel, A. Chilkoti, R. Jordan, R. Luxenhofer, *Macromol. Biosci.* **2016**.
[167] O. Nuyken, G. Maier, A. Groß, H. Fischer, *Macromol. Chem. Phys.* **1996**, *197*, 83.
[168] M. Litt, A. Levy, J. Herz, *J. Macromol. Sci., Chemistry* **1975**, *9*, 703.
[169] a) R. Hoogenboom, R. M. Paulus, M. W. M. Fijten, U. S. Schubert, *J. Polym. Sci. A Polym. Chem.* **2005**, *43*, 1487; b) J. M. Warakomski, B. P. Thill, *J. Polym. Sci. A Polym. Chem.* **1990**, *28*, 3551.
[170] J.-S. Park, K. Kataoka, *Macromolecules* **2006**, *39*, 6622.
[171] M. Sahn, D. Bandelli, M. Dirauf, C. Weber, U. S. Schubert, *Macromol. Rapid Commun.* **2017**, *38*.
[172] F. Wiesbrock, R. Hoogenboom, C. H. Abeln, U. S. Schubert, *Macromol. Rapid Commun.* **2004**, *25*, 1895.
[173] F. Wiesbrock, R. Hoogenboom, M. A. M. Leenen, M. A. R. Meier, U. S. Schubert, *Macromolecules* **2005**, *38*, 5025.
[174] R. Hoogenboom, M. W. M. Fijten, H. M. L. Thijs, B. M. van Lankvelt, U. S. Schubert, *des monomers polym* **2005**, *8*, 659.
[175] R. Hoogenboom, B. D. Monnery, US20170210853A1, **2017**.
[176] J. M. Kranenburg, C. A. Tweedie, R. Hoogenboom, F. Wiesbrock, H. M. L. Thijs, C. E. Hendriks, K. J. van Vliet, U. S. Schubert, *J. Mater. Chem.* **2007**, *17*, 2713.
[177] E. F.-J. Rettler, J. M. Kranenburg, H. M.L. Lambermont-Thijs, R. Hoogenboom, U. S. Schubert, *Macromol. Chem. Phys.* **2010**, *211*, 2443.
[178] C. Weber, R. Hoogenboom, U. S. Schubert, *Prog. Polym. Sci.* **2012**, *37*, 686.
[179] S. Huber, N. Hutter, R. Jordan, *Colloid Polym. Sci.* **2008**, *286*, 1653.
[180] a) P. Lin, C. Clash, E. M. Pearce, T. K. Kwei, M. A. Aponte, *J. Polym. Sci., Part B: Polym. Phys.* **1988**, *26*, 603; b) D. Christova, R. Velichkova, W. Loos, E. J. Goethals, F. Du Prez, *Polymer* **2003**, *44*, 2255.
[181] R. Konefał, J. Spěváček, P. Černoch, *Eur. Polym. J.* **2018**, *100*, 241.
[182] J.-S. Park, K. Kataoka, *Macromolecules* **2007**, *40*, 3599.
[183] M. M. Bloksma, C. Weber, I. Y. Perevyazko, A. Kuse, A. Baumgärtel, A. Vollrath, R. Hoogenboom, U. S. Schubert, *Macromolecules* **2011**, *44*, 4057.
[184] S. Salzinger, S. Huber, S. Jaksch, P. Busch, R. Jordan, C. M. Papadakis, *Colloid Polym. Sci.* **2012**, *290*, 385.
[185] Y. Jung, J.-H. Kim, W.-D. Jang, *Eur. Polym. J.* **2017**, *88*, 605.
[186] M. M. Bloksma, D. J. Bakker, C. Weber, R. Hoogenboom, U. S. Schubert, *Macromol. Rapid Commun.* **2010**, *31*, 724.
[187] P. Tatar Güner, A. L. Demirel, *J. Phys. Chem. B* **2012**, *116*, 14510.
[188] X. Zhimin, Y. Chuanyu, Z. Xinhui, Y. Dongkun, M. Tiancheng, *Acta Physico-Chimica Sinca* **2018**, 0.

[189] a) N. Zhang, R. Luxenhofer, R. Jordan, *Macromol. Chem. Phys.* **2012**, *213*, 973; b) S. Huber, R. Jordan, *Colloid Polym. Sci.* **2008**, *286*, 395; c) G. Le Fer, C. Amiel, G. Volet, *Eur. Polym. J.* **2015**, *71*, 523; d) M. Hruby, S. K. Filippov, J. Panek, M. Novakova, H. Mackova, J. Kucka, D. Vetvicka, K. Ulbrich, *Macromol. Biosci.* **2010**, *10*, 916; e) N. Oleszko-Torbus, A. Utrata-Wesołek, W. Wałach, A. Dworak, *Eur. Polym. J.* **2017**, *88*, 613.

[190] A. Zahoranová, M. Mrlík, K. Tomanová, J. Kronek, R. Luxenhofer, *Macromol. Chem. Phys.* **2017**, *28*, 1700031.

[191] A. S. Gubarev, B. D. Monnery, A. A. Lezov, O. Sedlacek, N. V. Tsvetkov, R. Hoogenboom, S. K. Filippov, *Polym. Chem.* **2018**, *33*, 1648.

[192] a) V. V. Jerca, K. Lava, B. Verbraeken, R. Hoogenboom, *Polym. Chem.* **2016**; b) F. Wiesbrock, R. Hoogenboom, M. Leenen, S. F. G. M. van Nispen, M. van der Loop, C. H. Abeln, A. M. J. van den Berg, U. S. Schubert, *Macromolecules* **2005**, *38*, 7957.

[193] P. Bouten, K. Lava, J. van Hest, R. Hoogenboom, *Polymers* **2015**, *7*, 1998.

[194] K. Kempe, M. Lobert, R. Hoogenboom, U. S. Schubert, *J. Polym. Sci. A Polym. Chem.* **2009**, *47*, 3829.

[195] C. Wang, L. Feng, H. Yang, G. Xin, W. Li, J. Zheng, W. Tian, X. Li, *Phys. Chem. Chem. Phys.* **2012**, *14*, 13233.

[196] J. M. Rodriguez-Parada, M. Kaku, D. Y. Sogah, *Macromolecules* **1994**, *27*, 1571.

[197] A. L. Demirel, P. Tatar Güner, B. Verbraeken, H. Schlaad, U. S. Schubert, R. Hoogenboom, *J. Polym. Sci., Part B: Polym. Phys.* **2016**, *54*, 721.

[198] K. Kempe, E. F.-J. Rettler, R. M. Paulus, A. Kuse, R. Hoogenboom, U. S. Schubert, *Polymer* **2013**, *54*, 2036.

[199] T. Saegusa, Y. Nagura, S. Kobayashi, *Macromolecules* **1973**, *6*, 495.

[200] S. Nam, J. Seo, S. Woo, W. H. Kim, H. Kim, D. D. C. Bradley, Y. Kim, *Nat. Commun.* **2015**, *6*, 8929.

[201] W. Chen, Y. Zhu, Y. Yu, L. Xu, G. Zhang, Z. He, *Chem. Mater.* **2016**, *28*, 4879.

[202] H. Lin, L. Zhu, H. Huang, C. J. Reckmeier, C. Liang, A. L. Rogach, W. C. H. Choy, *Nanoscale* **2016**, *8*, 19846.

[203] J.-H. Kim, Y. Jung, D. Lee, W.-D. Jang, *Adv. Mater.* **2016**, *28*, 3499.

[204] M. Bauer, S. Schroeder, L. Tauhardt, K. Kempe, U. S. Schubert, D. Fischer, *J. Polym. Sci., Part A: Polym. Chem.* **2013**, *51*, 1816.

[205] a) M. N. Leiske, A.-K. Trützschler, S. Armoneit, P. Sungur, S. Hoeppener, M. Lehmann, A. Traeger, U. S. Schubert, *J. Mater. Chem. B* **2017**, *5*, 9102; b) J. Kronek, Z. Kroneková, J. Lustoň, E. Paulovičová, L. Paulovičová, B. Mendrek, *J. Mater. Sci. Mater. Med.* **2011**, *22*, 1725.

[206] M. Grube, M. N. Leiske, U. S. Schubert, I. Nischang, *Macromolecules* **2018**, *51*, 1905.

[207] Z. Kronekova, M. Mikulec, N. Petrencikova, E. Paulovicova, L. Paulovicova, V. Jancinova, R. Nosal', P. S. Reddy, G. D. Shimoga, D. Chorvat, JR et al., *Macromol. Biosci.* **2016**, *16*, 1200.

[208] a) S. Cheon Lee, C. Kim, I. Chan Kwon, H. Chung, S. Young Jeong, *J. Control. Release* **2003**, *89*, 437; b) B. Guillerm, V. Darcos, V. Lapinte, S. Monge, J. Coudane, J.-J. Robin, *Chem. Commun.* **2012**, *48*, 2879.

[209] W. Wu, S. Cui, Z. Li, J. Liu, H. Wang, X. Wang, Q. Zhang, H. Wu, K. Guo, *Polym. Chem.* **2015**, *6*, 2970.

[210] G. Le Fer, C. Le Cœur, J.-M. Guigner, C. Amiel, G. Volet, *Eur. Polym. J.* **2017**, *88*, 656.

[211] V. M. Gaspar, P. Baril, E. C. Costa, D. de Melo-Diogo, F. Foucher, J. A. Queiroz, F. Sousa, C. Pichon, I. J. Correia, *J. Control. Release* **2015**, *213*, 175.

[212] a) X. Pan, Y. Liu, Z. Li, S. Cui, H. Gebru, J. Xu, S. Xu, J. Liu, K. Guo, *Macromol. Chem. Phys.* **2017**, 1600483; b) L. Tauhardt, D. Pretzel, K. Kempe, M. Gottschaldt, D. Pohlers, U. S. Schubert, *Polym. Chem.* **2014**, *5*, 5751; c) R. Shah, Z. Kronekova, A. Zahoranová, L. Roller, N. Saha, P. Saha, J. Kronek, *J. Mater. Sci. Mater. Med.* **2015**, *26*, 157; d) M. Wang, O. J. R. Gustafsson, G. Siddiqui, I. Javed, H. G. Kelly, T. Blin, H. Yin, S. J. Kent, D. J. Creek, K. Kempe et al., *Nanoscale* **2018**.

[213] H. P. C. van Kuringen, J. Lenoir, E. Adriaens, J. Bender, B. G. de Geest, R. Hoogenboom, *Macromol. Biosci.* **2012**, *12*, 1114.

[214] P. Goddard, L. E. Hutchinson, J. Brown, L. J. Brookman, *J. Control. Release* **1989**, *10*, 5.

[215] F. C. Gaertner, R. Luxenhofer, B. Blechert, R. Jordan, M. Essler, *J. Control. Release* **2007**, *119*, 291.

[216] L. Wyffels, T. Verbrugghen, B. D. Monnery, M. Glassner, S. Stroobants, R. Hoogenboom, S. Staelens, *J. Control. Release* **2016**, *235*, 63.

[217] a) H. M. L. Lambermont-Thijs, F. S. van der Woerdt, A. Baumgaertel, L. Bonami, F. E. Du Prez, U. S. Schubert, R. Hoogenboom, *Macromolecules* **2010**, *43*, 927; b) M. Thomas, J. J. Lu, Q. Ge, C. Zhang, J. Chen, A. M. Klibanov, *Proc. Natl. Acad. Sci. U.S.A.* **2005**, *102*, 5679.

[218] a) J. C. Fernandes, X. Qiu, F. M. Winnik, M. Benderdour, X. Zhang, K. Dai, Q. Shi, *Int. J. Nanomedicine* **2013**, *8*, 4091; b) M. Mees, E. Haladjova, D. Momekova, G. Momekov, P. S. Shestakova, C. B. Tsvetanov, R. Hoogenboom, S. Rangelov, *Biomacromolecules* **2016**, *17*, 3580.

[219] J. Ulbricht, R. Jordan, R. Luxenhofer, *Biomaterials* **2014**, *35*, 4848.

[220] K. P. Luef, C. Petit, B. Ottersböck, G. Oreski, F. Ehrenfeld, B. Grassl, S. Reynaud, F. Wiesbrock, *Eur. Polym. J.* **2017**, *88*, 701.

[221] T. Lühmann, M. Schmidt, M. N. Leiske, V. Spieler, T. C. Majdanski, M. Grube, M. Hartlieb, I. Nischang, S. Schubert, U. S. Schubert et al., *ACS Biomater. Sci. Eng.* **2017**, *3*, 304.

[222] K. L. Eskow Jaunarajs, D. G. Standaert, T. X. Viegas, M. D. Bentley, Z. Fang, B. Dizman, K. Yoon, R. Weimer, P. Ravenscroft, T. H. Johnston et al., *Mov. Disord.* **2013**, *28*, 1675.

[223] a) R. Luxenhofer, A. Schulz, C. Roques, S. Li, T. K. Bronich, E. V. Batrakova, R. Jordan, A. V. Kabanov, *Biomaterials* **2010**, *31*, 4972; b) Z. He, A. Schulz, X. Wan, J. Seitz, H. Bludau, D. Y. Alakhova, D. B. Darr, C. M. Perou, R. Jordan, I. Ojima et al., *J. Control. Release* **2015**, *208*, 67; c) Z. He, X. Wan, A. Schulz, H. Bludau, M. A. Dobrovolskaia, S. T. Stern, S. A. Montgomery, H. Yuan, Z. Li, D. Alakhova et al., *Biomaterials* **2016**, *101*, 296.

[224] a) Y. Chujo, Y. Yoshifuji, K. Sada, T. Saegusa, *Macromolecules* **1989**, *22*, 1074; b) Y. Chujo, K. Sada, A. Naka, R. Nomura, T. Saegusa, *Macromolecules* **1993**, *26*, 883; c) Y. Chujo, K. Sada, R. Nomura, A. Naka, T. Saegusa, *Macromolecules* **1993**, *26*, 5611; d) Y. Chujo, K. Sada, T. Saegusa, *Macromolecules* **1993**, *26*, 6315; e) Y. Chujo, K. Sada, T. Saegusa, *Macromolecules* **1993**, *26*, 6320.

[225] Y. Chujo, K. Sada, K. Matsumoto, T. Saegusa, *Macromolecules* **1990**, *23*, 1234.

[226] a) T. R. Dargaville, R. Forster, B. L. Farrugia, K. Kempe, L. Voorhaar, U. S. Schubert, R. Hoogenboom, *Macromol. Rapid Commun.* **2012**, *33*, 1695; b) S. Cesana, J. Auernheimer, R. Jordan, H. Kessler, O. Nuyken, *Macromol. Chem. Phys.* **2006**, *207*, 183.

[227] a) A. Zahoranová, Z. Kroneková, M. Zahoran, D. Chorvát, I. Janigová, J. Kronek, *J. Polym. Sci. Part A: Polym. Chem.* **2016**, *54*, 1548; b) M. Hartlieb, S. Schubert, K. Kempe, N. Windhab, U. S. Schubert, *J. Polym. Sci. Part A: Polym. Chem.* **2015**, *53*, 10; c) J. C. Rueda, H. Komber, B. Voit, *J. Polym. Sci. A Polym. Chem.* **2005**, *43*, 122.

[228] V. Schenk, E. Rossegger, C. Ebner, F. Bangerl, K. Reichmann, B. Hoffmann, M. Höpfner, F. Wiesbrock, *Polymers* **2014**, *6*, 264.

[229] Y. Chujo, K. Sada, K. Matsumoto, T. Saegusa, *Polym. Bull.* **1989**, *21*, 353.

[230] a) H. Uyama, S. Kobayashi, *Chem. Lett.* **1992**, *21*, 1643; b) D. Christova, R. Velichkova, E. J. Goethals, *Macromol. Rapid Commun.* **1997**, *18*, 1067; c) Z. Zhu, X. Li, *J. Appl. Polym. Sci.* **2014**, *131*, n/a-n/a.

[231] O. Sedlacek, J. Kucka, B. D. Monnery, M. Slouf, M. Vetrik, R. Hoogenboom, M. Hruby, *Polym. Degrad. Stab.* **2017**, *137*, 1.

[232] B. L. Farrugia, K. Kempe, U. S. Schubert, R. Hoogenboom, T. R. Dargaville, *Biomacromolecules* **2013**, *14*, 2724.

[233] J. N. Haigh, Y.-M. Chuang, B. Farrugia, R. Hoogenboom, P. D. Dalton, T. R. Dargaville, *Macromol. Rapid Commun.* **2016**, *37*, 93.

[234] a) M. Hartlieb, D. Pretzel, M. Wagner, S. Hoeppener, P. Bellstedt, M. Görlach, C. Englert, K. Kempe, U. S. Schubert, *J. Mater. Chem. B* **2015**, *3*, 1748; b) C. Legros, A.-L. Wirotius, M.-C. de Pauw-Gillet, K. C. Tam, D. Taton, S. Lecommandoux, *Biomacromolecules* **2015**, *16*, 183; c) M. Platen, E. Mathieu, S. Lück, R. Schubel, R. Jordan, S. Pautot, *Biomacromolecules* **2015**, *16*, 1516; d) M. Hartlieb, T. Bus, J. Kübel, D. Pretzel, S. Hoeppener, M. N. Leiske, K. Kempe, B. Dietzek, U. S. Schubert, *Bioconjugate Chem.* **2017**, *28*, 1229.

[235] X. Wang, X. Li, Y. Li, Y. Zhou, C. Fan, W. Li, S. Ma, Y. Fan, Y. Huang, N. Li et al., *Acta Biomater.* **2011**, *7*, 4149.

[236] a) B. Berman, *Business Horizons* **2012**, *55*, 155; b) S. C. Ligon, R. Liska, J. Stampfl, M. Gurr, R. Mülhaupt, *Chem. Rev.* **2017**, *117*, 10212.

[237] R. Langer, J. Vacanti, *Science* **1993**, *260*, 920.

[238] C. Mason, P. Dunnill, *Regen. Med.* **2008**, *3*, 1.

[239] a) M. Castilho, D. Feyen, M. Flandes-Iparraguirre, G. Hochleitner, J. Groll, P. A. F. Doevendans, T. Vermonden, K. Ito, J. P. G. Sluijter, J. Malda, *Adv. Healthcare Mater.* **2017**, *6*; b) B. L. Farrugia, T. D. Brown, Z. Upton, D. W. Hutmacher, P. D. Dalton, T. R. Dargaville, *Biofabrication* **2013**, *5*, 25001.

[240] G. Hochleitner, J. F. Hümmer, R. Luxenhofer, J. Groll, *Polymer* **2014**, *55*, 5017.

[241] a) K. F. Leong, C. M. Cheah, C. K. Chua, *Biomaterials* **2003**, *24*, 2363; b) S. J. Hollister, *Nat. Mater. (Nature Materials)* **2005**, *4*, 518; c) A. Khademhosseini, R. Langer, J. Borenstein, J. P. Vacanti, *Proc. Natl. Acad. Sci. U.S.A.* **2006**, *103*, 2480; d) S. Yang, K.-F. Leong, Z. Du, C.-K. Chua, *Tissue Eng.* **2002**, *8*, 1; e) W.-Y. Yeong, C.-K. Chua, K.-F. Leong, M. Chandrasekaran, *Trends Biotechnol.* **2004**, *22*, 643.

[242] D. W. Hutmacher, M. Sittinger, M. V. Risbud, *Trends Biotechnol.* **2004**, *22*, 354.

[243] T. J. Klein, S. C. Rizzi, J. C. Reichert, N. Georgi, J. Malda, W. Schuurman, R. W. Crawford, D. W. Hutmacher, *Macromol. Biosci.* **2009**, *9*, 1049.

[244] A. M. Tatara, A. G. Mikos, *J. Bone. Joint Surg. Am.* **2016**, *98*, 1132.

[245] G. Hochleitner, T. Jüngst, T. D. Brown, K. Hahn, C. Moseke, F. Jakob, P. D. Dalton, J. Groll, *Biofabrication* **2015**, *7*, 35002.

[246] a) V. Mironov, T. Boland, T. Trusk, G. Forgacs, R. R. Markwald, *Trends Biotechnol.* **2003**, *21*, 157; b) B. Derby, *Science (New York, N.Y.)* **2012**, *338*, 921.

[247] J. Groll, T. Boland, T. Blunk, J. A. Burdick, D.-W. Cho, P. D. Dalton, B. Derby, G. Forgacs, Q. Li, V. A. Mironov et al., *Biofabrication* **2016**, *8*, 13001.

[248] a) C. J. Ferris, K. G. Gilmore, G. G. Wallace, M. in het Panhuis, *Appl. Microbiol. Biotechnol.* **2013**, *97*, 4243; b) F. P.W. Melchels, M. A.N. Domingos, T. J. Klein, J. Malda, P. J. Bartolo, D. W. Hutmacher, *Prog. Polym. Sci.* **2012**, *37*, 1079; c) L. Moroni, T. Boland, J. A. Burdick, C. de Maria, B. Derby, G. Forgacs, J. Groll, Q. Li, J. Malda, V. A. Mironov et al., *Trends Biotechnol.* **2017**; d) P. A. Wieringa, A. R. Gonçalves de Pinho, S. Micera, R. J. A. van Wezel, L. Moroni, *Adv. Healthcare Mater.* **2018**, *7*, e1701164; e) S. Patra, V. Young, *Cell biochemistry and biophysics* **2016**, *74*, 93; f) A. A. Zadpoor, J. Malda, *Ann. Biomed. Eng.* **2017**, *45*, 1.

[249] S. V. Murphy, A. Atala, *Nat. Biotechnol.* **2014**, *32*, 773.

[250] D. H. Reneker, I. Chun, *Nanotechnology* **1996**, *7*, 216.

[251] a) T. D. Brown, P. D. Dalton, D. W. Hutmacher, *Adv. Mater.* **2011**, *23*, 5651; b) C. Wei, J. Dong, *J. Micromech. Microeng.* **2013**, *23*, 25017; c) N. Ristovski, N. Bock, S. Liao, S. K. Powell, J. Ren, G. T. S. Kirby, K. A. Blackwood, M. A. Woodruff, *Biointerphases* **2015**, *10*, 11006; d) T. D. Brown, F. Edin, N. Detta, A. D. Skelton, D. W. Hutmacher, P. D. Dalton, *Mater. Sci. Eng. C Mater. Biol. Appl.* **2014**, *45*, 698.

[252] T. D. Brown, A. Slotosch, L. Thibaudeau, A. Taubenberger, D. Loessner, C. Vaquette, P. D. Dalton, D. W. Hutmacher, *Biointerphases* **2012**, *7*, 13.

[253] a) T. Jüngst, M. L. Muerza-Cascante, T. D. Brown, M. Standfest, D. W. Hutmacher, J. Groll, P. D. Dalton, *Polym. Int.* **2015**, *64*, 1086; b) E. McColl, J. Groll, T. Jungst, P. D. Dalton, *Mater. Des.* **2018**.

[254] a) T. D. Brown, P. D. Dalton, D. W. Hutmacher, *Prog. Polym. Sci.* **2016**, *56*, 116; b) M. A. Woodruff, D. W. Hutmacher, *Prog. Polym. Sci.* **2010**, *35*, 1217.

[255] J. N. Haigh, T. R. Dargaville, P. D. Dalton, *Mater. Sci. Eng. C Mater. Biol. Appl.* **2017**, *77*, 883.

[256] G. Hochleitner, M. Kessler, M. Schmitz, A. R. Boccaccini, J. Teßmar, J. Groll, *Mater. Lett.* **2017**, *205*, 257.

[257] F. Chen, G. Hochleitner, T. Woodfield, J. Groll, P. D. Dalton, B. G. Amsden, *Biomacromolecules* **2016**, *17*, 208.

[258] G. Hochleitner, E. Fürsattel, R. Giesa, J. Groll, H.-W. Schmidt, P. D. Dalton, *Macromol. Rapid Commun.* **2018**, e1800055.

[259] a) M. de Ruijter, A. Hrynevich, J. N. Haigh, G. Hochleitner, M. Castilho, J. Groll, J. Malda, P. D. Dalton, *Small* **2018**, *14*; b) M. de Ruijter, A. Ribeiro, I. Dokter, M. Castilho, J. Malda, *Adv. Healthcare Mater.* **2018**, e1800418.

[260] J. Visser, F. P. W. Melchels, J. E. Jeon, E. M. van Bussel, L. S. Kimpton, H. M. Byrne, W. J. A. Dhert, P. D. Dalton, D. W. Hutmacher, J. Malda, *Nat. Commun.* **2015**, *6*, 6933.

[261] a) L. Thibaudeau, A. V. Taubenberger, B. M. Holzapfel, V. M. Quent, T. Fuehrmann, P. Hesami, T. D. Brown, P. D. Dalton, C. A. Power, B. G. Hollier et al., *Disease Models & Mechanisms* **2014**, *7*, 299; b) B. M. Holzapfel, F. Wagner, D. Loessner, N. P. Holzapfel, L. Thibaudeau, R. Crawford, M.-T. Ling, J. A. Clements, P. J. Russell, D. W. Hutmacher, *Biomaterials* **2014**, *35*, 4108; c) M. L. Muerza-Cascante, D. Haylock, D. W. Hutmacher, P. D. Dalton, *Tissue Eng. Part B Rev.* **2015**, *21*, 187.

[262] A. Youssef, S. J. Hollister, P. D. Dalton, *Biofabrication* **2017**, *9*, 12002.

[263] S. C. Woodward, P. S. Brewer, F. Moatamed, A. Schindler, C. G. Pitt, *J. Biomed. Mater. Res.* **1985**, *19*, 437.

[264] L. Faxälv, T. Ekblad, B. Liedberg, T. L. Lindahl, *Acta Biomater.* **2010**, *6*, 2599.

[265] M. P. Chhaya, P. S. P. Poh, E. R. Balmayor, M. van Griensven, J.-T. Schantz, D. W. Hutmacher, *Expert review of medical devices* **2015**, *12*, 537.

[266] F. Guillemot, V. Mironov, M. Nakamura, *Biofabrication* **2010**, *2*, 10201.

[267] a) J.-F. Xing, M.-L. Zheng, X.-M. Duan, *Chem. Soc. Rev.* **2015**, *44*, 5031; b) M. T. Raimondi, S. M. Eaton, M. M. Nava, M. Laganà, G. Cerullo, R. Osellame, *J. Appl. Biomater. Biom.* **2012**, 0.

[268] S. Wüst, R. Müller, S. Hofmann, *J. Funct. Biomater.* **2011**, *2*, 119.

[269] a) J. R. Tumbleston, D. Shirvanyants, N. Ermoshkin, R. Janusziewicz, A. R. Johnson, D. Kelly, K. Chen, R. Pinschmidt, J. P. Rolland, A. Ermoshkin et al., *Science (New York, N.Y.)* **2015**, *347*, 1349; b) A. T. Miller, D. L. Safranski, C. Wood, R. E. Guldberg, K. Gall, *J. Mech. Behav. Biomed. Mater.* **2017**, *75*, 1.

[270] C. J. Bloomquist, M. B. Mecham, M. D. Paradzinsky, R. Janusziewicz, S. B. Warner, J. C. Luft, S. J. Mecham, A. Z. Wang, J. M. DeSimone, *J. Control. Release* **2018**, *278*, 9.

[271] a) J. Jang, J. Y. Park, G. Gao, D.-W. Cho, *Biomaterials* **2018**, *156*, 88; b) J. M. Lee, W. Y. Yeong, *Adv. Healthcare Mater.* **2016**, *5*, 2856; c) D. Richards, J. Jia, M. Yost, R. Markwald, Y. Mei, *Ann. Biomed. Eng.* **2017**, *45*, 132; d) R. Suntornnond, J. An, C. K. Chua, *Macromol. Mater. Eng.* **2017**, *302*, 1600266; e) L. Moroni, J. A. Burdick, C. Highley, S. J. Lee, Y. Morimoto, S. Takeuchi, J. J. Yoo, *Nat. Rev. Mater.* **2018**, *3*, 21.

[272] J. Malda, J. Visser, F. P. Melchels, T. Jüngst, W. E. Hennink, W. J. A. Dhert, J. Groll, D. W. Hutmacher, *Adv. Mater.* **2013**, *25*, 5011.

[273] K. Hölzl, S. Lin, L. Tytgat, S. van Vlierberghe, L. Gu, A. Ovsianikov, *Biofabrication* **2016**, *8*, 32002.

[274] a) N. R. Schiele, D. T. Corr, Y. Huang, N. A. Raof, Y. Xie, D. B. Chrisey, *Biofabrication* **2010**, *2*, 32001; b) B. R. Ringeisen, C. M. Othon, J. A. Barron, D. Young, B. J. Spargo, *Biotechnol. J.* **2006**, *1*, 930.

[275] a) M. Gruene, M. Pflaum, C. Hess, S. Diamantouros, S. Schlie, A. Deiwick, L. Koch, M. Wilhelmi, S. Jockenhoevel, A. Haverich et al., *Tissue Eng. Part C Methods* **2011**, *17*, 973; b) L. Koch, A. Deiwick, S. Schlie, S. Michael, M. Gruene, V. Coger, D. Zychlinski, A. Schambach, K. Reimers, P. M. Vogt et al., *Biotechnol. Bioeng.* **2012**, *109*, 1855; c) S. Catros, J.-C. Fricain, B. Guillotin, B. Pippenger, R. Bareille, M. Remy, E. Lebraud, B. Desbat, J. Amédée, F. Guillemot, *Biofabrication* **2011**, *3*, 25001.

[276] F. Guillemot, A. Souquet, S. Catros, B. Guillotin, J. Lopez, M. Faucon, B. Pippenger, R. Bareille, M. Rémy, S. Bellance et al., *Acta Biomater.* **2010**, *6*, 2494.

[277] B. R. Ringeisen, H. Kim, J. A. Barron, D. B. Krizman, D. B. Chrisey, S. Jackman, R. Y. C. Auyeung, B. J. Spargo, *Tissue Eng.* **2004**, *10*, 483.

[278] J. A. Barron, P. Wu, H. D. Ladouceur, B. R. Ringeisen, *Biomedical Microdevices* **2004**, *6*, 139.

[279] B. Hopp, T. Smausz, N. Kresz, N. Barna, Z. Bor, L. Kolozsvári, D. B. Chrisey, A. Szabó, A. Nógrádi, *Tissue Eng.* **2005**, *11*, 1817.

[280] J. Zhang, B. Hartmann, J. Siegel, G. Marchi, H. Clausen-Schaumann, S. Sudhop, H. P. Huber, *PLOS ONE* **2018**, *13*, e0195479.

[281] a) Y. Lin, G. Huang, Y. Huang, T.-R. Jeremy Tzeng, D. Chrisey, *Rapid Prototyp. J.* **2010**, *16*, 202; b) J. A. Barron, B. R. Ringeisen, H. Kim, B. J. Spargo, D. B. Chrisey, *Thin Solid Films* **2004**, *453-454*, 383.

[282] R. Xiong, Z. Zhang, W. Chai, D. B. Chrisey, Y. Huang, *Biofabrication* **2017**, *9*, 24103.

[283] B. Guillotin, A. Souquet, S. Catros, M. Duocastella, B. Pippenger, S. Bellance, R. Bareille, M. Rémy, L. Bordenave, J. Amédée et al., *Biomaterials* **2010**, *31*, 7250.

[284] a) T. Xu, H. Kincaid, A. Atala, J. J. Yoo, *J. Manuf. Sci. Eng.* **2008**, *130*, 21017; b) W. C. Wilson, T. Boland, *Anat. Rec. A Discov. Mol. Cell. Evol. Biol.* **2003**, *272*, 491.

[285] B. Derby, *Annu. Rev. Mater. Res.* **2010**, *40*, 395.

[286] C. Xu, M. Zhang, Y. Huang, A. Ogale, J. Fu, R. R. Markwald, *Langmuir* **2014**, *30*, 9130.

[287] a) P. G. Campbell, L. E. Weiss, *Expert Opin. Biol. Ther.* **2007**, *7*, 1123; b) H. Gudapati, M. Dey, I. Ozbolat, *Biomaterials* **2016**, *102*, 20.

[288] R. E. Saunders, B. Derby, *Int. Mater. Rev.* **2014**, *59*, 430.

[289] a) T. Xu, W. Zhao, J.-M. Zhu, M. Z. Albanna, J. J. Yoo, A. Atala, *Biomaterials* **2013**, *34*, 130; b) X. Cui, K. Breitenkamp, M. G. Finn, M. Lotz, D. D. D'Lima, *Tissue Eng. Part A* **2012**, *18*, 1304; c) X. Cui, D. Dean, Z. M. Ruggeri, T. Boland, *Biotechnol. Bioeng.* **2010**, *106*, 963; d) G. Gao, T. Yonezawa, K. Hubbell, G. Dai, X. Cui, *Biotechnol. J.* **2015**, *10*, 1568.

[290] T. Xu, J. Jin, C. Gregory, J. J. J. J. Hickman, T. Boland, *Biomaterials* **2005**, *26*, 93.

[291] a) B. Lorber, W.-K. Hsiao, I. M. Hutchings, K. R. Martin, *Biofabrication* **2014**, *6*, 15001; b) K. Arai, S. Iwanaga, H. Toda, C. Genci, Y. Nishiyama, M. Nakamura, *Biofabrication* **2011**, *3*, 34113.

[292] R. E. Saunders, J. E. Gough, B. Derby, *Biomaterials* **2008**, *29*, 193.

[293] X. Cui, T. Boland, D. D.D'Lima, M. K. Lotz, *DDF* **2012**, *6*, 149.

[294] J. A. Phillippi, E. Miller, L. Weiss, J. Huard, A. Waggoner, P. Campbell, *Stem Cells* **2008**, *26*, 127.

[295] P. Calvert, *Chem. Mater.* **2001**, *13*, 3299.

[296] a) J. H. Y. Chung, S. Naficy, Z. Yue, R. Kapsa, A. Quigley, S. E. Moulton, G. G. Wallace, *Biomater. Sci.* **2013**, *1*, 763; b) I. T. Ozbolat, M. Hospodiuk, *Biomaterials* **2016**, *76*, 321.

[297] I. T. Ozbolat, Y. Yu, *IEEE transactions on bio-medical engineering* **2013**, *60*, 691.

[298] a) N. E. Fedorovich, J. R. de Wijn, A. J. Verbout, J. Alblas, W. J. A. Dhert, *Tissue Eng. Part A* **2008**, *14*, 127; b) D. F. Duarte Campos, A. Blaeser, M. Weber, J. Jäkel, S. Neuss, W. Jahnen-Dechent, H. Fischer, *Biofabrication* **2013**, *5*, 15003.

[299] S. Stichler, T. Jüngst, M. Schamel, I. Zilkowski, M. Kuhlmann, T. Böck, T. Blunk, J. Teßmar, J. Groll, *Ann. Biomed. Eng.* **2017**, *45*, 273.

[300] E. Y. S. Tan, W. Y. Yeong, *Int. J. Bioprinting* **2015**.

[301] a) V. Mironov, V. Kasyanov, R. R. Markwald, *Curr. Opin. Biotechnol.* **2011**, *22*, 667; b) F. Marga, K. Jakab, C. Khatiwala, B. Shepherd, S. Dorfman, B. Hubbard, S. Colbert, F. Gabor, *Biofabrication* **2012**, *4*, 22001.

[302] a) W. Wu, A. DeConinck, J. A. Lewis, *Adv. Mater.* **2011**, *23*, H178-83; b) C. B. Highley, C. B. Rodell, J. A. Burdick, *Adv. Mater.* **2015**, *27*, 5075.

[303] T. J. Hinton, Q. Jallerat, R. N. Palchesko, J. H. Park, M. S. Grodzicki, H.-J. Shue, M. H. Ramadan, A. R. Hudson, A. W. Feinberg, *Sci. Adv.* **2015**, *1*, e1500758.

[304] a) R. Levato, J. Visser, J. A. Planell, E. Engel, J. Malda, M. A. Mateos-Timoneda, *Biofabrication* **2014**, *6*, 35020; b) A. Skardal, M. Devarasetty, H.-W. Kang, I. Mead, C. Bishop, T. Shupe, S. J. Lee, J. Jackson, J. Yoo, S. Soker et al., *Acta Biomater.* **2015**, *25*, 24.

[305] M. Guvendiren, H. D. Lu, J. A. Burdick, *Soft Matter* **2012**, *8*, 260.

[306] H. A. Barnes, J. F. Hutton, K. Walters, *An introduction to rheology*, Elsevier, Amsterdam, **1993**.

[307] N. Paxton, W. Smolan, T. Böck, F. Melchels, J. Groll, T. Jüngst, *Biofabrication* **2017**, *9*, 44107.

[308] M. L. Oyen, *Int. Mater. Rev.* **2013**, *59*, 44.

[309] P. S. Maher, R. P. Keatch, K. Donnelly, R. E. Mackay, J. Z. Paxton, *Rapid Prototyp. J.* **2009**, *15*, 204.

[310] N. E. Fedorovich, I. Swennen, J. Girones, L. Moroni, C. A. van Blitterswijk, E. Schacht, J. Alblas, W. J. A. Dhert, *Biomacromolecules* **2009**, *10*, 1689.

[311] a) S. Bertlein, G. Brown, K. S. Lim, T. Jungst, T. Boeck, T. Blunk, J. Tessmar, G. J. Hooper, T. B. F. Woodfield, J. Groll, *Adv. Mater.* **2017**, *29*; b) R. Holmes, X.-B. Yang, A. Dunne, L. Florea, D. Wood, G. Tronci, *Polymers* **2017**, *9*, 226; c) E. Lallana, A. Sousa-Herves, F. Fernandez-Trillo, R. Riguera, E. Fernandez-Megia, *Pharm. Res.* **2012**, *29*, 1.

[312] R. Censi, P. J. Fieten, P. Di Martino, W. E. Hennink, T. Vermonden, *Macromolecules* **2010**, *43*, 5771.

[313] L. S. M. Teixeira, J. Feijen, C. A. van Blitterswijk, P. J. Dijkstra, M. Karperien, *Biomaterials* **2012**, *33*, 1281.

[314] a) M. P. Lutolf, J. A. Hubbell, *Nat. Biotechnol.* **2005**, *23*, 47; b) M. P. Lutolf, J. L. Lauer-Fields, H. G. Schmoekel, A. T. Metters, F. E. Weber, G. B. Fields, J. A. Hubbell,

Proc. Natl. Acad. Sci. U.S.A. **2003**, *100*, 5413; c) S. Kim, K. E. Healy, *Biomacromolecules* **2003**, *4*, 1214.

[315] Y. Liu, E. Kim, R. Ghodssi, G. W. Rubloff, J. N. Culver, W. E. Bentley, G. F. Payne, *Biofabrication* **2010**, *2*, 22002.

[316] Y. S. Zhang, K. Yue, J. Aleman, K. M. Moghaddam, S. M. Bakht, J. Yang, W. Jia, V. Dell'Erba, P. Assawes, S. R. Shin et al., *Ann. Biomed. Eng.* **2017**, *45*, 148.

[317] R. Luxenhofer, *Nanomedicine* **2015**, *10*, 3109.

[318] A. Das, K. Petkau-Milroy, G. Klerks, B. van Genabeek, R. P. M. Lafleur, A. R. A. Palmans, E. W. Meijer, *ACS Macro Lett.* **2018**, *7*, 546.

[319] N. Gangloff, J. Ulbricht, T. Lorson, H. Schlaad, R. Luxenhofer, *Chem. Rev.* **2016**, *116*, 1753.

[320] C. Fetsch, A. Grossmann, L. Holz, J. F. Nawroth, R. Luxenhofer, *Macromolecules* **2011**, *44*, 6746.

[321] N. Gangloff, C. Fetsch, R. Luxenhofer, *Macromol. Rapid Commun.* **2013**, *34*, 997.

[322] R. J. Simon, R. S. Kania, R. N. Zuckermann, V. D. Huebner, D. A. Jewell, S. Banville, S. Ng, L. Wang, S. Rosenberg, C. K. Marlowe, *Proc. Natl. Acad. Sci. U.S.A.* **1992**, *89*, 9367.

[323] M. M. Lübtow, L. Hahn, M. S. Haider, R. Luxenhofer, *J. Am. Chem. Soc.* **2017**, *139*, 10980.

[324] Dr. Anita Schulz, *Dissertation*, TU Dresden, Dresden, **2014**.

[325] M. M. Lübtow, L. C. Nelke, A. Brown, G. Sahay, G. Dandekar, R. Luxenhofer **2017**.

[326] N. Toncheva, C. Tsvetanov, S. Rangelov, B. Trzebicka, A. Dworak, *Polymer* **2013**, *54*, 5166.

[327] K. O'Driscoll, R. A. Sanayei, *Macromolecules* **1991**, *24*, 4479.

[328] D. Cohn, A. Sosnik, A. Levy, *Biomaterials* **2003**, *24*, 3707.

[329] K. C. Tam, X. Y. Wu, R. H. Pelton, *Polymer* **1992**, *33*, 436.

[330] T. Mezger, *Das Rheologie Handbuch. Für Anwender von Rotations- und Oszillations-Rheometern*, Vincentz, Hannover, **2016**.

[331] L. Ouyang, R. Yao, Y. Zhao, W. Sun, *Biofabrication* **2016**, *8*, 35020.

[332] T. Gao, G. J. Gillispie, J. S. Copus, A. K. Pr, Y.-J. Seol, A. Atala, J. J. Yoo, S. J. Lee, *Biofabrication* **2018**, *10*, 34106.

[333] A. Ribeiro, M. M. Blokzijl, R. Levato, C. W. Visser, M. Castilho, W. E. Hennink, T. Vermonden, J. Malda, *Biofabrication* **2017**, *10*, 14102.

[334] a) C. Li, N. J. Buurma, I. Haq, C. Turner, S. P. Armes, V. Castelletto, I. W. Hamley, A. L. Lewis, *Langmuir* **2005**, *21*, 11026; b) S. Xuan, C.-U. Lee, C. Chen, A. B. Doyle, Y. Zhang, L. Guo, V. T. John, D. Hayes, D. Zhang, *Chem. Mater.* **2016**, *28*, 727.

[335] K. H. Sun, Y. S. Sohn, B. Jeong, *Biomacromolecules* **2006**, *7*, 2871.

[336] J. Jiang, R. Malal, C. Li, M. Y. Lin, R. H. Colby, D. Gersappe, M. H. Rafailovich, J. C. Sokolov, D. Cohn, *Macromolecules* **2008**, *41*, 3646.

[337] L. Yu, H. Zhang, J. Ding, *Angew. Chem., Int. Ed.* **2006**, *45*, 2232.

[338] G. Grassi, A. Crevatin, R. Farra, G. Guarnieri, A. Pascotto, B. Rehimers, R. Lapasin, M. Grassi, *J. Colloid Interface Sci.* **2006**, *301*, 282.

[339] a) N. ten Brummelhuis, C. Secker, H. Schlaad, *Macromol. Rapid Commun.* **2012**, *33*, 1690; b) M. Schroffenegger, R. Zirbs, S. Kurzhals, E. Reimhult, *Polymers* **2018**, *10*, 451.

[340] T. Lorson, S. Jaksch, M. M. Lübtow, T. Jüngst, J. Groll, T. Lühmann, R. Luxenhofer, *Biomacromolecules* **2017**, *18*, 2161.

[341] M. Teubner, R. Strey, *J. Chem. Phys.* **1987**, *87*, 3195.

[342] M. E. Vigild, K. Almdal, K. Mortensen, I. W. Hamley, J. P. A. Fairclough, A. J. Ryan, *Macromolecules* **1998**, *31*, 5702.

[343] K. Fischer, M. Schmidt, *Biomaterials* **2016**, *98*, 79.

[344] Wolfgang Schärtl, *Light Scattering from Polymer Solutions and Nanoparticle Dispersions*, Springer Berlin Heidelberg, Berlin, Heidelberg, **2007**.

[345] D. W. Lee, W. S. Choi, M. W. Byun, H. J. Park, Y.-M. Yu, C. M. Lee, *J. Agric. Food Chem.* **2003**, *51*, 4819.

[346] Z. Kroneková, T. Lorson, J. Kronek, R. Luxenhofer, *Cytotoxicity of 2-oxazines and poly(2-oxazine)s in mouse fibroblast*, **2018**.

[347] J. Kronek, J. Lustoň, Z. Kroneková, E. Paulovičová, P. Farkaš, N. Petrenčíková, L. Paulovičová, I. Janigová, *J. Mater. Sci. Mater. Med.* **2010**, *21*, 879.

[348] S. F. Khattak, S. R. Bhatia, S. C. Roberts, *Tissue Eng.* **2005**, *11*, 974.

[349] a) R. Luxenhofer, R. Jordan, *Macromolecules* **2006**, *39*, 3509; b) M. Schmitz, M. Kuhlmann, O. Reimann, C. P. R. Hackenberger, J. Groll, *Biomacromolecules* **2015**, *16*, 1088.

[350] V. H. M. Mouser, F. P. W. Melchels, J. Visser, W. J. A. Dhert, D. Gawlitta, J. Malda, *Biofabrication* **2016**, *8*, 35003.

[351] A. V. Feoktystov, H. Frielinghaus, Z. Di, S. Jaksch, V. Pipich, M.-S. Appavou, E. Babcock, R. Hanslik, R. Engels, G. Kemmerling et al., *J. Appl. Crystallogr.* **2015**, *48*, 61.

[352] K. Rausch, A. Reuter, K. Fischer, M. Schmidt, *Biomacromolecules* **2010**, *11*, 2836.

[353] M. Gutmann, E. Memmel, A. Braun, J. Seibel, L. Meinel, T. Lühmann, *ChemBioChem* **2016**, *17*, 886-875.

[354] a) D. D. Ross, C. C. Joneckis, J. V. Ordóñez, A. M. Sisk, R. K. Wu, A. W. Hamburger, R. E. Nora, *Cancer Res.* **1989**, *49*, 3776; b) K. H. Jones, J. A. Senft, *J. Histochem. Cytochem.* **1985**, *33*, 77; c) J. M. Clarke, M. R. Gillings, N. Altavilla, A. J. Beattie, *J. Microbiol. Methods* **2001**, *46*, 261.

[355] L. Piñeiro, M. Novo, W. Al-Soufi, *Adv. Colloid Interface Sci.* **2015**, *215*, 1.

[356] K. Kalyanasundaram, J. K. Thomas, *J. Am. Chem. Soc.* **1977**, *99*, 2039.

Affidavit

I hereby confirm that my thesis entitled “Novel Poly(2-oxazoline) Based Bioinks” is the result of my own work. I did not receive any help or support from commercial consultants. All sources and / or materials applied are listed and specified in the thesis.

Furthermore, I confirm that this thesis has not yet been submitted as part of another examination process neither in identical nor in similar form.

Place, Date Signature

Hiermit erkläre ich an Eides statt, die Dissertation „Neuartige Poly(2-oxazolin) Basierte Biotinten“ eigenständig, d.h. insbesondere selbstständig und ohne Hilfe eines kommerziellen Promotionsberaters, angefertigt und keine anderen als die von mir angegebenen Quellen und Hilfsmittel verwendet habe.

Ich erkläre außerdem, dass die Dissertation weder in gleicher noch in ähnlicher Form bereits in einem anderen Prüfungsverfahren vorgelegen hat.

Ort, Datum Unterschrift